HEMODYNAMIC ASSESSMENT OF PROPOSED SOLUTIONS FOR FONTAN FAILURE

A Dissertation

Presented to

The Academic Faculty

by

Phillip Michael Trusty

In Partial Fulfillment

Of the requirements for the Degree

Doctor of Philosophy in

Bioengineering

Georgia Institute of Technology

May 2019

HEMODYNAMIC ASSESSMENT OF PROPOSED SOLUTIONS FOR FONTAN FAILURE

Approved by:

Ajit P. Yoganathan, PhD, Advisor
School of Biomedical Engineering
Georgia Institute of Technology

Shriprasad Deshpande, MD
Department of Pediatrics
Emory University

J. Brandon Dixon, PhD
School of Mechanical Engineering
Georgia Institute of Technology

Mark A. Fogel, MD
Division of Cardiology
Children's Hospital of Philadelphia

John N. Oshinski, PhD
School of Biomedical Engineering
Georgia Institute of Technology

Timothy C. Slesnick, MD
Department of Pediatrics
Emory University

Date Approved: March 5, 2019

ACKNOWLEDGEMENTS

The work accomplished in this thesis would not have been possible without the assistance of a number of people along the way. I would like to acknowledge all those who contributed to the completion of this work spanning from study design to data analysis:

- **Undergraduate students:** Alexa Graham, Megan Sales, Kasey Rice, Sarah Hall, Adriana Bodlak, Jake Sebring, Emelia Funnell, Wenjun Wu
- **Graduate students:** Mike Tree, Alan Wei, Eric Pierce, Maria Restrepo, Mark Luffel
- **Clinicians:** Timothy Slesnick, Shri Deshpande, Mark Fogel, Jack Rychik, Kirk Kanter, Kevin Maher, Jan Fernandez
- **Industry:** Doug Vincent, Jeff Naber, Kartik Sundareswaran, Daniel Crandall
- **Faculty/Staff:** Brandon Dixon, John Oshinski, Jarek Rossignac, Sandra Maffey, Steven Marzec

Finally, I would like to thank Dr. Yoganathan for the opportunity to work in the Cardiovascular Fluid Mechanics Lab. I benefited from long-standing collaborations he has developed over the years and I was the recipient of his discretionary funds in a number of projects. I was encouraged and funded to attend every conference that accepted my work where I gained valuable exposure and experience. Dr. Yoganathan allowed me to pursue my own research interests throughout my PhD, for which I am grateful.

TABLE OF CONTENTS

LIST OF TABLES

LIST OF FIGURES

NOMENCLATURE

AZ	azygous vein
BSA	body surface area
CD	collagen deposition
CFD	computational fluid dynamics
CI	cardiac index
CMR	cardiac magnetic resonance
CO	cardiac output
ECC	extracardiac conduit
EDV	end diastolic volume
EF	ejection fraction
ESV	end systolic volume
HFD	hepatic flow distribution
iPL	indexed power loss
IVC	inferior vena cava
LPA	left pulmonary artery
LT	lateral tunnel
MRI	magnetic resonance imaging
PA	pulmonary artery
PAVM	pulmonary arteriovenous malformations
PC-MRI	phase contrast magnetic resonance imaging
PFD	pulmonary flow distribution
PI	pulsatility index

PL	power loss
PVR	pulmonary vascular resistance
Qs	systemic flow
RPA	right pulmonary artery
SV	stroke volume
SVC	superior vena cava
TCPC	total cavopulmonary connection
VAD	ventricular assist device
VMTK	vascular modeling toolkit
WU	Wood units

SUMMARY

Single ventricle heart defects are among the most severe types of congenital heart problems and require surgical intervention for survival. The common procedure is to use a set of three, staged palliative surgeries to re-route blood around the non-functioning ventricle resuling in a “Fontan” physiology, which connects the vena cave directly to the pulmonary arteries in what is referred to as a total cavopulmonary connection (TCPC). Short term outcomes of this approach are promising, but almost all patients suffer from long term morbities including a variety of issues with the lungs, liver, lymphatics and gastrointestinal system.

This thesis focuses on evaluating currently proposed solutions for two of the most common problems faced by Fontan patients: pulmonary arteriovenous malformation (PAVMs) and Fontan associated liver disease (FALD). The use of (1) surgical planning and (2) Y-grafts are hypothesized to offer more balanced hepatic flow distrubtion (HFD), a key factor in PAVM formation. These methods are currently being implemented in a small portion of Fontan patients. In terms of FALD, both (1) improved TCPC efficiency and (2) mechanical circulatory support (MCS) are hypothesized to reduce hepatic congestion and stop or delay the progression of liver disease in these patients.

These four proposed solutions were investigated using patient specific computational modeling, medical image analysis, and in vitro testing. A total of ~220 patient data sets were analyzed in this thesis. Four MCS devices were tested. Surgical planning was found to offer accurate HFD predictions for specific graft types and was used to correct PAVMs in several Fontan revision cases. Y-grafts offered similar HFD to traditional connection types at the immediate post-operative state but showed significantly more balanced HFD at ~3 year follow up. TCPC efficiency and LPA stenosis approximately 7 years prior to biopsy were predictive of future liver

disease. MCS devices varied in their ability to reduce hepatic congestion, with the more powerful devices being the most successful. Overall, the proposed solutions for both PAVMs and FALD seem to be viable options.

1. INTRODUCTION

Congenital heart defects are the most common types of birth defects and are responsible for the largest proportion of infant mortality attributable to birth defects.[1] Over 1.3 million babies are born with a congenital heart defect each year.[2] The most severe of these congenital heart defects can result in a "single ventricle" physiology where both the pulmonary and systemic circulations are pumped in parallel by a single functioning ventricle. This physiology can damage the heart and lungs, and results in the mixing of oxygenated and deoxygenated blood. If left untreated, the newborn will not survive.

Over the last 40 years surgeons have pioneered a set of 3 staged surgeries to palliate single ventricle heart defects. These surgeries are known as the Norwood, Glenn and Fontan procedures, and take place when the patient is around 3 days, 3 months, and 3 years of age, respectively. The final result of these operations is a total cavopulmonary connection (TCPC), which is a complete anastomosis of the inferior and superior vena cava to the pulmonary arteries. In this new configuration, blood bypasses the right side of the heart and passively flows to the lungs for oxygenation. The single ventricle is left to pump oxygenated blood throughout the body. These patients are often referred to as "Fontan" patients.

Short term outcomes of the Fontan palliation are very promising, with a 1-year survival rate around 95%. However, as these patients age, long term complications are inevitable. Pulmonary arteriovenous malformations (PAVMs) and liver disease are two of the most prevalent morbitities, and are thought to be directly related to poor Fontan hemodynamics. Currently, the first and second "generation" of Fontan patients are beginning to experience these complications and clinicians are actively looking for solutions to these problems.

The central purpose of this thesis is to investigate the effectiveness of current, clinically implemented "solutions" for two of the most common modes of Fontan failure including PAVMs and liver disease. The work in this thesis will utilize both computational and experimental modeling and will involve around 150 patient data sets. This work is possible through collaborations with both Children's Healthcare of Atlanta and Children's Hospital of Philadelphia, as well as ventricular assist device companies including Medtronic (Heartware), Design Mentor and Abbott (Thoratec).

This thesis will consist of two specific aims, with Specific Aim 1 focused on PAVMs and Specific Aim 2 focused on liver disease. Specific Aim 1 will test if surgical planning can be used to accurately predict post-operative hepatic flow distribution (a factor in PAVM formation), and if Y-grafts can provide more balanced hepatic flow distribution than traditional Fontan connections. Specific Aim 2 will test if the extent of liver fibrosis in Fontan patients is associated with poor Fontan hemodynamics, and if ventricular assist devices can decrease Fontan hepatic congestion by augmenting flow and decreasing inferior vena cava pressure.

2. HYPOTHESES AND SPECIFIC AIMS

Specific Aim 1a: Evaluate the accuracy of Surgical Planning to predict post-operative hepatic flow distribution and resolve pulmonary arteriovenous malformations.

Hypothesis: Surgical planning can accurately predict post-operative hepatic flow distribution.

While surgical planning has been used in a plethora of previous studies, no conclusive evidence or long-term follow up data exists showing whether surgical planning was accurate or beneficial. Specific Aim 1a will use patient-specific, computational fluid dynamic (CFD) modeling to analyze the accuracy of surgical planning predictions of hepatic flow distribution (HFD), a known factor in pulmonary arteriovenous malformation (PAVM) formation. This aim will include all patients in the Georgia Tech Fontan database who were part of a surgical planning protocol and underwent a "Fontan revision" due to the formation of PAVMs (5-10 patients). Pre- and post-operative MRI and clinical data exist for each patient. Predicted results will be compared with long-term follow up data to determine if surgical planning was effective in predicting HFD. The relationship between HFD and PAVM resolution will also be explored.

Specific Aim 1b: Evaluate the ability of Y-grafts to provide balanced hepatic flow distribution and therefore prevent pulmonary arteriovenous malformations.

Hypothesis: Y-grafts will provide more balanced hepatic flow distribution than traditional Fontan connections.

Y-grafts are a relatively new option for Fontan completion, and are hypothesized to provide balanced HFD to the left and right pulmonary arteries via the Y-graft's two outlets (thus preventing the formation of PAVMs). Specific Aim 1b will use patient-specific CFD modeling to analyze the

ability of a Y-graft to offer balanced HFD, preventing the formation of PAVMs. We will perform a direct comparison between 30 consecutive Y-graft patients and 30 age and BSA matched traditional Fontan patients. In this comparison we will determine if a Y-graft provides more balanced HFD than a traditional Fontan connection. In addition, we will also study how HFD changes over time in Y-graft patients. To do this, we have acquired long-term follow up MRI and clinical data, in addition to immediate post-operative data, for 10 Y-graft patients.

Specific Aim 2a: Investigate the relationship between total cavopulmonary connection hemodynamics and Fontan associated liver failure.

Hypothesis: The extent of liver fibrosis in Fontan patients is associated with poor Fontan hemodynamics.

Specific Aim 2a will use CFD modeling to investigate potential relationships between Fontan hemodynamics and liver failure. This aim will assess if (a) liver failure is correlated with concurrent TCPC hemodynamics (at the same time point), and if (b) prior TCPC hemodynamics are predictive of future liver failure. Through our collaboration with the Children's Hospital of Philadelphia and their Single Ventricle Survivorship program, we have acquired concurrent MRI, catheterization and liver biopsy data for 35 Fontan patients. In addition, we have serial data (at a time point prior to the liver biopsy) for 25 of these patients. For each dataset, we will perform patient-specific simulations using MRI derived anatomy and blood flow waveforms. Hemodynamic metrics including pressure drop, TCPC resistance, energy loss, vessel size and percent stenosis will be calculated. Percent collagen deposition, as a measure of liver fibrosis, will be quantified using digital image analysis of Sirius Red stained slides.

Specific Aim 2b: Evaluate the use of ventricular assist devices to support the Fontan circulation and prolong liver health as a bridge to heart transplantation.

Hypothesis: Ventricular assist devices can decrease Fontan hepatic congestion by augmenting flow and decreasing inferior vena cava pressure.

Heart transplantation is currently the only option to fundamentally correct a failing Fontan heart. However, Fontan associated liver disease can be a contraindication to heart transplant, and combined heart and liver transplantation is extremely rare. Therefore, the purpose of Specific Aim 2b is to determine if VADs can be used to promote liver health in a failing Fontan patient until heart transplantation. In this aim we will use both experimental and computational modeling to determine if VADs are a viable option for right-sided Fontan support, and if VADs can decrease hepatic congestion in order to delay liver failure. To accomplish this, we will test 4 currently available pumps (Circulite, VentriFlo, PediMag and CentriMag) in a previously designed and validated Fontan mock circulatory loop. The experimental loop will be tuned to match "failing" Fontan pressures and flows acquired from clinical data. During these experiments we will evaluate each pump's ability to decrease hepatic pressure while increasing cardiac output. Additionally, the experimental data will be used to validate mechanically assisted Fontan computational fluid dynamic model. The computational model will then be used to determine if a VAD will work for multiple patient anatomies and multiple cannula varitions.

3. BACKGROUND AND SIGNIFICANCE

3.1 Cardiac Physiology

The heart is a muscular organ that powers the cardiovascular system. Each day, the heart beats around 100,000 times and pumps approximately 1,800 gallons of blood. A normally functioning heart is separated into two sides and four chambers (Figure 3-1). The right side of the heart consists of the right atrium and right ventricle. The right atrium is basically a reservoir which collects deoxygenated blood returning from the upper and lower body via the superior and inferior vena cava (IVC and SVC). The right atrium pumps blood through the tricuspid valve into the right ventricle. Once filled, the right ventricle begins to contract. The increased pressure causes the tricuspid valve to close and the blood moves through the pulmonary valve to the left and right lungs via the left and right pulmonary arteries (LPA and RPA).

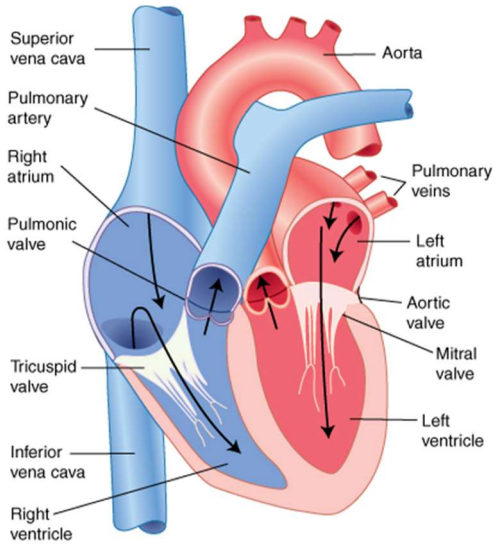

Figure 3-1 Cardiac Physiology. A four-chambered, cross-sectional view of the healthy heart.

The left side of the heart receives oxygenated blood from the pulmonary veins into the left atrium. When the pressure in the left atrium exceeds left ventricular pressure, blood moves into

the left ventricle through the mitral valve. The left ventricle is the stronger of the two ventricles and is responsible for delivering oxygenated blood throughout the body. As the left ventricle begins to contract, the mitral valve closes and blood travels through the aortic valve into the aorta. The aorta branches into several vessels taking blood to the upper and lower body.

3.2 Single Ventricle Congenital Heart Defects

A normally functioning heart prevents the mixing of oxygenated and deoxygenated blood, allowing for well oxygenated blood to promote proper organ function and sustain life. Arterial blood oxygen saturation is typically around 95-100% in a healthy individual, falling to near 70% on the venous side before entering the pulmonary circulation. An arterial oxygen saturation below 90% is considered low.

However, there are a number of congenital heart defects that can result in a single ventricle physiology, where oxygenated and deoxygenated blood can freely mix within the heart. These defects impose immediate danger to the child and require immediate surgical action to avoid death. Two of the most common single ventricle congenital heart defects include tricuspid atresia and hypoplastic left heart syndrome, which will be discussed in the following sections.

3.2.1 Tricuspid atresia

Tricuspid atresia is severe congenital heart defect where the tricuspid valve does not exist, or is completely closed. This is obviously a major problem since blood can no longer travel through the four chambers of the heart as designed. In addition, it is very common for a number of other defects to accompany tricuspid atresia, including an underdeveloped right ventricle, and both atrial

and ventricular septal defects (Figure 3-2). Tricuspid atresia is often associated with pulmonary stenosis and transposition of the great arteries.

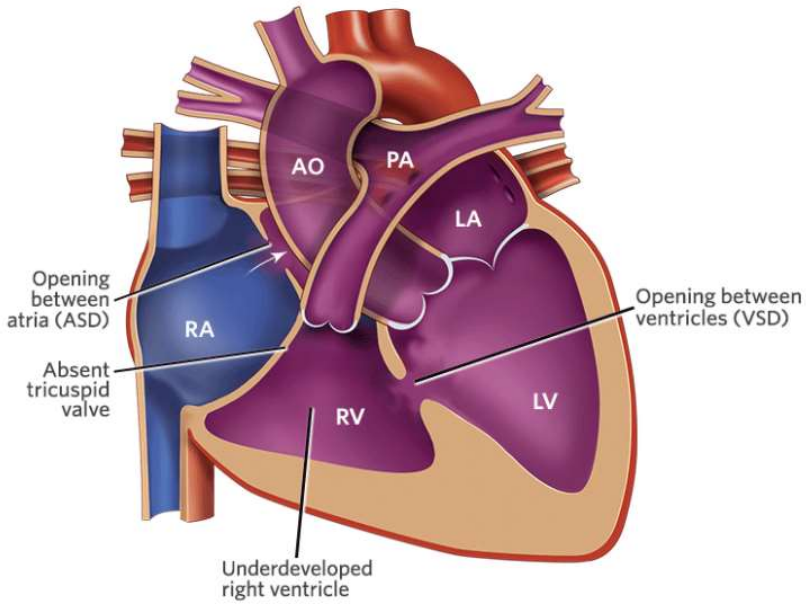

Figure 3-2 Tricuspid atresia. Aorta (AO), left and right atrium (LA, RA), left and right ventricle (LV, RV), pulmonary artery (PA).

The consequence of this defect is a single ventricle physiology. Blood is free to mix between the atria and ventricles, which causes semi-oxygenated blood to be sent to both the pulmonary and systemic circulations. The only pathway for blood to enter the pulmonary circulation is through the left ventricle to the right ventricle and then the pulmonary arteries.

3.2.2 Hypoplastic left heart syndrome

Hypoplastic left heart syndrome is a congenital heart defect where the left side of the heart is severely underdeveloped. As shown in Figure 3-3, the left ventricle is much smaller than the right ventricle. Other abnormalities associated with hypoplastic left heart syndrome can include a

very small or closed mitral or aortic valve, or septal defects between the atria or ventricles. In this situation, the abnormally small left ventricle cannot adequately pump blood through the systemic circulation, and the various related defects allow the mixing of oxygenated and deoxygenated blood.

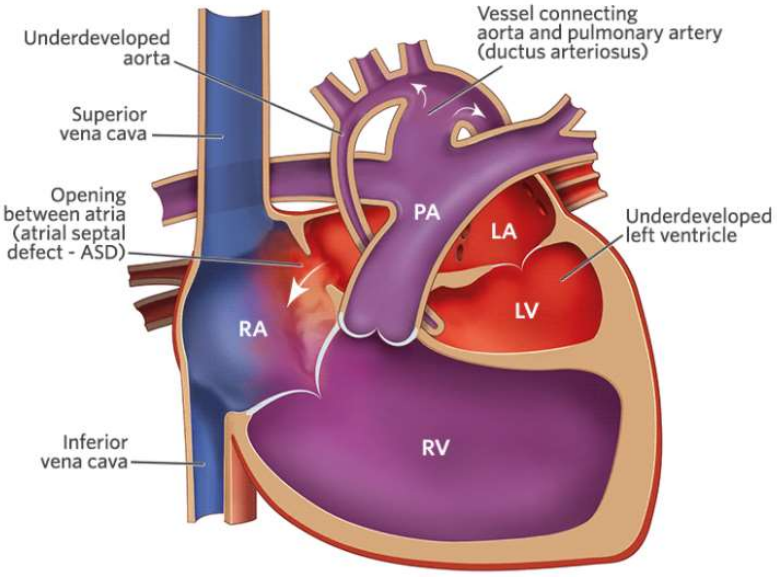

Figure 3-3 Hypoplastic left heart syndrome. Left and right atrium (LA, RA), left and right ventricle (LV, RV), pulmonary artery (PA).

Consequently, the right ventricle becomes the only functioning pump in the cardiovascular system and must drive blood through both the systemic and pulmonary circulations. The right ventricle is not made for this workload, as it is designed to operate at a much lower pressure. This can be detrimental to the patient if corrective actions are not taken. Additionally, the blood that is moving throughout the body is not completely oxygenated due to the mixing of oxygenated and deoxygenated blood in the heart, and therefore cannot supply the body with sufficient oxygen. This condition is fatal is left untreated.

3.3 Fontan Palliation

The Fontan procedure is the current strategy of choice to palliate single ventricle congenital heart defects. This surgical procedure must be accomplished through several stages since a complete right heart bypass is impossible at birth (vessels are too small and pulmonary vascular resistance is too high). The end result of this procedure is referred to as a total cavopulmonary connection (TCPC), where deoxygenated blood returning from the body bypasses the heart and moves passively to the lungs. This configuration successfully separates oxygenated and deoxygenated blood, but creates a one "pump" circulatory system (Figure 3-4). The individual stages of this procedure are detailed in the following sections.

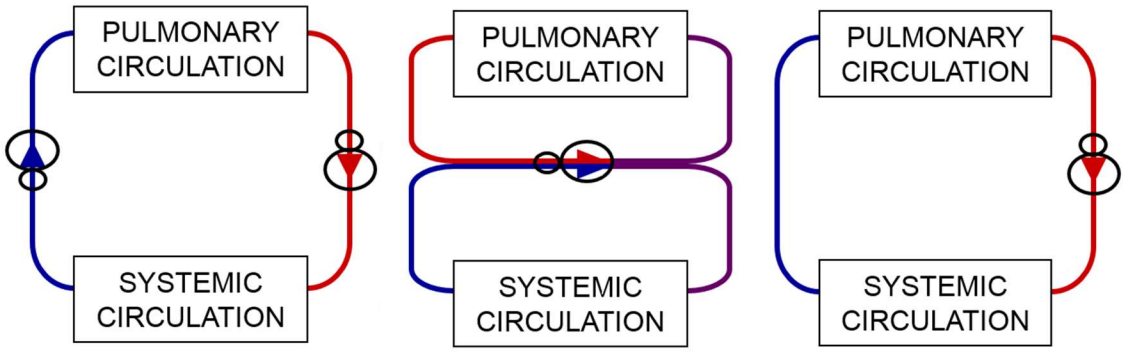

Figure 3-4 Schematics of healthy circulation (left), single ventricle congenital heart defect circulation (middle) and Fontan circulation (right).

3.3.1 Stage 1: Norwood Procedure

The Norwood procedure was introduced by Dr. William Norwood and is performed within the first days to weeks of life.[3] There are several versions of the Norwood procedure (Figure 3-5), but the general purpose of the procedure is to implement a shunt that allows for increased blood

flow to the lungs, with the goal of increasing blood oxygenation. The operation is usually accompanied by reconstruction of the hypoplastic aorta.

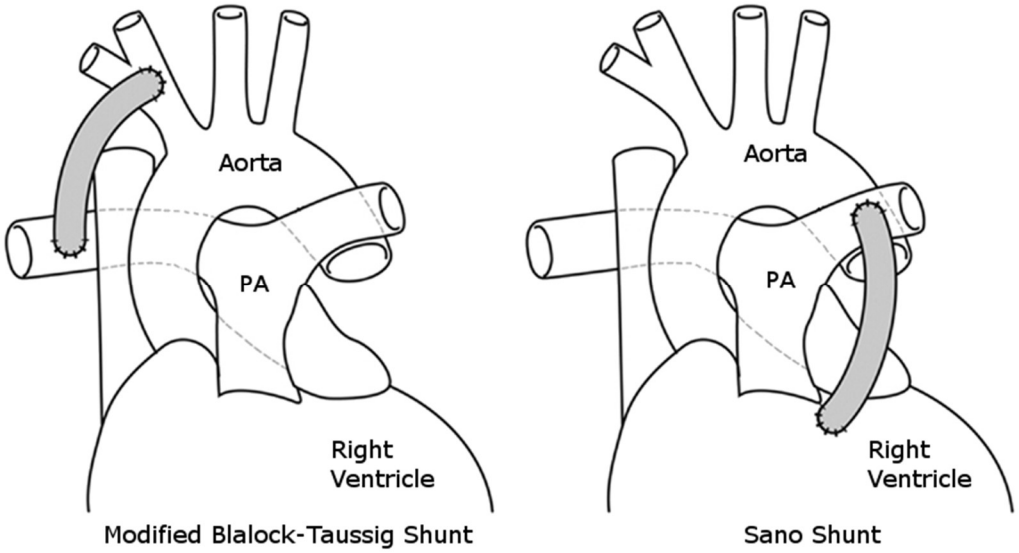

Figure 3-5 Norwood procedure variations.

The various versions of this procedure all shunt blood from the systemic to pulmonary circulation, but have different insertion sites for the inlet and outlet of the shunt. The modified Blalock-Taussig shunt takes blood from the right subclavian artery and empties into the right pulmonary artery, while the Sano procedure shunts directly from the right ventricle to the pulmonary arteries.[3,4] This stage allows for sufficient oxygenation for several months until the next stage of the operation.

3.3.2 Stage 2: Glenn Procedure

The second stage of Fontan palliation is known as the Glenn procedure. The goal of this stage is to increase lung perfusion and begin separating oxygenated and deoxygenated blood. This stage occurs between 3-6 months of age, once the relatively high pulmonary vascular resistance

associated with the neonatal circulation has decreased. The first step in this procedure is to remove the shunt from stage 1. The SVC is then disconnected from the right atrium and directly connected to the pulmonary arteries (Figure 3-6).

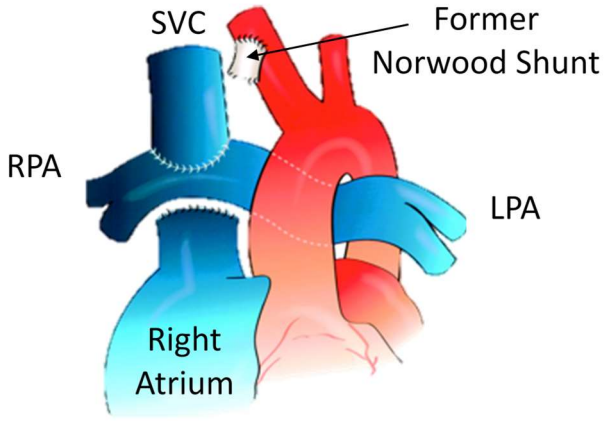

Figure 3-6 Glenn procedure.

Deoxygenated blood from the upper body now bypasses the heart and flows passively through the pulmonary circulation. At this stage of life, upper body flow accounts for approximately 60% of cardiac output, so more than half of deoxygenated blood is now separated from oxygenated blood. This configuration remains for several years until the final stage of palliation.

3.3.3 Stage 3: Fontan procedure

The final stage is known as the Fontan procedure. In this stage, the complete separation of deoxygenated and oxygenated blood is completed by re-routing blood from the IVC to the pulmonary arteries, bypassing the right atrium. In this configuration, only oxygenated blood enters the heart, and the two ventricles effectively function as a single pump pushing blood throughout

the systemic circulation. Without further complications, patient oxygen saturation can stabilize in the 90's, promoting growth and proper organ function.

The Fontan procedure was first reported in 1971 by Fontan and Baudet.[5] Since their first procedure, the Fontan procedure has progressed through several iterations including the atrio-pulmonary connection, lateral tunnel connection and the extracardiac conduit (Figure 3-7).[6,7] Each design change was motivated by health problems including arrhythmias and thrombus formation.[8,9] More recent configurations continue to surface including the Y-graft, hepatic to azygous shunt and hepatic to innominate vein connection.[10,11]

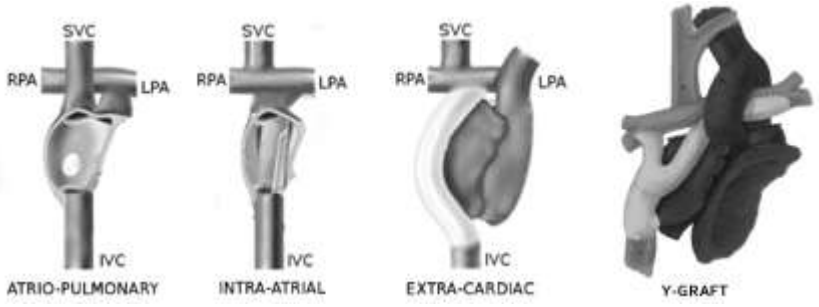

Figure 3-7 Progression of Fontan connection options.

3.4 Patient Outcomes

Fontan patient outcomes have improved substantially since the surgery was first performed. However, there remains much room for improvement. A study by Pundi et al. provides an overall assessment of Fontan outcomes up to 40 years after surgery and includes approximately 1000 patients.[12] Overall survival at 10, 20, and 30 years after surgery were 74, 61 and 43 percent respectively (Figure 3-8A). When divided into surgical era, obvious improvements in 10-year survival rates can be seen in the more recent decades (Figure 3-8B), with approximately 70% and 90% survival rates in surgeries performed before 1990 and after 2001 respectively.

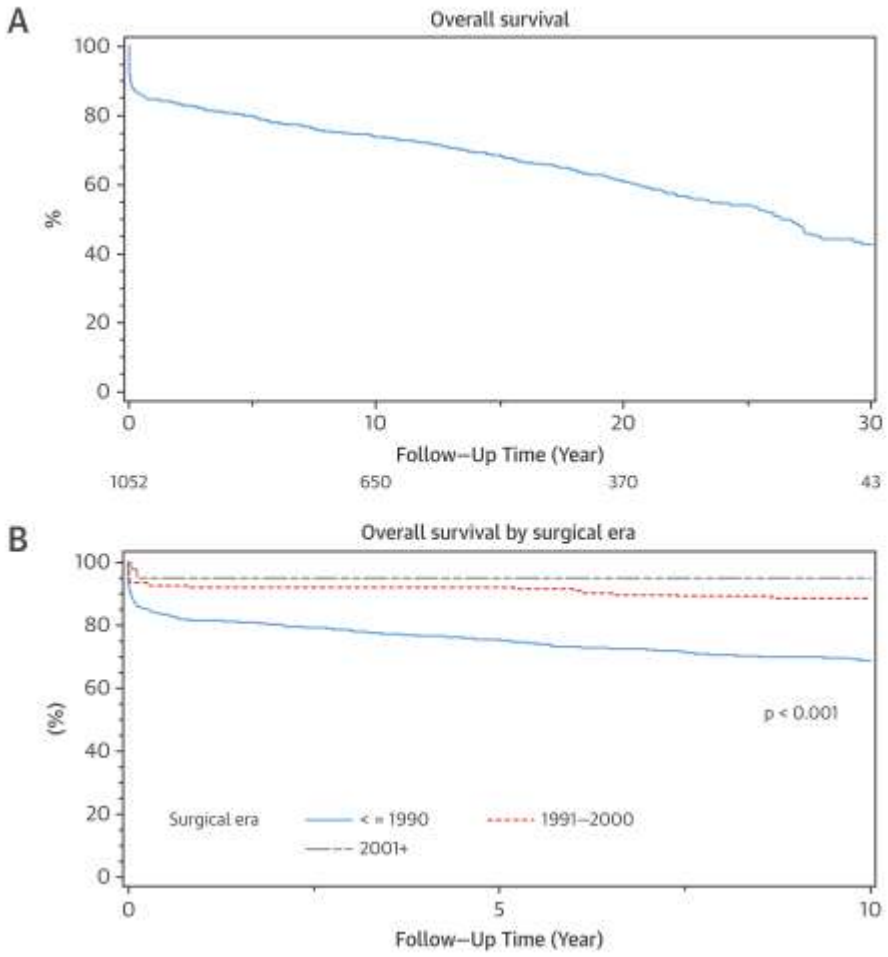

Figure 3-8 Fontan survival in terms of (A) overall patient cohort and (B) surgical era. Taken from Pundi et al., "40 year Follow up…", JACC 2015.

Significant differences were also seen in 10-year survival rates based on type of Fontan, with the extracardiac conduit outperforming all other connection types (Figure 3-9). Lateral tunnel, atriopulmonary and all other non-extracardiac conduit options performed similarly in terms of 10-year survival rate. Of the 1052 patients in this study, 177 (17%) had at least 1 early reoperation due to various complications including bleeding and need for a pacemaker. The major cause of death among these patients was primarily a cardiac cause, however the cause of death in many

patients was multifactorial and included respiratory failure, renal insufficiency, hepatic insufficiency, bleeding etc.

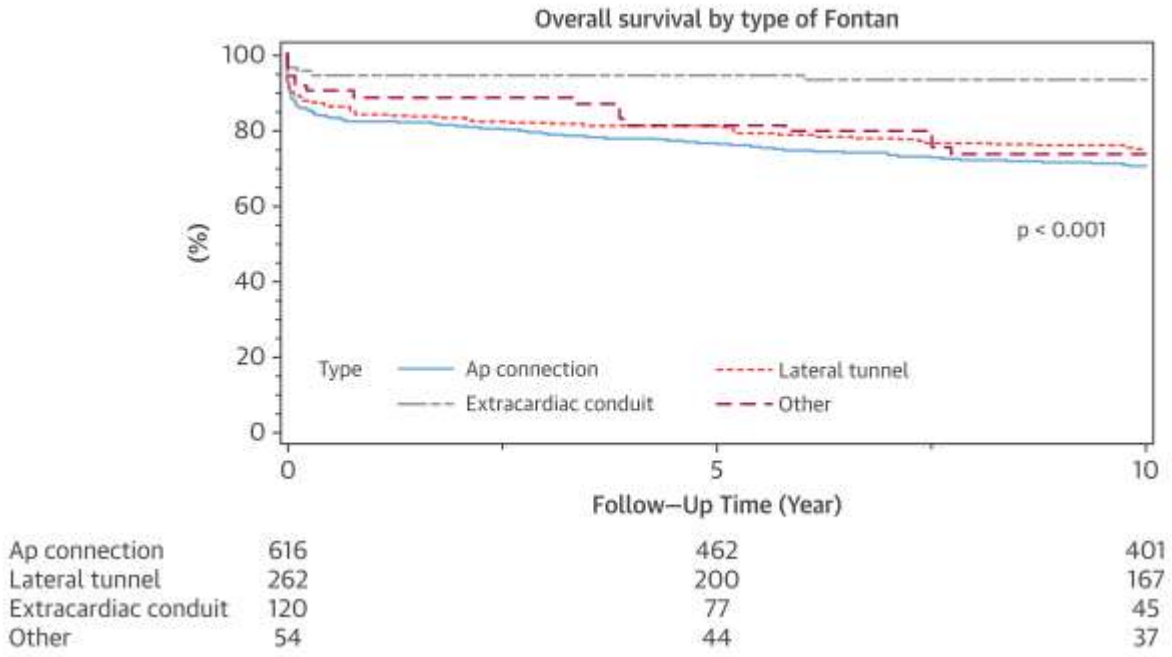

Figure 3-9 Fontan survival by type of Fontan. Taken from Pundi et al., "40 year Follow up…", JACC 2015.

3.5 Complications

A number of complications have been associated with the Fontan circulation. Relatively short-term issues including pulmonary arteriovenous malformations (PAVMs), Fontan associated liver disease (FALD), protein losing enteropathy, arrhythmias and plastic bronchitis are often seen in this population.[12–18] Additionally, long-term complications including heart failure, respiratory failure, renal insufficiency, poor quality of life and death are unfortunately inevitable as these patients age.[12,19–21] These numerous issues have led experts to say that "…freedom from morbidity is likely close to zero" and conclude that Fontan patients are "doomed to a circulatory failure."[12,22]

While each of these morbidities deserves in depth study, this thesis focusses on two of the most common issues including PAVMs and liver disease. These two complications are hypothesized to be hemodynamic driven, which we are well equipped to study in our lab. Additionally, there are currently proposed "solutions" to each of these problems that need to be explored and potentially validated. Finally, through existing collaborations we have obtained very rare data sets that will allow me to investigate the efficacy of these proposed solutions. A more detailed description of PAVMs and Fontan associated liver disease, as well as a description of the proposed solutions, is given in the following sections.

3.5.1 Pulmonary Arteriovenous Malformations

Pulmonary arteriovenous malformations are a common morbidity in Fontan patients in which abnormally dilated vessels create a right-to-left shunt between the pulmonary arteries and pulmonary veins.[13,18,23,24] When this occurs, the dilated vessels offer the path of least resistance and receive a large proportion of pulmonary blood flow.[25] Gas transport cannot occur adequately in blood moving quickly through these large vessels and the patient suffers from low oxygen saturation (Figure 3-10). PAVMs are very rare in the average population, with an incidence of only 2-3 per 100,000.[25] This condition is often asymptomatic, but can lead to dyspnea, embolic events and poor organ function.

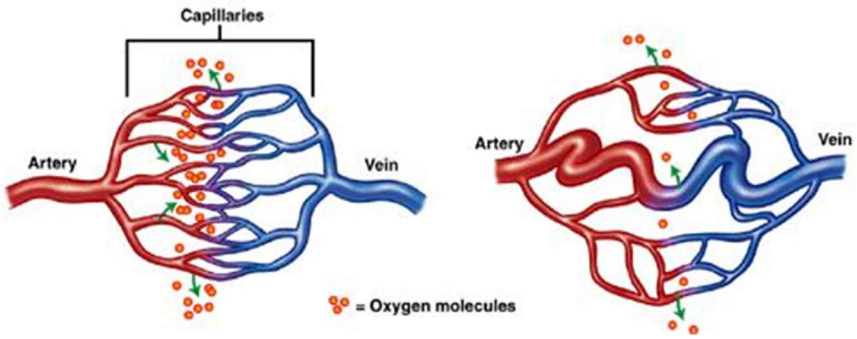

Figure 3-10 Pulmonary arteriovenous malformations. Right to left shunting decreases blood oxygenation.

Despite the rarity of this disease in the average population, PAVMs are commonly seen in Fontan patients.[13,18,23] Previous work has investigated the exact cause of this discrepancy, and though not fully understood, the lack of a "hepatic factor" (lack of IVC flow) to a specific lung has been shown to cause PAVMs.[14,26,27] Hepatic factor is delivered from the liver, through the right heart or TCPC (for 2-ventricle or Fontan circulation respectively), and finally through the LPA and RPA to the left and right lungs. A balanced hepatic flow distribution (HFD) to the left and right lungs is needed to prevent PAVMs.[14] Poor HFD (leading to PAVMs) is often the cause for a Fontan revision surgery, where the surgeon will perform an additional open heart surgery in order to improve the surgical design of the TCPC.[28,29]

Achieving a balanced HFD is inherently different for a 2-ventricle or Fontan circulation (Figure 3-11), which explains the discrepancy in PAVM prevalence between the healthy and Fontan populations. In a normal 2-ventricle circulation, hepatic blood joins blood returning from the lower body in the IVC, and then mixes with blood from the upper body in the right atrium and right ventricle before moving through the pulmonary arteries towards the lungs. This opportunity for hepatic blood to thoroughly mix in the right heart with all lower and upper body blood flow

allows for the concentration of this "hepatic factor" to be relatively consistent throughout the entire volume of blood entering the left and right pulmonary arteries. This allows an ample amount of hepatic factor to reach both the left and right lungs and prevent the formation of PAVMs.

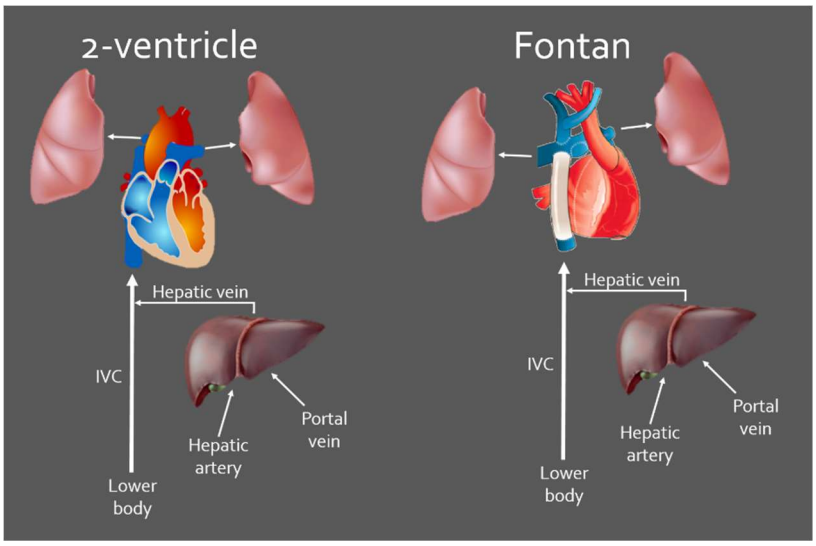

Figure 3-11 Schematic of hepatic flow and positioning of liver for 2-ventricle (left) and Fontan (right) circulation.

In contrast, the Fontan circulation (lacking a right atrium and ventricle) allows very little opportunity for hepatic flow to mix with blood returning from the upper body. After hepatic blood enters the IVC and mixes with blood returning from the lower body, the only time it comes into contact with upper body blood flow is while moving through the TCPC. The amount of mixing that will occur in the TCPC is highly dependent on TCPC design and individual vessel flow rates. Therefore, in the setting of a TCPC, hepatic flow distribution (HFD) becomes a fluid mechanics problem. Unfortunately, due to surgical freedom, patient circumstances and sometimes a lack of planning, many TCPCs are not ideal connections (Figure 3-12). Potential solutions to this problem focus on creating an optimal TCPC design in order to achieve balanced HFD to the left and right lungs.

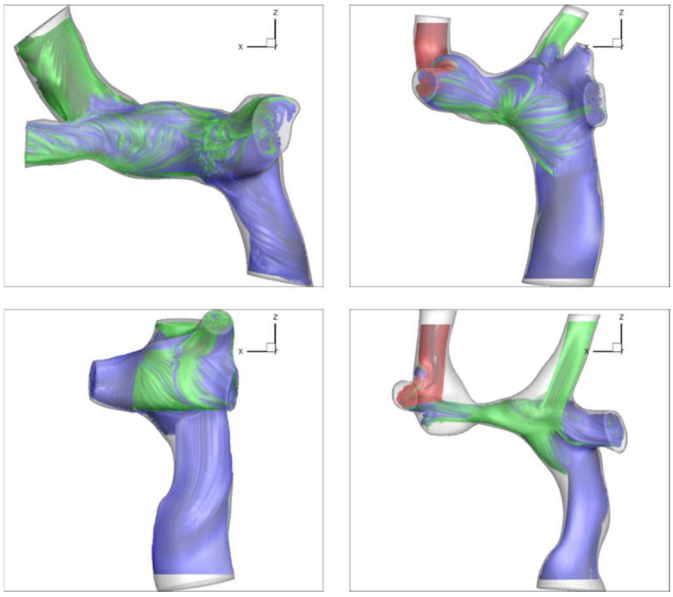

Figure 3-12 Representative examples of total cavopulmonary connections. Streamlines colored by inlet: IVC (blue), SVC (green), LSVC (red).

3.5.2 Fontan Associated Liver Disease

Fontan associated liver disease (FALD) is a well-documented complication which may have its roots in genetic, biochemical and hemodynamic origins (Figure 3-13). Additionally, liver insult may occur at birth (hypoxia and hypoperfusion), during the various perioperative states (Norwood, bidirectional Glenn and Fontan surgeries), and throughout the chronic condition of elevated CVP and relatively diminished CO.[15] Regardless of cause, FALD is now recognized as "universal" and likely a progressive process affecting all Fontan survivors.[30]

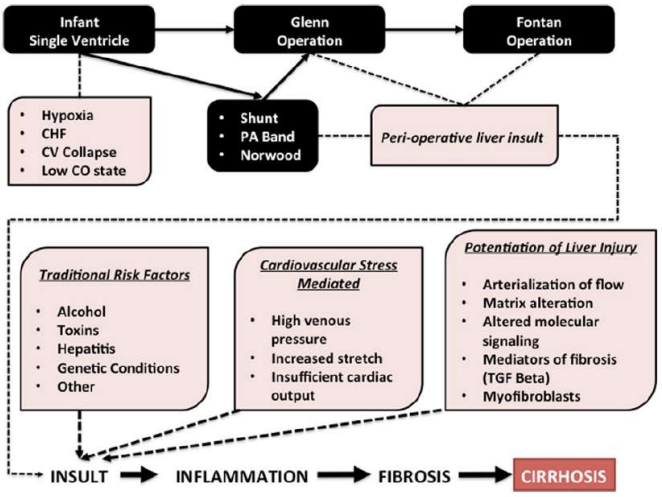

Figure 3-13 Potential mechanisms that initiate and cause progression of Fontan associated liver disease.

Liver disease results from chronic damage to the liver and is accompanied by the accumulation of extracellular matrix (ECM) proteins. These ECM proteins distort the architecture of the liver and form fibrous scars, leading to the development of arterialized nodules and eventual cirrhosis (Figure 3-14).[31] Typically caused by alcohol abuse and the hepatitis C virus, Fontan patients free from either of these risk factors begin developing liver disease as early as the teenage years.[30]

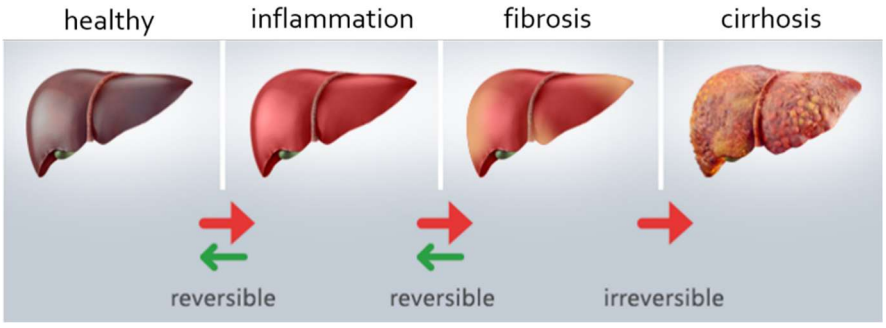

Figure 3-14 Progression of liver disease.

It is hypothesized that the elevated CVP and low CO inherent to the Fontan physiology lead to this early progression of liver disease.[15,32,33] The reason for elevated CVP and low CO in Fontan patients is illustrated in Figure 3-15. In a 2-ventricle circulation, the right ventricle provides the energy needed to move blood through the pulmonary circulation. This allows blood returning from the body to be at very low pressure (low central venous pressure). However, in the Fontan circulation with no right-sided pump, blood must move passively from the vena cava through the pulmonary circulation. This requires blood pressure upstream of the pulmonary arteries to be higher than the pulmonary arteries (high central venous pressure).

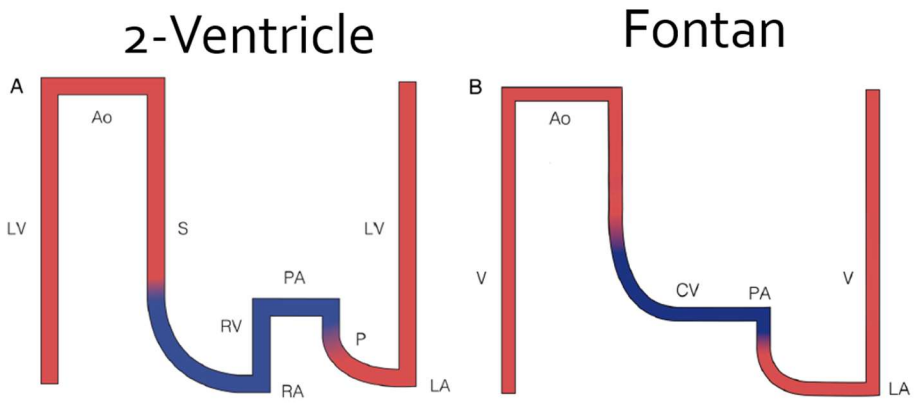

Figure 3-15 Relative pressure changes in 2-ventricle circulation (left) and Fontan circulation (right). LV: left ventricle, Ao: aorta, S: systemic circulation, RV: right ventricle, RA: right atrium, PA: pulmonary arteries, P: pulmonary circulation, LA: left atrium, LV: left ventricle.

A general consensus among experts is that "hepatic congestion" (high hepatic pressure and low flow through the liver) is the hemodynamic mechanism that leads to liver disease in Fontan patients.[22,34,35] Hepatic congestion can be a result of low cardiac output and elevated central venous pressure as previously mentioned, but may also be affected by the overburdened single ventricle, the TCPC, and high pulmonary vascular resistance. Potential solutions to this problem focus on reducing hepatic congestion.

3.6 Proposed Solutions

To address these two common modes of Fontan failure, clinicians are actively seeking and "trying out" potential solutions. Surgical planning and Y-graft use are hypothesized to improve hepatic flow distribution and therefore prevent/resolve PAVMs, and TCPC design optimization and mechanical circulatory support are hypothesized to delay/prevent the progression of Fontan associated liver disease. Though several of these "solutions" are currently being implemented clinically, their efficacy remains to be assessed. A description of the aforementioned proposed solutions for PAVMs and FALD is given below.

3.6.1 Surgical Planning (PAVMs)

Fontan surgical planning is an image-based, collaborative effort which is hypothesized to result in improved patient outcomes. The current surgical planning paradigm is a multi-step process that involves collaboration between clinicians and engineers. The major steps include preoperative image acquisition, image processing, creation of virtual surgical options, and numerical simulations of those proposed options (Figure 3-16).[11,36–38] Communication between clinicians and engineers is essential to verify segmented images, discuss the viability of surgical options and review simulation results. Overall, surgical planning is meant to analyze the performance of potential surgical options and therefore help inform the decision of graft type and positioning.

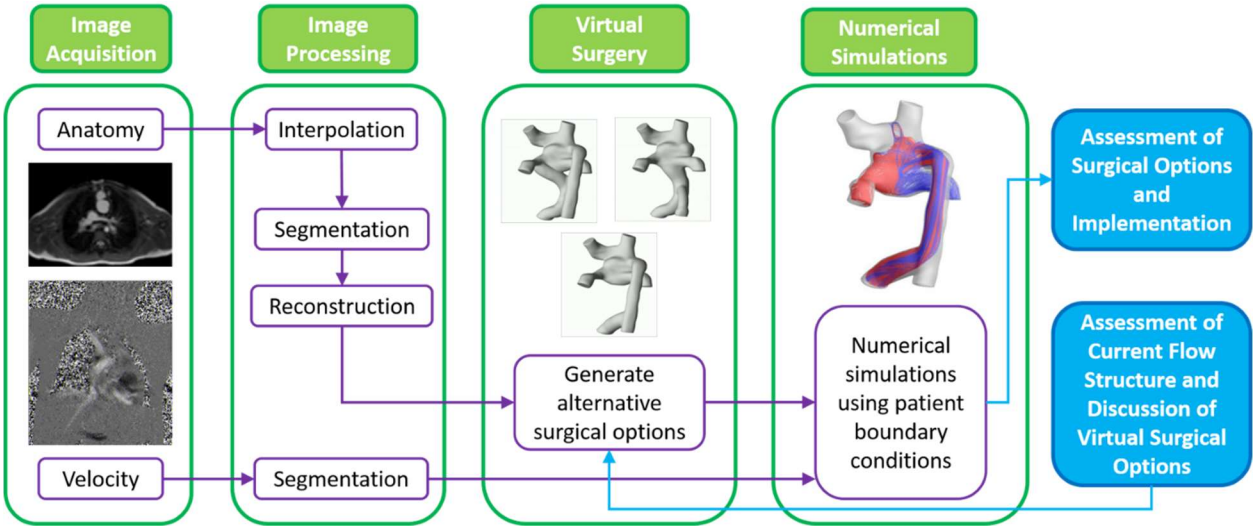

Figure 3-16 Surgical planning paradigm.

The data flow, order of events, and forms of data transfer between the clinical and engineering setting are shown in Figure 3-17. The only physical transfer of data from the clinical setting to engineering setting is the imaging data which begins the surgical planning process. Analyses including 3D reconstructions of the preoperative anatomy and proposed surgical options, as well as a final surgical planning report, are ultimately sent back to the clinic at the respective steps in the surgical planning process. Frequent communication between the two settings is important during the entire process, including segmentation, creation of realistic surgical options (requires the most clinical input), and review of comprehensive results.

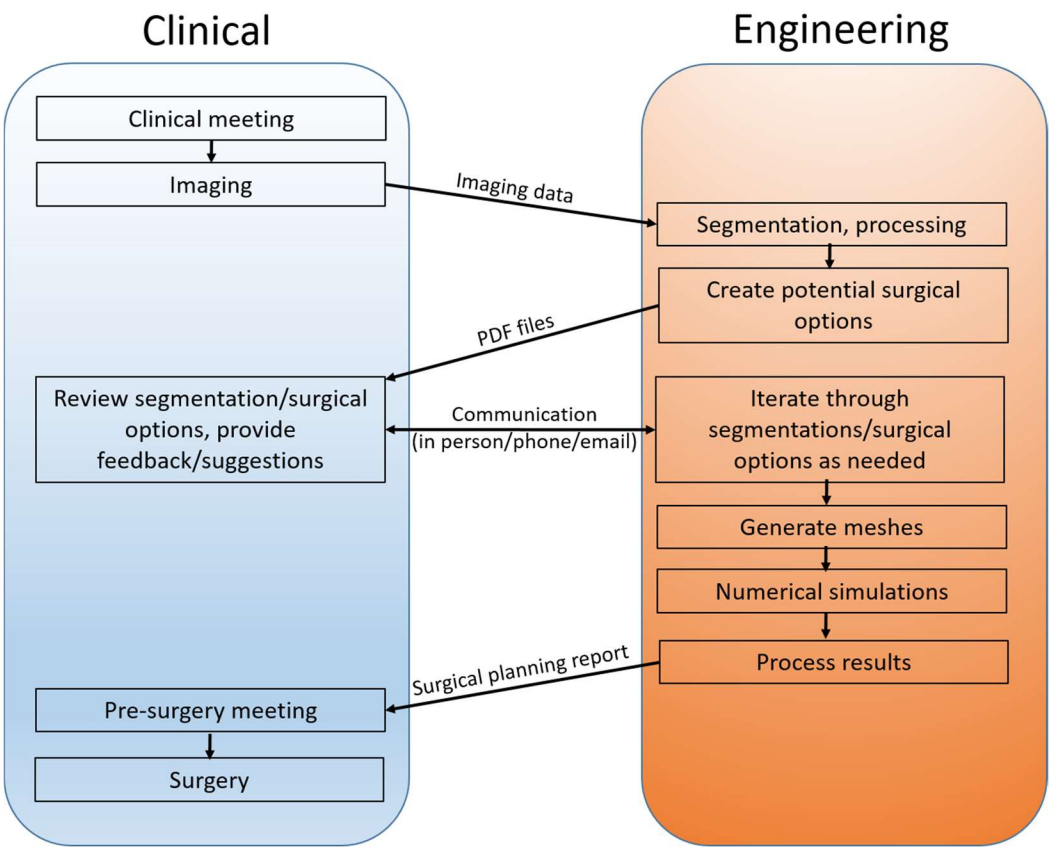

Figure 3-17 Interaction and types of data transfer between clinical and academic settings. Events are positioned chronologically from top to bottom.

A common motivation for Fontan surgical planning is the progression (or concern for progression) of pulmonary arteriovenous malformations (PAVMs). PAVMs are extremely rare in the average population (2/100,000), but are much more common in Fontan patients where a poorly designed total cavopulmonary connection (TCPC) may lead to unbalanced hepatic flow distribution (HFD), a known factor in PAVM formation/progression.[13,14,18,23,25–27] This type of surgical planning can involve both Fontan revision cases (a previous Fontan surgery resulted in PAVMs and therefore must be revised) as well as stage 2-3 cases (often performed on patients with more complex anatomies and hence the need for added insight to determine the best surgical

strategy). The goal to optimize patient outcomes has led to a variety of Fontan connections (Figure 3-18).

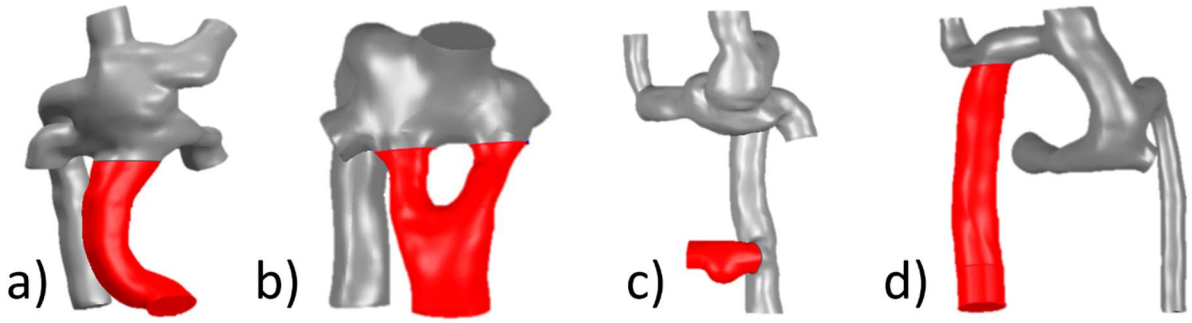

Figure 3-18 Representative post-operative anatomies including (a) standard extracardiac conduit, (b) Y-graft, (c) hepatic to azygous, and (d) hepatic to innominate vein Fontan connections. The graft is highlighted red.

Though limited to case studies and relatively short-term follow up data, several previous studies have provided a preliminary understanding of surgical planning prediction accuracy.[38] Sundareswaran et al published the first use of surgical planning to correct PAVMs (determined by an increase in oxygen saturation) in 2009.[28] Unfortunately, this single patient case report included no post-operative imaging data to compare the predicted and post-operative HFD. Haggerty et al provided the most thorough study to date which included only four patients with short follow up times (2 patients less than one month).[39] This study compared HFD and graft resistance and found "sufficient agreement" between the predicted and post-operative states. However, the use of steady flow conditions and fixed outlet flow splits, as well as the small sample size, limit the generalizability of these findings.

3.6.2 Y-grafts (PAVMs)

The use of Y-grafts for Fontan completion is a recent modification (2012) that is proposed to offer more balanced hepatic flow distribution, therefore preventing the formation of PAVMs (Figure 3-19). This option was motivated by intuition that directing hepatic flow through two Y-graft arms would encourage a more balanced HFD. Y-grafts are not specifically made for Fontan use, so these procedures use commercially available aorta-illiac grafts "off-label", and upside-down compared to their designed use. The diameter of the "trunk" of these grafts is divided in half for the two arms. For example, a 20mm Y-graft has a 20mm (diameter) trunk and two 10mm arms. A simple calculation reveals that these grafts have a 50% decrease in total cross-sectional area as blood moves from the trunk into the two Y-graft arms. Y-grafts are made of polytetrafluoroethylene (PTFE). One of the initial concerns about this option was the additional surgery time and sutures needed for 3 anastomosis locations rather than two.

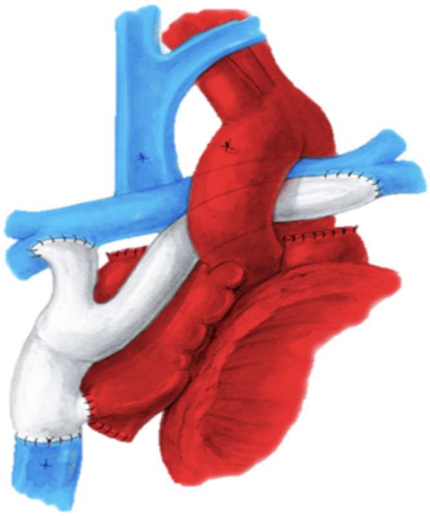

Figure 3-19 Y-graft for Fontan completion. Hepatic blood flow is directed towards the left and right pulmonary arteries via two Y-graft arms.

Y-graft use has been limited to several institutions including Children's Healthcare of Atlanta (CHOA), Children's Hospital of Philadelphia, Hospital for SickKids and University of

California San Francisco among others. There have been roughly 70 Y-graft Fontan cases to date, with ~50 of them performed by Dr. Kirk Kanter at CHOA. Our clinical collaboration with CHOA and Dr. Kanter have given us access this data.

Relatively few studies exist examining these patients as this is a new patient cohort with small numbers. A feasibility study was first published by Dr. Kanter addressing the intra-operative details as well as hospitalization times and general hemodynamics for six consecutive patients.[10] Several engineering studies then assessed energy losses and hepatic flow distribution in these patients.[40–42] Substantial effort was then directed towards optimizing Y-graft design to achieve better outcomes.[43,44] Each of these studies used a very small patients cohort ($n<6$) which limited the generalizability and statistical power of their analyses and results. Additionally, most studies were based on immediate post-operative imaging data which may not be representative of the patient's adapted state. Overall, due to the rarity of these patients, no studies exist with any substantial sized patient cohort or longer-term follow up data.

3.6.3 Improved Fontan Energetics (FALD)

In addition to the overburdened single ventricle in a Fontan patient, the total cavopulmonary connection constitutes a major bottleneck in the Fontan circulation.[22] It is hypothesized that the efficiency of the TCPC plays a major role in patient outcomes and that the TCPC is the limiting resistance in the Fontan circulatory system (Figure 3-20). Though pulmonary vascular resistance may be a major player is some cases, the interest in improving

Fontan energetics stems from the fact that TCPC design is something that can be controlled (to a point).

Figure 3-20 Simplistic representation of flow through several constrictions. Only the most severe constriction (c) will determine flow rate.

Importantly, the location of the liver with respect to the TCPC has generated much concern for the potential pressure build up and eventual hepatic congestion that could be caused by an inefficient TCPC. The liver is located immediately upstream of the TCPC, and therefore any increase in resistance of the TCPC would lead to an increased pressure in the liver. Therefore, the idea is that by decreasing TCPC resistance, the liver will experience a lower pressure and less hepatic congestion, hopefully leading to decreased liver disease. Figure 3-21 shows a simple illustration of this relationship.

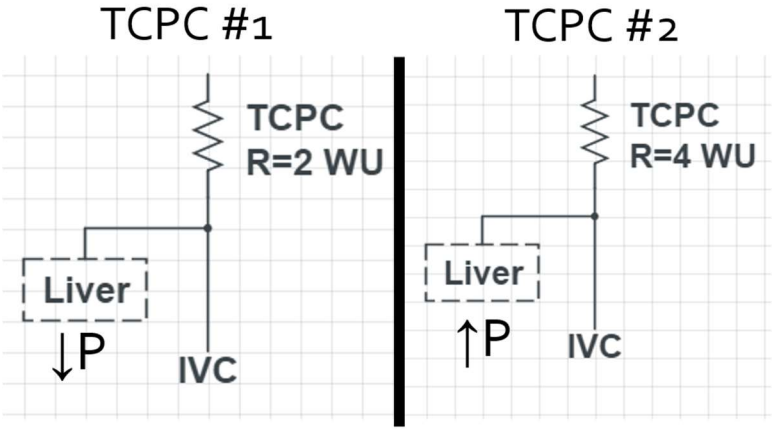

Figure 3-21 Simplistic comparison of the effect of TCPC resistance.

Fontan energetics have been the focus of numerous previous studies which sought solely to characterize the TCPC and determine important factors that influence energy efficiency.[45,46] Studies have also correlated TCPC energy loss with exercise performance in terms of minute oxygen consumption and work at anaerobic threshold.[47–50] Several current (unpublished) studies have investigated relationships between energy loss and patient outcomes including transplant, protein losing enteropathy, quality of life and death as endpoints.

An area left mostly untouched by these previous studies is the use of detailed cardiac magnetic resonance (CMR) derived flow dynamics and computational fluid dynamics (CFD) to assess and correlate local Fontan flows and energetics with liver fibrosis. Individual vessel flow rates could provide new information regarding factors not seen in previous studies using more global flow metrics. Additionally, investigating the energetics of the Fontan pathway and the TCPC may offer insights into surgical optimization and novel design as a method to potentially combat liver fibrosis.

3.6.4 Mechanical Circulatory Support (FALD)

The current methodology of Fontan palliation results in a one "pump" circulatory system with passive, non-pulsatile flow to the lungs. Inherent hemodynamic differences exist between a biventricular circulatory system and this modified physiology, including elevated central venous pressures (CVP) and insufficient cardiac output (CO), as well as a myriad of ventricular function, impedance and congestion issues.[12,16,22,32,51] As these patients survive into early adulthood, numerous long-term complications are common, with liver disease, protein losing enteropathy and plastic bronchitis among the most prevalent.[15,16,52–54]

In order to moderate these long-term problems, a circulatory correction rather than palliation is needed; and with a limited number of immediate heart transplants available, mechanical circulatory support (MCS) has become a potential option as a bridge to transplant therapy (Figure 3-22). However, the use of MCS in Fontan patients poses unique challenges including low preload and afterload, an absent upstream capacitance chamber, and potentially difficult anatomic implementation.[55]

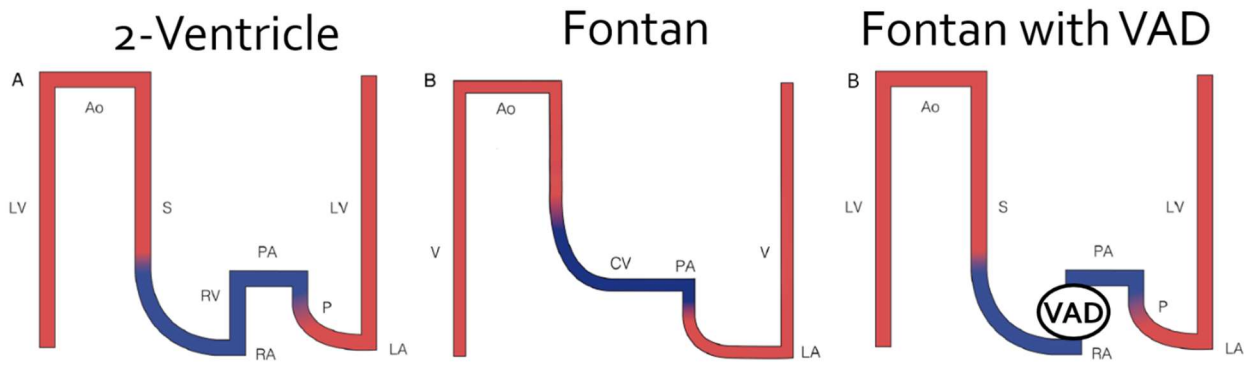

Figure 3-22 Relative pressure changes in 2-ventricle circulation (left), Fontan circulation (center, and Fontan with VAD (right). The VAD is positioned to replace to function of the right ventricle. LV: left ventricle, Ao: aorta, S: systemic circulation, RV: right ventricle, RA: right atrium, PA: pulmonary arteries, P: pulmonary circulation, LA: left atrium, LV: left ventricle.

The two approaches for Fontan MCS include (1) designing a new pump specifically for Fontan use, or (2) using an existing pump off-label with the hope that it can provide adequate support in an environment other than its intended use. Option 1 requires significant lead time for design iterations, testing, and regulatory approval with the hope that such development will provide an ideal Fontan MCS solution. On the other hand, option 2 trades the benefits of using a device specifically tailored for Fontan MCS for the immediate availability of existing pumps. Proponents of option 2 argue that Fontan patients are failing now, and the clinic cannot wait for the ideal solution to arrive.

A very limited number of studies exist that explore MCS use in the Fontan physiology, and even fewer studies exist that investigate either right-sided Fontan support or failing Fontan support. Weinstein et al. reported lower bridge-to-transplant/recovery success rates in single vs biventricular patients using the Berlin Heart EXCOR device.[56] In this study, only 3 of 5 patients with a total cavopulmonary connection (TCPC) were successfully supported. Niebler et al. presented a single case report showing successful ventricular support (148 days) using a HeartWare HVAD.[57] In terms of right-sided support (the focus of the present study), Rodefeld et al. reported a 6 hour MCS support in a Fontan animal model, Prêtre et al. demonstrated successful support (11 months) in a single patient using a Berlin Heart, and Tree et al. studied the Circulite device using a benchtop model.[58–60] These few studies constitute the majority of literature investigating right-sided support in a failing Fontan physiology. Clearly, further effort is needed to evaluate MCS devices in this scenario and potentially offer improved support for failing Fontan patients as a bridge-to-transplant.

3.7 Previous Fontan Hemodynamic Studies

In additional to those mentioned in the previous sections, numerous other studies have investigated Fontan hemodynamics from both a clinical and engineering standpoint. Three of the main areas of interest for these studies include TCPC characterization, exercise capacity and liver disease. The following sections will summarize some of the major findings in each of these areas.

3.7.1 TCPC characterization

A substantial amount of effort has been focused on characterizing the total cavopulmonary connection. This characterization includes the geometry, flow rates, and local hemodynamics, as well as the relationship between the three and how they change over time. Tang et al. performed a study including 108 Fontan patients with the goal of identifying important geometric characteristics that influence Fontan hemodynamics (indexed power loss and HFD in this study).[61] They investigated vessel diameter, connection angle, and distances between vessels among other parameters. Computational fluid dynamics were used to assess hemodynamics on each patient. They found that indexed power loss was inversely correlated with minimum Fontan pathway diameter, and left and right pulmonary artery diameters. Hepatic flow distribution was correlated with caval offset, pulmonary flow distribution and the angle between the Fontan pathway and superior vena cava. Though none of these correlations were very strong, they conclude that these findings have important implications on future connection design as well as a better understanding of what may cause unbalanced HFD and therefore PAVM formation.

Haggerty et al. similarly characterized TCPC hemodynamics in a large cohort (n=100) to provide reference values for future studies and quantify the variability between patients.[45] This study found that power loss varied by two orders of magnitude, and Fontan resistance was around 15-20% of published values of pulmonary vascular resistance in these patients. No differences were seen (in terms of power loss) between intra-atrial and extracardiac connections. Additionally, severe stenosis was seen to be the major determinant for the least efficient Fontan connections.

Other studies have used serial imaging data to quantify geometric and hemodynamic changes over time in Fontan patients. Restrepo et al. examined Fontan pathway growth in lateral tunnel and extracardiac connections.[62] Lateral tunnel connections were seen to increase in size over time (the heart wall is growing) while extracardiac connections did not (GoreTex cannot grow). In general, vessel sizes and growth over time were highly varied among patients. All flow rate (except SVC) increased proportionally to body surface area. In another study by the same group, although flow rates increased proportionally to body surface area, vessel diameters did not match somatic growth.[63] As a result, energy losses increased significantly with time.

In general, these studies effectively characterize the geometry, flow rates, growth and hemodynamics of the TCPC. The main limitation in these studies, from a translational standpoint, is the lack of association with patient outcomes. Due to data availability this may have not been possible. These studies were an important first step in understanding the makeup of the Fontan population and describing the fluid dynamics within the TCPC.

3.7.2 Exercise capacity

Exercise capacity has been an area of interest in the Fontan population for a number of years. This has been used as a measure of a patient's ability to sustain a normal activity level as

well as participate in more vigorous activities. A plethora of studies have been devoted to this topic.

Cheng et al. quantified vessel flow rates in Fontan patients both at rest and at exercise, finding that all flow rates increased (as expected).[64] Additionally, the LPA/RPA flow ratio was consistent between rest and exercise, suggesting that blood flow distribution is dominated by distal pulmonary resistance. In this cohort of patients, IVC/SVC flow split was 50/50% at rest. During exercise, the IVC flow rate increased by approximately 3x while the SVC flow rate remained constant. Several studies have also found that heart rate, cardiac output and stroke volume are sub-normal during exercise after the Fontan procedure.[65,66] However, exercise tolerance was found to be approved post-Fontan compared with pre-Fontan, with arterial oxygen saturation, respiratory rate, minute ventilation etc. all improving.

Using serial data, Giardini et al. found that exercise capacity progressively declines in Fontan patients.[67] Ventricular morphology and type of Fontan operation were the only significant predictors of the rate of deterioration. Gewillig et al. found no limitations in heart rate, afterload or contractility in Fontan patients, and reason that poor ventricular filling is the cause of diminished exercise performance.[51] Others have further studied the effects of vena cava flow and ventricular function on exercise tolerance, as well as prognostic implications, and comparisons with the resting state and normal population.[68–70]

In terms of engineering analysis, Khiabani et al. found that exercise capacity in single ventricle patient after Fontan correlates with energy loss in the TCPC.[50] A significant, negative correlation was seen between indexed power loss at exercise and minute oxygen consumption and work at anaerobic threshold. Indexed power loss was seen to increase at an exponential rate during exercise. Similarly, Whitehead et al. showed that power loss increases in a non-linear manner as

activity level increases.[49] Some opponents to these engineering studies claim that local energy losses in the TCPC are much less important than more global metrics and heart function parameters, but the relative importance of these factors remains to be seen.

3.7.3 Fontan associated liver disease

As Fontan associated liver disease has become a well-recognized problem in this population, a number of clinical studies have investigated its causes. Asrani et al. summarize the relationship between congenital heart disease and the liver and suggest that chronic, passive venous congestion and decreased cardiac output may promote hepatic complications.[53] They also suggest that hepatic complications are in part related to time since the Fontan procedure and that the need for early cardiac transplantation and optimized management of the disease are imperative. A number of studies have stressed that liver disease is universal in the Fontan population.[30,34] These studies found varying levels in hepatic abnormalities in all Fontan patients, regardless of time since Fontan procedure.

Others have described the "precarious" state of the liver after the Fontan operation.[15,17,22] These studies again refer to diminished cardiac output and chronically elevated central venous pressure as potential culprits, and suggest that liver insult may occur at each level of the staged palliative operations. Importantly, groups are working towards improved, non-invasive methods to quantify liver fibrosis using elastography, imaging and biomarkers.[71,72] Liver biopsies are currently the gold standard, but suffer from sampling error and invasiveness. Other methods may offer an improved "global" view of the state of the liver and encourage increased monitoring. Currently, no engineering studies exist investigating the relationship between detailed fluid

mechanics of the TCPC and the extent of liver disease. Whether TCPC design/efficiency is a major factor in the progression of liver disease is currently unknown.

3.8 Study Significance

Within the last several years, experts have stated that "…it is reasonable to conclude that freedom from morbidity [for Fontan patients] is likely close to zero" and that Fontan patients are "doomed to a circulatory failure."[17,59] PAVMs are often the cause for Fontan revision surgeries and FALD has been termed a "universal" disease in Fontan patients.[28,30] Clinicians are actively looking for solutions to these problems.

As many as 25% of Fontan patients will develop clinically significant PAVMs with increasing cyanosis.[23] The prevention of PAVMs can substantially improve the quality of life for Fontan patients. Additionally, for patients who currently have PAVMs, the use of surgical planning to revise the Fontan connection and resolve the PAVMs may substantially reverse this morbidity.[28,29]

In relation to FALD, it is highly unlikely that a Fontan patient with liver disease will ever receive a heart transplant.[73] Therefore, knowing when and how to intervene is a significant and challenging question. The proposed work is aimed at building healthier lives for Fontan patients by preventing the progression of cardiovascular related liver disease. This not only addresses Fontan associated liver disease, but would also increase the likelihood of Fontan heart transplantation. Lifelong health for these patients is dependent upon preventing long term

complications. The purpose of testing currently available VADs is to potentially offer immediate support for failing Fontan patients, before long term complications progress.

4. METHODS

4.1 Medical Image Processing

4.1.1 Image Acquisition

All CMRs were performed at either the Children's Hospital of Philadelphia or Children's Healthcare of Atlanta with Siemens 1.5 T magnetic resonance imaging systems (Siemens Medical Solutions, Malvern PA). Patients were scanned supine, head first in the scanner with ECG leads placed under a breath-held protocol. After localizers were obtained, a stack of contiguous, static, diastolic steady state free precession (SSFP) images were obtained from the diaphragm to thoracic inlet to assess anatomy and provide inputs for CFD modeling. Slice thickness was generally 1-5 mm and in plane resolution was 1.2x1.2 mm.

Through plane, retrospectively gated, phase contrast magnetic resonance (PC-MRI) was used to assess flows in the cavae, branch pulmonary arteries, pulmonary veins and across the aortic valve. IVC flow was measured supra-hepatic. The location of these planes in relation to the TCPC for one representative patient is shown in Figure 4-1. Velocity encoding (VENC) was generally 150 cm/sec for the aorta and 60 cm/sec for the other vessels. Slice thickness was generally 4-5 mm with in plane resolution of 1.25x1.25 mm. The number of phases was a function of the heart rate and ranged from 20-30.

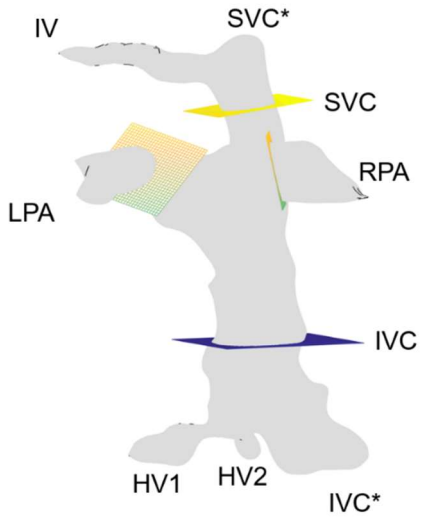

Figure 4-1 Location of PC-MRI planes for blood flow velocity measurement for a representative patient.

Global ventricular function was calculated from cine images of the ventricular short axis. Endocardial and epicardial borders were semi-automatically traced and ventricular volumes were determined by multiplying the slice thickness with the segmented area. Slice volume was integrated along the ventricular longitudinal axis using Simpson's rule to extract the total volume of the ventricle in a cardiac phase. This method was applied at end diastole and end systole to calculate end-diastolic volume (EDV) and end-systolic volume (ESV) respectively. Stroke Volume (SV) and ejection fraction (EF) were calculated as the EDV-ESV and SV/EDV respectively.

4.1.2 Anatomy Segmentation

Patient specific anatomies were reconstructed from CMR images. For convenience, images were often re-oriented to give axial images for segmentation. Images were then loaded into an open-source segmentation software, InVesalius or ITK-Snap, both of which have been validated for medical image reconstruction.[74–77] In either software, various levels of automation can be used

to assist with segmenting the TCPC. Due to the high degree of variability among Fontan anatomies, fully automatic segmentation (and even semi-automatic in some cases) has been unfruitful, requiring manual segmentation. In either case, the TCPC is segmented from the IVC at the level of the diaphragm up to the innominate vein on the SVC. Pulmonary arteries are segmented until a branching point. The segmented anatomy was outputted as a .stl file for further processing in Geomagic.

4.1.3 Blood waveform segmentation

Blood flow waveforms for all vessels of interest were reconstructed from PC-MRI images to provide boundary conditions for modeling purposes. These vessels include the IVC, SVC, LPA, RPA, LSVC and AZ as appropriate. An open-source software (Segment, http://segment.heiberg.se) was used to segment the blood flow waveforms for all patients. Segment provides a straightforward and user friendly workflow for segmentation, and offers a wide variety of functionality including automatic region of interest refining and propagation, vessel tracking throughout the cardiac cycle, automatic parameter calculation and 3D velocity profile segmentation among others.[77,78] To segment a blood flow waveform, a contour was drawn around the vessel of interest and propagated throughout all phases in the cardiac cycle (typically 20-30). Segment then calculated the flow rate at each phase by spatially registering the magnitude and directionality information of each pixel and computing the total flow rate within the specified contour. These data were outputted as a matrix with variables including time and flow rate among others.

4.2 Computational Fluid Dynamics

A general methodology overview of patient specific CFD simulations can be seen below in Figure 4-2 .[11]

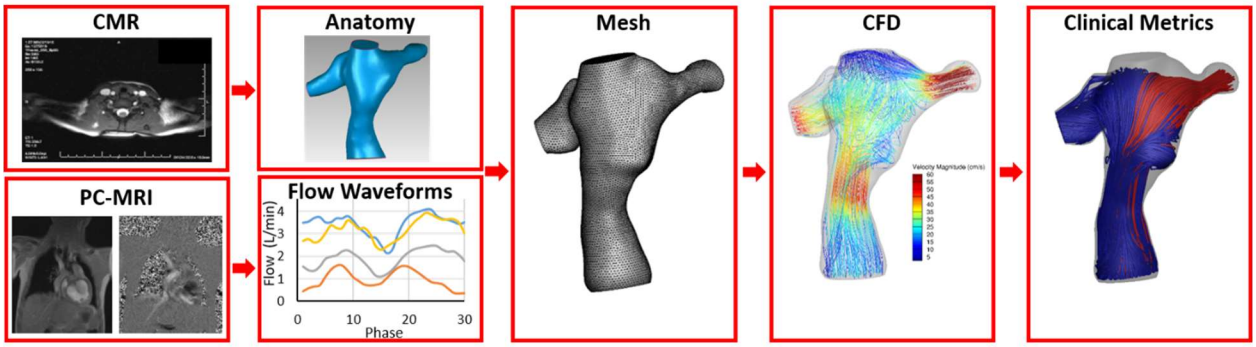

Figure 4-2 General process for patient-specific CFD simulations.

4.2.1 Mesh Generation

The step by step process for mesh generation can be found in Appendix 0. In general, a polyhedral mesh of approximately $D_{IVC}/20$ mm elements was used in order to achieve mesh independent results, where D_{IVC} is the diameter of the IVC.[79] Mesh sizing was varied across the model and flow extensions in order to create a high-quality mesh with as few elements as possible. An inflation layer was used to capture near wall velocity and pressure gradients. ANSYS Workbench was used to add flow extensions, control meshing parameters and check mesh quality as detailed in Section 0

.

4.2.2 Blood waveform processing

The blood flow waveforms segmented from the phase contrast CMR data must be processed before implementing as boundary conditions in a CFD simulation. This is the case because of errors associated with medical imaging. For example, in the case of the TCPC, the flow

rate of the inlets (IVC and SVC) must be equal to the flow rates of the outlets (LPA and RPA) over a cardiac cycle (conservation of mass). However, this is never the case. It is common for inlets and outlets to be around 20% different in magnitude. To account for this, it is common practice to scale the outlet waveforms (while maintaining the LPA/RPA flow ratio at each time point) in order the match the inlet flow magnitude and achieve conservation of mass. The outlets are scaled (rather than the inlets) because clinical experience has shown that measuring flow rates from the larger vessels (IVC and SVC) are more accurate. Clinicians ensure that trusting the LPA/RPA ratio is accurate because similar errors may occur in each vessel. After scaling the outlet waveforms appropriately, a fast Fourier transform is then used to create a repeatable waveform that can be used in simulations. The top 30 frequency components were used for waveform modeling to allow for a well-fitted curve (r^2=0.999). A custom MATLAB script for scaling and creating the FFT waveform can be found in Appendix 0.

4.2.3 Simulation Parameters

A step by step guide to simulation set-up, including the various fluid and solver parameters (fluid properties, convergence criteria, number of time steps etc.) can be found in Appendix 0. All simulations were performed using ANSYS Fluent (Release 17.0) which is a finite volume pressure-based Navier-Stokes solver. Blood was modeled as a single-phase Newtonian fluid (μ=0.04 g/(cm·s), ρ=1.06 g/cm^3). Patient specific blood flow waveforms extracted from PC-MRI were used as boundary conditions for each TCPC inlet and outlet. Twenty cardiac cycles were simulated to overcome transition effects and achieve period stability, using the final cycle for data

analysis. All simulations assumed rigid walls and employed flow extensions to develop velocity profiles.

4.2.4 Flow field visualization

Tecplot 360 (2013, Release 1) was used for flow visualization using the output of CFD simulations. Fluent outputs including a case and data file (.dat files) were opened in Tecplot. Slices were taken at desired locations from which streamlines were created. The velocity information at each data point was used to produce flow field animations, streamtraces and streamlines as needed. Various built in Tecplot functions were used to visualize velocity and pressure contours. Streamlines were exported for analysis in MATLAB. A custom MATLAB script and Tecplot macro were used to color streamlines by outlet. This procedure and associated codes can be found in Appendix 0.

4.3 In vitro modeling

4.3.1 Experimental loop design

An overall schematic of the in vitro Fontan circulatory loop is shown in Figure 4-3. A programmable piston pump (Vivitro SuperPump, Model SPL 39891; Vivitro Systems Inc, Victoria, British Columbia) powered the loop, representing the single systemic ventricle (70 bpm), with a bileaflet mechanical heart valve (BMHV) on either side representing the atrioventricular and aortic valves. Compliance chambers and ball valves were used to model aortic and systemic compliance and resistance respectively. All pathways were designed as 3-element Windkessel models, employing a resistance-compliance-resistance circuit (only one resistance shown in Figure 4-3 for clarity). Pressures and flows were recorded at each of the TCPC vessels.

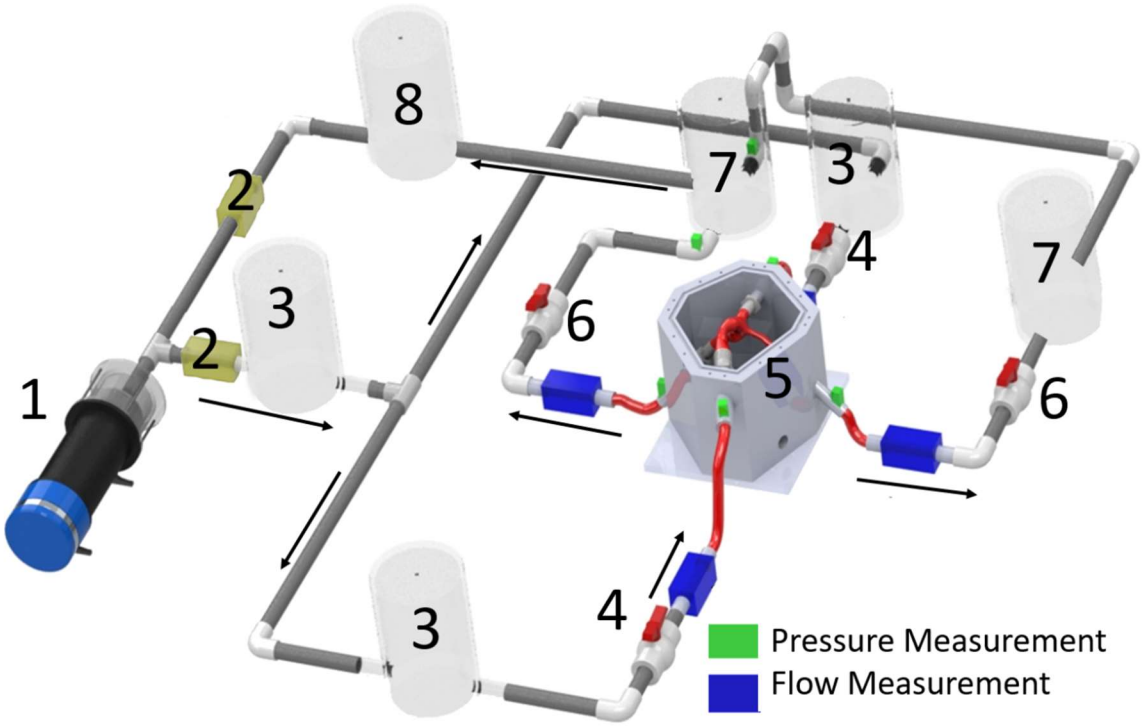

Figure 4-3 Fontan in vitro loop design. Schematic of in vitro Fontan circulatory loop with labeled components: (1) programmable piston pump (single ventricle), (2) bileaflet mechanical heart valves, (3) aortic and system compliance chambers, (4) systemic resistance, (5) patient-specific total cavopulmonary connection, (6) pulmonary resistance, (7) pulmonary compliance chambers, (8) single atrium compliance chamber.

Blood was modeled with a 36%/74% glycerin-saline solution (by volume) with 3.47 cSt kinematic viscosity. The in vitro loop employed a patient-specific, flexible total cavopulmonary connection (TCPC) anatomy reconstructed from magnetic resonance imaging with institutional review board (IRB) approval (H09279). The TCPC model was constructed of transparent silicone with a patient-specific matched bulk compliance (1.36 mL/mmHg).[80] The model walls were 1.4±0.1 mm thick and constructed of a shore 30A hardness flexibile silicone material that was dip molded to the segmented patient specific geometry.

A National Instruments data acquisition (DAQ) system and custom LabVIEW virtual instrument were used to control the piston pump and record pressure and flow measurements (see

section 0). Data were collected for 4 flow rates (IVC, SVC, LPA, RPA) and 6 pressures (IVC, SVC, LPA, RPA, single atrium, single ventricle). The custom LabVIEW virtual instrument controlled the system and allowed the investigator to acquire, calibrate, and display all 16 analog input voltage signals. Acquisition sampling frequency was adjustable, and the incoming signals were used in the real-time calculation of several important verification parameters: signal mean, signal maximum, and signal minimum. The time period over which each of these parameters was calculated was set independent of the sampling frequency. This allowed for cyclic averages during pulsatile experimental conditions. These parameters could be calculated on multiple signals simultaneously, which allowed for additional flow pulsatility and resistance verification.

4.3.2 Data collection

Flow probes and pressure transducers were positioned at every TCPC inlet and outlet as shown in Figure 4-3. Pressure relative to atmospheric pressure was measured via fluid-filled strain gauge pressure transducers (Model 6199; Utah Medical Products Inc., Midvale, UT). The pressure transducers had a measurement range of -50 to 300 mmHg and a sensitivity of 5 μV/V/mmHg, or ± 2 %. The pressure transducer excitation voltage and signal amplification was provided by a custom-built signal conditioning box constructed by the Georgia Tech Mechanical Engineering Electronics Lab. Signal output from the conditioning box was read by LabVIEW.

Flow rates were measured with 3 in-line and 1 clamp-on ultrasonic flow probes (Transonic Systems, Ithaca, NY). The 3 in-line flow measurements were performed with model 10PXN probes. The clamp-on measurement was with a model 8PXL probe. The flow probes utilized the Doppler effect to measure the flow at a frequency of 1.2 MHz. The flow signal from each probe was sent to a TS410 tubing flow module housed within a T402 multi-channel research console.

The research console applied a low pass filter at 100 Hz to each signal before the signal was read by LabVIEW. All flow probes had a resolution of 0.01 L/min.

4.3.3 Experimental parameters

Baseline failing Fontan conditions will first be established in each experiment. Baseline failing Fontan conditions were defined as a cardiac output (CO) of 3.5 L/min with Fontan pressures near 15-20 mmHg. The inferior and superior vena cava (IVC and SVC) and left and right pulmonary artery (LPA and RPA) flow splits were set to 60/40 and 50/50 respectively. Identical baseline conditions were used for all tested devices. Device parameters including flow rate, frequency, and filling/ejection times were investigated.

4.3.3.1 Cannula and baffle restriction strategies

Multiple cannula and baffle restriction strategies were tested including placing the VAD (1) in parallel with the Fontan baffle (inflow placed in the IVC near the diaphragm and egress located at the LPA/RPA confluence, Figure 4-4a), (2) in series with the Fontan baffle (same cannulation as (1) with baffle completely restricted, Figure 4-4c), and (3) performing a Fontan "takedown" and using the VAD as a true (albeit extracorporeal) right ventricle.

Additionally, in an attempt to reduce potential recirculation, a Y-graft outflow cannula (inserting downstream in each pulmonary artery, Figure 4-4b) was tested in series and in parallel. The main difference between scenario 2 and 3 is that SVC flow can move directly into the LPA/RPA in scenario 2, therefore it is not a complete Fontan "takedown." In scenario 3, all IVC/SVC flow must pass through the assist device before entering the pulmonary circulation. To experimentally achieve scenario 3, the pulmonary arteries were separated from the IVC/SVC using

two clamps (Figure 4-4d). In addition to these 3 scenarios, various levels of baffle restriction (0-100%) were explored in the "in parallel" configuration. A schematic of the TCPC and VAD with vessels and cannula labeled is shown in Figure 4-4e. Outflow cannula will vary based on cannulation strategy.

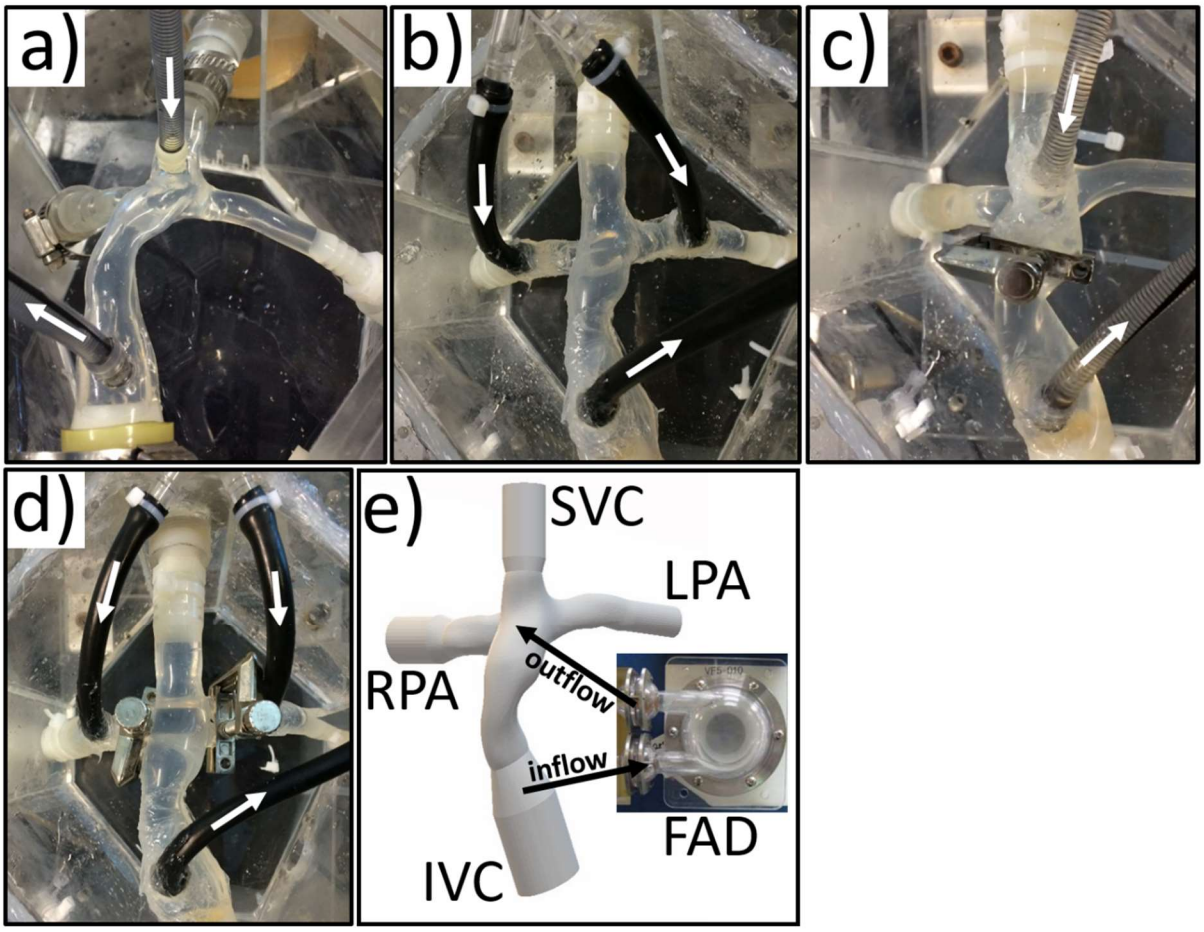

Figure 4-4 Cannulation strategies. (a) Fontan assist device (VAD) in parallel with single outflow cannula. (b) VAD in parallel with Y-graft outflow cannula. (c) VAD in series (complete Fontan baffle restriction). (d) Fontan takedown configuration (vena cava separated from pulmonary arteries). (e) Schematic of total cavopulmonary connection and VAD with vessels and cannula labeled. Outflow cannula will vary based on cannulation strategy.

4.3.3.2 Banding designs

A further investigation was performed looking into the effect of Fontan baffle banding design on hemodynamics. This was undertaken after realizing that complete baffle restriction was needed for certain devices. Five banding designs were 3D printed for testing. Each band was designed to theoretically produce the same resistance to flow. A description in shown in Figure 4-5.

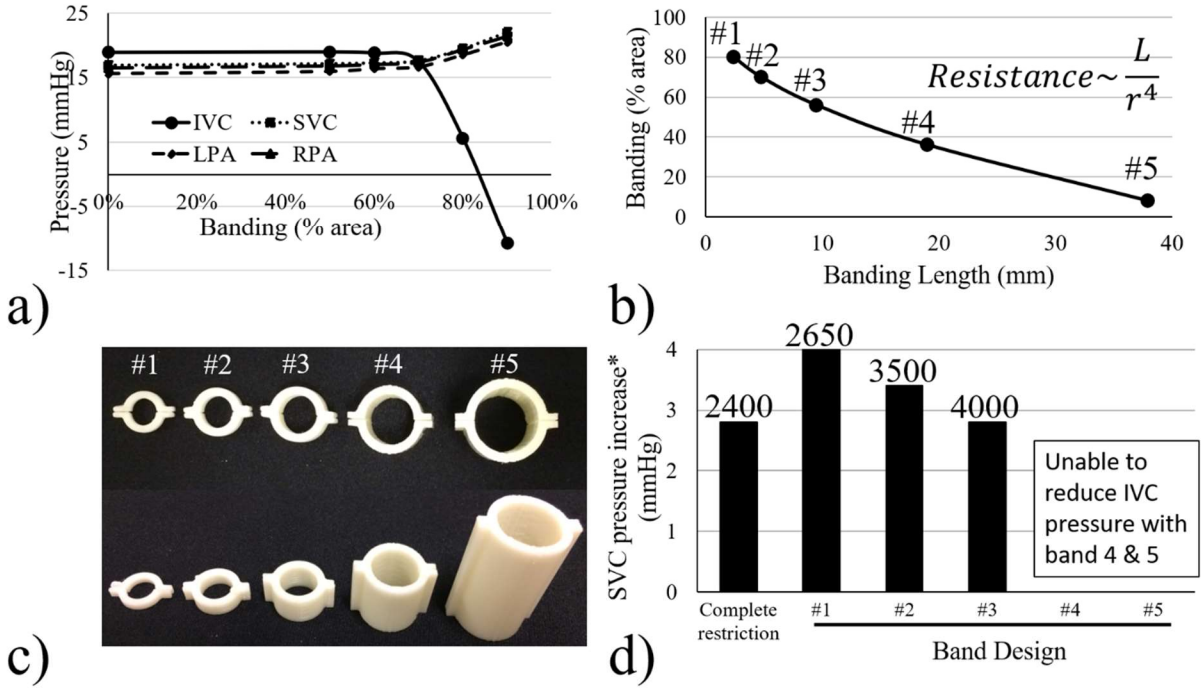

Figure 4-5 Effect of banding design on hemodynamics. (a) Effect of banding on pressure; (b) Theoretical relationship between banding length (L) and area to maintain resistance (r=radius); (c) Top and side views of the five custom banding designs; (d) Effect of banding design on SVC pressure (VAD rpms labeled above each bar). Banding is calculated as percent constriction by area. All points on the curve in (b) theoretically offer the same resistance. The asterisk in (d) indicates that SVC pressure increase was measured at the point when IVC pressure was reduced by 10 mmHg.

4.3.4 Mechanical circulatory support

Four mechanical circulatory support devices will be assessed in this thesis. Each device will be tested as a Fontan assist device (VAD), where the inflow cannula will be attached to the IVC and the outflow cannula will insert into the center of the TCPC junction. Various configurations will be tested and described in further detail in Chapter 8. For use as a Fontan assist device, each of these devices must be used "off-label." A description of each device is given in the following sections.

The two approaches for Fontan MCS include (1) designing a new pump specifically for Fontan use, or (2) using an existing pump off-label with the hope that it can provide adequate support in an environment other than its intended use. Option 1 requires significant lead time for design iterations, testing, and regulatory approval with the hope that such development will provide an ideal Fontan MCS solution. On the other hand, option 2 trades the benefits of using a device specifically tailored for Fontan MCS for the immediate availability of existing pumps. In this thesis, we are using the second approach and testing devices "off-label" with the goal of determining which devices may be able to provide immediate support to these patients.

4.3.4.1 CircuLite

The Circulite (Medtronic, Minneapolis, MN) device is a small, implantable ventricular support system (Figure 4-6). The device prides itself on requiring only a minimally invasive procedure for implantation. Circulite is designed for patients with chronic heart failure. The pump can provide up to 4.24 L/min of blood flow under the pressure conditions of the left ventricle in

heart failure. The device is meant to supplement the heart's cardiac output and not completely replace the function of the left ventricle. Circulite is controlled and powered by a wearable external controller and battery pack connected via a percutaneous lead.

Figure 4-6 Circulite ventricular assist device.

4.3.4.2 VENTRIFLO™ True Pulse Pump

The VENTRIFLO™ (Design Mentor, Pelham, NH) True Pulse Pump system is an extracorporeal blood pump that produces pulsatile blood flow using a flexible membrane as its key enabling technology (Figure 4-7). This device is designed for cardiopulmonary bypass, but it very tunable which may lend itself to "off-label" uses. The pump driver incorporates an electromagnetic linear motor with a suspended magnet between the motor coils, providing unique pressure sensitivity with automatic stroke volume adjustment for a given motor current and vasculature pressure.[81] Cadence, stroke strength and cycle timing of the pump are defined by the user. VENTRIFLO™ employs one-way ball valves on either side of the pump to ensure unidirectional flow. This device champions the importance of providing biomimetic, pulsatile flow.

Figure 4-7 VENTRIFLO™ True Pulse Pump.

4.3.4.3 PediMag

The Pedimag (Abbott (Thoratec), Pleasanton, CA) device is an extracorporeal circulatory support device used to stabilize patients in need of cardiopulmonary assistance (Figure 4-8). Pedimag is currently approved for clinical use up to six hours, as a short-term solution while surgical/long-term circulatory support decisions can be made. This device uses a magnetically levitated pump impeller which is hypothesized to reduce hemolysis issues.[82] Under left ventricle pressures, Pedimag is rated to output up to 1.5 L/min. The entire pump system is made to be transportable.

Figure 4-8 PediMag ventricular assist device.

4.3.4.4 CentriMag

The Centrimag (Abbott (Thoratec), Pleasanton, CA) device is a "scaled-up" version of the Pedimag device (Figure 4-9). Centrimag uses the magnetically driven pump impellar technology as the Pedimag device. CentriMag is currently approved for use as a right ventricle assist device for up to 30 days in patients in cardiogenic shock due to acute right ventricular failure. The Centrimag and Pedimag pumps use identical hardware. CentrMag is more powerful than the smaller PediMag device, and can deliver 9.9 L/min under left cardiac failure conditions.[83]

Figure 4-9 CentriMag ventricular assist device.

4.4 Data Analysis

4.4.1 Anatomy characterization

Vascular modeling toolkit (VMTK) was used to characterize patient specific anatomies. A detailed protocol can be found in Appendix 0. Parameters including average, minimum and

maximum vessel diameters, centerlines, and stenosis were calculated. Overall PA stenosis was defined using the following equation:

$$Overall\ PA\ Stenosis\ \% = 100\left(\frac{A_{min,LPA} + A_{min,RPA}}{A_{avg,LPA} + A_{avg,RPA}}\right)$$

where $A_{min,LPA}$ and $A_{min,RPA}$ are the minimum cross-sectional areas of the LPA and RPA, and $A_{avg,LPA}$ and $A_{avg,RPA}$ are the average cross-sectional areas of the LPA and RPA. A combined outlet stenosis value was used in place of unilateral PA stenosis measurements to give a more accurate representation of the total outlet obstruction to flow and allow a better comparison between patients. Additionally, IVCs and SVCs showed negligible percent stenosis and therefore were not included in this calculation.

4.4.2 Hepatic flow distribution

Hepatic flow distribution was quantified by seeding massless particles at the IVC and calculating the total flux of particles leaving the left and right pulmonary arteries. Hepatic flow distribution is defined as $HFD = \frac{\theta_{LPA}}{\theta_{LPA}+\theta_{RPA}}$ where θ is the total flux of particles throughout a cardiac cycle. The error in HFD prediction is defined as:

$$HFD_{Prediction\ Error} = \left|HFD_{post-op} - HFD_{predicted}\right|$$

HFD will also be discussed in terms of "HFD deviation from 50%", and an even (50/50) split of hepatic flow to the LPA and RPA is assumed as ideal. This convention gives a "0" HFD deviation for balanced HFD cases, and an HFD deviation of 50 for extreme cases (all hepatic flow to either the LPA and RPA. HFD deviation is calculated as:

$$HFD\ Deviation\ from\ 50\% = |HFD - 50|$$

4.4.3 Energy loss

Calculations were performed to compute several TCPC efficiency related metrics including power loss (PL), indexed power loss (iPL) and TCPC resistance. The TCPC is thought to be a major "bottleneck" of the single ventricle circulatory system, and these metrics quantify how inefficient this connection is. Power loss was calculated from a simplified control volume approach as follows:

$$PL = \sum_{inlets} \int_A \left(p + \frac{1}{2}\rho v^2\right) v \cdot dA - \sum_{outlets} \int_A \left(p + \frac{1}{2}\rho v^2\right) v \cdot dA$$

where p is the static pressure, ρ is the blood density, A is the area of the inlet/outlet and v the velocity at the respective inlets or outlets. Power loss was calculated at every millisecond throughout the cardiac cycle and then averaged to obtain an overall PL value. Power loss was indexed (iPL) as $\left(\frac{PL}{\rho Q_s^3/BSA^2}\right)$ and a TCPC resistance was calculated $\left(\frac{\Delta P_{TCPC}}{Q_s}\right)$ where Q_s is the systemic venous flow ($L \cdot min^{-1}$), BSA is body surface area (m^2), ΔP_{TCPC} is the pressure drop across the TCPC and ρ is blood density ($kg \cdot m^{-3}$).[84] A custom post-processing MATLAB code was used to calculate these variables and check their convergence over multiple cardiac cycles. Results changing less than 5% between cardiac cycles were defined as converged. This code with details is included in Appendix 0.

4.4.4 Additional metrics

Several additional metrics were calculated including pulmonary flow distribution (PFD), aortic to pulmonary collateral flow, particle residence time (PRT) and pulsatility index (PI). PFD was calculated as $PFD = \frac{Q_{LPA}}{Q_{LPA}+Q_{RPA}}$ where Q is flow rate. Collateral flow was calculated as the difference between aortic and vena cava flow: $Collateral\ flow = Q_{AO} - Q_{IVC} - Q_{SVC}$. This is

an important clinical metric which describes how much of the cardiac output is bypassing the TCPC. Particle residence time was calculated from CFD results by recording the amount of time required for 95% of all seeded particles to exit the TCPC domain. Pulsatility index was defined as follows:

$$PI = \frac{Q_{max} - Q_{min}}{2 * Q_{avg}}$$

where Q_{max}, Q_{min}, and Q_{avg} are the maximum, minimum and average flow rates during the cardiac cycle, respectively, as determined from the phase contrast CMR data. In general, the Fontan circulatory system is much less pulsatile than a normal, biventricular system. Pulsatility is thought to affect mechanotransduction and therefore may affect a number of biological processes potentially leading to diseased conditions in the single ventricle patient.

4.5 Statistical Analysis

SPSS (IBM Corp., Version 24, Armonk, NY) was used for statistical analyses. The Shapiro-Wilk test was used to determine normality for each parameter. Pearson's and Spearman's correlations were used to investigate bivariate correlations for parametric and nonparametric data respectively. For SA 2A, data was also binned into tertiles or quartiles based on liver score for further analysis. Depending on normality, either a Wilcoxon rank sum test or an independent sample t-test was used to test for equal medians between groups.

For data with serial timepoints, a paired-sample t-test or Wilcoxon signed-rank test was used to investigate differences between timepoints. A multiple regression analysis, using the forward stepping method, was used to investigate if a combination of several parameters were predictive of another parameter. The DFBETA test and Grubb's test were used to determine and remove

overly influential data points and outliers respectively. To account for multiple comparisons in the liver studies, a more stringent significance level of $\alpha=0.01$ was chosen to account for multiple testing. Standard descriptive statistics were calculated for all metrics. In most cases, statistical significance was determined using $p<0.05$ (except when correcting for multiple comparisons). Values are shown as average ± standard deviation [range]. Power analyses (G*Power, version 3.1.9.2) were used to determine the required effect size needed for statistical significance at a given sample size.

4.6 Institutional Review Board

All patient data incorporated in this thesis were collected, shared and used under appropriate approval of each center's institutional review boards ensuring the ethical treatment of human subject data. The respective IRB approval identification numbers are given below:

Table 4-1 List of IRB approvlas for the patient data used in this thesis.

Data (SA #)	IRB approval #
Surgical planning (SA 1A)	H09279, H17434
Y-grafts (SA 1B)	H14005
Comparison patients (SA 1B)	H05236
Liver study (SA 2A)	H17229
Models for VAD testing (SA 2B)	H05236

5. SPECIFIC AIM 1A

Purpose: To evaluate the accuracy of surgical planning to predict post-operative hepatic flow distribution and resolve pulmonary arteriovenous malformations.

Hypothesis: Surgical planning can accurately predict post-operative hepatic flow distribution.

5.1 Overview

While surgical planning has been used in a number of previous studies, no conclusive evidence or long-term follow up data exists showing whether surgical planning was accurate or beneficial. Specific Aim 1A will use patient-specific, computational fluid dynamic (CFD) modeling to analyze the accuracy of surgical planning predictions of hepatic flow distribution (HFD), a known factor in pulmonary arteriovenous malformation (PAVM) progression. This aim will include all patients in the Georgia Tech Fontan database who were enrolled in a prospective surgical planning protocol before surgery. This included both Fontan revisions (n=5) as well as Stage 2-3 surgeries (n=7). Pre- and post-operative MRI and clinical data exist for each patient. Predicted results will be compared with long-term follow up data to determine if surgical planning was effective in predicting HFD.

5.2 Methods

This Specific Aim utilizes medical image processing, computational fluid dynamics, anatomy characterization and statistical analysis. Please refer to Chapter 4 for a detailed description of the methodology for each.

5.2.1 Study Design

Surgical planning accuracy was investigated for both Fontan revisions and Fontan completions. To do this, each patient was prospectively enrolled in a surgical planning protocol prior to the respective surgery. A flow chart is used to explain the clinical history and points of evaluation for both the Fontan revision (Figure 5-1) and Fontan completion cases (Figure 5-2). All Fontan revision patients had previously developed PAVMs and were undergoing a revision surgery to correct the PAVMs. All fontan completion cases were enrolled in surgical planning due to their complex anatomies and concern for future development of PAVMs.

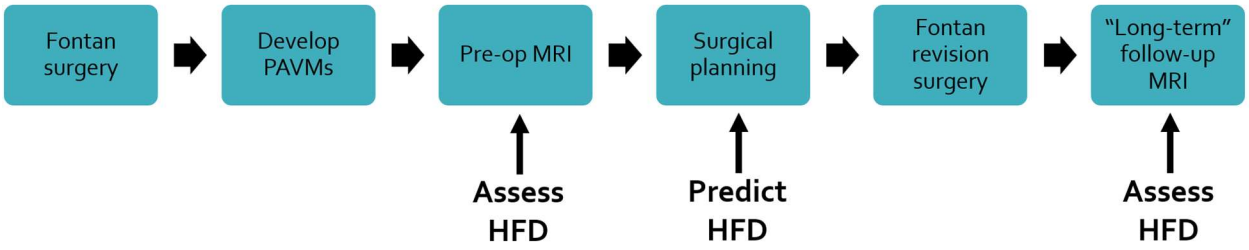

Figure 5-1 Series of events required for all Fontan revision patients included in this study. In each case, the formation of PAVMs was the main cause for the re-operation. Hepatic flow distribution will be assessed at each of the timepoints indicated.

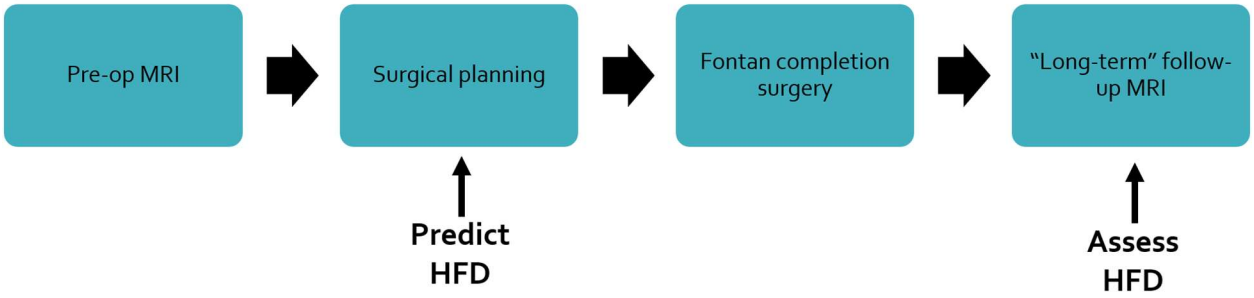

Figure 5-2 Series of events required for all Fontan completion patients included in this study. Hepatic flow distribution will be assessed at each of the timepoints indicated.

5.2.2 Patient Selection

A total of 12 single ventricle patients were included in this study. All patient data was received from the Children's Hospital of Philadelphia and Children's Healthcare of Atlanta under IRB approval (17-014377 and H09279 respectively) with a waiver of consent. Inclusion criteria were that the patient: (i) was enrolled in the surgical planning process prior to surgery, (ii) patient had pre- and post-operative cardiac magnetic resonance (CMR) and phase contrast CMR imaging, and (iii) imaging quality was sufficient for accurate anatomical segmentation as well as flow segmentation at every TCPC inlet/outlet. This resulted in both Fontan revision cases (n=5) and stage 2-3 cases (n=7). Clinical data including age, gender, body surface area (BSA), imaging and surgery dates, and diagnosis was obtained for each patient.

5.2.3 Surgical Planning

5.2.3.1 General Process

The current surgical planning paradigm is a multi-step process that involves collaboration between clinicians and engineers. The major steps include preoperative image acquisition, image processing, creation of virtual surgical options, and numerical simulations of those proposed

options (Figure 5-3).[36–38] Communication between clinicians and engineers is essential to verify segmented images, discuss the viability of surgical options and review simulation results. Overall, surgical planning is meant to analyze the performance of potential surgical options and therefore help inform the decision of graft type and positioning.

Potential surgical options are evaluated and ranked according to various clinically important metrics. To date, the major goals of Fontan surgical planning have included minimizing energy loss in the total cavopulmonary connection (TCPC), providing a balanced hepatic flow distribution (HFD) to the left and right lungs, and avoiding extreme wall shear stress. Energy loss has been related to exercise intolerance and is hypothesized to affect overall patient outcomes and HFD is a known factor in PAVM progression.[28,41,50,85,86] In situations where one specific surgical option is not optimal for all metrics, clinicians must evaluate which complication is of most concern for a given patient. For example, the progression of PAVMs is a very common motivation for surgical planning and therefore would focus on achieving balanced HFD.

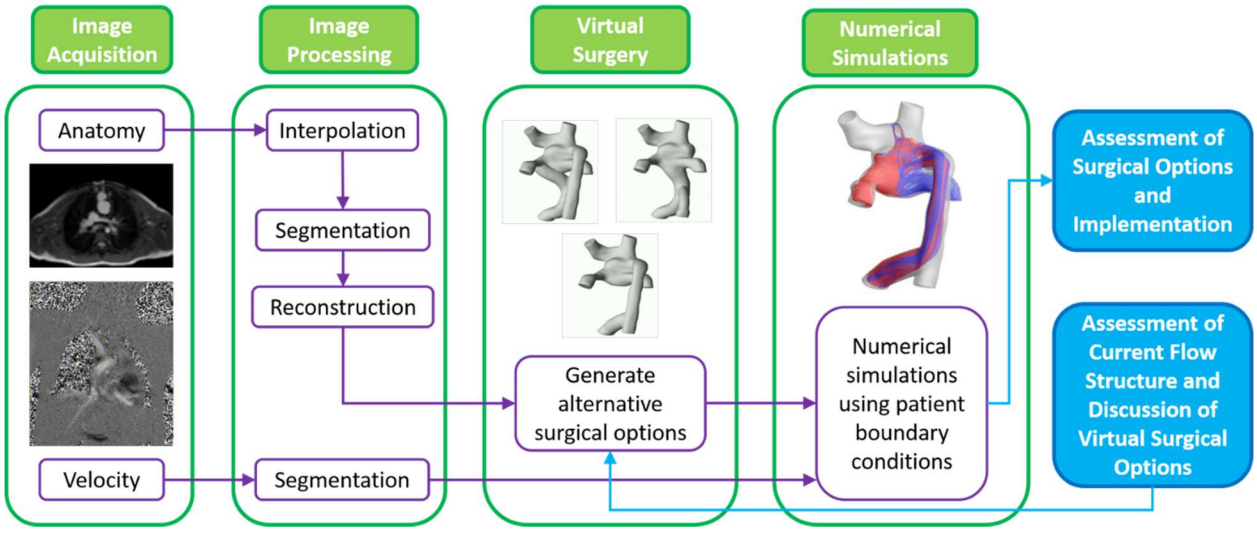

Figure 5-3 Surgical planning paradigm.

The data flow, order of events, and forms of data transfer between the clinical and engineering setting are shown in Figure 5-4. The only physical transfer of data from the clinical setting to engineering setting is the imaging data which begins the surgical planning process. Analyses including 3D reconstructions of the preoperative anatomy and proposed surgical options, as well as a final surgical planning report, are ultimately sent back to the clinic at the respective steps in the surgical planning process. Frequent communication between the two settings is important during the entire process, including segmentation, creation of realistic surgical options (requires the most clinical input), and review of comprehensive results.

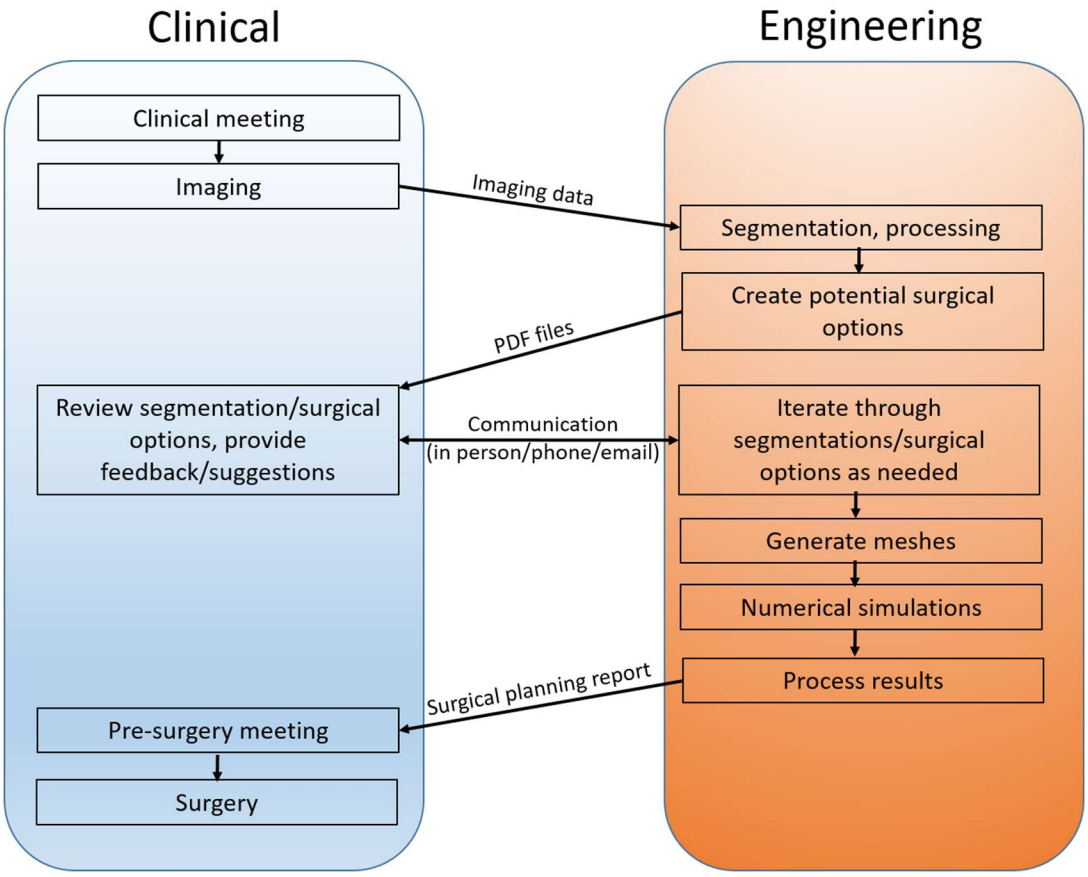

Figure 5-4 Interaction and types of data transfer between clinical and academic settings. Events are positioned chronologically from top to bottom.

5.2.3.2 Anatomy prediction

The preoperative anatomical segmentation is the basis for generating potential surgical options, which is performed following detailed discussion with the clinicians. The Glenn anatomy (for pre-Fontan planning) or original Fontan anatomy (for Fontan revisions), as well as structures that could create anatomical constraints for the proposed options (heart, aorta etc.) are included in the modeling. While standard CAD software can be used to generate surgical options, the use of modeling software specifically designed for Fontan surgical planning drastically reduces the time and effort required, and reduces the need for any prior modeling expertise. For example, SURGEM III is a software which has been developed over the last decade specifically for Fontan surgical planning.[37,87,88] SURGEM III is an interactive solid modeling tool whose name stems from "surgery modeler." It is designed to simplify and accelerate the surgical planning process, specifically the steps involved in creating and evaluating potential surgical options. With this software, a user can easily choose a graft type (traditional conduit or Y-graft) and graft size (in 2 mm increments) and position the insertion locations as desired (Figure 5-5). The user can modify graft centerline placement, insertion angle and offset options as needed (Figure 5-5c). SURGEM III can also automatically generate a large number of combinations of graft size and insertion angles/offsets in order to evaluate the robustness of given surgical option.[89] Finally, this software can preview and export a surface mesh of the proposed surgical option for the next step in the surgical planning process (Figure 5-5d).

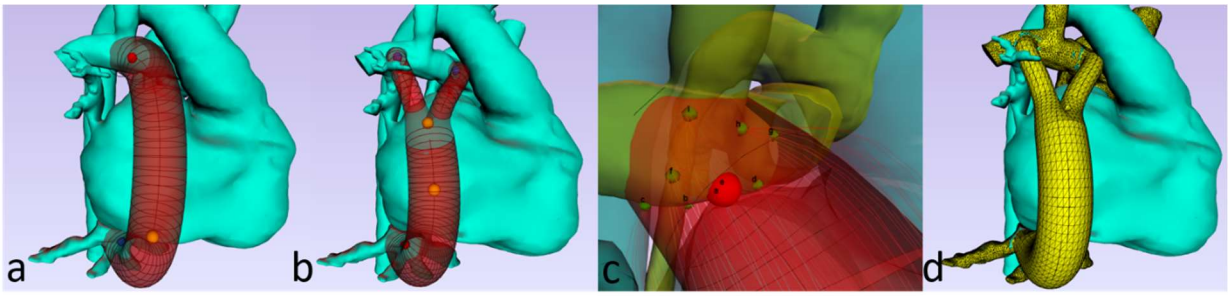

Figure 5-5 Creation of surgical options. (a) Fontan extracardiac baffle option. (b) Fontan bifurcated Y-graft option. (c) Automatic creation of baffle insertion angle/offset variations. (d) Preview of unioned (pre-op anatomy with proposed graft placement) mesh.

5.2.3.3 Blood flow waveform prediction

In this study, the pre-operative flow waveforms reconstructed from PC-MRI were directly used as the "predicted" flow waveforms. This prediction was used because it is the fastest prediction method and can fit within the relatively short clinical timeline.

5.2.3.4 Additional metrics

HFD prediction error is defined as:

$$HFD_{Prediction\ Error} = \left|HFD_{post-} - HFD_{predicted}\right|.$$

An absolute value is used to focus on total error rather than the direction of the discrepancy. Changes in flows pre- to post-operative are calculated as:

$$Flow\ Change = \left|Q_{post} - Q_{pre}\right|$$

where Q represents flow rate.

5.2.3.5 Pre-operative vs post-operative anatomy comparison

To compare the predicted and post-operative anatomies, the TCPCs were first registered (Geomagic, 3D Systems, Rock Hill, SC) to account for differences in imaging coordinate systems. A mesh comparison software (CloudCompare, version 2.10, open source) was then used to

quantify average and maximum deviations between the surfaces of the two TCPCs. A detailed description of this process can be found in Appendix 13.6: Anatomy Comparison. This was done for both the full TCPC and the graft alone. Graft insertion offset was calculated by measuring the distance between the predicted and post-operative anastomosis locations. For Y-grafts, the largest insertion offset of the two branches was used.

5.3 Results

5.3.1 Clinical Data

Clinical and surgical data is given in Table 5-1. The cohort consisted of 5 Fontan revisions and 7 Stage 2-3 cases. Implemented surgical options included 4 hepatic to azygous shunts, 4 Y-grafts, 3 traditional extracardiac conduits and 1 hepatic to innominate vein connection. Average follow up time was 22±32 [0.2-98] months. All raw data for both pre and post time points as well as Georgia Tech patient IDs etc. are given in Appendix C.

Table 5-1 Demographic and surgical data.

Patient ID	Gender	Diagnosis	Surgery Type	PAVMs*	Surgical Option	Age at surgery (years)	Age at follow up (years)	Follow up (months)	HFD prediction (%LPA)	HFD post-op (%LPA)	HFD Error
Patient 1	F	H, PA	Revision	Left	Hep to AZ	4.7	12.8	97.8	60	56	4
Patient 2	F	H	Revision	Left	Y-graft	19.0	19.0	0.3	38	45	7
Patient 3	M	H, D	Revision	Right	Hep to AZ	11.6	15.0	40.4	100	100	0
Patient 4	F	U	Revision	Right	Y-graft	12.7	12.8	1.6	53	32	21
Patient 5	M	H, PA	Revision	Left	ECC	17.5	18.3	9.0	26	71	45
Patient 6	M	HLHS	Stage 2-3	-	ECC	1.3	4.3	35.9	17	51	34
Patient 7	M	H, HLHS,	Stage 2-3	-	Y-graft	2.6	2.6	0.2	27	48	21
Patient 8	F	PA, TH	Stage 2-3	-	Y-graft	3.0	8.3	63.7	60	77	17
Patient 9	M	PA, DILV	Stage 2-3	-	ECC	2.2	2.2	0.3	73	80	7
Patient 10	F	H	Stage 2-3	-	Hep to AZ	1.1	1.1	0.3	51	56	5
Patient 11	F	H, DORV	Stage 2-3	-	Hep to AZ	3.2	4.2	11.7	71	87	16
Patient 12	F	H, HLHS	Stage 2-3	-	Hep to Inn	1.4	1.5	2.1	48	25	23

**The pulmonary arteriovenous malformations (PAVMs) column indicates which lung contained the malformations. Diagnoses are abbreviated as heterotaxy (H), pulmonary atresia (PA), dextrocardia (D), hypoplastic left heart syndrome (HLHS), tricuspid hypoplasia (TH), double inlet left ventricle (DILV), unbalanced canal (U) and double outlet right ventricle (DORV). Surgical options are abbreviated as hepatic to azygous shunt (Hep to AZ), extracardiac conduit (ECC) and hepatic to innominate vein (Hep to Inn). HFD is hepatic flow distribution.*

5.3.2 Revisions vs Stage 2-3

Age at surgery and age at follow up were significantly different between the revision (13.1±5.7 and 15.6±2.9 years) and Stage 2-3 (2.1±0.9 and 3.5±2.5 years) cases respectively ($p<0.001$ for both, Table 5-2). Follow up time was not significantly different between the revision and Stage 2-3 cases (30±41 and 16±25 months respectively, $p=0.49$, Table 5-2). No significant differences in pre- to post-operative changes in flow rates were seen between the revision and Stage 2-3 cases (Table 5-2). Additionally, no flow rates (grouped by surgery type or vessel) showed consistent directionality in flow rate changes. Significant differences in geometric variations (between the predicted and actual post-operative anatomy) were seen between the revision and Stage 2-3 cases both in terms of the TCPC as a whole and the graft alone (Table 5-2).

Table 5-2 Fontan revision and Stage 2-3 comparison.

	Revision	Stage 2-3	p-value
Age at surgery (yrs)	13.1±5.7	2.1±0.9	<0.001
Age at follow up (yrs)	15.6±2.9	3.5±2.5	<0.001
Follow up time (months)	30±41	16±25	0.492
HFD prediction error	15±18	18±10	0.795
IVC flow change (L/min)	0.22±0.16	0.25±0.19	0.782
SVC flow change (L/min)	0.35±0.13	0.44±0.32	0.573
AZ flow change (L/min)	0.61±0.45	0.20±0.17	0.104
LPA flow change (L/min)	0.57±0.19	0.48±0.37	0.638
RPA flow change (L/min)	0.80±0.60	0.25±0.22	0.052
IVC flow change (%)	42±42	41±26	0.955
SVC flow change (%)	36±21	48±29	0.462
AZ flow change (%)	49±30	40±28	0.656
LPA flow change (%)	38±21	59±35	0.274
RPA flow change (%)	62±40	41±53	0.471
PFD change (%)	9±9	14±6	0.261
TCPC deviation (mm)	3.3±0.8	1.6±0.5	0.001
TCPC max deviation (mm)	17.6±2.0	9.2±3.7	0.004
Graft deviation (mm)	5.6±2.8	2.8±1.9	0.062
Graft max deviation (mm)	15.3±4.4	9.3±4.5	0.046
Graft insertion offset (mm)	13.5±8.3	5.8±4.5	0.063

Change represents absolute difference between pre-operative and post-operative flows. Hepatic flow distribution (HFD); inferior and superior vena cava (IVC and SVC); left and right pulmonary artery (LPA and RPA); azygous vein (AZ); pulmonary flow distribution (PFD); total cavopulmonary connection (TCPC).

5.3.3 HFD Prediction Error

The predicted and post-operative HFD can be found in Table 5-1. Overall, $HFD_{prediction\ error}$ was 17±13%, and was not significantly different between revisions (15±18%) and Stage 2-3

(18±10%) cases (p=0.73, Table 5-2). Stage 2-3 predictions underestimated HFD in 6/7 cases, while revisions were evenly split between overestimations and underestimations. CFD results comparing the predicted and post-operative streamlines for all Fontan revisions and Stage 2-3 cases are shown in Figure 5-6 and Figure 5-7 respectively. In addition, Figure 5-6 shows the pre-operative HFD for all Fontan revisions, confirming a lack of hepatic flow to the lung with PAVMs. Overall, no significant correlations were found between HFD prediction error and age at surgery, age at follow up, or follow up time. Moderate correlations were seen between the percent change in IVC flow rate (r=0.60, p=0.04) and the change in PFD (r=0.60, p=0.04) from pre- to post-op with HFD prediction error.

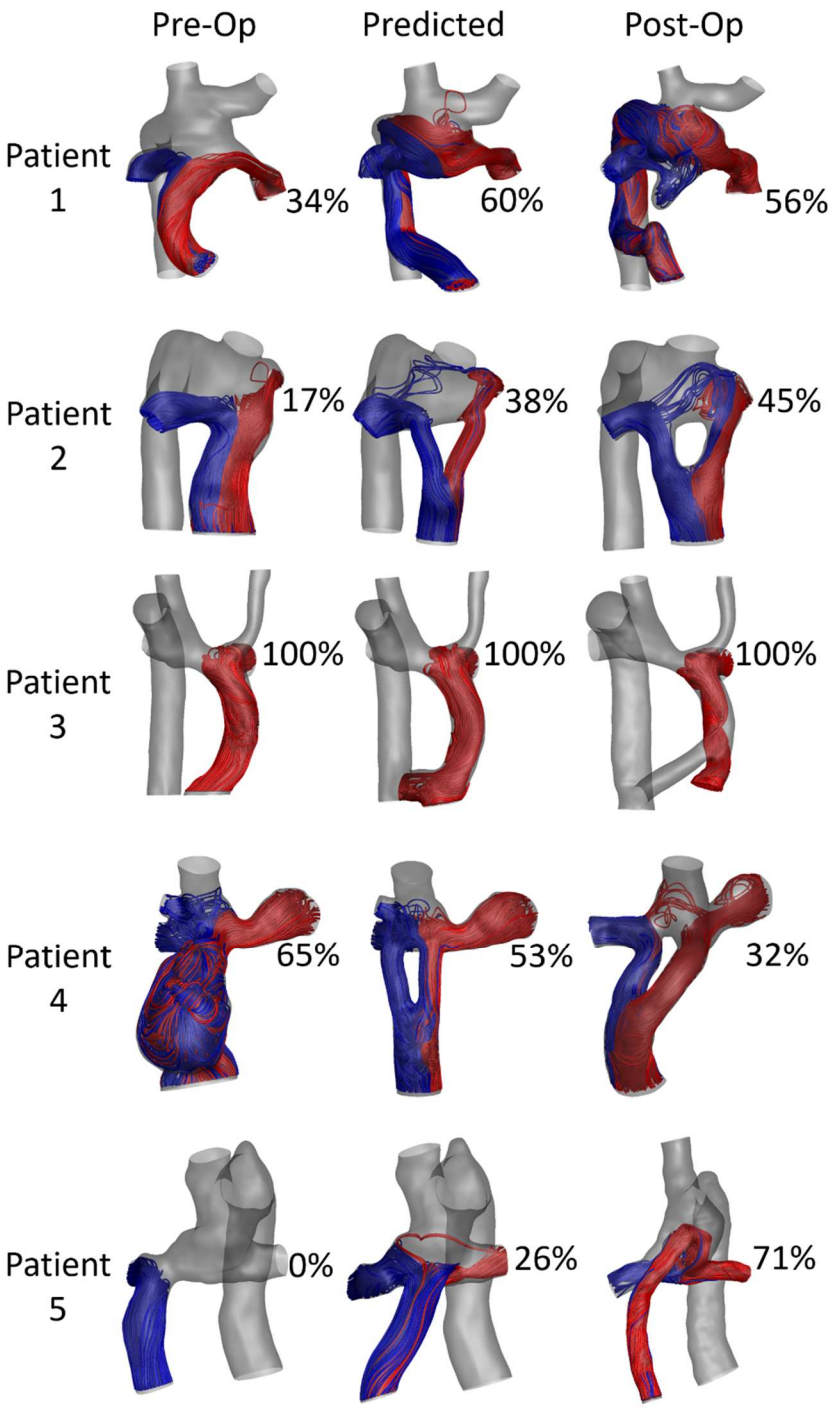

Figure 5-6 Streamline comparison for the pre-operative, predicted, and post-operative states for all Fontan revision cases. Patients 1, 2 and 5 were diagnosed with left-sided pulmonary arteriovenous malformations (PAVMs), and Patients 3 and 4 with right-sided PAVM.

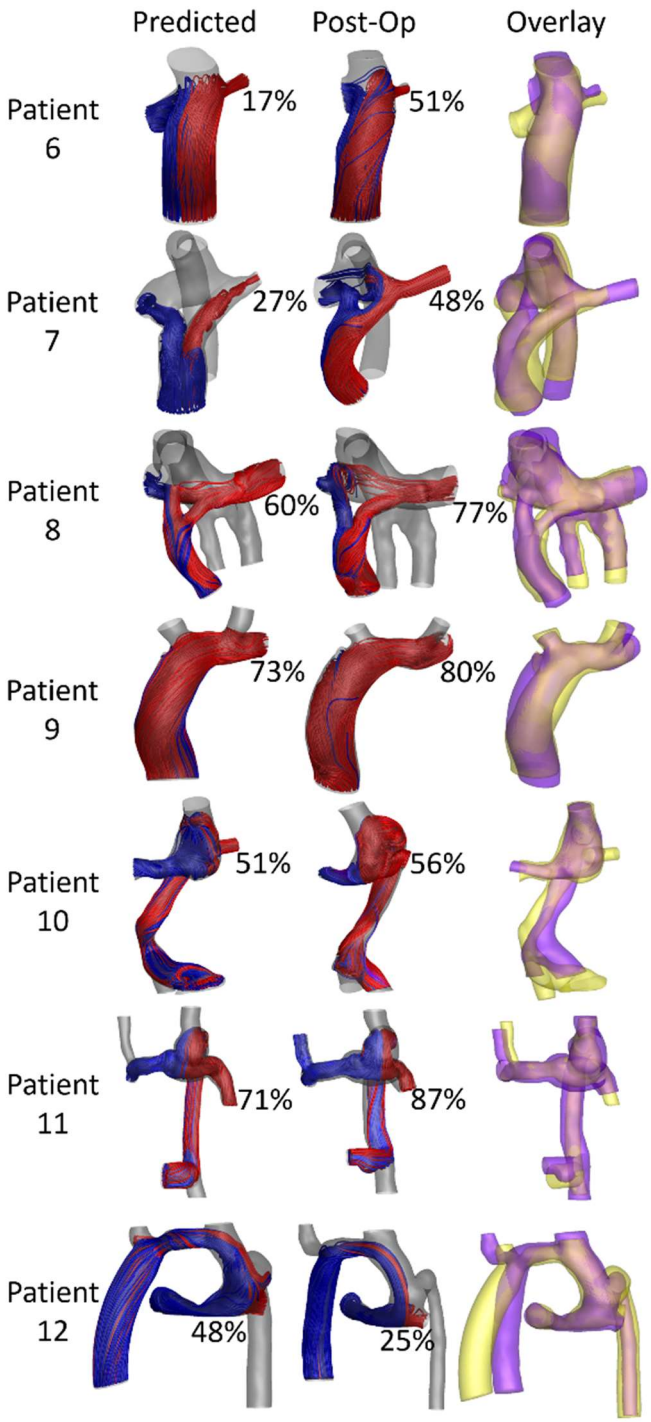

Figure 5-7 Streamline comparison between the predicted and post-operative states for all Stage 2-3 patients. Hepatic flow distribution is noted as the percent of HFD to the left pulmonary artery. The overlay column compares the predicted (yellow) and post-operative (purple) anatomies.

5.3.4 *Connection Types*

$HFD_{prediction\ error}$ was found to be associated with surgical connection type. A comparison of $HFD_{prediction\ error}$ between graft types can be seen in Figure 5-8. Hepatic to azygous shunts had significantly lower prediction errors than other connection types (6±7% vs 22±13% respectively, p=0.05, Figure 5-8b). In addition, a strong, positive correlation was seen between HFD prediction error and graft insertion offset within the Y-graft and ECC group (r=0.99, p<0.001, Figure 5-9d). Example cases of low, moderate and high graft insertion offsets are shown in Figure 5-9a-c.

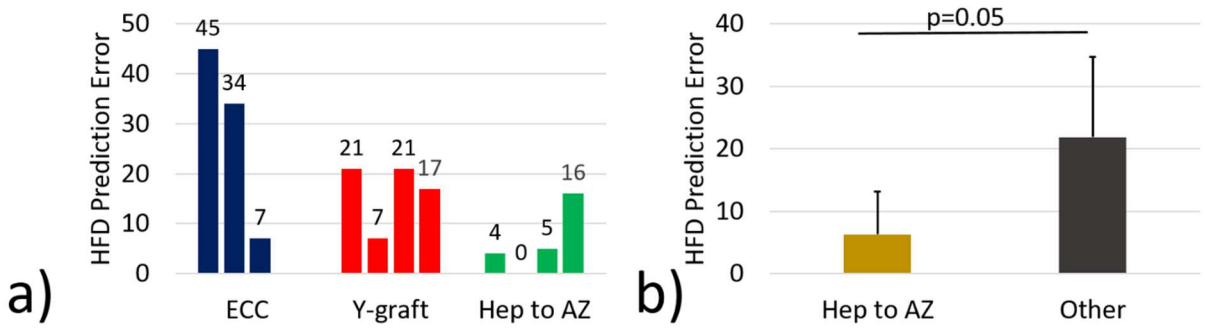

Figure 5-8 Effect of connection type on HFD prediction error. (a) Comparison between graft types. (b) Hepatic to azygous (Hep to AZ) shunts versus all other connection types. Extracardiac conduit: (ECC).

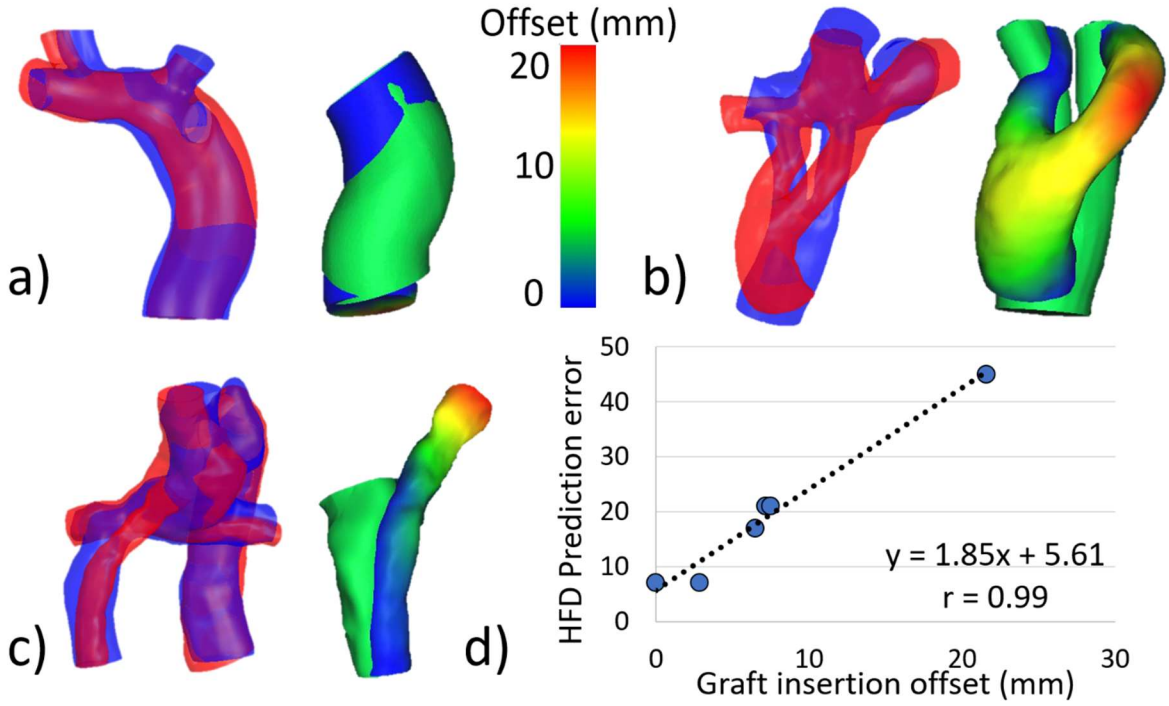

Figure 5-9 Relationship between HFD prediction error and graft insertion offset for extracardiac conduit and Y-graft Fontan connections. Representative cases are shown for (a) low, (b) moderate, and (c) high graft insertion offsets. A strong correlation (d) was se seen between prediction error and offset for these connection types. The overlay figures compare the predicted (blue) and post-operative (red) TCPCs on the left, and show a colormap of the offset between the predicted and post-operative grafts on the right for each representative case. All cases use the same color scale.

5.3.5 Potential Methodological Improvements

The HFD prediction error associated with the "improved" post-operative anatomy and flow predictions and the current methodology is shown in Table 5-3. While a reduced or identical prediction error was seen for the majority of patients using either methodological improvement, (8/12 and 7/12 for the improved anatomy and improved flow scenarios respectively), a more substantial reduction in error was seen when using the improved anatomy prediction. The current HFD prediction error (17±13%) was significantly reduced by improving anatomy prediction (9±6%, p=0.03, paired-sample t-test), but remained nearly the same when using only an improved

flow prediction (18±17%, p=0.73, paired-sample t-test). When comparing the two potential methodological improvements, improved post-operative anatomy prediction resulted in equivalent or more accurate HFD predictions for 9/12 patients when compared with improved flow prediction.

Table 5-3 Comparison of HFD prediction errors between the current surgical planning process and potential methodological improvements.

			HFD Prediction Error		
Patient ID	**Surgery Type**	**Connection Type**	**Current**	**Improved anatomy prediction**	**Improved flow prediction**
Patient 1	Revision	Hep to AZ	4	6	11
Patient 2	Revision	Y-graft	7	13	1
Patient 3	Revision	Hep to AZ	0	0	0
Patient 4	Revision	Y-graft	21	10	29
Patient 5	Revision	ECC	45	16	58
Patient 6	Stage 2-3	ECC	34	18	18
Patient 7	Stage 2-3	Y-graft	21	7	38
Patient 8	Stage 2-3	Y-graft	17	6	14
Patient 9	Stage 2-3	ECC	7	13	5
Patient 10	Stage 2-3	Hep to AZ	5	2	3
Patient 11	Stage 2-3	Hep to AZ	16	3	23
Patient 12	Stage 2-3	Hep to Inn	23	18	13
Average	-	-	17±13	9±6*	18±17

Hepatic flow distribution (HFD); hepatic to azygous shunt (Hep to AZ); extracardiac conduit (ECC); hepatic to innominate connection (Hep to Inn). Asterisk indicates statistically significant difference (paired sample t-test) from the current method.

5.4 Discussion

Previously limited by a lack of post-operative data, the current study offers the first assessment of prospective Fontan surgical planning accuracy for both Fontan revisions and Stage 2-3 conversions using medium-term post-operative data. This study incorporates a unique data set resulting from more than a decade of surgical planning experience, and provides a methodological assessment necessary for the improvement of surgical planning accuracy.

Though an exact "cut-off" for HFD to prevent PAVMs is currently unknown, and may vary between patients, the Fontan revision results (Table 5-1, Figure 5-6) confirm a lack of hepatic flow to the lung with PAVMs in each case. Furthermore, PAVMs regressed in each case where the revision resulted in increased hepatic flow to the affected lung. In combination with previous studies, these results emphasize the importance of achieving a balanced hepatic flow distribution through appropriate TCPC design.

In this study, HFD prediction error averaged 17±13% across all patients. Prediction error was similar between revision and Stage 2-3 cases, but differed across connection types. Intuitively, hepatic to azygous connections are more robust to variations in surgical implementation since all hepatic flow will join the azygous flow and then travel through the entire azygous vein before interacting with other flows regardless of exact placement of the shunt. No colliding flows from multiple vessels are present locally in hepatic to azygous connections, in contrast with Y-graft and ECC connections where slight offsets may substantially change the interactions between various inlets and therefore stray from predicted results (Figure 5-10).[89] Therefore, hepatic to azygous predictions were found to be quite accurate, while predictions for other connection types were more varied. This agrees with previous work evaluating the robustness of various types of surgical connections.[89]

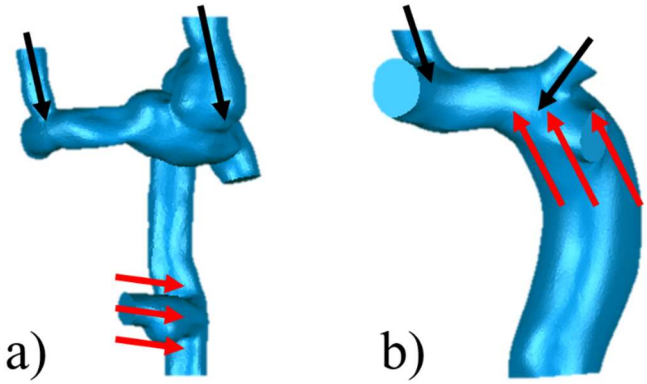

Figure 5-10 Schematic representation showing differences between (a) hepatic to azygous and (b) extracardiac conduits (ECC). Black arrows indicate inlet flows and red arrows indicate potential variations in graft placement. Differences in graft placement can affect flow collisions much more in ECC connections.

Capitalizing on the available post-operative data, various simulations were run using the post-operative anatomy or flows as a surrogate for an "improved" prediction. While it is unlikely that anatomy or flow prediction techniques will ever produce exact matches to post-operative outcomes, this analysis is instructive by showing the full potential of surgical planning accuracy if methodological improvements in either of these areas offered extremely accurate predictions. To reiterate, improvements in anatomy prediction led to a significant ($p=0.03$) reduction in HFD prediction error. Interestingly, improvements in flow prediction did not result in similar error reduction (Table 5-3). These findings stress two critical points: (i) post-operative anatomy prediction is a primary factor in HFD prediction, and (ii) anatomy prediction methods must improve in order for Fontan surgical planning to offer more accurate HFD predictions.

Again, improved flow prediction alone did not result in more accurate HFD predictions ($p=0.73$, Table 5-3). In general, HFD is primarily driven by graft placement.[61] In a complex connection such as the TCPC, relatively small offsets in graft placement and angulation can largely alter the collisions and interactions among flows from various vessels.[61] These variations can affect

the preferential streaming of inlet flows including hepatic flow, which in turn will determine hepatic flow distribution. Naturally, severe changes in individual flow rates can affect HFD prediction, however this was not observed in this cohort.

Though it is common to use indexed flow rates (normalized by BSA) in pediatric studies involving changes over time, raw flow rates are shown in this study (Table 5-2) to emphasize the changes in actual inputs to the surgical planning process. While an indexed flow rate may remain constant over a several year follow up, the actual flow rate (and therefore the flow rate that needs to be predicted) does not. This raw data better represents how boundary conditions for the surgical planning process change over time.

Multiple methods exist to predict post-operative Fontan anatomies and flows, ranging from simple (basic CAD software and using pre-operative flows as the "predicted" post-op flows) to more sophisticated (designated surgical planning software and lumped parameter modeling) methods.[88,90] As the methods have progressed in complexity, anatomy prediction methods have become faster (software is designed specifically for Fontan surgical planning) and flow prediction methods have become slower (more complex calculations and "full body" modeling). Meeting the clinical timeline for most surgical planning cases requires accelerated analysis.[11] Conveniently, the present results indicate that anatomy prediction is a primary shortcoming, which can hopefully be improved without lengthening the surgical planning process.

Accurate anatomy prediction involves both predicting a viable surgical option and accurately implementing that option. Modeling a viable surgical option is heavily dependent on high quality imaging data, clinician involvement and inclusion of relevant anatomical landmarks. Current methods include the heart, aorta and pulmonary circulation, but future efforts could potentially add additional organs and the process of chest closure. Once a surgeon has selected the surgical option

to implement, closely replicating that option in vivo may be challenging. Little intra-operative guidance is currently offered as part of the surgical planning process. Some efforts have explored 3D printing and augmented/virtual reality as planning/guidance tools, but further refinements are needed.[91–94] In addition, growth is another difficult factor to model, but may be necessary to improve surgical planning results.[62,63] It is possible that "variations" between a predicted and post-operative anatomy are due to growth rather than imperfect surgical implementation.

If Fontan surgical planning is to be used in clinical practice, the importance and necessity of follow up data and validation studies such as this cannot be overstated. Understanding the current accuracy and methodological shortcomings is imperative in order to correctly use the results and progress the field. Future efforts and refinements to the surgical planning process will greatly benefit from an improved understanding of the current state.

6. SPECIFIC AIM 1B

Purpose: To evaluate the ability of Y-grafts to provide balanced hepatic flow distribution and therefore prevent pulmonary arteriovenous malformations.

Hypothesis: Y-grafts provide more balanced hepatic flow distribution than traditional Fontan connections.

6.1 Overview

Y-grafts are a relatively new option for Fontan completion, and are hypothesized to provide balanced HFD to the left and right pulmonary arteries via the Y-graft's two branches (thus preventing the progression of PAVMs)[10,40]. Specific Aim 1B used patient-specific CFD modeling to analyze the ability of a Y-graft to offer balanced HFD, preventing the progression of PAVMs. We will perform a direct comparison between 30 consecutive Y-graft patients and 30 age and BSA matched traditional Fontan patients. In this comparison we will determine if Y-grafts provide more balanced HFD than a traditional Fontan connection. In addition, we will also study how HFD changes over time in Y-graft patients. To do this, we have acquired medium-term follow up MRI and clinical data, in addition to immediate post-operative data, for 10 Y-graft patients.

6.2 Methods

This Specific Aim utilizes medical image processing, computational fluid dynamics, anatomy characterization and statistical analysis. Please refer to Chapter 4 for a detailed description of the methodology for each.

6.2.1 Study Design

This study is composed of two parts: (1) a direct comparison between Y-grafts and traditional grafts, and (2) a serial study assessing the hemodynamic changes in Y-grafts over time. This design is illustrated in Figure 6-1

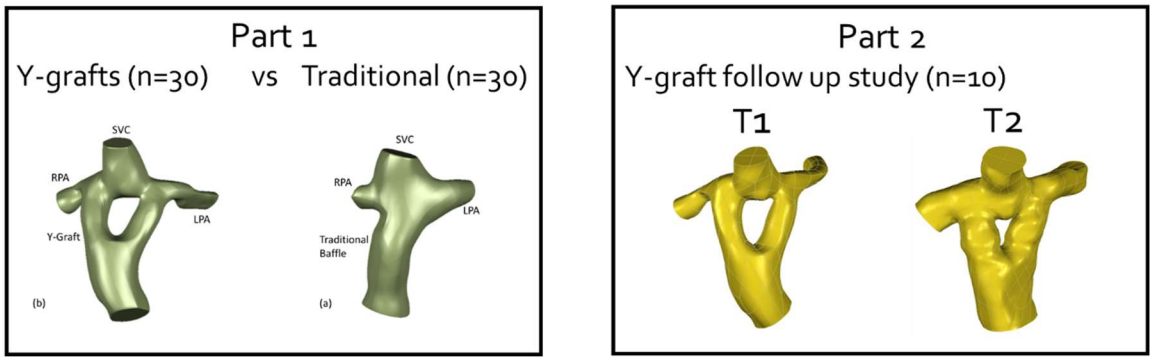

Figure 6-1 Study design for Specific Aim 2B. Patient number in part 2 is limited by available data.

6.2.2 Patient Selection

For the first part of this study, a total of 60 patients were used. All LT/ECC patient data (n=30) were received from Children's Healthcare of Philadelphia and all Y-Graft patient data (n=30) were received from Children's Healthcare of Atlanta. Thirty consecutive Y-grafts performed by Dr. Kirk Kanter were used; LT/ECC patients were chosen to match age and BSA between groups. All Y-graft Fontan connections used commercially available Y-grafts. Clinical

data including age, gender, and BSA were obtained for each patient. All patient data for this part of the study can be found in Appendix D – Specific Aim 1B Cross-Sectional patient data.

For the serial investigation, 10 Fontan patients with Y-graft connections were included. Inclusion criteria included (i) single ventricle patient with Y-graft Fontan connection, (ii) serial, post-operative CMR and phase-contrast CMR data, and (iii) sufficient image quality to accurately segment the TCPC and blood flow waveforms at each TCPC inlet/outlet. All Y-graft patient data was received from Children's Healthcare of Atlanta (IRB: H09279). All Y-graft connections used commercially available aorto-iliac Y-grafts.

A LT/ECC comparison group with identical follow up times was not available. Therefore, several, unique LT/ECC groups were chosen (each n=10) with follow up times both before and after the Y-graft cohort. All LT/ECC patient data was received from Children's Hospital of Philadelphia (IRB: H05236). Clinical data including age, body surface area (BSA), gender, ventricle morphology, presence of fenestration and dates of surgery and CMR studies were obtained for each patient. All patient data for the longitudinal part of this study as well as the comparison groups can be found in Appendix E – Specific Aim 1B Longitudinal patient data.

6.2.3 Statistical analysis

The cross-sectional portion of this specific aim follows the statistical methods stated in Chapter 4.5. The longitudinal follows the same statistical methods, but a description is given here to clarify the statistical methods used. In the serial study of 10 Y-grafts, a paired sample t-test is used to determine if there is a significant directional change in HFD over time. This test will give a significant result if patients are moving in the same direction. For example, if all patients improved in HFD by 1% then a paired sample t-test will give a significant result. An independent

samples t-test was also used to show if the Y-graft group at timepoint 2 was more balanced in terms of HFD than at timepint 1. For example, if all patients improve in HFD by 1 %, the group will not have a significantly better HFD at timepoint 2, even though all patients changed in the same direction. A paired sample t-test will tell if the Y-grafts are improving, an independent sample t-test will show if that amount of improvement makes a significant difference between the two timepoints.

For the comparison between the Y-graft and ECC control groups in the longitudinal study, comparisons were made between the Y-grafts at timepoint 2 with the various control groups. As we did not care how the control groups compared with one another, we did not use an ANOVA for a multiple group comparison. We compared the Y-graft at timepoint 2 with the control groups on an individual basis, and therefore used an independent sameple t-test for analysis.

6.3 Results

6.3.1 Cross-sectional study

6.3.1.1 Y-graft Hemodynamic Performance

Figure 6-2 shows several clinically important hemodynamic metrics for the Y-graft cohort. The average PFD and HFD deviations from an ideal 50/50 split were 13.4±10.6 and 25.9±15.1, respectively (Figure 6-2a). Figure 6-2b illustrates the effect of LPA stenosis on indexed power loss. A moderate positive correlation ($r=0.67$, $p<0.01$) was found between LPA stenosis and indexed power loss. The distributions of TCPC resistance and HFD deviation are shown in Figure 6-2c Figure 6-2d. The distribution of TCPC resistance is skewed to the right with approximately

53% and 70% of Y-graft patients having resistances less than 1 and 2 Wood Units respectively. HFD deviation was relatively evenly distributed (Figure 6-2d). Only 13% of Y-graft patients have HFD deviations less than 10 (ideal) and 24% of Y-graft patients have deviations greater than 40 (poor).

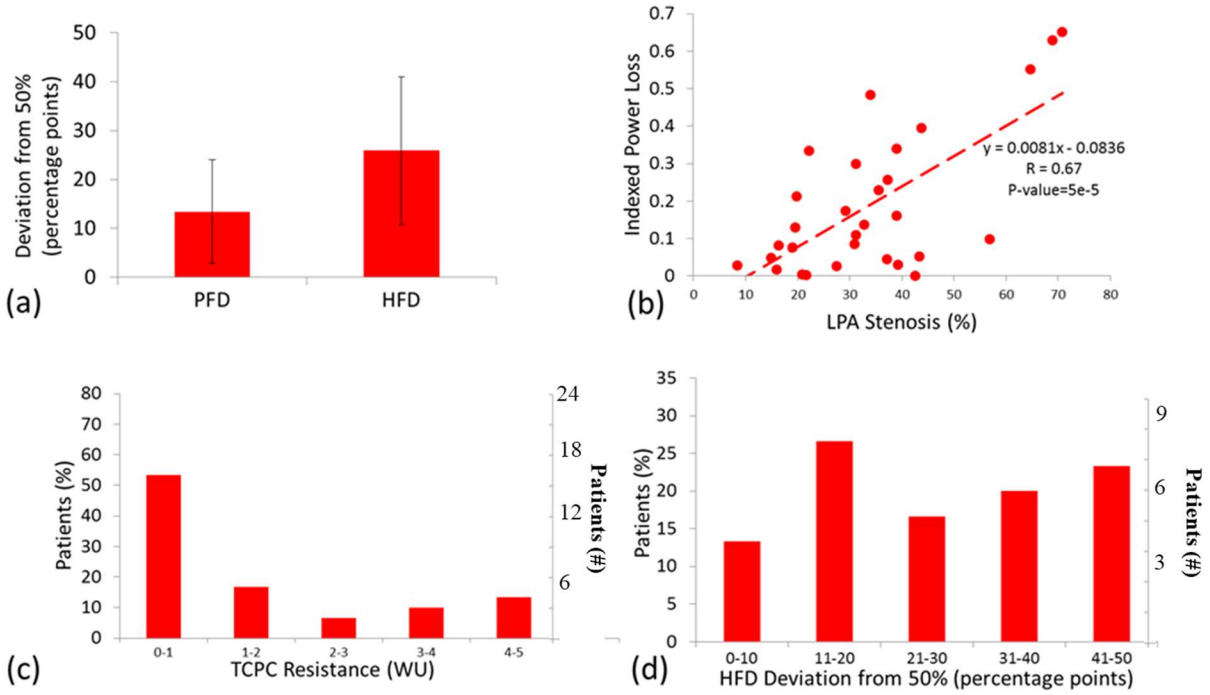

Figure 6-2 Y-Graft hemodynamic performance. (a) Pulmonary and hepatic flow distribution (PFD and HFD) deviations. (b) Effect of LPA stenosis on index power loss (iPL). (c) Distribution of TCPC resistance. (d) Distribution of HFD deviation.

6.3.1.2 Representative Y-graft Cases

Figure 6-3 shows streamlines for six representative cases from the 30 patient Y-graft cohort. Patients Y1, Y2, andY3 show balanced HFD (low HFD deviation) while the final three (Y4, Y5, andY6) are unbalanced. Y1 represents an “ideal” case with balanced PFD, normal SVC positioning and no mid-PA stenosis. Y2 represents uneven PFD with mid-PA stenosis on the low PFD side. Y3 has bilateral SVCs, balanced PFD and mid-PA stenosis. Y4 has balanced PFD with the SVC positioned superior to a y-branch anastomosis. Y5 has unbalanced PFD with mid-PA stenosis on the high PFD side and Y6 represents balanced PFD with y-branch stenosis. HFD to the

LPA is noted for each model in Figure 6-3. (The posterior views for a variety of these patients can be found in Appendix D – Specific Aim 1B Cross-Sectional patient data Animations for several important comparative cases are provided in Appendix H.

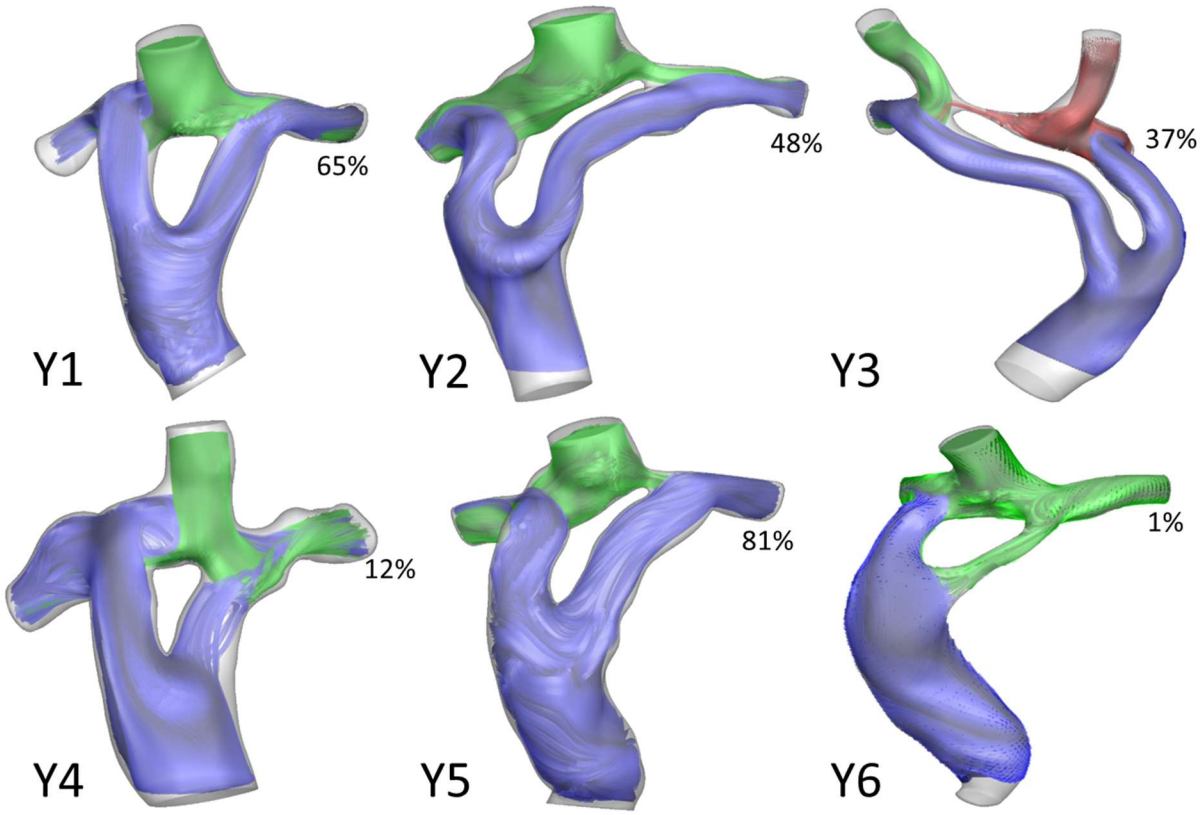

Figure 6-3 Representative Y-Graft cases with HFD noted. Streamlines colored by origin: IVC(blue), SVC(green) and LSVC(red). Percentages shown are percent of hepatic flow to the left pulmonary artery.

6.3.1.3 Y-graft vs LT/ECC

To further evaluate the commercially available Y-graft, a direct hemodynamic comparison was performed between the Y-graft and LT/ECC cohorts. Clinical data are shown in Table 6-1 for each graft type. Patients were selected to best match age and BSA between groups. Y-graft resistance was significantly higher ($p=0.03$) than LT/ECC resistance, with averages of 1.51±1.52 and 0.56±0.54 WU, respectively (Figure 6-4a). Overall, HFD deviation was not significantly

different between the groups with an average of 21±13 for the LT/ECC and 26±15 for Y-grafts (Figure 6-4b). Figure 6-4c shows no significant differences in particle residence time.

Figure 6-4d and Figure 6-4e compare the distribution of TCPC resistance and HFD deviation between graft types, respectively. Almost 77% of LT/ECC patients have a resistance less than 1 WU, compared to 53% of the Y-grafts. Additionally, 30% of commercially available Y-graft patients exhibit a resistance greater than 2 WU, while only 3% of the LT/ECC cohort have values this high (Figure 6-4d). Focusing on the two extremes of HFD deviation, 30% of LT/ECC patients had ideal HFD deviations (<10) compared to only 10% of Y-graft patients. At the other extreme, more than twice as many Y-graft patients (23%) have HFD deviations greater than 40 (poor) than LT/ECC patients (10%).

Figure 6-4f compares the sensitivity of iPL to LPA stenosis for both graft types. Commercially available Y-grafts were found to be more sensitive to LPA stenosis in terms of iPL with a significant difference between the two correlations (Fisher's exact test, one-tailed, $z=-1.76$, $p=0.04$).

Table 6-1 Averaged clinical data for all patients separated by graft type.

	LT/ECC (n=30)	Y-Graft (n=30)	p-value
BSA (m^2)	0.67 ± 0.12	0.66 ± 0.20	0.19
Age (years)	3.65 ± 1.14	3.68 ± 2.49	0.17
Gender (male)	70%	53%	0.19
PA Stenosis (%)*	33.99 ± 12.60	26.82 ± 10.69	0.02
Systemic Venous Flow (L/min)*	2.07 ± 0.61	1.57 ± 0.59	<0.01
Pulmonary Flow Distribution (% LPA)	46.01 ± 15.00	46.00 ± 16.78	0.99
PFD Deviation from 50% (percentage points)	13.13 ± 7.91	13.40 ± 10.60	0.78
Pulsatility Index (IVC)	0.66 ± 0.65	0.93 ± 0.72	0.14
Pulsatility Index (SVC)	0.51 ± 0.50	0.42 ± 0.12	0.76

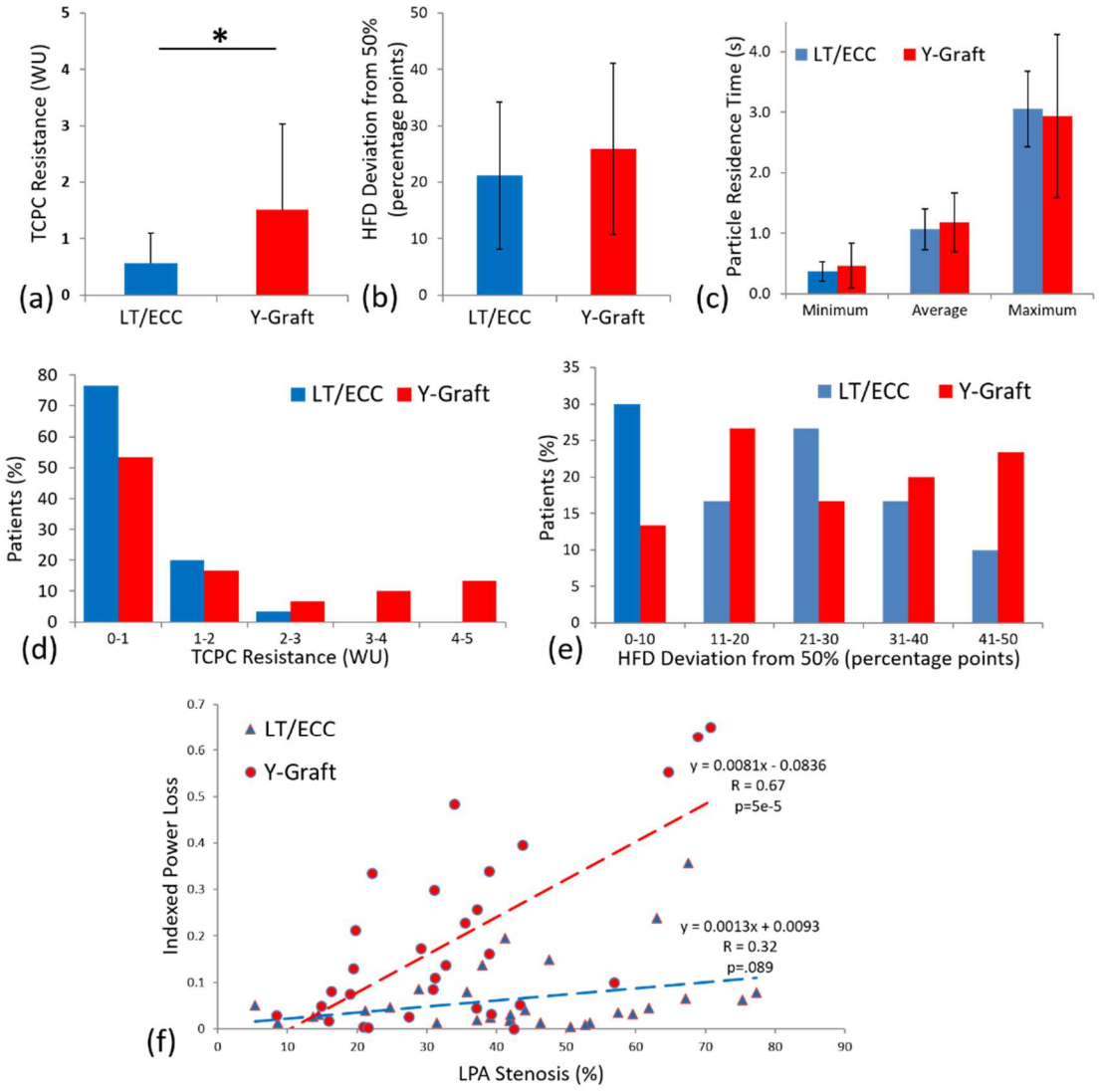

Figure 6-4 Hemodynamic Comparison of the Y-graft and LT/ECC. (a) Indexed power loss. (b) HFD deviation from 50%. (c) Particle residence time. (d) Distribution of iPL. (e) Distribution of HFD deviation. (f) Effect of LPA stenosis on iPL.

6.3.2 Serial Y-graft study

6.3.2.1 Clinical Data

Clinical and hemodynamic data for all Y-grafts at both timepoints are shown in Table 6-2. Age increased from 3 [2.75-4.0] to 6 [5-6.25] years across the two timepoints, with a median follow

up time of 14 [7-25] days and 3.02 [2.13-3.31] years respectively. The cohort included 4/6 male/female and 3/7 HLHS/non-HLHS.

Indexed IVC flow increased from 0.57 [0.45-0.89] to 0.9 [0.66-1.1] L/min/m2 (p=0.005). Similarly, Qs increased from 1.83 [1.62-1.91] to 2.28 [1.93-2.83] L/min/m2 (p=0.020). SVC, LPA, RPA, collateral flow and cardiac index showed no significant changes between timepoints. PFD became more balanced (PFD deviation from 50% decreased from 9 [5-26] to 6 [4-11]) though not statistically significant (p=0.173). Finally, pulmonary artery stenosis did not significantly change over time.

Table 6-2 Clinical and hemodynamic data for the Y-graft cohort.

	Y-graft (n=10)		Paired sample t-test
	Timepoint 1	Timepoint 2	p-value
Age (years)	3 [2.75-4.0]	6 [5-6.25]	<1e-3*
BSA (m^2)	0.62 [0.60-0.76]	0.87 [0.76-0.99]	<1e-3*
Follow up time (years)	0.04 [0.02-0.07]	3.02 [2.13-3.31]	<1e-3*
Gender	4/10 male		-
Morphology	3/10 HLHS		-
Fenestrated	9/10		-
Cardiac Index (L/min/m^2)	3.09 [2.8-3.8]	3.11 [2.89-3.69]	0.982
IVC flow (L/min/m^2)	0.57 [0.45-0.89]	0.9 [0.66-1.1]	0.005*
SVC flow (L/min/m^2)	1.16 [0.99-1.41]	1.1 [0.87-1.6]	0.224
LPA flow (L/min/m^2)	0.82 [0.58-1.23]	0.9 [0.65-1.07]	0.374
RPA flow (L/min/m^2)	0.905 [0.56-1.23]	0.82 [0.59-1.2]	0.200
Qs (L/min/m^2)	1.83 [1.62-1.91]	2.28 [1.93-2.83]	0.020*
Collateral flow (L/min/m^2)	1.14 [0.94-2.08]	0.59 [0.16-1.39]	0.264
PFD deviation (percentage points)	9 [5-26]	6 [4-11]	0.173
LPA stenosis (%)	14 [11-27]	13 [8-30]	0.987
RPA stenosis (%)	13 [4-29]	13 [5-32]	0.760
Overall PA stenosis (%)	15 [11-26]	14 [7-31]	0.847
TCPC resistance (WU)	0.26 [0.12-0.42]	0.15 [0.12-0.20]	0.117
HFD deviation (percentage points)	16 [6-30]	5 [2-16]	0.015*

BSA: body surface area; IVC/SVC: inferior and superior vena cava; LPA/RPA: left and right pulmonary artery; Qs: systemic return; PFD: pulmonary flow distribution; HFD: hepatic flow distribution; TCPC: total cavopulmonary connection.

6.3.2.2 HFD and TCPC Resistance

Hepatic flow distribution significantly improved over time (paired sample t-test, p=0.015, Table 6-2). HFD deviation decreased from 16 [6-30] to 5 [2-16]. Nine out of ten patients had more balanced HFD at timepoint 2 than timepoint 1 (Figure 6-5). On average, there was a 13 [3-18] point improvement in HFD deviation. In general, a HFD deviation <10 is clinically acceptable, though no exact cut-offs have been determined. Individual HFD values and follow up times can be found in Figure 6-5a. Streamlines for all Y-grafts at both timepoints are shown in Figure 6-6. Overall, HFD was relatively balanced at timepoint 2 with an HFD deviation of only 5 [2-16].

a)

	Y1 (42m)	Y2 (39m)	Y3 (45m)	Y4 (39m)	Y5 (36m)	Y6 (29m)	Y7 (15m)	Y8 (4m)	Y9 (36m)	Y10 (30m)
HFD T1	14	54	68	63	48	92	68	37	44	78
HFD T2	28	49	49	52	65	71	52	43	53	58

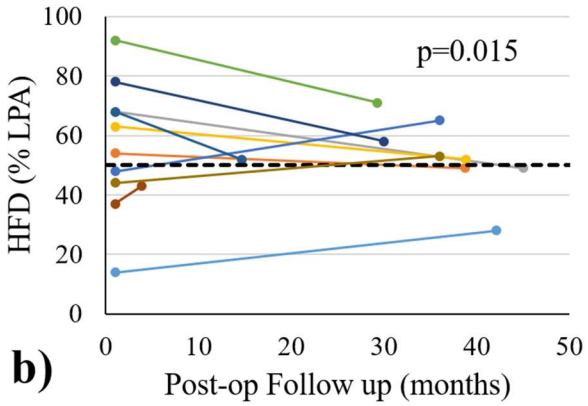

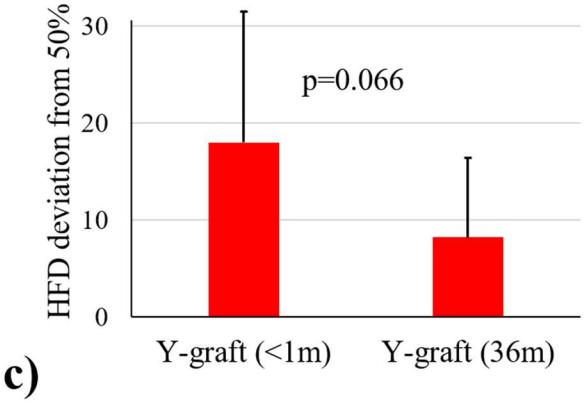

Figure 6-5 Serial comparison of Y-graft hepatic flow distribution (HFD). (a) Individual patient HFD values at timepoint 1 and 2 (T1 and T2). (b) Change in HFD over time. Each line represents a single patient. P-value indicates significance of paired sample t-test. (c) Overall comparison of HFD deviation for entire cohort. P-value indicates significance of independent sample t-test. Follow up time is indicated as number of months (##m). Dashed black line represents "ideal" HFD.

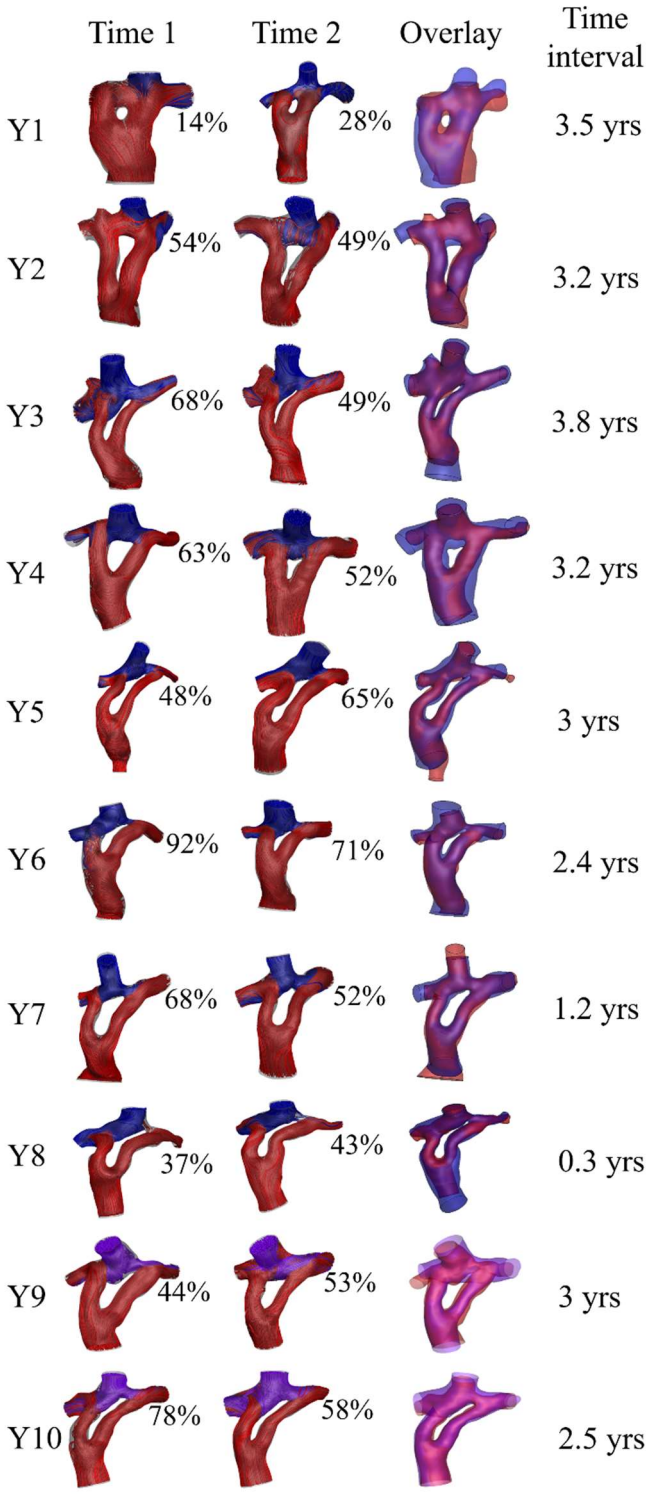

Figure 6-6 Streamlines for all Y-graft patients. The overlay image compares anatomies at time 1 (red) and time 2 (blue). Time interval shows time between time 1 and time 2. Hepatic flow distribution (HFD) is indicated by percent of HFD to the left pulmonary artery.

TCPC resistance decreased from 0.26 [0.12-0.42] to 0.15 [0.12-0.20] WU, but was not statistically significant (paired sample t-test, p=0.117, Table 6-2). TCPC resistance decreased for eight out of ten patients (Figure 6-7). On average, TCPC resistance decreased by 0.10 [-0.25, 0.01] WU. Individual resistance values can be found in Figure 6-7a.

a)

	Y1 (42m)	Y2 (39m)	Y3 (45m)	Y4 (39m)	Y5 (36m)	Y6 (29m)	Y7 (15m)	Y8 (4m)	Y9 (36m)	Y10 (30m)
R_{TCPC} T1	0.06	0.13	0.22	0.70	0.60	0.18	0.31	0.34	0.35	0.12
R_{TCPC} T2	0.33	0.15	0.14	0.11	0.18	0.13	0.14	0.23	0.17	0.11

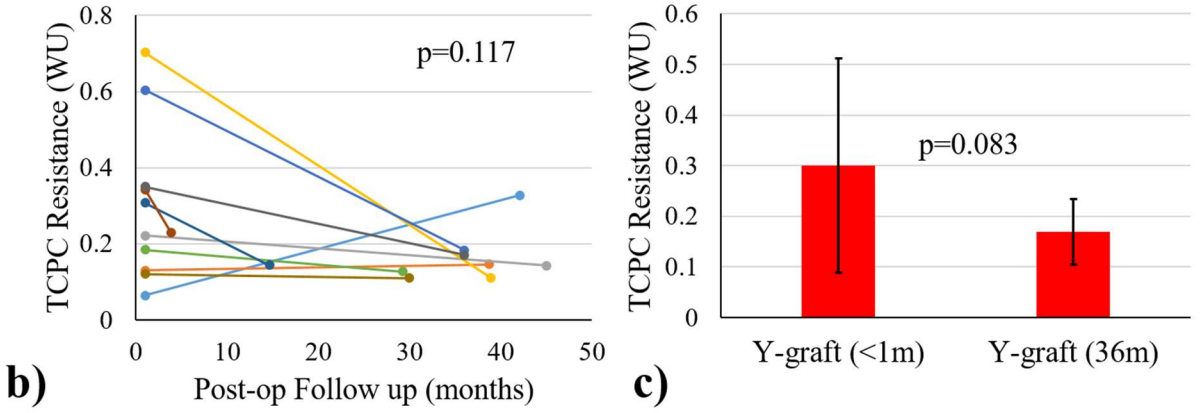

Figure 6-7 Serial comparison of Y-graft TCPC resistance (R_{TCPC}). (a) Individual patient R_{TCPC} values at timepoint 1 and 2 (T1 and T2). (b) Change in R_{TCPC} over time. Each line represents a single patient. P-value indicates significance of paired sample t-test. (c) Overall comparison of R_{TCPC} for entire cohort. P-value indicates significance of independent sample t-test. Follow up time is indicated as number of months (##m). TCPC: total cavopulmonary connection, WU: Wood units.

6.3.2.3 Comparison with LT/ECC

Three LT/ECC comparison groups were chosen using consecutive patients with (i) <3 year follow up, (ii) 3-6 year follow up, and (iii) >10 year follow up (n=10 for each group). These three groups were chosen in order to straddle the Y-graft follow up times since a comparison group with

identical, serial follow up times was not available. These 10 Y-graft patients are a subset of the 30 Y-graft patients included in the cross-sectional study. The clinical and hemodynamic data for all three LT/ECC comparison groups are shown in Table 6-3. Follow up times were significantly different for the three comparison groups: 0.57 [0.45-0.68], 5.25 [4.4-5.4], and 12.87 [12-15.7] years respectively ($p<0.001$ for each).

Table 6-3 Clinical and hemodynamic data for the LT/ECC comparison groups.

	LT/ECC Group 1 (FU <3 year) n=10	LT/ECC Group 2 (FU=3-6 year) n=10	LT/ECC Group 3 (FU >10 year) n=10
Age (years)	3 [2.75-4]	7 [6-7.25]	15 [14-17.75]
BSA (m^2)	0.63 [0.58-0.67]	0.83 [0.725-1]	1.55 [1.24-1.64]
Follow up time (years)	0.57 [0.45-0.68]	5.25 [4.4-5.4]	12.87 [12-15.7]
Gender	4/10 male	6/8 male	3/10 male
Morphology	5/10 HLHS	6/10 HLHS	5/10 HLHS
Fenestrated	7/10	7/10	6/10
Cardiac Index (L/min/m^2)	4.49 [3.48-4.78]	3.67 [2.82-4.09]	3.39 [3.02-3.64]
IVC flow (L/min/m^2)	1.05 [0.83-1.35]	1.55 [1.14-2.73]	1.60 [1.29-2.09]
SVC flow (L/min/m^2)	1.56 [1.19-2.47]	1.26 [0.94-1.84]	0.78 [0.57-0.98]
LPA flow (L/min/m^2)	1.13 [0.85-1.47]	1.01 [0.74-1.29]	10.6 [0.85-1.27]
RPA flow (L/min/m^2)	1.06 [0.88-1.44]	1.42 [1.09-2.49]	1.32 [0.95-1.69]
Qs (L/min/m^2)	2.85 [2.34-3.65]	2.80 [2.43-3.55]	2.46 [2.17-2.81]
Collateral flow (L/min/m^2)	1.76 [0.70-2.90]	0.32 [0.0-1.81]	0.67 [0.31-1.56]
PFD deviation (percentage points)	12 [5-21]	9 [4-16]	8 [3-15]
LPA stenosis (%)	39 [13-49]	47 [33-66]	32 [17-45]
RPA stenosis (%)	20 [9-31]	35 [10-58]	19 [8-32]
Overall PA stenosis (%)	31 [13-36]	38 [30-54]	22 [13-22]
TCPC resistance (WU)	0.16 [0.13-0.29]	0.10 [0.07-0.21]	0.18 [0.13-0.22]
HFD deviation (percentage points)	21 [13-37]	17 [6-44]	13 [7-16]

LT: lateral tunnel; ECC: extracardiac conduit; FU: follow up; BSA: body surface area; IVC/SVC: inferior and superior vena cava; LPA/RPA: left and right pulmonary artery; Qs: systemic return; PFD: pulmonary flow distribution; HFD: hepatic flow distribution; TCPC: total cavopulmonary connection.

Both Y-grafts and LT/ECC patients showed more balanced HFD as patients aged (Figure 6-8). Y-grafts improved quicker than LT/ECC. The Y-grafts at timepoint 2 (36 month follow up)

were significantly more balanced than the LT/ECC group with an earlier follow up time (p=0.009), and more balanced, though not statistically significant, than the two LT/ECC groups with later follow up times (p=0.059 and p=0.209 respectively, Figure 6-8a). TCPC resistance was not significantly different between any two groups (Figure 6-9). Large variations in TCPC resistance were seen at the earliest timepoints in both Y-grafts and LT/ECC patients, and decreased in the later timepoints.

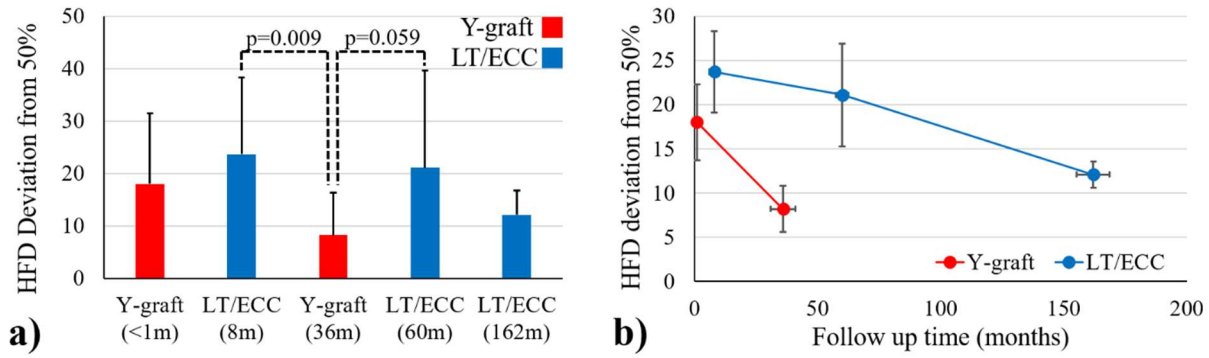

Figure 6-8 HFD comparison of Y-grafts and LT/ECC patients. Results are represented as both a (a) bar chart and (b) line graph to better compare groups. Error bars represent standard error in (b) for clarity. P-value indicates significance of independent sample t-test. No other comparison was significant. Follow up time is indicated as number of months (##m). HFD: hepatic flow distribution, LT: lateral tunnel, ECC: extracardiac conduit.

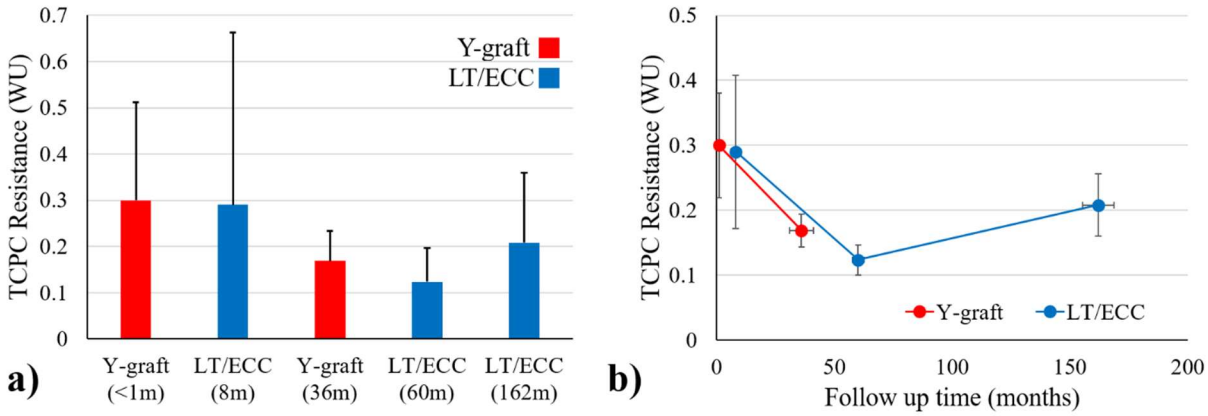

Figure 6-9 TCPC resistance comparison of Y-grafts and LT/ECC patients. Results are represented as both a (a) bar chart and (b) line graph to better compare groups. Error bars represent standard error in (b) for clarity. No statistical comparison between groups was significant. Follow up time is indicated as number of months (##m). TCPC: total cavopulmonary connection, LT: lateral tunnel, ECC: extracardiac conduit, WU: Wood units.

6.4 Discussion

6.4.1 Cross-sectional comparison

6.4.1.1 Y-Graft Hemodynamic Performance

As expected, PFD deviation is relatively low and on average there is about a 25% difference in overall flow rates to the LPA and RPA. This flow split is determined partially by branch pulmonary artery stenosis as well as overall lung resistance.[95] HFD deviation was higher and more variable than expected and will be discussed in the following section. The effect of LPA stenosis on iPL is also an expected result. Blood accelerates through the stenosis region and then decelerates as the vessel returns to its original size according to the conservation of momentum principle. These changes in velocity result in an increased pressure drop across the TCPC (lower efficiency) which leads to an increased iPL. The LPA is a common site for stenosis and Figure 6-2 shows that the most severe LPA stenosis anatomies have the highest iPL.[61]

The distribution of TCPC resistance raises concern for a number of Y-graft patients. In this study, Y-graft TCPCs are seen to have resistances as high as 4.7 Woods units, and this increased level of vascular resistance could lead to venous hypertension/congestion. Liver failure and protein-losing enteropathy are thought to be direct results of elevated Fontan venous pressures.[34,52,53] The relatively even distribution of HFD deviation suggests that the Y-graft is not a "one size fits all" solution to accomplish evenly split hepatic flow to the lungs. While 13% of Y-graft patients had very balanced HFD, nearly a quarter of patients had >90% hepatic flow directed to either the left or right lung. The effectiveness of Y-graft use seems to be multi-factorial and extremely patient specific, suggesting the need for pre-operative, individual surgical planning via computational modeling.

6.4.1.2 Representative Y-Graft Cases

The ability of a Y-graft to evenly split hepatic flow is highly dependent on PFD, the location of branch PA stenosis and IVC/SVC flow collisions, among other factors. A difference in PFD can cause two Y-grafts with very similar anatomies to have drastically different HFDs. This can be seen in Figure 6-3, where Y2 and Y5 have PFDs of 24% and 65%, respectively. Despite similar anatomies and Y-grafts, the HFD for these cases are considerably different (48% and 81% to the LPA, respectively). A comparison between Y1 and Y4 illustrates the effect of IVC/SVC flow collision on HFD. Both cases have balanced PFD and similar sized PAs, but Y1 has a medially positioned SVC, while Y4's SVC is positioned more superior to the left Y-branch. The SVC flow collision in Y4 forces some SVC flow into the left Y-branch which causes hepatic flow to preferentially course through the right Y-branch. The result is a very unbalanced HFD for Y4 (12% to the LPA) and relatively balanced HFD for Y1 (65% to the LPA).

Stenosis is commonly seen in Fontan anatomies;[61] Y2, Y3, Y5 and Y6 all have severe stenosis in either the pulmonary arteries or Y-graft branches. For single SVC anatomies (Y2, Y5), mid-PA stenosis influences SVC flow which will preferentially follow the path of least resistance (in these cases towards the RPA). For an unbalanced PFD case, if the mid-PA stenosis is located on the same side as the PA receiving the majority of pulmonary flow, then the stenosis blocks most SVC flow and this PA receives the majority of its flow from the hepatics and will therefore have an unbalanced HFD (Y5). However, the opposite is true if the stenosis is located on the low PFD side; in this case hepatic flow is able to move towards both PAs resulting in more balanced HFD (Y2). For bilateral SVC anatomies (Y3), mid-PA stenosis can "separate" the two SVC flows and HFD will be highly dependent on the individual SVC and overall PA flows. If SVC flows are similar and PFD is balanced, a balanced HFD is expected. Y6 shows a case with severe stenosis located in the left Y-branch, and as a result hepatic flow is very limited through the stenosed branch. With the full range of flow rates, flow ratios, pulsatilities, unique geometries and stenosis locations, the ability of a specific Y-graft to achieve balanced HFD may not be intuitive. Again, Y-graft performance needs to be evaluated on an individual basis and all of these factors must be considered.

6.4.1.3 Y-graft vs LT/ECC

Average TCPC resistance was approximately 3x higher for Y-grafts than LT/ECCs. The most apparent explanation stems from the geometry of the Y-graft itself. With commercially available Y-grafts, the diameter of the base of the Y-graft is evenly split between the two branches. For example, a 20mm (diameter) Y-graft will have two 10mm (diameter) branches. A basic calculation reveals that preserving diameter does not preserve area; this design results in a 50% reduction in

cross-sectional area as blood moves into the Y-graft branches. In essence, Y-grafts have a built-in 50% long segment "stenosis". In order to preserve cross-sectional area, the Y-graft branch diameter must be r*sqrt(2), where r is equal to the radius of the Y-graft before it splits into the two branches. Additionally, resistance is inversely proportional to the fourth power of the radius (Poiseuille's law). Therefore, blood traveling through 2 Y-branches with diameters half the size of the LT/ECC would analytically yield an 4x increase in resistance. According to the results presented here, the reduction in diameter and cross-sectional area inherent to commercially available Y-grafts has a greater negative impact on TCPC resistance than the venous flow collisions inherent to LT/ECCs. Therefore, "custom" Y-grafts which preserve cross sectional area as shown by Yang et al. may be the more promising option for successful Y-graft use, and may potentially provide an advantage over the LT/ECC Fontan pathway.[43,44]

Overall, HFD deviation was not significantly different between graft types. Both graft types were highly variable. The most important observation is the discrepancy in the number of patients at both the lowest (ideal) and highest (poor) HFD deviation (Figure 6-4e). In this study, Y-grafts have almost twice as many poor differential cases as ideal cases, while LT/ECCs show the opposite trend. These results highlight the need for pre-operative planning with Y-graft use as well as the design of individualized Y-grafts which are tailored for a specific patient. Potential modifications such as the angle of insertion, branch size and overall shape could lead to better HFD performance on an individual basis. A surgical modification already explored by surgeons includes "flaring" of the Y-graft branches at the anastomosis location. This allows the Y-graft branches to connect to the PAs in a more streamlined deisgn, rather than a perpendicular connection.

6.4.1.4 Additional Considerations

Particle residence time (PRT) was investigated for its potential impact on flow-induced thrombus formation, as well as to provide quantitative information about flow stagnation.[96,97] No differences between Y-grafts and LT/ECC were seen for minimum, mean or maximum residence times. As seen in Figure 6-4f, Y-graft iPL was more sensitive to LPA stenosis than LT/ECC iPL. PA stenosis may have a greater influence on the reduced flow through the closest Y-branch than it does on the total hepatic flow traveling through a LT/ECC connection. This difference would lead to a greater effect of stenosis on iPL for Y-grafts than LT/ECCs.

Several additional comparisons between graft types are important to note. First, PFD was identical between graft types at 46% to the left lung, indicating that graft type does not affect PFD. Additionally, there was significantly more PA stenosis ($p=0.02$) in the LT/ECC cohort as seen in Table 6-1. Even with significantly more PA stenosis, which is known to increase resistance, the LT/ECC cohort still had lower TCPC resistance than the Y-grafts. This strengthens the finding that commercially available Y-grafts inherently create higher TCPC resistance. Finally, the LT/ECC group includes both intra-atrial and extracardiac connections, while Y-grafts are always extracardiac. In this study, 10 of the LT/ECCs were intra-atrial. To ensure that these results were a consequence of graft type and not the intra-atrial vs. extracardiac variation, a sub-comparison was performed between these two groups. No statistically significant differences were found in this sub-comparison for iPL ($p=0.40$), PFD ($p=0.34$), or HFD deviation ($p=0.14$), and therefore the comparative results presented here are due to graft choice and not the difference between LT or ECC.

6.4.2 Serial Y-graft study

6.4.2.1 Hepatic Flow Distribution

Both Y-grafts and LT/ECC patients showed more balanced HFD as follow up time increased. However, Y-grafts improved at a faster rate (Figure 6-8). The Y-grafts (at 36 month follow up) had an HFD deviation less than half of the LT/ECC group at 60 month follow up. In addition, no LT/ECC timepoint (even at 13 year follow up) was as balanced as the Y-graft cohort.

In general, a more balanced HFD over time (for either graft type) may be explained in part by two main reasons: (i) more balanced overall pulmonary flow distribution and (ii) hepatic flow constituting a larger percentage of Qs as patients age. Though HFD is multifactorial, one key component is pulmonary flow distribution. In most cases, as PFD becomes more balanced, HFD becomes more balanced. In this study, both patient cohorts showed more balanced PFD as age increased, though not statistically significant (Table 6-2,Table 6-3). Secondly, it is well known that the IVC receives a larger portion of Qs as patients age.[98] As this percentage increases, graft positioning, flow interactions, and the location of stenosis etc. may have a diminished effect.

To illustrate with an extreme example, if 100% of Qs originates from the IVC (which includes hepatic flow), IVC flow will travel to the LPA and RPA regardless of graft placement. In this scenario, HFD would be completely determined by PFD, which is seldom extremely unbalanced (PFD deviation averaged 11±8 in this study). Therefore, as age and IVC flow increases it is expected that HFD will become more balanced regardless of graft type. Though both of these factors occurred at similar rates for the Y-graft and LT/ECC groups, Y-grafts exhibited an accelerated improvement in HFD when compared with the LT/ECC group (Figure 6-8b). This suggests that using a Y-graft provides an advantage over LT/ECC connections in terms of achieving a balanced HFD. The accelerated improvmenet in HFD likely occurs because Y-grafts are an inherently better option for achieving a balanced HFD. In the immediate pre-operative state,

patients have similar HFD despite which graft was used. This early similarity occurs because the body has not yet adapted to the new Fontan connection and factors such as pleural effusions are common which may mask the true performance of the surgical option. However, as follow up time increases and the body adapts, the differences between Y-grafts and traditional connections become more clear.

6.4.2.2 TCPC Resistance

Even with the "built in" 50% stenosis inherent to the design of commercially available Y-grafts, TCPC resistance was not significantly different between the Y-graft and LT/ECC groups. Overall PA stenosis was higher in the LT/ECC groups, but not to the extent of equaling the total (Y-graft + PA) stenosis seen in Y-graft patients. Therefore, avoiding caval flow collisions through Y-graft use must play a role in decreasing energy losses and lowering TCPC resistance. This encourages the use of a customized Y-graft design which would preserve cross-sectional area throughout the bifurcation.[40] By combining a "stenosis-free" graft design with the ability to avoid caval flow collisions, it is reasonable to think that Y-grafts could offer lower TCPC resistance than the standard LT/ECC connections. It remains unknown how TCPC resistance will differ between Y-grafts and LT/ECC connections at follow up times later than 31 months (our longest Y-graft follow up time). With increasing cardiac output as patients age, avoiding caval flow collisions may become a progressively more important factor. However, investigating this hypothesis will require longer-term follow up data.

6.4.2.3 Future Y-graft Use

While the cross-sectional study showed no significant difference in HFD between Y-grafts and LT/ECC, and significantly higher TCPC resistance in Y-grafts, these results may have been influenced by using the immediate post-operative state for Y-graft analysis. It is very challenging

to make long-term predictions of hemodynamics based on immediate post-operative MR data. Post-operative transient changes, such as fluid retention, pleural effusions, and acute changes to loading conditions all may have influenced the immediate post-operative scans. As more data emerge and further follow up information for these early Y-graft Fontan patients become available, the true utility in this technique will continue to be unveiled. Even though it is a more complex operation, with increasing experience the technical challenges of a bifurcated Fontan can be overcome, and the streamlining of caval flow may prove to be more beneficial for long-term hemodynamics.

Based on the current data, Y-graft Fontan connections are a viable surgical option with comparable hemodynamic performance. After the immediate post-operative state, Y-grafts offered more balanced HFD than LT/ECC connections without sacrificing energy efficiency. Though longer follow up data on this unique cohort will be instructive, future Y-graft use may be a proactive step to balance HFD and reduce PAVM development. Additionally, as suggested in previous studies, the use of an area preserving Y-graft design may offer further hemodynamic benefits.[40,43] As technology and biomaterials improve, the possibility to 3D print a Y-graft specifically designed for a patient may offer improved results.

7. SPECIFIC AIM 2A

Purpose: To investigate the relationship between total cavopulmonary connection hemodynamics and Fontan associated liver failure.

Hypothesis: The extent of liver fibrosis in Fontan patients is associated with poor Fontan hemodynamics.

7.1 Overview

Specific Aim 2A will use CFD modeling to investigate potential relationships between Fontan hemodynamics and liver failure. This aim will assess if (a) liver fibrosis is correlated with concurrent TCPC hemodynamics (at the same time point), and if (b) prior TCPC hemodynamics are predictive of future liver failure. Through our collaboration with the Children's Hospital of Philadelphia and their Single Ventricle Survivorship program, we have acquired concurrent MRI, catheterization and liver biopsy data for 33 Fontan patients. In addition, we have serial data (at a time point prior to the liver biopsy) for 21 of these patients. For each dataset, we will perform patient-specific simulations using MRI derived anatomy and blood flow waveforms. Fluid mechanic and anatomical metrics including pressure drop, TCPC resistance, energy loss, vessel size and percent stenosis will be calculated. Percent collagen deposition, as a measure of liver fibrosis, will be quantified using digital image analysis of Sirius Red stained slides.

7.2 Methods

This Specific Aim utilizes medical image processing, computational fluid dynamics, anatomy characterization and statistical analysis. Please refer to Chapter 4 for a detailed description of the methodology for each.

7.2.1 Study Design

This study includes two parts as shown in Figure 7-1. The first investiages the relationship between hemodynamics and liver fibrosis at the same time point, while the second part analyzes hemodynamic data collected more than 1 year prior to the liver biopsy to determine if hemodynamics are predictive of future liver fibrosis.

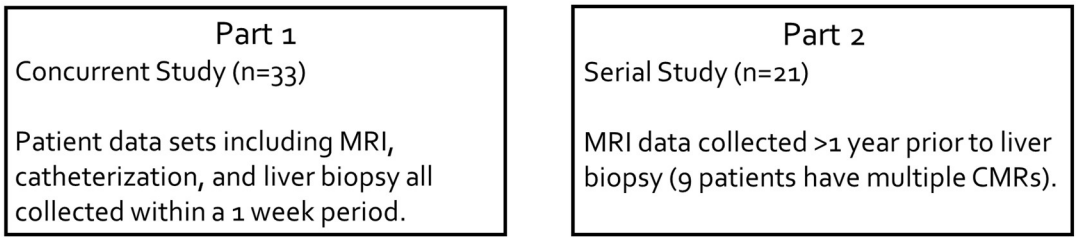

Figure 7-1 Two-part study design of Specific Aim 2a.

7.2.2 Patient Selection

Thirty-three single ventricle patients after Fontan completion were studied with concurrent CMR, cardiac catheterization and liver biopsy. All subjects were evaluated as part of an institutional recommended clinical care protocol for elective comprehensive assessment who are more than 10 years from their Fontan operation.[15] Indication for assessment was institutional recommendation for comprehensive surveillance, and not for any specific signs or symptoms of Fontan circulatory failure. No subject had any clinical signs or symptoms of hepatic dysfunction. This study cohort of 33 is a subset of a larger cohort of 67 patients who had catheterization and liver biopsy performed. Inclusion in the current cohort required that the cardiac catheterization,

MRI and liver biopsy were all performed within a six-month period. In most cases, CMR was obtained just prior to catheterization, and liver biopsy performed immediately following catheterization. Demographic data including age, gender, body surface area (BSA), Fontan type and Fontan duration was obtained for each patient. Fontan duration is defined as the time between the Fontan surgery and data collection. All patient data was obtained from the Children's Hospital of Philadelphia and was collected under IRB approval (IRB 12-009791) with written informed consent. All patient data for the concurrent portion of the study can be found in Appendix F – Specific Aim 2A Cross-sectional Patient data.

For part 2 of this aim (serial study), 21 single ventricle patients after Fontan completion were studied with CMR more than 1 year prior to liver biopsy. Similar to part 1, all liver biopsies were conducted as part of an institutional recommended clinical care protocol for elective comprehensive assessment who are more than 10 years from their Fontan operation. Indication for assessment was an institutional recommendation for comprehensive surveillance, and not for any specific signs or symptoms of Fontan circulatory failure. No subject had any clinical signs or symptoms of hepatic dysfunction. Inclusion in the current cohort required that the CMR was performed more than 1 year prior to liver biopsy. Demographic data including age, gender, body surface area (BSA), Fontan type and duration of Fontan physiology was obtained for each patient. Fontan duration is defined as the time between the Fontan surgery and data collection. All patient data were obtained from the Children's Hospital of Philadelphia and were collected under IRB approval (IRB 12-009791) with written informed consent. Ten of the 21 patients also had a CMR at the time of biopsy; these patients were included in a serial study investigating the relationship between changes in fluid mechanics and liver fibrosis. All patient data for the serial part of the study can be found in Appendix G – Specific Aim 2A Serial Study Patient data.

7.2.2.1 Hepatic Fibrosis Quantification

Liver biopsies were obtained using ultrasound guided percutaneous needle biopsy. Percutaneous biopsy was chosen over a transvenous approach in order to obtain a more representative sample of liver tissue and eliminate sampling bias in which more severe fibrosis may, theoretically, be found surrounding the hepatic veins. Anticoagulation was reversed with protamine at completion of the cardiac catheterization and liver biopsy performed by an interventional radiologist, obtaining one or two sample cores.

Quantitative determination of hepatic fibrosis was performed by an experienced pathologist using Sirius red staining for collagen with automated calculation of percent positive staining per slide.[30,99] Slides were stained with Sirius red and digitally scanned using Aperio Scanscope CS-O (Leica Biosystems, Vista CA). Whole slide image analysis with Color Deconvolution V9 algorithm was used to calculate quantitative percent collagen deposition by automated detection of the percentage of area containing Sirius red staining (Leica Biosystems, Vista CA). For subjects with biopsy specimens on multiple slides, the percentage of Sirius red staining was averaged across all slides.

7.2.2.2 Catheterization Protocol

All subjects were in a fasting state for eight hours prior to the catheterization, as per institutional policy. The use of light sedation, deep sedation, or general anesthesia was at the discretion of the catheterization team. Original pressure tracings and data from cardiac catheterization were reviewed and measurements were repeated to assure consistency of data

interpretation for all study subjects. Protocol included obtaining a hemoglobin level 6-12 hours after liver biopsy with comparison to pre-biopsy level, and overnight observation in a post-procedure recovery unit.

7.2.2.3 Hemodynamic Metrics

In addition to the hemodynamic metrics listed in the Methods chapter, two additional metrics were calculated in this study. Total ventricular power output was defined as the flow energy produced by the single ventricle in one cardiac cycle. This metric was calculated as $Power_{sv} = CO * P_{avg,sv}$ where the subscript 'sv' signifies single ventricle, CO is cardiac output and $P_{avg,sv}$ is the average pressure of the single ventricle. Ventricular power was converted to units of milliwatts. The percentage of total power output lost in the TCPC was calculated as $X_{TCPC} = 100 * \frac{PL}{P_{sv}}$, where PL is power loss in the TCPC.

7.3 Results

7.3.1 Concurrent Study (part 1)

7.3.1.1 Demographic Data

Patient demographic data is given in Table 7-1. The cohort was balanced in terms of gender and Fontan type. Single ventricle morphology included 45% hypoplastic left heart syndrome (HLHS) and 55% non-HLHS. Average patient age was 16.2±4.7 [7-26] years, with an average Fontan duration of 14.2±4.6 [5-24] years. The average percent collagen deposition was 21.3±8.7 [9-49] %, incorporating a wide range of hepatic fibrosis. No significant correlations were found between percent collagen deposition and age, BSA or Fontan duration. Percent collagen deposition was not significantly different when analyzed by gender, Fontan type or presence of

fenestration (Table 7-1). The average time between CMR and liver biopsy was 14±27 days, with a range of 0-102 and median of 1 day.

Table 7-1 Patient demographic data (n=33).

	Mean±SD [range]	Correlation Coefficient (rho)	p-value
Age (years)	16.2±4.7 [7-26]	-0.055	0.766
BSA (m^2)	1.5±0.3 [0.76-2]	0.044	0.811
Gender (male/female)	16/17	-	0.734
Fontan duration (years)	14.2±4.6 [5-24]	-0.073	0.693
Fontan type (extracardiac/intra-atrial)	17/16	-	0.236
Single ventricle morphology (HLHS/non-HLHS)	15/18	-	0.457
Presence of fenestration (yes/no)	13/20	-	0.803
Time between CMR and liver biopsy (days)	14±27 [0-102]	-	-

Correlations with percent collagen deposition are shown. Categorical variables show p-values for the appropriate independent samples test. Values are mean ± standard deviation [range]. BSA: body surface area; Fontan duration: time since Fontan procedure.

7.3.1.2 Fibrosis and Hemodynamics

A significant, positive correlation was found between percent collagen deposition and indexed IVC flow rate (rho=0.624, p<0.001, Figure 7-2a). Similarly, indexed IVC flow rate was significantly higher (p=0.008) in the upper tertile of percent collagen deposition scores compared to the lowest tertile (Figure 7-2b). Cardiac output was positively correlated with percent collagen deposition and approached statistical significance (rho=0.297, p=0.062, Table 7-2). No significant correlations were found between percent collagen deposition and caval or branch pulmonary artery pressures or flow rates. In addition, there were no correlations with pulmonary venous flow rates (Qp) or systemic to pulmonary collateral flow. Similarly, systemic vascular resistance (SVR), pulmonary vascular resistance (PVR), and IVC pulsatility index showed no significant correlations with percent collagen deposition (Table 7-2).

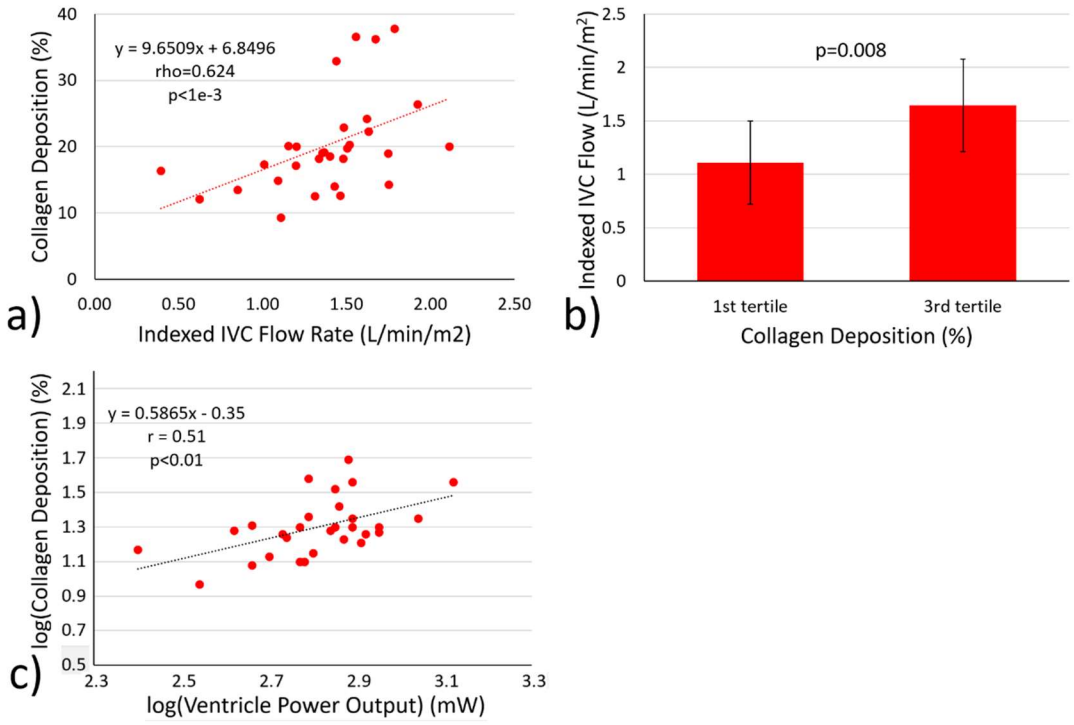

Figure 7-2 Effect of fibrosis on IVC flow and ventricle power output: (a) Correlation between IVC flow and percent collagen deposition; (b) Collagen deposition tertile comparison; (c) Correlation between percent collagen deposition and ventricle power output.

Table 7-2 Correlations between hemodynamics and percent collagen deposition.

	Mean±SD [range]	Correlation coefficient (rho)	p-value
Cardiac Index (L/min/m^2)	3.2±0.77 [1.6-5.4]	0.307	0.088
Cardiac Output (L/min)†	4.7±1.3 [2.5-7.5]	0.297	0.062
IVC flow (L/min/m^2)*	1.4±0.42 [0.39-2.6]	0.624	<1e-3
SVC flow (L/min/m^2)	0.80±0.36 [0.22-1.8]	0.160	0.390
LPA flow (L/min/m^2)	0.91±0.27 [0.32-1.7]	-0.105	0.575
RPA flow (L/min/m^2)	1.3±0.39 [0.71-2.4]	0.178	0.329
LPV flow (L/min/m^2)	1.3±0.32 [0.82-2.3]	0.037	0.849
RPV flow (L/min/m^2)	1.6±0.40 [1.0-3.1]	0.382	0.041
Collateral Flow (L/min/m^2)	1.07±0.71 [0.0-3.0]	0.091	0.625
IVC pressure (mmHg)	12.3±2.5 [6-16]	-0.038	0.840
SVC pressure (mmHg)	12.2±2.4 [6-16]	-0.051	0.787
LPA pressure (mmHg)	11.8±2.6 [6-17]	-0.154	0.417
RPA pressure (mmHg)	11.8±2.4 [6-16]	-0.096	0.607
SVR (WU/m^2)	20.7±8.3 [10.0-48.4]	-0.136	0.472
PVR (WU/m^2)	1.4±0.6 [0.37-2.9]	-0.247	0.181
IVC pulsatility index (%)	54±35 [19-162]	-0.159	0.401

*Values are mean ± standard deviation [range]. IVC: inferior vena cava; LPA: left pulmonary artery; LPV: left pulmonary vein; PVR: pulmonary vascular resistance; RPA: right pulmonary artery; RPV: right pulmonary vein; SVC: superior vena cava; SVR: systemic vascular resistance: * signifies statistical significance, † signifies a log transformation of the data.*

7.3.1.3 Fibrosis and Ventricular Function

Ventricular power output was positively correlated with percent collagen deposition (r=0.51, p<0.01, Figure 7-2c). Ventricular power output averaged 675±227 [253-1317] mW. No significant correlations were seen between percent collagen deposition and end diastolic volume, end systolic volume, stroke volume or ejection fraction (Table 7-3).

Table 7-3 Correlations between ventricular function and percent collagen deposition.

	Mean±SD [range]	Correlation coefficient (rho)	p-value
End diastolic volume (mL/m^2)	106±33 [45-181]	0.0061	0.974
End systolic volume (mL/m^2)	50±27 [7-125]	0.015	0.940
Stroke Volume (mL/m^2)	56±14 [35-87]	0.143	0.460
Ejection Fraction (%)	55±12 [27-85]	0.038	0.846
Ventricular power output (mW) *†	676±227 [253-1317]	0.51	<0.01

*Values are mean ± standard deviation [range]. * signifies statistical significance, † signifies a log transformation of the data. A Pearson correlation was used for the transformed data.*

7.3.1.4 Fibrosis and the Total Cavopulmonary Connection

LPA diameter was negatively correlated with percent collagen deposition and approached statistical significance (rho=-0.328, p=0.067, Table 7-4). There were no significant relationships between percent collagen deposition and IVC, SVC or RPA size, or the extent of caval or branch

pulmonary artery stenosis. Flow efficiency through the TCPC showed no significant correlations with percent collagen deposition (Figure 7-3). All individual data point values can be found in Appendix F – Specific Aim 2A Cross-sectional Patient data. TCPC resistance averaged 0.41±0.35 [0.10-1.63] WU. The percentage of total ventricular power output lost in the TCPC was 1.8±1.9 [0.24-8.17] percent. Indexed TCPC power loss averaged 0.11±0.09 [0.03-0.48]. Particle residence time did not correlate with percent collagen deposition with an average of 0.68±0.20 [0.18-1.11] seconds, corresponding to 0.84±0.26 [0.18-1.25] cardiac cycles. Velocity field and pressure drop maps are shown for a representative low and high percent collagen deposition case in Figure 7-4. Velocity magnitudes and pressure drops were slightly higher in the more severe fibrosis case, however this figure shows only a single time point in the cardiac cycle. These figures were made at the first timepoint in the cardiac cycle. The full simulation data is available on the server and may be used to create images at any point in the cardiac cycle for any patient of interest. Overall, no consistent, discernable differences in flow collisions, flow field features, streamlining, or pressure drop between low and high fibrosis cases were observed.

Table 7-4 Correlations between TCPC geometry, energetics and percent collagen deposition.

	Mean±SD [range]	Correlation coefficient (rho)	p-value
IVC diameter (mm/m^2)	11.6±2.9 [6.4-21.4]	-0.058	0.753
SVC diameter (mm/m^2)	9.4±2.5 [5.9-17.0]	-0.142	0.438
LPA diameter (mm/m^2)	7.1±1.1 [4.8-9.6]	-0.328	0.067
RPA diameter (mm/m^2)	7.4±2.1 [3.9-14.2]	0.016	0.933
IVC stenosis (%)	33±13 [10-58]	0.012	0.946
SVC stenosis (%)	29±15 [3-56]	-0.180	0.324
LPA stenosis (%)	51±18 [22-85]	0.112	0.543
RPA stenosis (%)	33±14 [1-66]	-0.025	0.892
IVC area (cm^2/m^2)	1.58±0.61 [0.56-2.72]	-0.025	0.892
TCPC resistance (WU)	0.41±0.35 [0.10-1.62]	-0.077	0.687
TCPC PL (% of total power output)	1.8±1.9 [0.24-8.2]	0.079	0.688
TCPC iPL	0.11±0.09 [0.03-4.9]	0.062	0.746
Particle residence time (s)	0.68±0.20 [0.18-1.12]	0.186	0.307

Values are mean ± standard deviation [range]. IVC: inferior vena cava; LPA: left pulmonary artery; RPA: right pulmonary artery; SVC: superior vena cava; TCPC: total cavopulmonary connection.

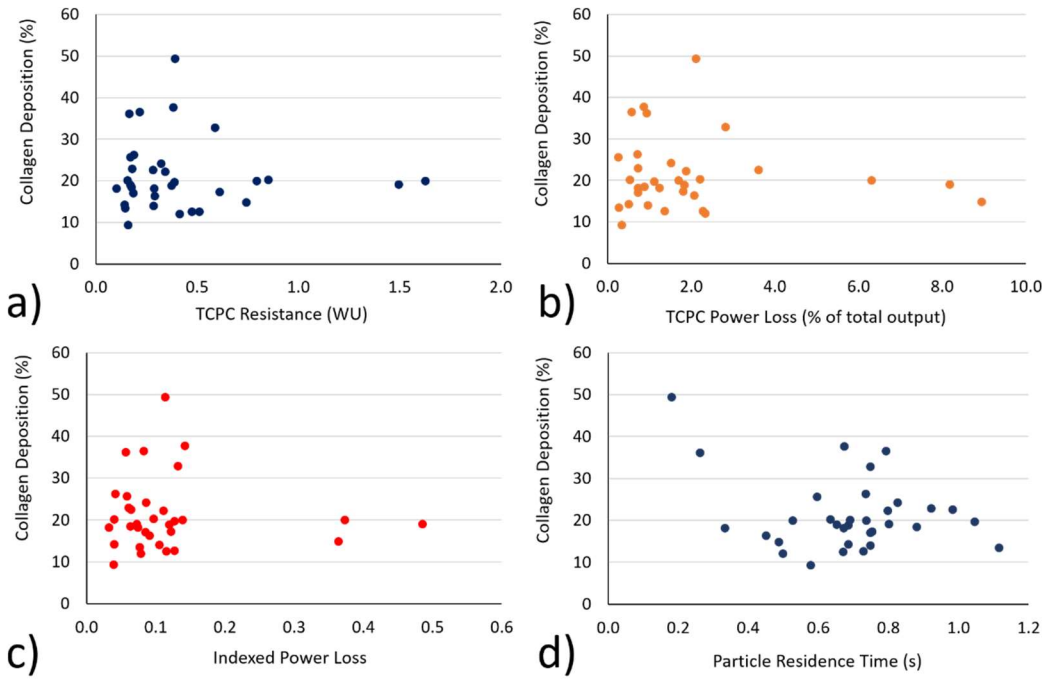

Figure 7-3 Relationship between TCPC energetics and liver fibrosis: Flow efficiency through the TCPC showed no significant correlations with percent collagen deposition. (a) TCPC resistance; (b) TCPC power loss (as percent of total power output); (c) indexed power loss; (d) particle residence time. TCPC = total cavopulmonary connection.

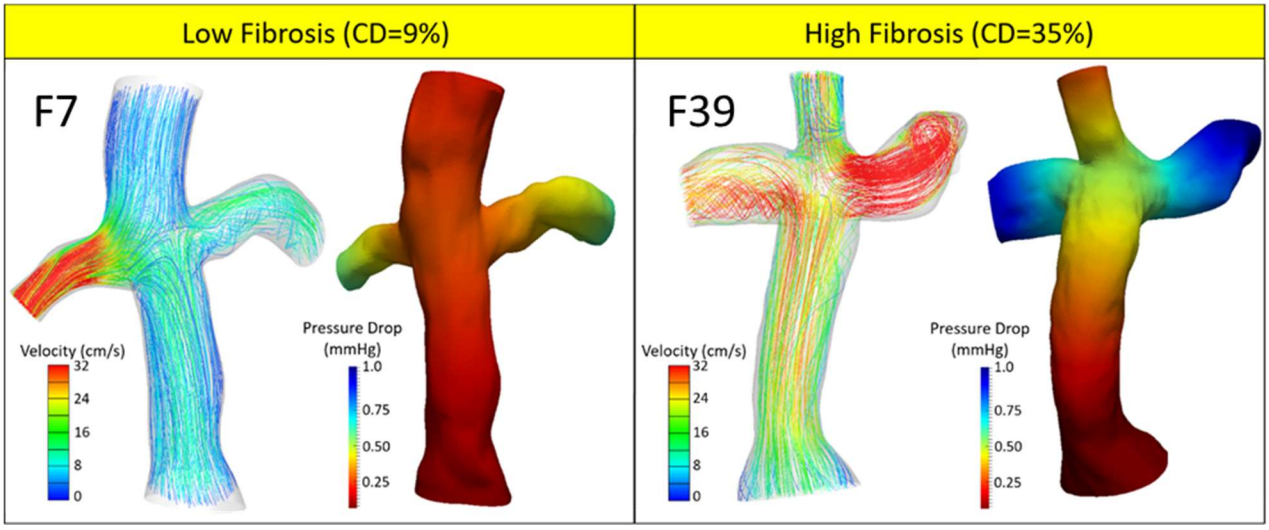

Figure 7-4 Total cavopulmonary connection velocity and pressure fields. Velocity field and pressure drop maps are shown for a representative low and high percent collagen deposition case. Overall, no consistent, discernable differences in flow collisions, flow field features, streamlining, or pressure drop between low and high fibrosis cases were observed. CD = collagen deposition.

7.3.2 Serial Study (part 2)

7.3.2.1 Demographic Data

Patient demographic data is given in Table 7-5. The cohort was 80% extracardiac conduits, 48% fenestrated and 38% male. Single ventricle morphology was composed of 66% hypoplastic left heart syndrome (HLHS) and 34% non-HLHS. All patients had CMR data at a time point >1 year before liver biopsy. Average patient age at CMR and biopsy was 11.6±5.9 [3-23] and 18.3±4.9 [11-29] years respectively, with an average time between CMR and biopsy of 6.7±2.9 [2-11] years. Fontan duration averaged 9.1±5.5 [0-21] and 15.8±4.7 [9-28] years at CMR and biopsy respectively. The average percent collagen deposition was 25±12 [7-49] %, incorporating a wide range of hepatic fibrosis. No significant correlations were found between percent collagen deposition and age, BSA or Fontan duration. Percent collagen deposition was not significantly different when analyzed by gender, Fontan type or presence of fenestration.

Table 7-5 Patient demographic data (n=21).

	Mean±SD [range]	Correlation coefficient (r)	p-value
Age at CMR (years)	11.6±5.9 [3-23]	-	-
Age at biopsy (years)	18.3±4.9 [11-29]	0.19	0.423
Time between CMR and liver biopsy (years)	6.7±2.9 [2-11]	-	-
Fontan duration at CMR (years)	9.1±5.5 [0-21]	-	-
Fontan duration at biopsy (years)	15.8±4.7 [9-28]	0.33	0.151
BSA at CMR (m^2)	1.1±0.4 [0.6-2.0]	-	-
Gender (male/female)	8/13	-	0.248
Single ventricle morphology (HLHS/non-HLHS)	14/7	-	0.684
Fontan type (extracardiac/intra-atrial)	17/4	-	0.341
Presence of fenestration (yes/no)	10/11	-	0.418
Collagen Deposition (%)	25±12 [7-49]	-	-

Values are mean ± standard deviation [range]. BSA: body surface area; Fontan duration: time since Fontan procedure. All correlation coefficients and p-values represent partial correlations between values and hepatic fibrosis controlling for the time between CMR and biopsy. P-value for categorical variables represents independent sample t-test.

7.3.2.2 Hemodynamics and ventricular function

No significant correlations were seen between percent collagen deposition and cardiac output, vessel flow rates, collateral flow or IVC pulsatility index (Table 7-6). Similarly, no

ventricular function metric was significantly correlated, including end diastolic volume, end systolic volume, stroke volume and ejection fraction (Table 7-6).

Table 7-6 Correlations between hemodynamics, ventricular function and percent collagen deposition.

	Mean±SD [range]	Correlation coefficient (r)	p-value
Cardiac Index (L/min/m^2)	3.3±0.6 [1.9-4.5]	-0.03	0.907
Cardiac Output (L/min)	3.9±1.4 [1.8-6.8]	-0.04	0.987
IVC flow (L/min/m^2)	1.5±0.4 [0.9-2.2]	0.19	0.434
SVC flow (L/min/m^2)	0.9±0.4 [0.2-1.7]	-0.32	0.166
LPA flow (L/min/m^2)	1.0±0.3 [0.5-1.7]	-0.04	0.876
RPA flow (L/min/m^2)	1.1±0.3 [0.6-1.7]	0.07	0.790
Collateral Flow (L/min/m^2)	1.0±0.7 [0.0-2.5]	0.48	0.276
IVC pulsatility index (%)	52±42 [8-146]	0.22	0.630
End diastolic volume (mL/BSA$^{1.3}$)	70±23 [36-100]	0.33	0.424
End systolic volume (mL/ BSA$^{1.3}$)	28±11 [11-40]	0.31	0.452
Stroke Volume (mL/ BSA$^{1.3}$)	43±13 [26-62]	0.25	0.405
Ejection Fraction (%)	62±6 [56-72]	-0.13	0.775

Values are mean ± standard deviation [range]. IVC: inferior vena cava; LPA: left pulmonary artery; RPA: right pulmonary artery; SVC: superior vena cava. All correlation coefficients and p-values represent partial correlations controlling for the time between CMR and biopsy.

7.3.2.3 TCPC geometry and energetics

TCPC resistance showed a positive correlation (r=0.54, p=0.026, Table 7-7) with percent collagen deposition (Figure 7-5a). TCPC resistance averaged 0.19±0.12 [0.06-0.44] WU. No significant relationships were seen with other efficiency related metrics including indexed power loss and pressure drop, which averaged 0.04±0.03 [0.01-0.11] and 0.49±0.25 [0.20-1.00] mmHg respectively. In terms of TCPC geometry, left pulmonary artery (LPA) stenosis averaged 32±26 [0-87]% and showed a positive correlation (r=0.55, p=0.028, Table 7-7) with percent collagen deposition (Figure 7-5b). Again, a conservative p=0.01 was used to determine significance to account for multiple testing. No other TCPC geometry metric, including vessel diameters or other measures of stenosis, were close to significant correlations with percent collagen deposition (Table 7-7). The streamlines and pressure drop for three representative cases of low, moderate and high percent collagen deposition with TCPC resistance and LPA stenosis noted are shown in Figure 7-6. All individual patient data used to create these plots can be found in Appendix G – Specific Aim 2A Serial Study Patient data.

Table 7-7 Correlations between TCPC geometry, energetics and percent collagen deposition.

	Mean±SD [range]	Correlation coefficient (r)	p-value
IVC diameter (mm/m^2)	18.0±6.5 [9.4-32.2]	-0.09	0.731
SVC diameter (mm/m^2)	13.8±4.9 [7.4-23.5]	-0.10	0.682
LPA diameter (mm/m^2)	10.9±3.4 [6.2-19.6]	-0.41	0.100
RPA diameter (mm/m^2)	11.7±4.8 [5.8-22.4]	-0.22	0.369
IVC stenosis (%)	21±12 [6-53]	-0.15	0.546
SVC stenosis (%)	10±13 [0-54]	0.13	0.629
LPA stenosis (%)	32±26 [0-87]	0.55	0.028*
RPA stenosis (%)	25±28 [0-84]	-0.24	0.316
TCPC resistance (WU)	0.19±0.12 [0.06-0.44]	0.54	0.026*
TCPC iPL	0.04±0.03 [0.01-0.11]	0.40	0.138
TCPC pressure drop (mm Hg)	0.49±0.25 [0.20-1.00]	0.06	0.817

Values are mean ± standard deviation [range]. IVC: inferior vena cava; LPA: left pulmonary artery; RPA: right pulmonary artery; SVC: superior vena cava; TCPC: total cavopulmonary connection. All correlation coefficients and p-values represent partial correlations controlling for the time between CMR and biopsy. An asterisk indicates statistical significance.

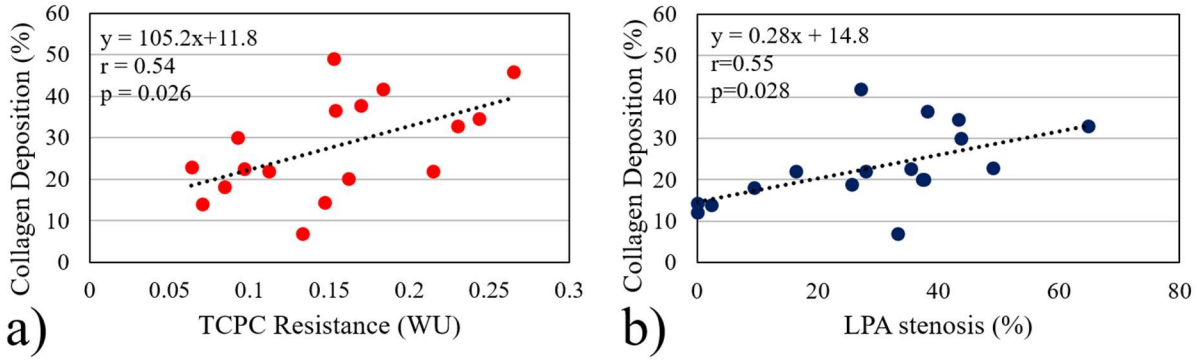

Figure 7-5 Effect of Fontan performance and stenosis on liver fibrosis: (a) Correlation between TCPC resistance and percent collagen deposition; (b) Correlation between LPA stenosis and percent collagen deposition. Correlation coefficient and p-value represent partial correlation controlling for time between CMR and biopsy. LPA: left pulmonary artery; TCPC: total cavopulmonary connection; WU: Wood units.

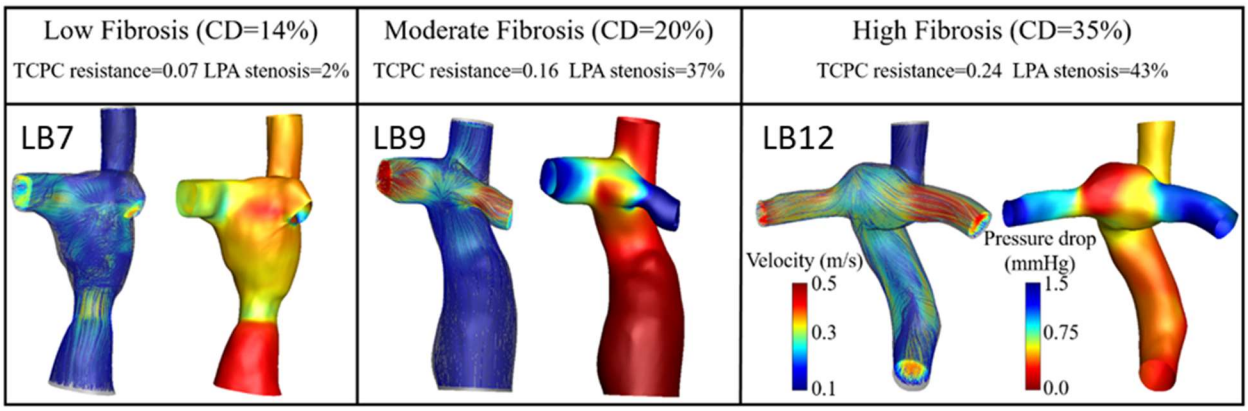

Figure 7-6 Velocity streamlines and pressure drop contours for representative (a) low, (b) moderate and (c) high fibrosis cases (in relation to this cohort). All panels use the same color scales shown in panel 3. TCPC resistance and LPA stenosis are noted for each patient. Resistance is given in Wood units. CD: collagen deposition; LPA: left pulmonary artery; TCPC: total cavopulmonary connection.

7.3.2.4 Serial CMR analysis

Ten of the 21 patients in this study had multiple CMRs (one >1 year prior to biopsy and another at the time of biopsy). This allowed for a preliminary investigation of potential

relationships between hemodynamic changes over time and liver fibrosis. One patient experienced premature ventricular complexes throughout one of their CMR examinations and was therefore excluded. Average time between serial CMRs was 7.3±3.3 [2, 12] years (Table 7-8). As seen with the full cohort in this study (Table 7-6), this subset of patients showed no significant relationship between IVC flow rate >1 year prior to biopsy and percent collagen deposition (Figure 7-7b). However, a significant, positive correlation ($r=0.91$, $p=0.001$, Table 7-8) was observed between the change in IVC flow rate (during the interval between the CMRs) and percent collagen deposition (Figure 7-7c). Similarly, an increase in TCPC resistance ($r=0.83$, $p=0.022$) showed a significant, positive correlation with percent collagen deposition. Importantly, these changes were not correlated to patient age, time between CMRs or Fontan duration. Finally, IVC flow rate at the time of biopsy was significantly related to percent collagen ($r=0.68$, $p=0.044$) deposition (Figure 7-7d), agreeing with our previous work. Figure 7-7a is provided to give a better understanding of the timing of the CMRs with respect to the biopsy, as well as the changes and absolute values for each patient.

Table 7-8 Correlations between changes in hemodynamic metrics over time with percent collagen deposition (n=9).

	Change between CMR1 and CMR2	Correlation coefficient (r)	p-value
Morphology (HLHS/other)	3/6	-	-
Gender (male/female)	3/6	-	-
Time between CMRs (years)	7.3±3.3 [2, 12]	-	-
BSA (m^2)	0.37±0.32 [-0.6, 0.85]	0.56	0.190
Cardiac Output (L/min)	0.94±1.0 [-0.15, 2.37]	0.71	0.072
Cardiac Index (L/min/m^2)	-0.32±0.43 [-1.0, 0.33]	0.05	0.912
IVC flow (L/min/m^2)	-0.03±0.22 [-0.31, 0.30]	0.91	0.001*
SVC flow (L/min/m^2)	-0.16±0.32 [-0.85, 0.14]	0.37	0.415
LPA flow (L/min/m^2)	-0.24±0.37 [-1.06, 0.08]	0.48	0.277
RPA flow (L/min/m^2)	0.10±0.34 [-0.52, 0.59]	0.36	0.433
Collateral flow (L/min/m^2)	0.17±0.46 [-0.52, 1.03]	-0.09	0.854
IVC stenosis (%)	11±11 [-2, 24]	0.03	0.957
SVC stenosis (%)	12±15 [-7, 45]	-0.31	0.492
LPA stenosis (%)	21±23 [-21, 50]	0.06	0.903
RPA stenosis (%)	11±34 [-54, 55]	-0.29	0.535
TCPC resistance (WU)	0.13±0.11 [-0.003, 0.29]	0.83	0.022*
iPL	0.05±0.05 [0.01, 0.157]	0.64	0.124
TCPC pressure drop (mmHg)	0.64±0.51 [0.07, 1.43]	0.73	0.062
IVC pulsatility (%)	-3±38 [-91, 36]	-0.36	0.423

Change is calculated as value at CMR2 – value at CMR1. Values are mean ± standard deviation [minimum, maximum]. IVC: inferior vena cava; LPA: left pulmonary artery; RPA: right pulmonary artery; SVC: superior vena cava; TCPC: total cavopulmonary connection. All correlation coefficients and p-values represent partial correlations controlling for the time between CMRs. An asterisk indicates statistical significance.

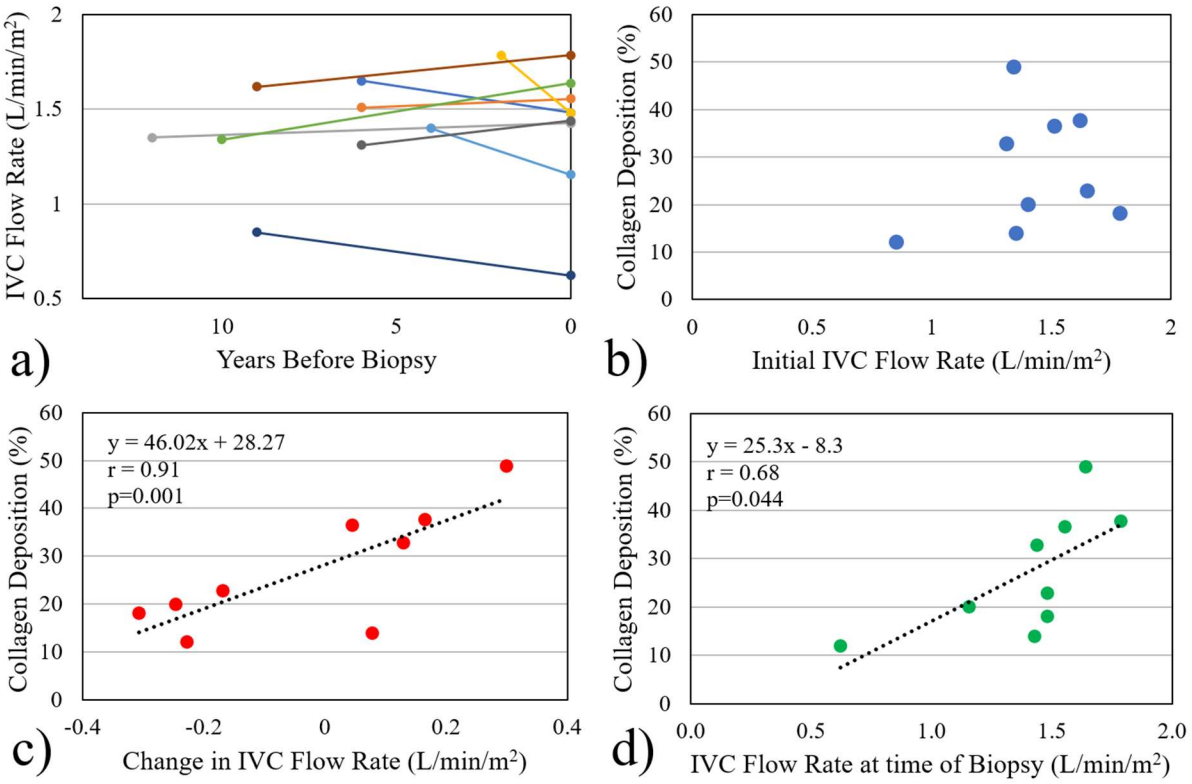

Figure 7-7 Relationship between percent collagen deposition and IVC flow rate. Changes in IVC flow rate over time are shown in (a). Each line represents an individual patient. Differences in correlations between percent collagen deposition and IVC flow rate were observed between time points before (b) and at the time of (d) biopsy. Additionally, the change in IVC flow rate (c) was significantly correlated with percent collagen deposition.

7.4 Discussion

Liver fibrosis is a serious complication of the current treatment strategy for Fontan survivors. In these patients, while achieving the benefits of reduced intra-cardiac mixing and increased oxygen saturation, this physiology comes at the obligatory cost of creating a state of chronically elevated central venous pressures. Given that venous congestion likely plays a primary role in this hepatopathy, we sought to investigate whether additional higher order variables such

as flow hemodynamics, efficiency, or pathway architecture might influence the degree of fibrosis seen by using CMR derived ventricular function, flows and computational flow dynamics.

Our study is particularly valuable as we have the unique opportunity of analyzing contemporaneous liver biopsy data in conjunction with detailed blood flow characteristics in each patient. The use of an accurate, high-resolution liver fibrosis quantification technique is necessary when investigating potential causes and risk factors of liver fibrosis. In this study, liver biopsy samples were analyzed in a unique manner specific to Fontan disease, by quantifying percent Sirius Red collagen staining.[30,99] This method of quantification allows for a more incremental, quantitative scale, which may be more sensitive to teasing out possible associative or causative processes than traditional, graded scoring systems developed for other (non-Fontan) fibrosis mechanisms.

This study demonstrated that in single ventricle patients exposed to Fontan physiology for a mean of approximately 14 years, significant positive associations exist between inferior vena caval flow (measured supra-hepatic) and ventricular power output at the time of biopsy. In addition, there was a significant positive correlation with cardiac output.

Interestingly, a positive association was seen between the degree of hepatic fibrosis and indexed IVC flow rate as well as cardiac output. We speculate that this is due to hepatic arterialization and thus increased hepatic venous return contributing to IVC flow and cardiac output. Hypervascular nodules and hepatic arterialization have been described in the patient with Fontan circulation, with localization of hypervascularity to the peripheral perfusion "watershed" areas of the liver.[100] This may reflect adaptation and attempt towards increased blood flow to regions of hypoperfusion and/or relative hypoxia, perhaps somewhat similar to the phenomenon of aorto-pulmonary collateral flow seen.[101] Liver angiogenesis and fibrogenesis have been linked,

with a complex interplay between the two processes based on the primary mechanism causing the fibrosis.[102] Although the precise mechanism is unclear, hepatic fibrosis after Fontan operation may lead to increased hepatic blood flow, increased venous return and may thus be a source for excessive volume loading of the single ventricle, again similar to systemic to pulmonary collateral flow or valve insufficiency scenarios. This notion requires further investigation. This idea dovetails with the finding of increased ventricular power output with increasing hepatic fibrosis. Progressive hepatic fibrosis may thus be a source for future ventricular failure. Interestingly, similar changes are seen in patients with alcoholic liver cirrhosis. Though the hepatic arterial buffer response is a complex system, scar tissue in the liver generally impedes flow from the portal vein and hepatic artery.[103] However, this may lead to the phenomena of arterilization which provides alternate, lower-resistance routes for blood through through liver. This can result in an overall increase in blood flow through the liver.

To investigate whether prior hemodynamics are associated with future fibrosis, the second part of this study included patients with CMR data obtained more than 1 year before liver biopsy. This study demonstrates that a significant, positive correlation exists between prior Fontan metrics (TCPC resistance and LPA stenosis) and future liver fibrosis in single ventricle patients after Fontan. Hemodynamic metrics were measured approximately seven years prior to liver biopsy. Fontan duration at the time of biopsy was approximately 16 years (Table 7-5).

With the TCPC positioned immediately downstream of the liver, increases in TCPC resistance and flow obstruction (LPA stenosis) may result in increased hepatic congestion. This worsened hemodynamic state may lead to progressive liver fibrosis over time, producing the positive correlations seen in this study. Though individual measurements of pulmonary vascular resistance (PVR) were not available for these patients at the time of CMR, PVR values reported in previous

studies suggest that the TCPC resistances calculated here are around 10% of PVR on average.[104] For the purposes of illustrating the variability between patients, if we assume a constant PVR of 2 WU for all patients (Egbe et al), TCPC resistance would range from 3% to 22% of PVR in this study (the ratio of TCPC resistance to PVR ranged from 4% to 107% in our previous study (Trusty et al.) including individual PVR measurements).[104,105] This approximation demonstrates the potential for TCPC inefficiencies to substantially affect total resistance downstream of the liver.

These findings encourage the consideration of pre-procedural planning to improve TCPC performance. Though commonly used for preventing or correcting pulmonary arteriovenous malformations by optimizing hepatic flow distribution (HFD), surgical planning can similarly be used to compare potential surgical options and optimize energy efficiency.[11,28,39] Furthermore, flow efficiency through a connection can be more difficult to visualize and predict than HFD since changes in velocity and pressure are nonlinear and not always intuitive.[106] Therefore, pre-procedural planning focused on flow efficiency may be even more informative for surgical decision making.

Similarly, interventional strategies may prove beneficial for patients post-Fontan with LPA stenosis or high TCPC resistance or those that demonstrate clinical hepatic decline. The significant, positive correlation between LPA stenosis and fibrosis seen in this study suggests that early correction of vessel stenosis may reduce the progression of liver disease in these patients. Whether this is due to the effect of LPA stenosis on TCPC resistance or some other factor, interventions such as balloon dilation may be important considerations in this post-Fontan population. Periodic monitoring of vessel stenosis may be useful to determine when or if these interventions are needed.

Important inferences can be made by comparing results between this longitudinal study and our previous cross-sectional study. One of the main conclusions from the previous cross-sectional

study was the positive correlation between IVC flow rate and percent collagen deposition (rho=0.624, p<0.001), reinforced by a significantly higher IVC flow rate in the upper tertile of fibrosis patients (p=0.008).[105] In the current study with IVC flow measured approximately 7 years prior to biopsy, no such relationship was observed (r=0.19, p=0.434). Though these results are the first of their kind and may serve only as preliminary results, they suggest that liver disease itself (fibrosis induced hepatic arterialization as hypothesized in our previous study) may be the cause of these significant differences in IVC flow at the time of biopsy. In addition, TCPC resistance and LPA stenosis showed significant correlations with fibrosis in this longitudinal study but not at the time of biopsy. This confirms our suspicion that hemodynamics at the time of biopsy may be more representative of the effects of liver disease rather than the cause.

Finally, the serial CMR analysis for the subset of nine patients in this study provides a more direct view of any causal relationships. In these nine patients, we see interesting changes in the correlations between IVC flow rate and percent collagen deposition over time. IVC flow rate showed no correlation with percent collagen deposition at a time point prior to biopsy (approximately 7 years before), but a significant relationship was seen in the change in IVC flow rate as well as the IVC flow rate at the time of biopsy (all flows indexed to BSA). These findings support the proposed mechanistic pathway illustrated in Figure 7-8. Data from this study suggests that an inefficient TCPC design and vessel stenosis may caused increased resistance to hepatic flow, therefore increasing pressure and resulting in increased hepatic congestion, contributing to the progression of liver fibrosis. In addition, the progression of liver disease may lead to hepatic arterialization (a compensatory mechanism) which decreases resistance to flow through the liver and leads to increases in IVC flow rate. Though the progression of liver disease in these patients

is undoubtedly a multifactorial issue, these data suggests that TCPC design and vessel stenosis are important contributing factors.

The relationship between hemodynamics and liver fibrosis may seem like a "chicken and the egg" scenario. With numerous and complex mechanicsms involved in the process, it can be difficult to tease out the cause and effect. Our preliminary explanation given here stems from the observation that TCPC resistance is corrected with liver fibrosis prior to biopsy, but not at the time of biopsy, and that the opposite is true for IVC flow (correlated at the time of biopsy but not prior to biopsy). We do not multiple liver biopsy measurements for these patients, so we cannot address how fast the liver fibrosis progressed or when it happened exactly. We are making the assumption that the time point prior to biopsy (~7 years before) the liver was relatively healthy without much fibrosis. Based on this assumption, we are proposing that metrics evaluated prior to biopsy are potentially a cause of liver fibrosis and not a result of liver fibrosis (since we are assuming liver fibrosis was minimal at this early timepoint). In addition, if a given metric was not correlated at the early timepoint, but is correlated at the time of biopsy, we are proposing that this change in relationship is a result of the progressing liver fibrosis. This logic will not hold in all situations, but in this preliminary study we feel it serves the reader well to propose a mechanistic link between these observations.

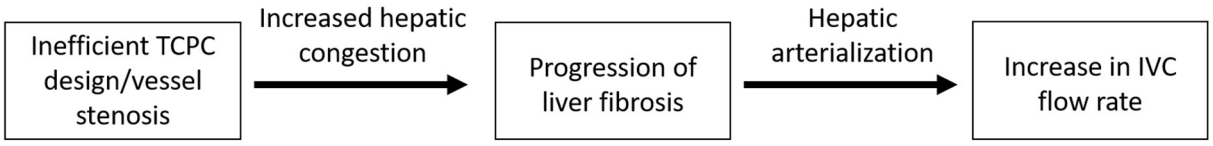

Figure 7-8 Proposed mechanism of the interaction between hemodynamics and liver fibrosis.

8. SPECIFIC AIM 2B

Purpose: To evaluate the use of ventricular assist devices to support the Fontan circulation and prolong liver health as a bridge to heart transplantation.

Hypothesis: Ventricular assist devices can decrease Fontan hepatic congestion by augmenting flow and decreasing inferior vena cava pressure.

8.1 Overview

Heart transplantation is currently the only option to fundamentally correct a failing Fontan heart. However, Fontan associated liver disease can be a contraindication to heart transplant, and combined heart and liver transplantation is extremely rare. Therefore, the purpose of Specific Aim 2B is to determine if VADs can be used to promote liver health in a failing Fontan patient until heart transplantation. In this aim we will use both experimental and computational modeling to determine if VADs are a viable option for right-sided Fontan support, and if VADs can decrease hepatic congestion in order to delay liver failure. To accomplish this, we will test 4 currently available pumps (Circulite, VentriFlo, PediMag and CentriMag) in a previously designed and validated Fontan mock circulatory loop. The experimental loop will be tuned to match "failing" Fontan pressures and flows acquired from clinical data. During these experiments we will evaluate each pump's ability to decrease hepatic pressure while increasing cardiac output. Additionally, the experimental data will be used to validate a mechanically assisted Fontan computational model. The computational model will then be used to investigate the effect of variations in cannula offset

and insertion angle, as well as address the generalizability of the experimental results across multiple patient anatomies.

8.2 Methods

This specific aim uses *in vitro* modeling to test several mechanical circulatory support devices in the context of a failing Fontan. Please refer to Chapter 4 for a detailed description of the mock circulatory loop, measurement techniques and devices tested.

8.2.1 Study Design

Four devices were tested in this specific aim. Each device following a similar experimental protocol as shown in Figure 8-1. A variety of cannulation strategies, baffle clamping methods and pumping parameters were investigated (depending on the individual device abilities and successes). These will be discussed in the following sections.

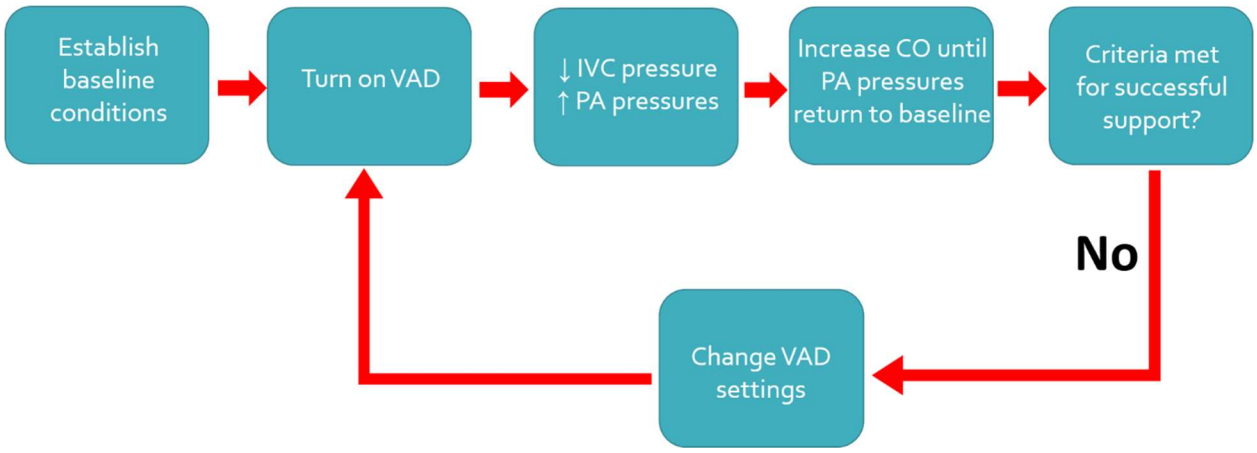

Figure 8-1 Experimental protocol for testing ventricular assist devices in the Fontan mock circulatory loop.

8.2.2 Patient Model

Substantial effort was spent in a previous study to develop a patient specific model that matches the bulk compliance of the actual TCPC.[80] This model represents a "standard" TCPC with two inlets and two outlets, a right-sided superior vena cava and typical levels of stenosis. The anatomy was segmented from CMR data under IRB approval (H092079). The TCPC model was constructed of transparent silicone with a bulk compliance of 1.36 mL/mmHg. Further details on the quantification of patient-specific compliance as well as the determination of the appropriate model wall thickness can be found in the study be Tree et al.[80]

8.2.3 Cannula and Baffle Restriction Strategies

Multiple cannula and baffle restriction strategies were tested including placing the VAD (1) in parallel with the Fontan baffle (inflow placed in the IVC near the diaphragm and egress located at the LPA/RPA confluence, Figure 8-2a), (2) in series with the Fontan baffle (same cannulation as (1) with baffle completely restricted, Figure 8-2c), and (3) performing a Fontan "takedown" and using the VAD as a true (albeit extracorporeal) right ventricle.

Additionally, in an attempt to reduce potential recirculation, a Y-graft outflow cannula (inserting downstream in each pulmonary artery, Figure 8-2b) was tested in series and in parallel. The main difference between scenario 2 and 3 is that SVC flow can move directly into the LPA/RPA in scenario 2, therefore it is not a complete Fontan "takedown." In scenario 3, all IVC/SVC flow must pass through the assist device before entering the pulmonary circulation. To experimentally achieve scenario 3, the pulmonary arteries were separated from the IVC/SVC using two clamps (Figure 8-2d). In addition to these 3 scenarios, various levels of baffle restriction (0-100%) were explored in the "in parallel" configuration. A schematic of the TCPC and VAD with vessels and cannula labeled is shown in Figure 8-2e. Outflow cannula position will vary based on

cannulation strategy. The results and implications of these cannulation options are discussed further in the following sections.

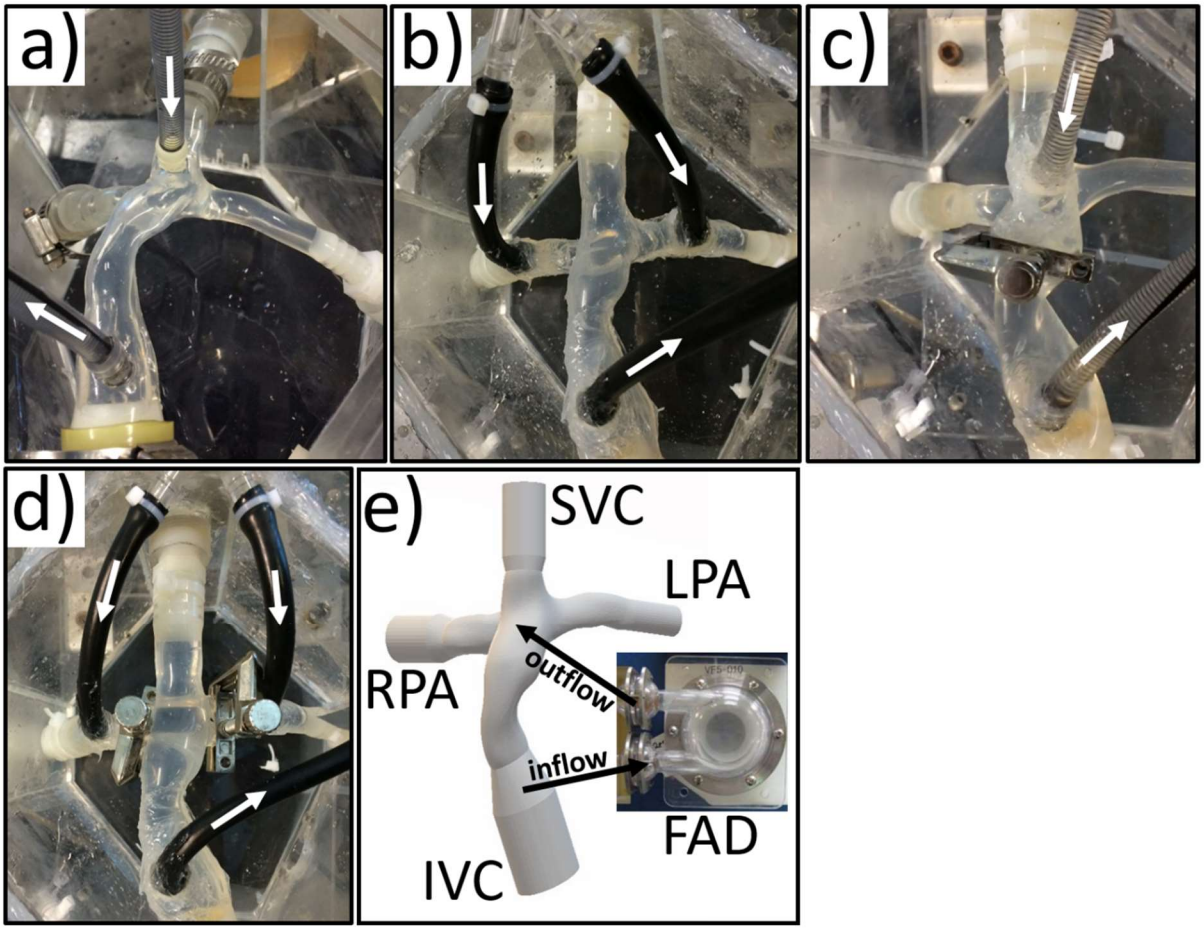

Figure 8-2 Cannulation strategies. (a) Ventricular assist device (VAD) in parallel with single outflow cannula. (b) VAD in parallel with Y-graft outflow cannula. (c) VAD in series (complete Fontan baffle restriction). (d) Fontan takedown configuration (vena cava separated from pulmonary arteries). (e) Schematic of total cavopulmonary connection and VAD with vessels and cannula labeled. Outflow cannula will vary based on cannulation strategy.

8.2.4 Banding Designs

A further investigation was performed looking into the effect of Fontan baffle banding design on hemodynamics. This was undertaken after realizing that complete baffle restriction was needed for certain devices. Five banding designs were 3D printed for evaluation. Following

Poiseuille's law, each band was designed to theoretically produce the same resistance to flow (resistance proportional to length/radius[4]). A description is shown in Figure 8-3. The results and implications of these banding options are discussed further in the following sections.

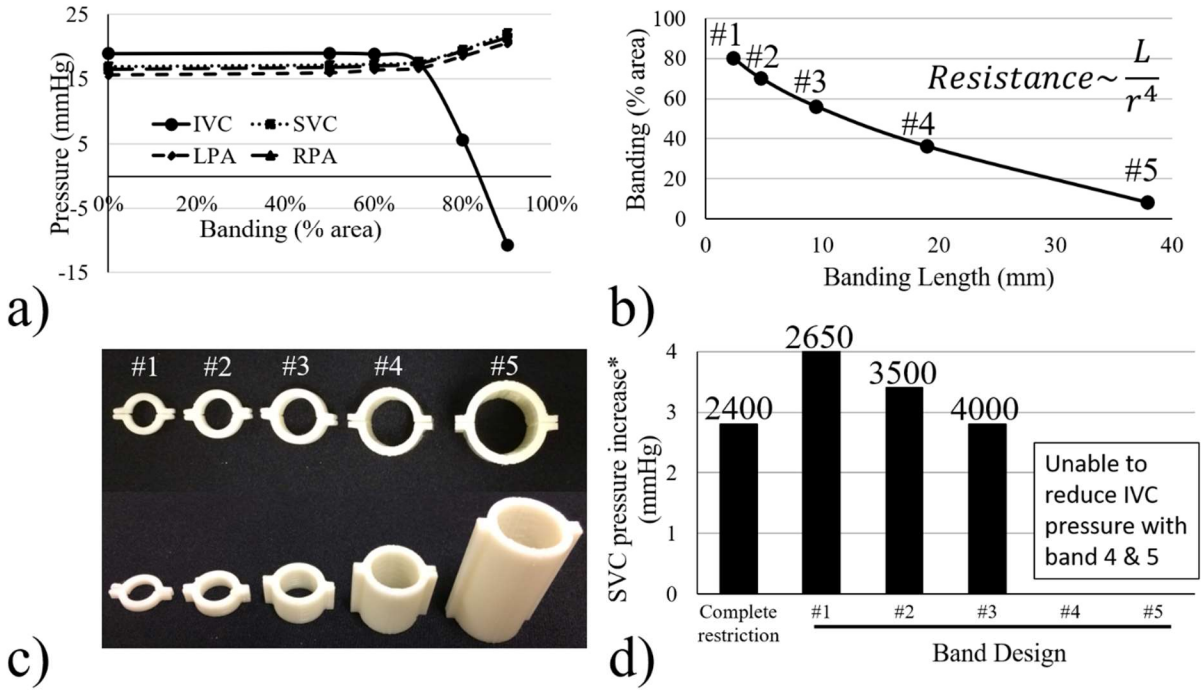

Figure 8-3 Effect of banding design on hemodynamics. (a) Effect of banding on pressure; (b) Theoretical relationship between banding length (L) and area to maintain resistance (r=radius); (c) Top and side views of the five custom banding designs; (d) Effect of banding design on SVC pressure (VAD rpms labeled above each bar). Banding is calculated as percent constriction by area. All points on the curve in (b) theoretically offer the same resistance. The asterisk in (d) indicates that SVC pressure increase was measured at the point when IVC pressure was reduced by 10 mmHg.

8.2.5 Experimental Protocol

In this study, successful Fontan support was defined as the ability to simultaneously decrease IVC pressure (Fontan pressure) by 5 mmHg and increase CO to 4.25 L/min (a 0.75 L/min increase).[107,108] These hemodynamic changes represent a significant improvement in the physiologic state of a patient. Patients with hemodynamics in this range are less likely to have

severe liver complications. If both criteria were met, the VAD configuration was deemed successful. Identical failing Fontan baseline conditions were first established in each scenario. The VAD was then turned on and a change in Fontan pressures was observed (as expected). If the IVC pressure decreased (reduced venous congestion) and PA pressures increased (improved ventricular filling and increased preload), ventricle adaptation (a shift in the pressure volume loop) was modeled by increasing the output of the "single ventricle" pump until the PA pressures returned to their baseline values (Figure 8-1). This is based on the assumption that the baseline PA pressures represent their homeostatic values. The resulting hemodynamic conditions were then compared to the criteria for success. If unsuccessful, the VAD configuration/parameters were adjusted and the process was repeated.

8.2.6 Computational Model

In addition to in vitro testing of commercially available mechanical assist devices, computational methods were used to explore Fontan circulatory support across multiple patient anatomies and cannulation variations. Importantly, computational methods were first validated by comparing with experimental results. The CentriMag device was modeled computationally after determining that it outperformed all other devices during in vitro testing. The CentriMag device was modeled computationally using a "fan" boundary condition in ANSYS Fluent. The pump performance curve from the instructions for use defining pressure and flow relationship for CentriMag was implemented into Fluent by fitting the performance curve with a third order polynomial. The coefficients for this curve were inputted into the fan boundary condition

parameters in Fluent. Computational fluid dynamics, anatomy and velocity segmentation methods followed those previously described in Chapter 4.

Six patients were modeled computationally (Table 8-1). Patients were chosen to offer a wide range of anatomies including variations in vessel sizes and IVC-SVC offsets, a variety of diagnoses and both intracardiac and extracardiac Fontan connections. All patient data were received from the Children's Hospital of Philadelphia with IRB approval (IRB: H05236). Cannulation options were modeling using SURGEM III. A baffle size of 10mm (diameter) was used as specified in the CentriMag IFU. Five unique combinations of insertion offset and insertion angle were modeled (all within the realm of surgical possibilities). Each position is spaced ½ cannula diameter horizontal or vertical from the other insertion locations. Five cannulation angles were modeled. Angle "n" represents an angle normal to the surface of the vessel wall. Angle "j", "l", "p" and "r" are positioned 50 degress away from normal as indicated in Figure 8-4. Fifty degrees was chosen to investigate extreme differences in cannula insertions. To focus on the most extreme possible cannulation insertions, specific combinations of position and angle were chosen to result in the most extreme differences in flow fields. For example, the combination of "ir" inserts the cannula to the "northeast" of the control ("en") and angles the cannula towards the "northeast", directing flow from the cannula to the "northeast" as much as possible. "en" serves as the control which represents the center position with an insertion angle normal to the vessel wall. The five cannulation variations investigated include "en", "ir", "gp", "cl", and "aj".

Table 8-1 Patient ID key for Specific Aim 2B.

Study ID	GT ID
Patient 1	CHOP011B
Patient 2	CHOP001B
Patient 3	CHOP057A
Patient 4	CHOP064A
Patient 5	CHOP081A
Patient 6	CHOP197A

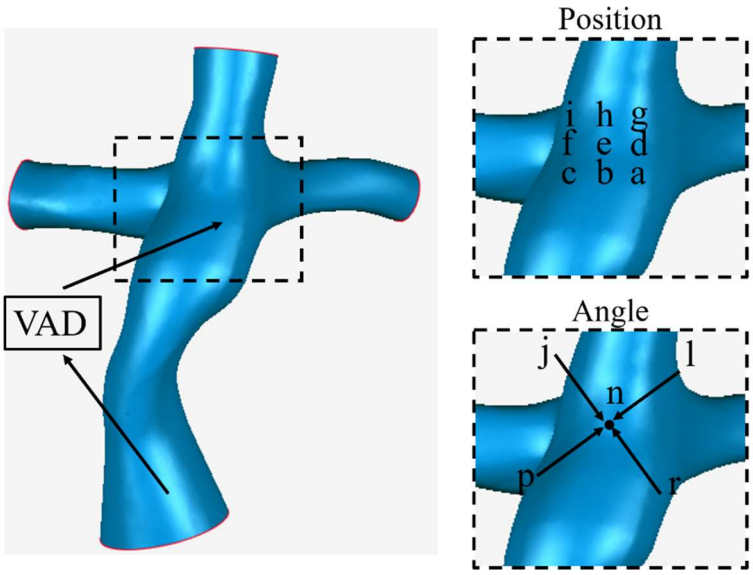

Figure 8-4 Cannulation options. A total of five options were investigated: "en", "ir", "gp", "cl", and "aj".

In addition, dye flow visualization techniques were utilized to better understand the fluid dynamics inside the TCPC. A 20% (by volume) solution of red dye was injected into the SVC at baseline failing Fontan conditions at various VAD rpms. A Phantom VEO 340L (AMETEK Vision Research, NJ, USA) high speed camera was used to record videos at 1000 frames per second to allow for a qualitative understanding of the flow fields within the TCPC.

Results from the computational modeling include wall shear stress, pressure gain from the vena cava to pulmonary arteries, power added and hepatic flow distribution. Wall shear stress was averaged over the cardiac cycle and across the entire surface area of the TCPC. Pressure gain was defined as the average pressure increase from the vena cava to the pulmonary arteries averaged over the cardiac cycle. The equation is given below:

$$Pressure\ gain = 0.5 * \left(P_{LPA,avg} + P_{RPA,avg} - P_{IVC,avg} - P_{SVC,avg}\right)$$

where $P_{LPA,avg}$, $P_{RPA,avg}$, $P_{IVC,avg}$, and $P_{SVC,avg}$ are the average pressure for the LPA, RPA, IVC and SVC, respectively, during the cardiac cycle. Power added was calculated using the same equation as commonly used for "power loss":

$$PL = \sum_{inlets} \int_A \left(p + \frac{1}{2}\rho v^2\right) v \cdot dA - \sum_{outlets} \int_A \left(p + \frac{1}{2}\rho v^2\right) v \cdot dA$$

where p is the static pressure, ρ is the blood density, A is the area of the inlet/outlet and v the velocity at the respective inlets or outlets. However, in this situation power is being added to the system, therefore the "power loss" value is negative. The percentage of TCPC wall area greater than 150 Pa was calculated as a measure of hemolysis potential. 150 Pa was chosen as a conservative estimate of the WSS threshold for hemolysis.[109] The percentage of wall area above 150 PA is defined as

$$\%\ Area\ above\ 150\ Pa = \ 100 * \frac{Area\ of\ TCPC\ wall\ above\ 150\ Pa}{Total\ surface\ area\ of\ TCPC\ wall}$$

8.3 Results

8.3.1 CircuLite

8.3.1.1 CircuLite in parallel

Figure 8-5 shows the mean pressure and flow rate changes induced by the VAD when placed in parallel with the Fontan connection (Figure 8-2a). The largest magnitude flow changes occur while running the VAD at 28,000 rpm, its fastest capable speed. At this speed, the IVC flow is increased by 0.07 L/min, but the SVC, LPA, and RPA flow rates decrease by 0.2, 0.06, and 0.07 L/min, respectively. The largest magnitude pressure changes also occur at 28,000 rpm VAD

rotational speed. The IVC, SVC, and LPA pressures decrease by 2.22, 1.08, and 0.43 mmHg respectively, and the RPA pressure increases by 0.63 mmHg at this rotational speed.

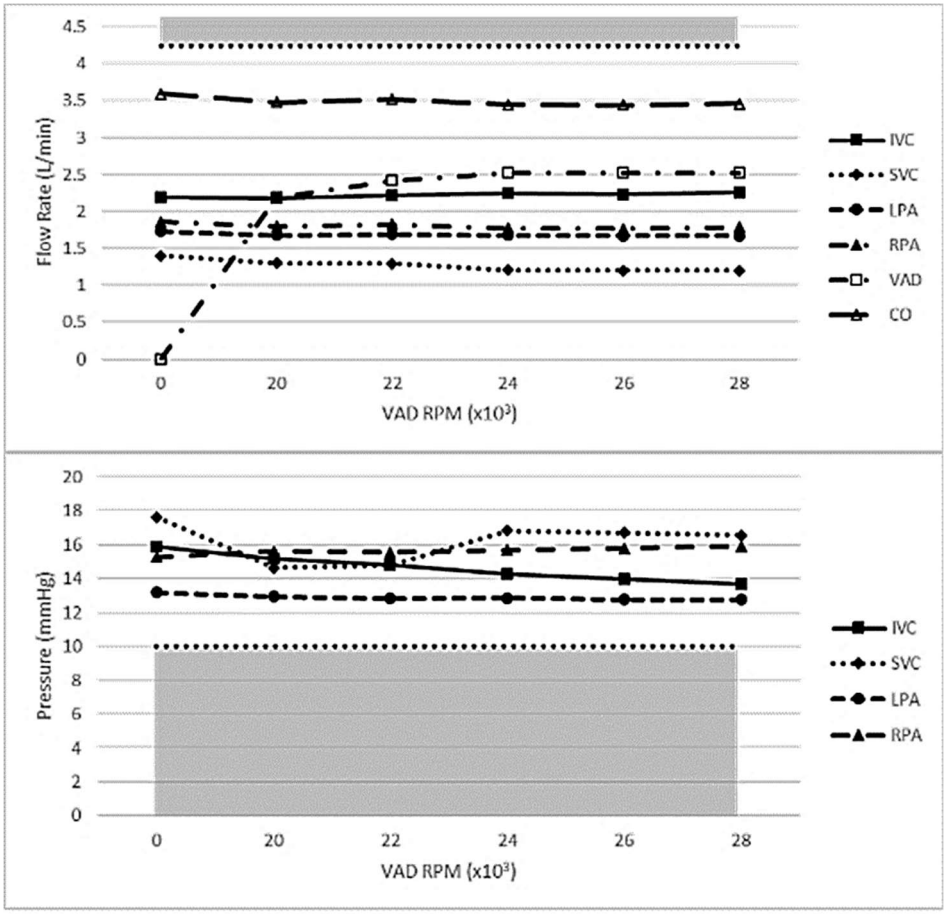

Figure 8-5 Fontan vessel mean flow rate (top) and pressure (bottom) values as a function of VAD rotational speed during the VAD in parallel scenario. The VAD flow rate is also shown for comparison. The shaded region defines areas of ideal circulatory support.

Ultimately, these results fall short of decreasing IVC pressure by 5 mmHg and augmenting CO by 0.75 L/min. Furthermore, although the VAD output was able to reach 2.5 L/min, (Figure 8-5) of flow, it only resulted in a negligible change in CO, suggesting significant recirculation. This was further confirmed by using a simple dye injection technique which demonstrated significant recirculation within the Fontan circuit and the VAD.

8.3.1.2 Restrictive banding

In order to minimize the recirculation observed in the previous configuration, graduated restriction was applied to test if restrictive banding would reduce the recirculation and what degree of restriction was needed.Figure 8-6 shows the mean pressure and flow rate changes with increasing levels of IVC banding while operating the VAD at 28,000 RPM. Table 8-2 lists the baseline mean flow rates and pressures when the VAD is not operating, for reference.

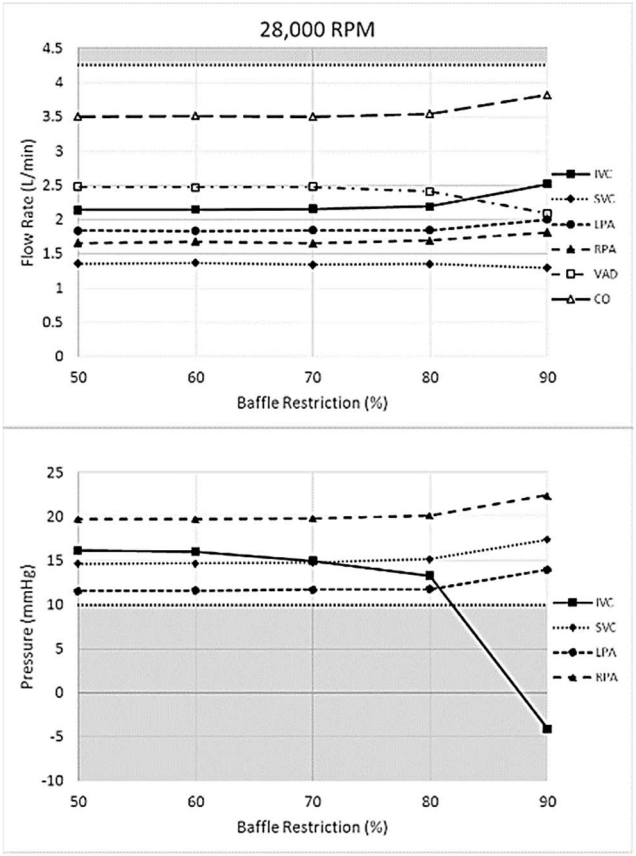

Figure 8-6 Flow rate (top) and pressure (bottom) changes as a function of baffle restriction %. The shaded region defines areas of ideal circulatory support.

Table 8-2 Fontan vessel flow rates and pressures at various VAD rotational speeds and baffle restriction levels during the baffle restriction examination scenario.

		Flow Rate (L/min)						Pressure (mmHg)			
VAD RPM	Baffle Restriction (%)	IVC	SVC	LPA	RPA	VAD	CO	IVC	SVC	LPA	RPA
0	0	2.15	1.36	1.89	1.62	--	3.51	16.78	14.96	12.18	19.17
28000	0	2.13	1.35	1.84	1.64	2.29	3.48	16.43	14.95	11.70	19.81
28000	50	2.14	1.36	1.84	1.66	2.48	3.50	16.16	14.65	11.57	19.72
28000	80	2.19	1.36	1.85	1.70	2.41	3.55	13.29	15.16	11.75	20.12
28000	90	2.52	1.30	2.00	1.82	2.09	3.82	-4.07	17.39	13.98	22.43

It was found that restrictive banding did not affect the Fontan connection mean flow rates and pressures and by extension, the degree of recirculation, until 80% restriction was applied. A 90% restriction caused nearly 0.4 L/min augmentation of CO, all of which was due to an increase in IVC contribution rather than recirculation. The same 90% restriction also caused 20.5 mmHg of pressure loss in the IVC, resulting in a negative pressure value and a physiologically collapsed vein. This suggested that separation of the SVC and IVC flow (with restrictive banding) reduced the preload for the VAD to the point where negative IVC pressure and suction events may become manifest. This would, therefore, be a sub-optimal, physiologically unacceptable operating scenario.

8.3.1.3 Circulite in series

VAD in parallel and restrictive banding scenarios resulted in less than ideal Fontan circulation support. Therefore, in an attempt to avoid recirculation and optimize the VAD preload, placement of the VAD in series was explored. As mentioned above, this involved take-down of the Fontan; with the new SVC IVC confluence serving as the preload chamber. The unifocalized branch pulmonary arteries served as the receiving vessel for the egress cannula. Figure 8-7 shows the mean pressure and flow rate changes induced by the VAD when placed in series with the Fontan connection.

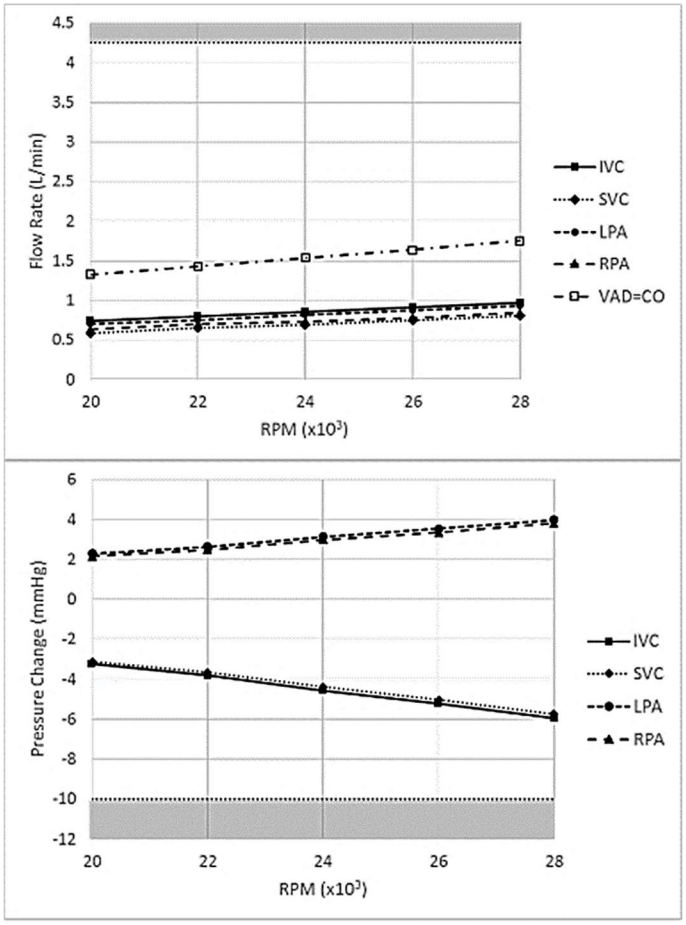

Figure 8-7 Flow rate (top) and pressure (bottom) changes as a function of VAD rotational speed during the VAD in series scenario. Note that during this scenario the VAD flow is equal to the cardiac output. The shaded region defines areas of ideal circulatory support.

The results show that the failing Fontan baseline set for the VAD in parallel and restrictive banding methods was not maintained during the VAD in series scenario (0 RPM). The failing Fontan baseline set was established with the Fontan connection intact. Taking down the Fontan connection to place the VAD in series with the caval veins and the pulmonary arteries forces an altered baseline condition, though all model resistances and compliances remain consistent. When the VAD is engaged, CO increases from 0.7 L/min to 1.75 L/min. This flow limit is achieved at the maximum speed of 28000 rpm which is the operating limit for the device. Additionally, IVC and SVC pressure drop by 5.9 mmHg while pulmonary artery pressure increases only 2 mmHg. Mean caval pressure drops an appropriate amount to be considered successful, and the CO is augmented by the VAD by ~ 1 L/min. However, the absolute magnitude of the CO is lower than previous scenarios, and much lower than physiological values of CO for Fontan patient support. Thus, the VAD in series scenario also fails to successfully meet both the support criteria, mainly due to the output capacity limitation.

8.3.2 Ventriflo

8.3.2.1 VentriFlo in parallel

When positioning the VAD in parallel with the Fontan baffle, a consistent pressure drop was observed across all vessels (Figure 8-8a). The pressure drop increased as VAD flow rate increased, with a pressure drop of approximately 4 mmHg as the VAD flow rate approached the total IVC flow rate. Following the experimental protocol, the inability of this configuration to

increase PA pressures prevented ventricle adaptation and no CO augmentation was achieved (Figure 8-8b). Values from selected experimental conditions are listed in Table 8-3.

The consistent pressure drop across all Fontan vessels, without a downstream increase in the PA pressures, indicates a significant amount of recirculation through the Fontan baffle as seen in our previous work.[60] Fluid exiting the egress cannula preferentially travels down through the Fontan baffle and back into the inflow cannula, effectively short-circuiting the Fontan connection and failing to add energy downstream in the PAs. In an attempt to decrease this recirculation, a Y-graft outflow cannula was used in order to deliver the VAD outflow further downstream in the PAs (Figure 8-2b). However, the results from this option were nearly identical to the single outflow cannula.

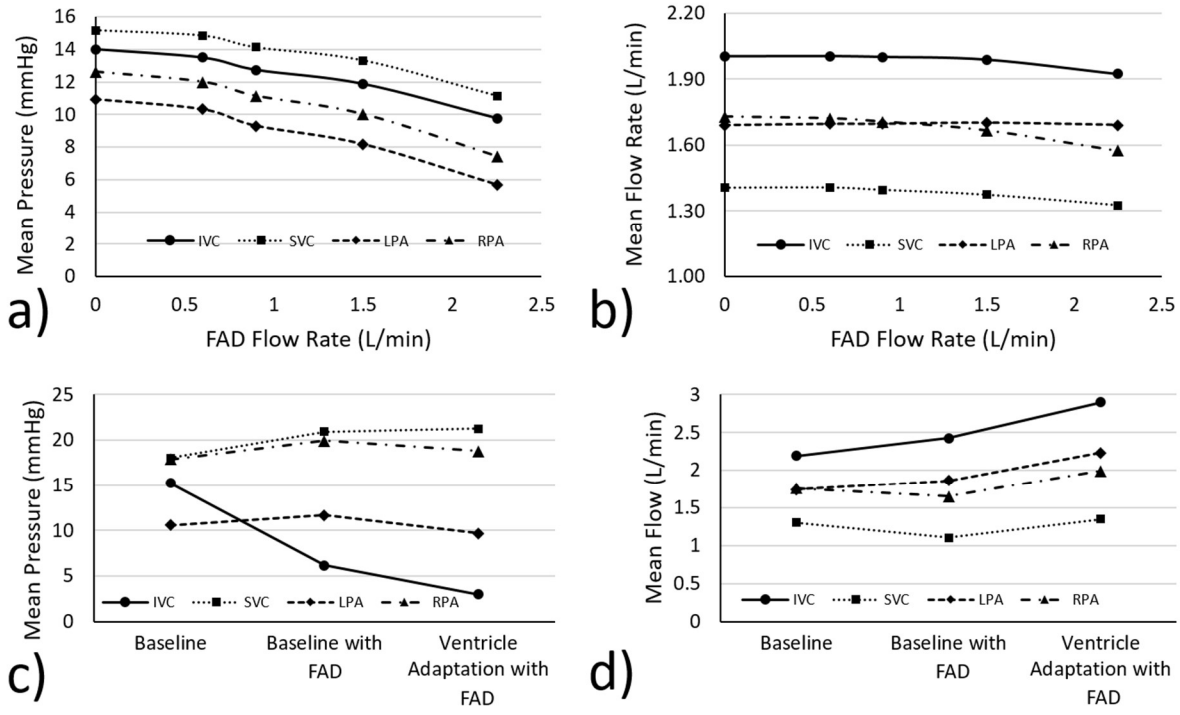

Figure 8-8 Hemodynamic changes caused by ventricular assist device (VAD) implementation. VAD in parallel: (a) mean pressures and (b) mean flow rates. Successful support achieved with VAD in series: (c) mean pressures and (d) mean flow rates.

Table 8-3 Hemodynamic measurements for ventricular assist device (VAD) configurations and parameter testing.

VAD Configuration		Average Flow Rate (L/min)					Average Pressure (mmHg)			
		VAD	IVC	SVC	LPA	RPA	IVC	SVC	LPA	RPA
In parallel (single outflow cannula)		0.0	2.0	1.4	1.7	1.7	14.0	15.2	10.9	12.6
		0.6	2.0	1.4	1.7	1.7	13.5	14.8	10.3	12.0
		0.9	2.0	1.4	1.7	1.7	12.7	14.1	9.3	11.1
		1.5	2.0	1.4	1.7	1.7	11.9	13.3	8.2	10.0
		2.3	1.9	1.3	1.7	1.6	9.8	11.2	5.7	7.4
In series (complete baffle restriction)	Baseline	0.0	2.2	1.3	1.7	1.8	15.2	18.0	10.6	17.9
	Baseline with VAD	2.4	2.4	1.1	1.9	1.7	6.2	20.9	11.7	19.9
	Ventricle Adaptation with VAD	2.9	2.9	1.4	2.2	2.0	3.0	21.3	9.7	18.8
Relative effects of VAD frequency	Baseline	0.0	2.2	1.3	1.7	1.8	15.2	18.0	10.6	17.9
	70 bpm	2.3	2.3	1.0	1.6	1.7	2.9	25.0	14.4	27.5
	140 bpm	2.4	2.5	1.1	1.8	1.8	2.8	21.3	11.1	22.7
	160 bpm	2.3	2.4	1.1	1.9	1.7	6.2	20.9	11.7	19.9
Relative effects of VAD ejection vs filling time	Baseline	0.0	2.1	1.4	1.8	1.8	19.0	21.8	13.4	21.7
	20%	2.1	2.2	1.3	1.8	1.8	5.8	22.8	12.1	22.2
	33%	2.1	2.2	1.3	1.7	1.8	5.8	21.9	11.5	21.3
	50%	2.1	2.2	1.3	1.7	1.7	6.1	21.5	11.4	20.7

The VAD was not in use during baseline measurements. Ejection vs filling time is indicated as ejection time (percent of VAD cycle).

8.3.2.2 VentriFlo in series

A restrictive banding around the Fontan baffle was then investigated as a means to decrease recirculation. The amount of restriction was iteratively increased from 0 to 100 percent (by area). Baffle restrictions up to 80% produced almost no hemodynamic differences when compared with the unrestricted option, and a 90% baffle restriction showed only minor differences in pressure

drop and flow augmentation. However, a complete restriction of the Fontan baffle was found to be a viable option.

With complete baffle restriction (effectively placing the VAD in series with the Fontan baffle), a substantial pressure drop in the IVC of approximately 10 mmHg was observed, along with a simultaneous increase in PA pressures of 1-2 mmHg (Figure 8-8c). These conditions promote ventricle adaptation, which was modeled by increasing CO until the PA pressures returned to their baseline values. In this "adapted" state, the mean flow rates were increased for all vessels with a resulting total cardiac output of 4.25 L/min (Figure 8-8d) and an IVC pressure approximately 10 mmHg lower than the baseline value (Figure 8-8c), thus meeting the defined criteria for successful support.

8.3.2.3 Complete Fontan "takedown"

Under the preload and afterload conditions that exist in the Fontan "takedown" configuration, the VAD could output a maximum of only 3.2 L/min, which was less than the baseline cardiac output. Therefore, this configuration was not successful.

8.3.2.4 VentriFlo pumping parameters

Achieving successful support required iterating through many different combinations of pumping parameters including flow rate, frequency, stroke volume, and ejection vs filling ratio (E/F ratio). During successful support, the VAD was operating at 160 bpm and a 66% E/F ratio, producing an output of 2.85 L/min with a stroke volume of approximately 17 mL. In an attempt to better understand the effects of these individual variables, a parametric sweep of VAD frequency and E/F (ejection to filling time) ratio was performed while holding all other parameters constant

(using the cannulation shown in Figure 8-2c). VAD frequency was varied between 70 and 160 bpm (holding VAD flow rate constant), and significant differences were noted in mean vessel pressure with IVC pressure increasing and PA/SVC pressure decreasing (Figure 8-9a). Varying the E/F ratio from 20% to 50% produced less significant hemodynamic changes than VAD frequency, with a maximum pressure drop of about 2 mmHg in the SVC/RPA (Figure 8-9b).

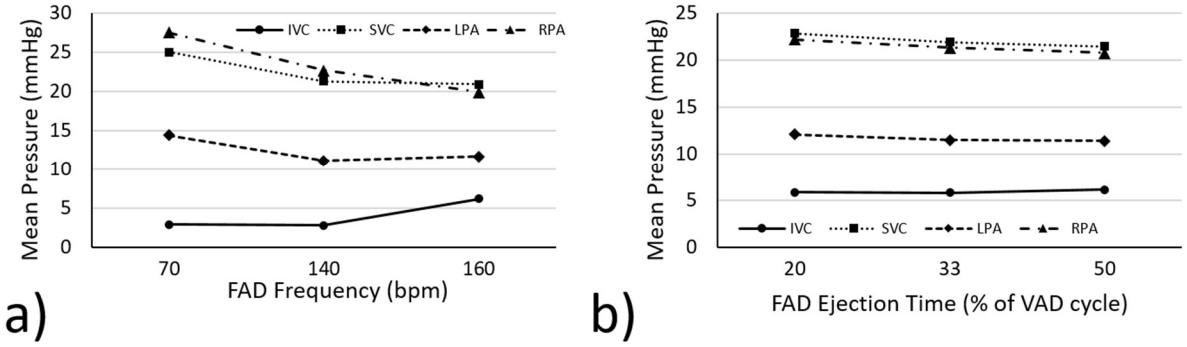

Figure 8-9 Effect of pumping parameters on hemodynamics. (a) Effect of ventricular assist device (VAD) frequency on Fontan pressures. (b) Effect of VAD ejection vs filling time on Fontan pressures. These measurements were taken using the VAD in series cannulation strategy (Figure 8-2c).

Altering VAD flow rate was inconsequential in the parallel configuration (affected only the amount of recirculation with no productive change in hemodynamics), and irrelevant in the Fontan takedown configuration (maximum VAD flow rate was less than the baseline cardiac output and therefore not a viable option). However, when positioned in series, VAD flow rate is the most important pumping parameter to achieve favorable changes in hemodynamics. Following intuition, if the VAD flow rate is below the original IVC flow rate it effectively limits the flow and substantially increases all upstream pressures. Conversely, if the VAD flow rate is greater than the original IVC flow rate it creates a "suction" and significantly decreases all upstream pressures.

Therefore, with a VAD flow rate greater than or equal to the original IVC flow rate, IVC pressure will decrease which may alleviate hepatic congestion, the hypothesized mechanicsm for Fontan associated liver disease.

8.3.3 PediMag

As with the CircuLite and VentriFlo devices, significant amounts of recirculation through the Fontan pathway (FP) were observed with the PediMag™ device. To reduce recirculation, various levels of FP banding were explored. Eighty percent FP restriction (by area) was required before any noticeable hemodynamic changes were observed (Figure 8-3a). Based on these findings, the impact of complete restriction of the Fontan pathway was assessed. With complete Fontan pathway restriction, PediMag™ was able to decrease IVC pressure by >10 mmHg while increasing PA pressures by approximately 2 mmHg at the baseline flow conditions (Table 8-4). Following the established experimental protocol, these favorable changes allow for ventricle adaptation, which was modeled by increasing cardiac output. PediMag™ easily surpassed the initial criteria for success, effectively maintaining decreased IVC pressure and increased PA pressures even up to a cardiac output of 5 L/min (Figure 8-10,Table 8-4). However, these improvements in hemodynamics were accompanied by an increase in SVC pressure of approximately 6 mmHg. Elevated SVC pressures may affect cerebral blood flow, enlarged veins in the head and neck and difficulty breathing and is therefore an unacceptable result.

Table 8-4 Hemodynamic measurements for PediMag™ and CentriMag™ at the baseline and adapted states. The asterisk indicates that PediMag™ required complete Fontan pathway restriction.

Device	Condition	VAD speed (rpms)	Average Flow Rate (L/min)					Average Pressure (mmHg)			
			CO	IVC	SVC	LPA	RPA	IVC	SVC	LPA	RPA
PediMag*	Baseline	0	3.5	2.1	1.4	1.76	1.74	16	16.6	14.0	15.2
	Baseline with VAD	2400	3.5	2.3	1.2	1.75	1.75	5.2	19.3	15.9	17.8
	Ventricle adaption to 4 L/min	2500	4.0	2.5	1.5	2.0	2.0	8.7	19.7	15.1	17.7
	Ventricle adaption to 4.5 L/min	2750	4.5	2.8	1.7	2.25	2.25	10.0	21.0	14.1	18.1
	Ventricle adaption to 5 L/min	3000	5.0	3.1	1.9	2.5	2.5	10.1	22.2	13.1	18.4
CentriMag	Baseline	0	3.5	2.1	1.4	1.75	1.75	17.2	16.0	14.0	16.4
	Baseline with VAD	2350	3.6	2.2	1.4	2.0	1.6	6.3	11.6	17.5	16.0
	Ventricle adaption to 4 L/min	2350	4.0	2.5	1.5	2.1	1.9	8.8	13.7	17.9	17.7
	Ventricle adaption to 4.5 L/min	2550	4.5	2.8	1.7	2.4	2.1	10.8	15.4	19.7	19.6
	Ventricle adaption to 5 L/min	3050	5.0	3.1	1.9	2.7	2.3	9.0	16.2	23.2	21.4

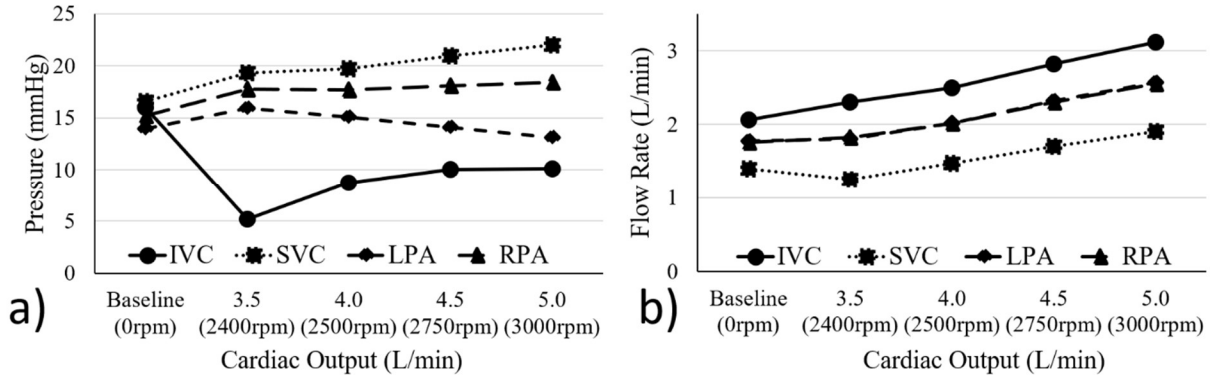

Figure 8-10 Hemodynamic changes achieved using PediMag™. (a) average pressures and (b) average flow rates. PediMag™ rpms are indicated below each cardiac output. LPA and RPA flow rates are nearly identical in (b) and therefore appear as a single line.

8.3.4 CentriMag

The need for higher output to overcome recirculation encouraged the testing of the CentriMag™ device. As shown in Figure 8-11, CentriMag™ was able to produce the desired hemodynamic changes with no FP banding. IVC pressure decreased ~10 mmHg while the average PA pressure increased ~1.5 mmHg (Table 8-4). In addition, SVC pressure decreased by ~4 mmHg, overcoming a major limitation of the PediMag™ device. Following these favorable changes, ventricle adaption was modeled (Figure 8-12). As with PediMag™, CentriMag™ could easily support a cardiac output up to 5 L/min while maintaining decreased IVC pressure and increased PA pressures (Table 8-4). Dye flow visualization techniques revealed that at high enough VAD output, SVC flow was pulled down through the FP and into the inflow cannula. This explains the decrease in SVC pressure seen with the CentriMag™ device while at the same time achieving increased forward flow through the pulmonary arteries.

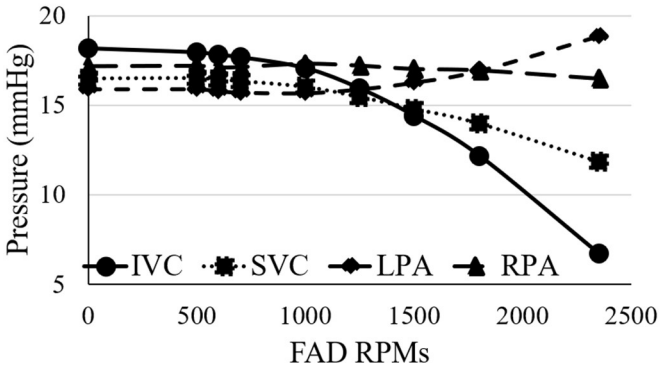

Figure 8-11 Effect of CentriMag™ rotational speed on Fontan pressures. This scenario required no banding of the Fontan pathway.

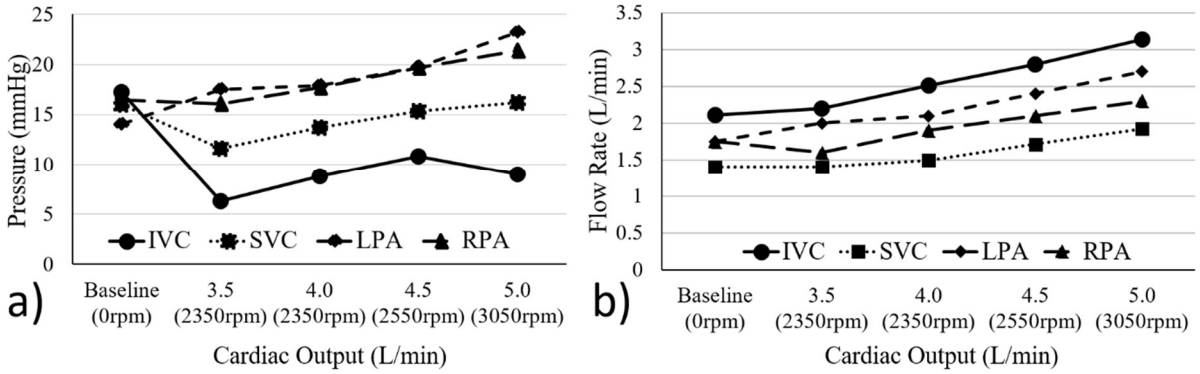

Figure 8-12 Hemodynamic changes achieved using CentriMag™. (a) average pressures and (b) average flow rates. This scenario required no banding of the Fontan pathway. CentriMag™ rpms are indicated below each cardiac output.

8.3.5 Computational modeling

8.3.5.1 Validation

Computational methods were first validated using the in vitro results. Figure 8-13 and Table 8-5 show very good agreement between the in vitro and computational results in terms flow rate and pressure changes. Importantly, the VAD flow rate was only 2% different between the two modeling techniques, proving that our method to model the pump computationally is accurate. Additionally, the average pressure increase from the vena cavae to the pulmonary arteries (the most important pressure metric) was only 1% different between techniques, again confirming the accuracy of the computational model.

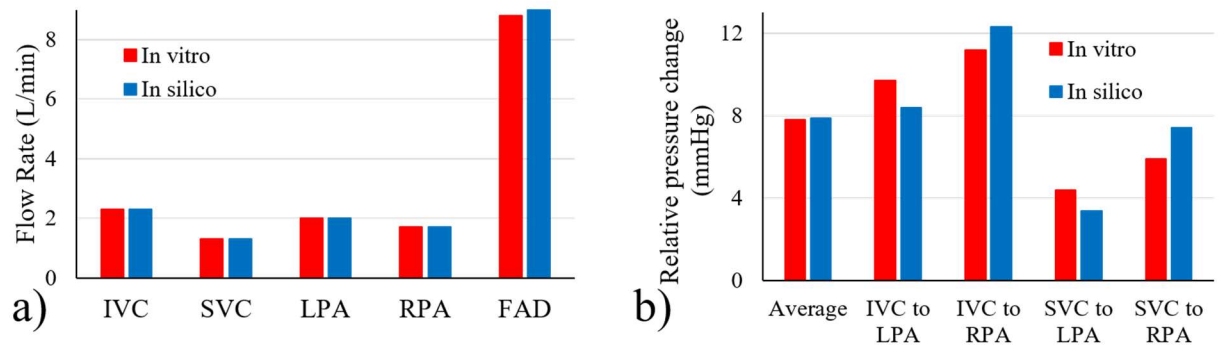

Figure 8-13 Comparison of (a) flow rates and (b) relative pressure changes between in vitro and computational results.

Table 8-5 Comparison of flow rates and relative pressure changes between in vitro and computational results.

Flows (L/min)	In vitro	In silico
IVC	2.3	2.3
SVC	1.3	1.3
LPA	2	2
RPA	1.7	1.7
FAD	8.8	9
Pressure Increase (mmHg)	In vitro	In silico
Average	7.8	7.9
IVC to LPA	9.7	8.4
IVC to RPA	11.2	12.3
SVC to LPA	4.4	3.4
SVC to RPA	5.9	7.4

Dye flow visualization techniques were used to better understand the flow fields within the TCPC. Dye was injected only into the SVC. Figure 8-14 shows good agreement between the in vitro and computational results at various VAD speeds. Slow motion dye flow visualization videos are provided for two rotational speeds in Appendix H.

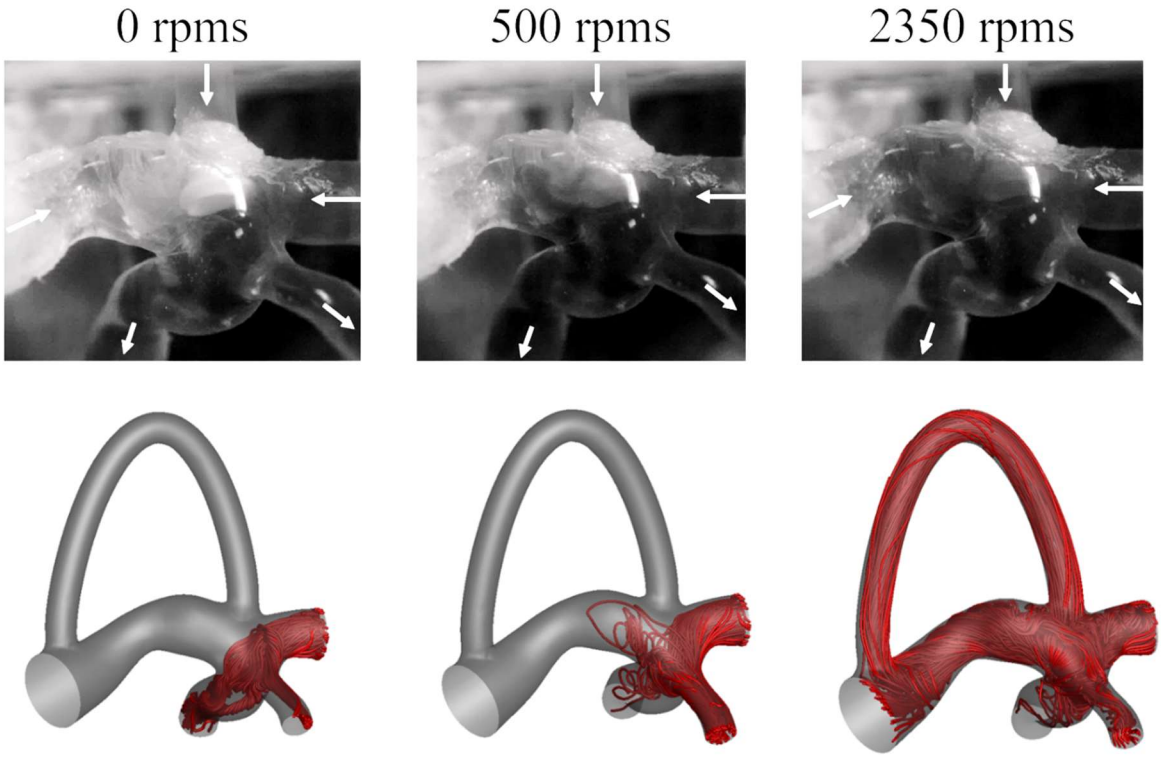

Figure 8-14 Comparison of "streamlines" from the SVC between in vitro (top row) and computational (bottom row) results. This comparison is made with the VAD at 0, 500 and 2350 rpms.

8.3.5.2 Computational results

Pump efficacy across different patient anatomies and different cannulations were investigated. Clinical data for the six patients modeled computationally is given in Table 8-6. These patients offered a wide range of age, BSA, diagnosis, cardiac output and flow splits.

Table 8-6 Patient clinical data for computational modeling. Patient 1 is the patient also used for in vitro experiments.

	Age (y)	Gender	BSA (m2)	Diagnosis	Fontan type	CO (L/min)	Inlet Flow ratio (IVC/SVC) %	Outlet flow distribution (LPA/RPA) %
Patient 1	21	F	1.69	HLHS, VSD	LT	3.91	73/27	45/55
Patient 2	16	F	1.23	HLHS	LT	2.33	71/29	40/60
Patient 3	21	F	1.6	TGA, VSD, TA	ECC	4.24	73/27	60/40
Patient 4	6	F	0.94	HLHS	LT	1.6	64/36	55/45
Patient 5	4	F	0.54	TGA, TA	ECC	3.88	32/68	35/65
Patient 6	17	M	1.65	HLHS	ECC	4.87	70/30	20/80

BSA: body surface area; HLHS: hypoplastic left heart syndrome; VSD: ventricular septal defect; TGA: transposition of the great arteries; TA: tricuspid atresia; LT: lateral tunnel; ECC: extracardiac conduit.

The CentriMag pump increased pressure from the vena cavae to the pulmonary arteries in all patient anatomies. The pump was run at 2350 rpms for all patients to focus on the effect of patient physiology on pump performance. Median pressure increase was 5.78 [1.2-7.9] mmHg, HFD was 52 [19-63] and the pump added 31 [19-47] mW of power. Average wall shear stress (WSS) across the entire TCPC wall was low for all anatomies at 29.5 [21-36] Pa with a maximum wall shear stress of 248 [167-337] Pa. The threshold of 150 Pa was chosen as a conservative wall shear stress for potential red blood cell damage.[109] This level of wall shear stress would require an exposure time on the order of 10^2 seconds which exceeds the exposure time experienced within the TCPC. Even at this threshold, only 1% of the total wall area experienced a WSS above 150 Pa for patient 6, while all other patients were less than 1% (Table 8-7).

Table 8-7 Comparison of VAD performance across patient anatomies.

	Pressure gain (mmHg)	Power added (mW)	HFD	Average WSS (Pa)	Max WSS (Pa)	Area WSS above 150
Patient 1	7.9	47	55	21	167	0%
Patient 2	5.3	28	48	25	183	0%
Patient 3	4.3	37	63	30	203	0%
Patient 4	7.4	19	62	32	316	0%
Patient 5	6.2	34	35	29	293	0%
Patient 6	1.2	28	19	36	337	1%

HFD: hepatic flow distribution; WSS: wall shear stress.

Wall shear stress, SVC streamlines, and relative pressure changes for the six patients can be visualized in Figure 8-15, Figure 8-16and Figure 8-17 respectively.

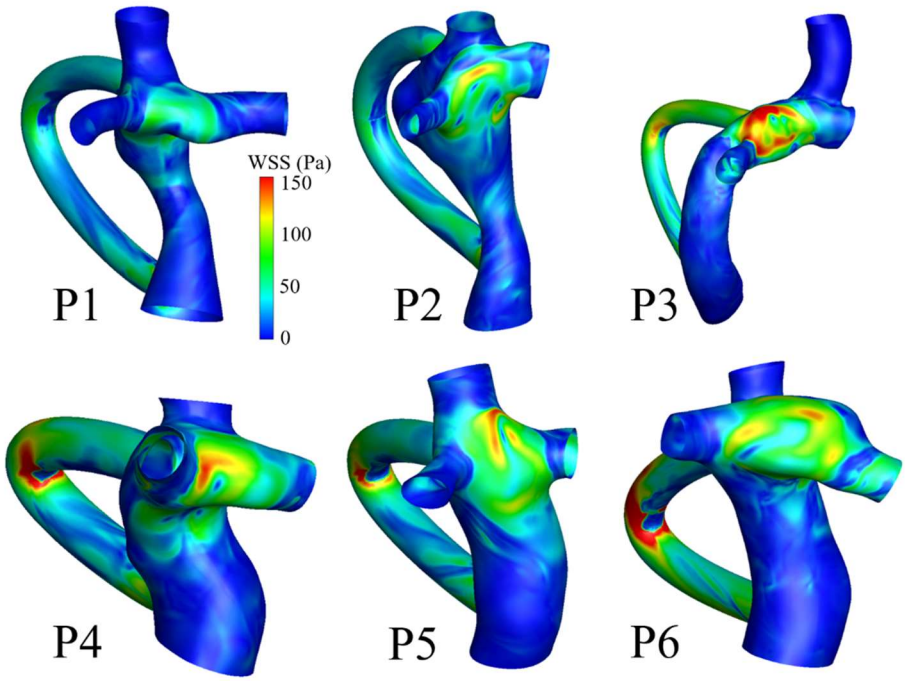

Figure 8-15 Wall shear stress for all patients. All patients use the same color scale.

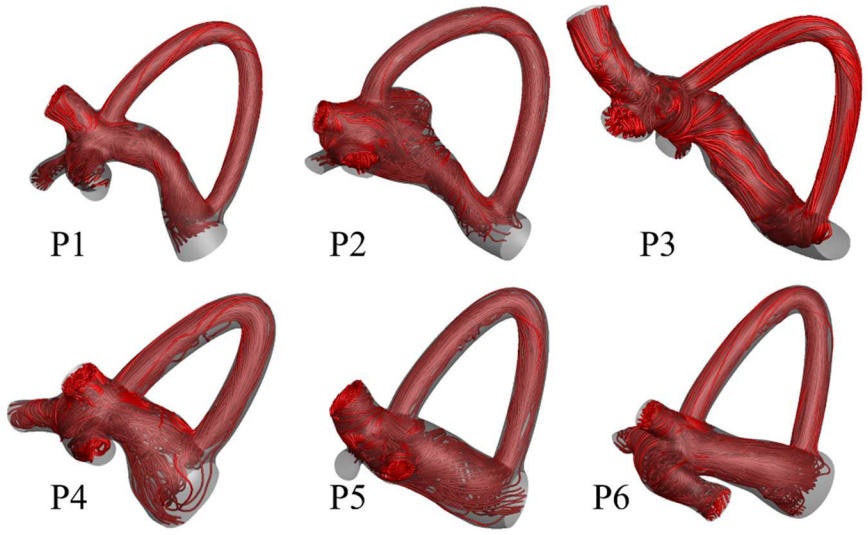

Figure 8-16 SVC streamlines for all patients. Streamlines are only seeded at the SVC. In each case, the VAD is pulling the SVC flow down through the Fontan pathway into the inflow cannula.

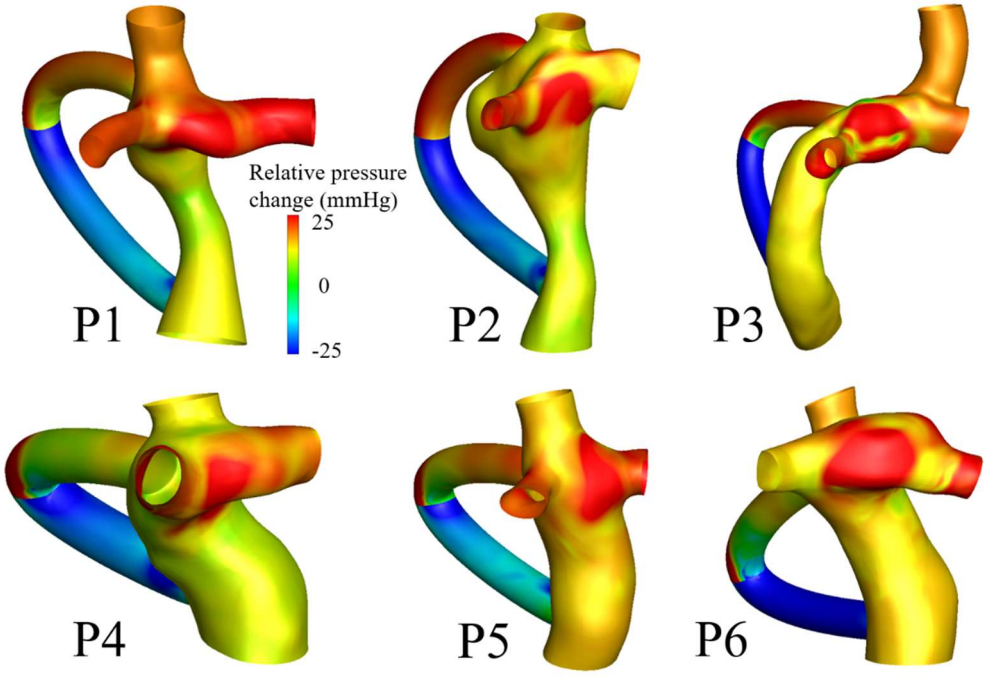

Figure 8-17 Relative pressure changes for all patients. All patients use the same color scale.

The effect of cannula insertion was also investigated. Various cannula insertions were modeled on Patient 1. Table 8-8 shows the results across the five cannulation variations. Pressure increased from the vena cava to the pulmonary arteries in each scenario with a median of 5 [2-7.9] mmHg. The pump added 40 [21-57] mW of power and HFD was 45 [43-55]. Average wall shear stress was 24 [21-26] Pa with a maximum WSS of 168 [125-193] Pa. All cannulations had 0% wall area with a WSS above 150 Pa.

Table 8-8 Effect of cannulation insertion on VAD performance.

	Position	Insertion angle	Pressure gain (mmHg)	Power added (mW)	HFD	Average WSS (Pa)	Max WSS (Pa)	Area WSS above 150 Pa
Cannulation 1	e	n	7.9	47	55	21	167	0%
Cannulation 2	a	j	4.6	34	43	23	168	0%
Cannulation 3	c	l	2	21	52	26	176	0%
Cannulation 4	g	p	6.3	57	45	26	125	0%
Cannulation 5	i	r	5	40	44	24	193	0%

Wall shear stress, SVC streamlines, and relative pressure changes for the five cannulations can be visualized in Figure 8-18, Figure 8-19 and Figure 8-20 respectively.

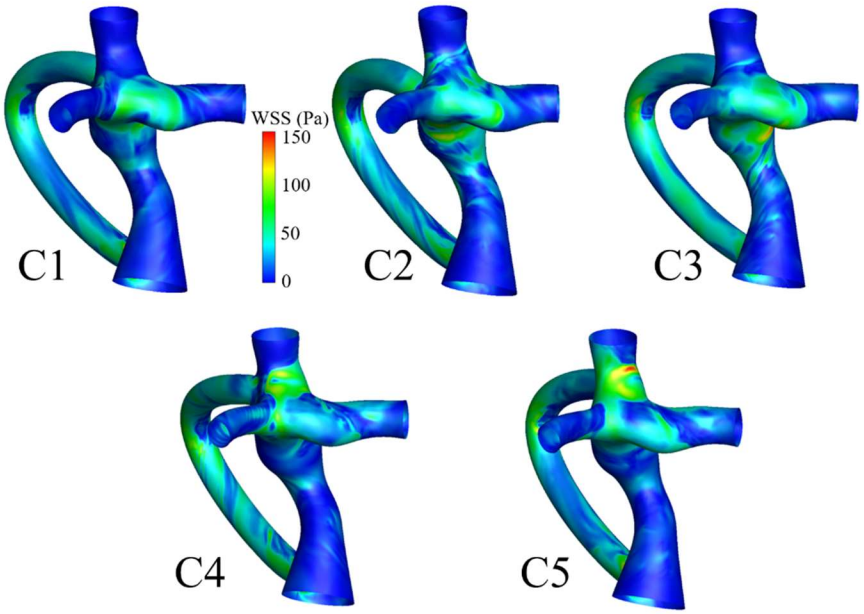

Figure 8-18 Wall shear stress contours for all cannulation options. All figures use the same color scale.

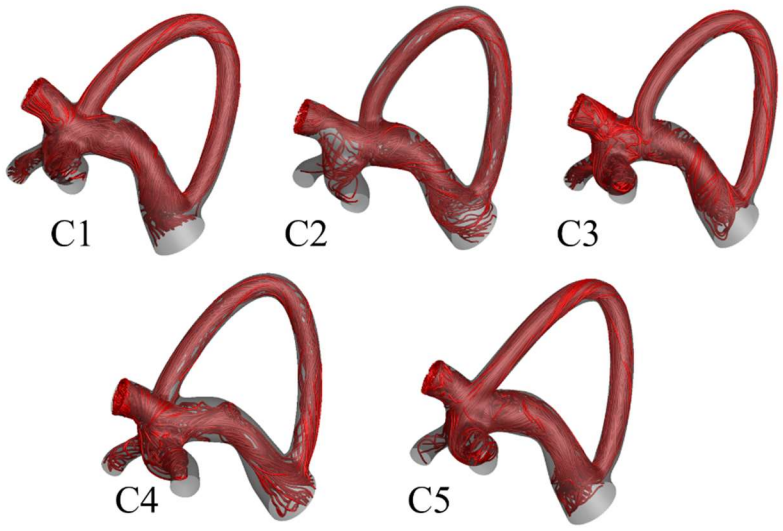

Figure 8-19 SVC streamlines for all cannulation options. Streamlines are only seeded from the SVC.

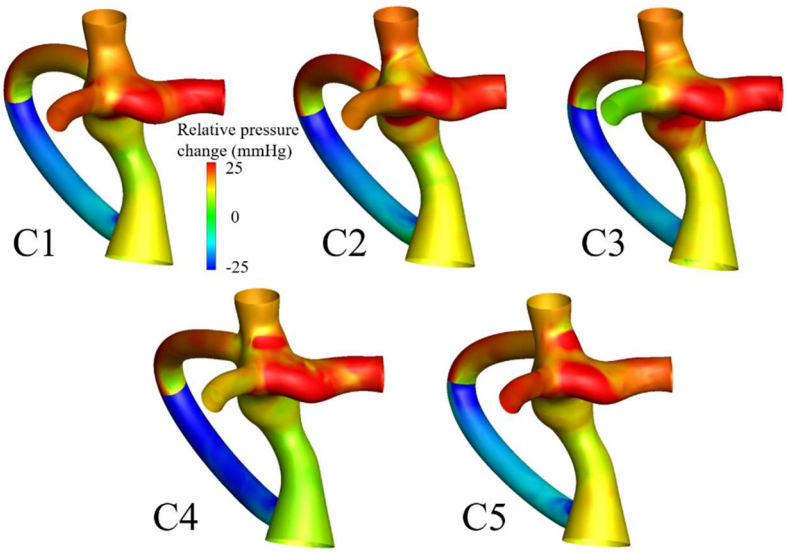

Figure 8-20 Relative pressure changes for all cannulation options. All figures use the same color scale.

A summary of the results from both the inter-patient comparison as well as intra-patient comparison (different cannulations) is given in Figure 8-21.

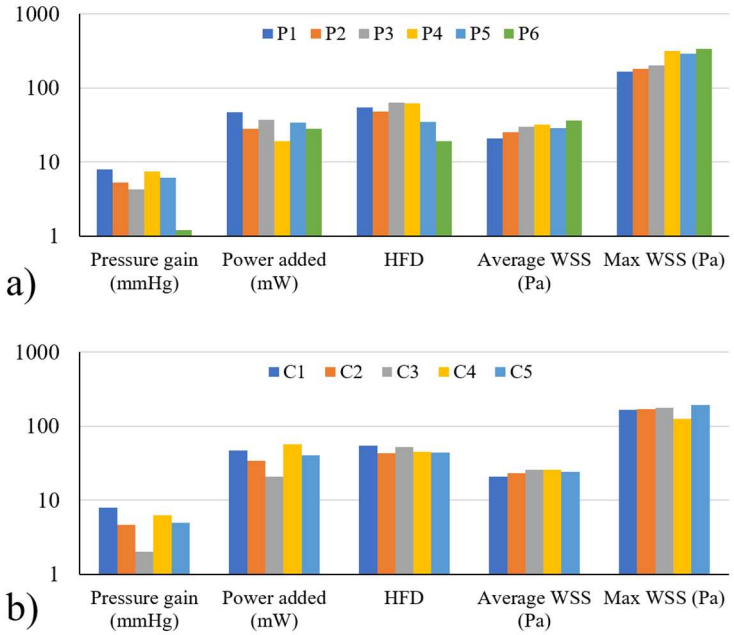

Figure 8-21 Summary of results for the (a) inter-patient and (b) intra-patient (different cannulations) comparisons.

8.4 Discussion

8.4.1 Device efficacy

A wide range in device efficacy was observed across the four devices tested. The devices tested include implantable and extracorporeal devices, pulsatile and continuous flow devices, and devices designed for partial and full ventricular support. Importantly, the lack of a Fontan animal model requires benchtop testing to determine which devices may potentially be beneficial for patient use. As seen in this work, some devices are clearly not suitable for failing Fontan support and therefore no in vivo trials are needed which may put patients in danger.

Overall, device efficacy improved with the output of the device. The HeartWare CircuLite VAD was the "weakest" of the devices tested and could not provide successful support in any scenario (in parallel, with Fontan pathway banding, Fontan takedown). Significant amounts of recirculation required Fontan pathway banding, which then resulted in a non-physiologic pressure drop in the IVC. In addition, when taking down the Fontan and positioning CircuLite as a true right ventricle, the VAD could not produce a full cardiac output and therefore this pump was not a successful option.

The VENTRIFLO™ True Pulse Pump was more powerful than the CircuLite VAD. VENTRIFLO™ showed similar recirculation patterns through the Fontan pathway. Severe pathway restriction was again needed to produce hemodynamic changes. With complete pathway banding, VENTRIFLO™ was able to provide successful support up to a CO of 4.25 L/min. However, this was accompanied by an unacceptable increase in SVC pressure and requires complete pathway restriction which makes the patient completely dependent on the VAD, raising concerns in the case of device durability/failure. In the Fontan takedown scenario, VENTRIFLO™ could only output a maximum of 3.2 L/min, which is less than the baseline cardiac output.

This work underscores the challenges of supporting a failing Fontan physiology. Similar to our previous studies, significant amounts of recirculation through the Fontan pathway (FP) limited the effectiveness of the PediMag™ device and required complete clamping of the FP. In this scenario, PediMag™ was able to outperform any device previously tested and successfully supported the failing Fontan circulation up to a cardiac output of 5 L/min. However, this scenario resulted in increased SVC pressure. Use of CentriMag™ as a Fontan assist device overcame these shortcomings and successfully achieved the goals of support in a native Fontan without the need for restrictive banding. Importantly, the drop in IVC pressure and augmentation of cardiac output achieved using CentriMag™ was accompanied by a drop in SVC pressure as well. This is possible because even with recirculation through the Fontan pathway, CentriMag™ is powerful enough to still provide sufficient forward flow to the pulmonary arteries allowing for successful support. In addition, the recirculating flow is able to entrain SVC flow, effectively "pulling" SVC flow and therefore decrease SVC pressure. These observations provide an important insight into the pump parameters needed for suitable Fontan assist devices.

The number of patients living with complex congenital heart disease continues to increase, and patients with single ventricle physiologies palliated with the Fontan TCPC continue to survive longer. This however sets them up for the inevitable Fontan failure; currently with very limited options for rescue, including heart transplant. The essential subtypes of Fontan failure have been described as 1) primary ventricular failure and 2) failure of the Fontan circulation in the setting of preserved ventricular function and pressure. Failure of the systemic ventricle can manifest similar to heart failure in anatomically normal hearts with increased end-diastolic pressure, increased left atrial pressure and decreased cardiac output with or without decreased systolic function. In this situation, at failure of medical therapy, ventricular assist devices can be implanted in the standard

fashion (systemic ventricle to aorta). Assistance in this manner has been shown to provide relief from such types of Fontan failure as a bridge to transplantation. Both pulsatile devices (Berlin Excor, Thoratec PVAD) as well as continuous flow devices (HeartWare HVAD, CentriMag™) have been used to support the systemic ventricle with varying success. Arnaoutakis, Weinstein and Poh all report high mortality rates and adverse events.[56,110,111] Therefore, although in theory supporting failing Fontan with ventricular dysfunction appears straightforward, the clinical experience is far from optimal.

Supporting a failing Fontan with preserved ventricular function is even more challenging in our view. This is supported by the fact that there are a large number of Fontan patients that develop this pathophysiology with essentially only a few reports of attempts to support these patients mechanically.[58,59] In addition, we believe that there may be under reporting of other unsuccessful attempts at such support. In all of the published attempts to support the Fontan side failure, modifications have been required in the form of a Fontan take down (Prêtre et al), vena cava banding (Rodefeld et al) or creation of a compliance chamber (Reardon and Lacour-Gayet).[58,59,112,113] One of our interests here was to assess the feasibility of offering successful support using off the shelf devices with no or minimal modification to the Fontan anatomy or MCS device.

In light of these limitations and challenges associated with supporting failing single ventricle patients, specifically failing Fontan patients, development of devices that allow for the adaptability necessary for practical use is critical. The current study provides data to support the notion that a centrifugal pump such as CentriMag™ may be able to assist the failing Fontan physiology. The advantage of this pump design is its high output (designed for full cardiac support) as well as the cannulation options adaptable to the TCPC anatomy. Allowing for both an inflow

and outflow cannula to be custom sized as needed depending on the patient anatomy permits optimal positioning of these cannula.

The devices investigated here offer paracorporeal support and are therefore not a long-term strategy. However, the study finding that CentriMag™ may be able to effectively support a failing Fontan circulation and potentially improve hemodynamics has important clinical implications. It provides an option for temporary relief of the failing Fontan scenario and the ability to optimize the patient prior to consideration for long term support or transplantation. CentriMag™ and PediMag™ have both been used as bridge to transplant devices in the pediatric population as LVADs.[55] Their ability to support the failing Fontan circulation provides a novel and clinically relevant application.

For long term support, currently available durable intracorporeal continuous flow devices however have fixed, short, inflow cannula (metal) that necessitate positioning of the device proximate to the ventricle. Such proximate positioning as well as the straight metal cannula is not well suited for attachment to the Fontan conduit. This therefore necessitates design modifications that would allow for flexibility in cannula length and positioning, as well as device positioning due to significant variations in Fontan pathway anatomy and intrathoracic relationships. A conceptual design for such a pump is shown in Figure 8-22. Here the intracorporeal, durable centrifugal pump is anchored to the right hemidiaphragm with inbuilt anchoring hooks. Additionally, the device can be anchored to the chest wall. The inflow and outflow cannula made of flexible material such as Dacron™ can be custom sized and appropriately sutured to the Fontan conduit. The driveline is externalized to be connected to the controller and power source. A design such as this may be able to provide long term support for this group of patients as a bridge to transplant or even as destination therapy.

8.4.2 Banding and cannulation strategies

Various methods of banding and cannulation strategies were attempted throughout these experiments on all of the devices tested. Even using advanced banding designs to account for restriction diameter and length, no banding strategy was more successful than a standard, narrow banding of 80% constriction by area. However, this would not be implemented clinically since 80% constriction is not feasible. Therefore, complete pathway restriction was found to be the best option to achieve successful support with the VENTRIFLO™ and PediMag™ devices.

Multiple cannulation strategies were attempted to reduce recirculation and avoid complete pathway restriction. Similar to the banding results, advanced cannulation techniques did not improve results and therefore are not worth the added complexity. Overall, advanced banding and cannulation strategies were superceded by using a pump powerful enough to overcome the effects of recirculation.

8.4.3 Generalizability

The computational analysis shows similar results across patient anatomies and cannula insertions. These are important findings that suggest failing Fontan support can be achieved using similar methods for different patients. The patients modeled were selected from a variety of diagnoses, anatomies and physiological conditions, and therefore give a decent representation of the range of Fontan patients that may need mechanical circulatory support. Though other unique

anatomies do exist, these patients give a preliminary understanding of the generalizability of VAD use in Fontan patients.

In addition, results were very similar across cannulation options. This provides confidence that slight variations in surgical implementation will not cause drastic differences in the pump's ability to support the failing Fontan. The cannula insertion options that were modeled span a generous set of offsets and angulations, and therefore should be representative of the full range of surgical variations that could exist. Figure 8-22 shows a conceptual design and placement of an intracorporeal durable centrifugal pump for failing Fontan support.

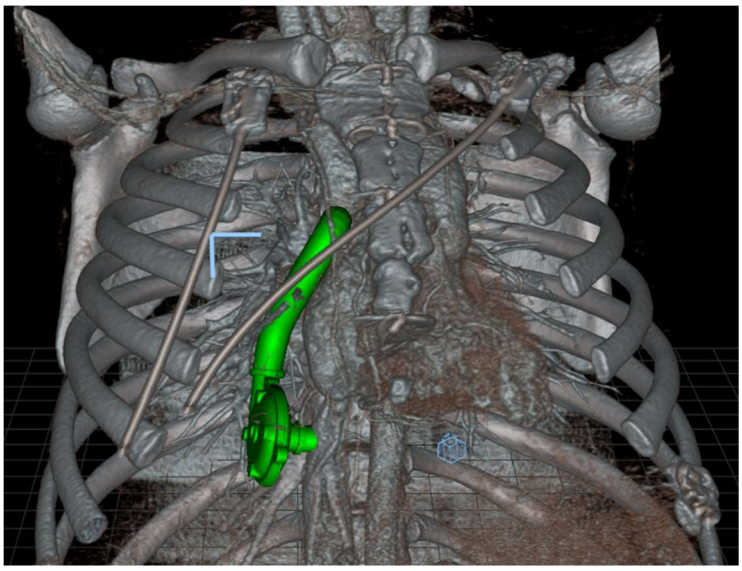

Figure 8-22 Conceptual design and placement of an intracorporeal durable centrifugal pump for failing Fontan support. Driveline not shown.

9. SUMMARY AND CLINICAL SIGNIFICANCE

This thesis investigated four potential solutions to two of the most common forms of Fontan failure (PAVMs and liver disease). As the number of Fontan patients continues to grow with increased life expectancies, it is obvious that solutions are needed for these problems. Specific Aim 1 focused on PAVMs and investigated the two proposed solutions of surgical planning and Y-graft use to balanced hepatic flow distribution (the mechanism to prevent/correct PAVMs). Specific Aim 2 focused on liver disease and investigated the two proposed solutions of improving TCPC efficiency and using mechanical circulatory support to decrease hepatic congestion (the mechanism cause liver fibrosis progression).

9.1 Surgical planning (PAVMs)

An important accomplishment in this thesis was the evaluation of surgical planning prediction accuracy. Overall, HFD prediction error was 17±13%. This error was significantly reduced when predicting HFD for hepatic to azygous shunts. These results are vital for proper implementation of surgical planning into clinical practice and engineering improvements to the surgical planning process.

Clinicians must evaluate the ranking of surgical options with the prediction error in mind. Aside from hepatic to azygous connections, the predicted HFD will be almost 20% off on average. Therefore, an option that has a predicted HFD to be very balanced, could potentially be unbalanced in either direction depending on surgical implementation and the change in flow rates from pre- to post-op conditions. Surgical planning can alert clinicians of extremely poor surgical options (i.e. all hepatic blood flow going to a single lung), where even a 20% error would still not be a

promising option. Again, with hepatic to azygous connections, surgical planning produced accurate predictions which can provide guidance to surgical decision making.

Both improved surgical implementation and more accurate surgical planning methodologies are needed to increase surgical planning accuracy. As discussed in section 5.4, little intra-operative guidance is currently available to help surgeons replicate virtual surgical options. Even if surgical planning methodologies could perfectly predict HFD for a given option, this is not completely useful if the surgeons cannot exactly replicate the option. On the other hand, current surgical planning methodologies are not perfect, and refinements are needed. A combination of these two aspects is likely necessary to improve surgical planning predictions.

As surgical planning improves, another serious barrier is the logistics of making this technology available to an increasing number of clinicians. Currently, our lab is heavily involved with CHOA and CHOP (plus other referring centers) on each of their surgical planning cases. A substantial amount of man hours and computational resources are needed for each surgical planning case, and therefore this is not a sustainable practice for widespread use.[11] Potential avenues could include a surgical planning based company or internal positions within each hospital that are responsible for surgical planning analysis. In either case, funding/reimbursement methods pose a potential challenge.

In the end, we do see that correction of unbalanced HFD leads to regression of PAVMs. In each Fontan revision in this study, the previously diagnosed PAVMs did regress once surgical planning was used to create a more balanced HFD. This is encouraging and proves the importance of choosing a correct TCPC design for a given patient. We see clearly that this must be decided in a patient-specific manner, which strengthens the need for surgical planning.

9.2 Y-grafts (PAVMs)

Overall, Y-grafts have proven to be a viable option for Fontan completion. Though additional follow-up data is needed for more generalizable results, the significant improvement in HFD over time is very encouraging. The results from the initial post-operative state were not as positive, but again this may have been an artifact of not allowing the body sufficient time for adaptation.

An important concern for Y-graft use is the increased number of sutures needed for three anastomosis sites instead of two. It is thought that this may be a potential cause of increased thrombus in these patients. Additionally, potential regions of extreme wall shear stress is another concern of Y-graft use. The validity of these concerns remains to be seen.

As a proposed solution for preventing the formation of PAVMs, the true validation will come from long-term follow up of these patients and the determination if PAVMs form less often in patients with Y-grafts. While HFD is an important and quantifiable metric related to PAVM formation, the existence of lung malformations is the actual outcome that must be measured.

Overall, our single-center Y-graft studies have shown that using Y-grafts are a clinically viable solution for Fontan completion, and that this option is not inferior to traditional Fontan options. As this patient cohort ages, further information can be gathered concerning potential thrombus issues and the intended benefits regarding PAVM formation. If Y-grafts prove to be a solution to preventing PAVMs, then this commercially available option will likely become more widespread.

9.3 TCPC efficiency (FALD)

Fontan hemodynamics measured approximately 8 years prior to liver biopsy were found to be predictive of future liver disease. Specifically, TCPC resistance and LPA stenosis showed the strongest correlations with liver fibrosis. An important, proposed mechanistic pathway was developed by combining results from the serial and concurrent portions of this study.

Data from this study suggests that an inefficient TCPC design and vessel stenosis may result in increased hepatic congestion, contributing to the progression of liver fibrosis. In addition, the progression of liver disease may lead to hepatic arterialization which decreases resistance to flow through the liver and leads to increases in IVC flow rate. Though the progression of liver disease in these patients is undoubtedly a multifactorial issue, these data suggest that TCPC design and vessel stenosis are important contributing factors.

These findings have important clinical implications. The results encourage the consideration of pre-procedural planning to improve TCPC performance. Though commonly used for preventing or correcting pulmonary arteriovenous malformations by optimizing hepatic flow distribution (HFD), surgical planning can similarly be used to compare potential surgical options and optimize energy efficiency. Furthermore, flow efficiency through a connection can be more difficult to visualize and predict than HFD since changes in velocity and pressure are nonlinear and not always intuitive.(18) Therefore, pre-procedural planning focused on flow efficiency may be even more informative for surgical decision making.

Similarly, interventional strategies may prove beneficial for patients post-Fontan with LPA stenosis or high TCPC resistance or those that demonstrate clinical hepatic decline. The significant, positive correlation between LPA stenosis and fibrosis seen in this study suggests that early correction of vessel stenosis may reduce the progression of liver disease in these patients. Whether

this is due to the effect of LPA stenosis on TCPC resistance or some other factor, interventions such as balloon dilation may be important considerations in this post-Fontan population. Periodic monitoring of vessel stenosis may be useful to determine when or if these interventions are needed.

9.4 Mechanical circulatory support (FALD)

In vitro testing proved very useful in evaluating the off-label use of various mechanical circulatory support devices. The CircuLite device was clearly not capable of supporting the Fontan circulation, and should therefore not be implemented in a patient. At its maximum output, the VentriFlo device was able to achieve our initial goals for successful Fontan support, and provides physiological, pulsatile flow which may prove necessary for proper perfusion. The PediMag device outperformed the VentriFlo device, with the ability to induce favorable hemodynamic changes and increase cardiac output up to 5 L/min (beyond our original goal).

However, each of these previous devices had two major drawbacks: (1) an increase in SVC pressure accompanied any decrease in IVC pressure and (2) complete baffle restriction was required to produce positive hemodynamic changes. The first concern trades improved liver health for potentially dangerous conditions for brain function, while the second concern forces the patient to be completely dependent on the VAD (deadly in the event of device malfunction/failure).

The CentriMag device was able to overcome both of these concerns. When run at a high enough output, the inflow of the CentriMag pump pulled flow from both the IVC and SVC, decreasing pressure in both vessels. The output from the pump was directed down the two pulmonary arteries, simultaneously increased both outlet pressures. This was accomplished without any baffle restriction. Following this favorable change in hemodynamics, ventricle

adaptation was modeled, and CentriMag was able to maintain these improved conditions up to a cardiac output of 5 L/min. Therefore, CentriMag was the most successful pump tested in this thesis, exceeding our original requirements for success.

A number of cannulation strategies and banding designs were tested in this study. However, the most successful scenario (using CentriMag) required no banding or non-standard cannulation and therefore these alternatives may be less impactful. Another potential factor in pump efficacy is the difference between pulsatile and steady flow. Though most devices produce steady flow, opponents argue that pulsatile flow is necessary for proper perfusion and clearance throughout the body. Though not the focus of this work, the potential consequences of either device type during the bridge-to-transplant period may warrant future work. A final concern is the high flow rate of the CentriMag device required to produce the desired hemodynamic changes.

Finally, there are two important clinical consideration to take from this specific aim. First, devices perform much different in these “off-label” scenarios and therefore performance curves published in the instructions for use will not be accurate. A new set of performance curves must be generated at the pressures of the intended use. Second, though the wall shear stress results did not indicate any concerns for hemolysis, blood damage within the pump is a potential problem which needs to be considered.

10. LIMITATIONS AND FUTURE DIRECTIONS

10.1 Specific Aim 1A (Surgical Planning)

10.1.1 Limitations

Though important conclusions can be drawn from this study, a more complete understanding of surgical planning accuracy and methodological needs with increased statistical power will require a substantial amount of data most likely through a multi-center grant. Acquiring post-operative data is unlikely without dedicated funds. Additionally, this study includes a broad range of follow up times and offers only a "snapshot" of the patients' post-operative hemodynamics. If available, the inclusion of serial data in a similar study could offer a better understanding of hemodynamic changes over time. The predicted results in this study are representative of the specific surgical planning process used. Results may vary with other prediction techniques. However, this study employs one of the most advanced anatomy prediction methods and still concludes that post-operative anatomy prediction is a limiting factor, which is unlikely to change based on prediction technique. Finally, two experienced surgeons were involved in these surgical planning cases. While we see no differences in prediction accuracy between these two surgeons, it is possible that results may vary based on the surgeon involved.

10.1.2 Future Directions

A number of relatively basic and necessary questions remain: Are patient outcomes improved as a result of surgical planning? Does surgical planning reduce operating times? Does surgical planning reduce clinical costs or the need for re-operations? Can surgical planning provide

useful insights even with patient growth and adaptation over time? To address these questions as well as evaluate current surgical planning methods, further validation must be a focus in the coming years. A substantial, multi-center clinical trial randomizing the use of Fontan surgical planning and funding post-op data collection may be necessary to acquire the data required to answer these questions.

Additionally, in order to refine the process of surgical planning, further validation is needed in order to determine which, if any, metrics are causal or correlated to long-term Fontan complications. Future studies are needed to identify specific metrics that may be associated with liver disease, protein losing enteropathy and thromboembolic events among others. Furthermore, the various simulation fidelities (steady vs pulsatile, free-breathing vs breath-held etc.) can be assessed for their impact on these metrics. Through this process, surgical planning can be improved and more substantially related to patient outcomes.

Finally, the results of Specific Aim 1A show the need for improved anatomy and flow prediction. Future efforts should focus on the improvement of anatomy and flow prediction tools as well as the surgical option implementation process. Little intra-operative guidance is currently offered as part of the surgical planning process. Some efforts have explored 3D printing and augmented/virtual reality as planning/guidance tools, but further refinements are needed.[91–94] In addition, a current shortcoming of the surgical planning process is the lack of feedback and interaction with the surgeon. Future work should push for more surgeon involvement throughout the process. It is vital to understand how the surgeon prefers to view the proposed surgical options and what methods work best to guide the surgeon to replicate that option. This information will provide valuable improvements to the creation of potential surgical options as well as define the best methods for pre-operative and intra-operative guidance.

10.2 Specific Aim 1B (Y-grafts)

10.2.1 Limitations

In the first part of this study, the period of time between the Fontan operation and the MRI scan was not identical for all patients. Y-graft patients were scanned within one month of the surgery, while LT/ECC patients were scanned around 6 months after the operation. This difference in recovery time may lead to variations in the amount of physiological adaptation which could affect flow rates (as seen in the difference between systemic venous flows) and pulmonary vascular resistance and therefore TCPC resistance and HFD. Additionally, the spatial velocity profiles used at the inlets of the CFD domain are assumed to be parabolic, which are not identical to the spatial velocity profiles obtained from the MRI velocity segmentations. However, this assumption is expected to have only minimal effects on the bulk hemodynamic metrics.

In the second part of this study (serial analysis), the small sample size limits the power of statistical analysis. However, even with the limited number of patients, a significant improvement in hepatic flow distribution was observed. Additionally, the lack of a LT/ECC comparison group with identical follow up times required the use of several unique comparison groups. Though this does not allow for a direct comparison with serial LT/ECC data, choosing follow up times that straddle the Y-grafts can provide meaningful comparisons. Finally, it is important to note that all Y-graft patients in this study used commercially available Y-grafts, and results may differ with more customized designs.

From a modeling perspective, this study focused only on the TCPC geometry and did not include interactions with the rest of the cardiovascular or pulmonary circulation. This localized TCPC modeling may omit significant global influences on the system. Finally, due to limited data,

the hepatic veins were not included in this modeling. The inclusion of the hepatic veins and their respective flow rates could potentially influence the mixing of hepatic factor with the IVC flow and therefore alter the presented HFD results. This study also assumes rigid walls in the CFD simulations.

10.2.2 Future Directions

Follow-up studies on an increased number of Y-graft patients is essential to thoroughly assess if Y-graft use is beneficial for these patients. Specifically, careful monitoring of pulmonary arteriovenous malformation progression is key since the motivation for this graft is to provide a balanced HFD and prevent PAVM formation. As more data is collected we will be able to better determine the benefits/shortcomings of Y-graft use.

Additionally, the potential of thrombus formation and the use of customized Y-graft designs should be explored further. Previous studies have brought up concerns for clot formation in the Y-graft arms due to regions of low wall shear stress. Clinicians should pay close attention to possible clot formation during follow-up imaging studies. As mentioned by the Marsden group, a customized Y-graft design may provide benefits by preserving cross-sectional area throughout the graft. These potential benefits have not been analyzed on a patient cohort large enough to draw any conclusions.

10.3 Specific Aim 2A (TCPC hemodynamics and liver disease)

10.3.1 Limitations

All results in the first part of Specific Aim 2A are based on concurrent CMR, catheterization, and liver biopsy data sets. As we demonstrate in this study, IVC flow rate is

associated with hepatic fibrosis. Therefore, hemodynamic metrics that are dependent on IVC flow rates may change as a result of fibrosis. Consequently, if prior flow rates or TCPC energetics (highly dependent on IVC flow rate) are a factor in future fibrosis progression (e.g. Fontan hemodynamics are predictive of future hepatic fibrosis), the use of concurrent data sets would not elucidate this relationship. This motivated the second part of Specific Aim 2A which analyzed CMR derived flow dynamics and CFD energetics at a time point prior to the liver biopsy.

In addition, because the TCPC is created from non-compliant materials (such as Gortex) and 2-3 staged surgeries would indeed cause fibrosis around systemic venous pathway vessels, rigid modeling is an acceptable assumption. Some variability is expected with liver biopsy data based on heterogeneity of the disease as well as sampling bias, however the current method remains the best available. Finally, all blood flow characteristics of the TCPC circuit were obtained with the patient at rest, in a supine position. Fontan hemodynamics are different with the patient upright, ambulatory and in particular during exercise. Perhaps our finding of LPA size in association with liver fibrosis may indeed suggest that important TCPC flow disturbances might be discovered in association with fibrosis if study could be undertaken in a more natural active daily state or under provocative testing.

10.3.2 Future Directions

To further investigate the relationship between liver fibrosis and Fontan hemodynamics, it may be important to explore another method of liver fibrosis quantification. There is an inherent sampling bias to liver biopsies from which these results were drawn. Before ruling out the possibility that Fontan hemodynamics play a role in liver fibrosis, comparisons with imaging or ultrasound derived liver scores should be investigated, as well as related biomarkers.

If in fact Fontan hemodynamics prove to not be a driving force in Fontan associated liver disease, genetics may be the next area of investigation. If genetics are determined to decide which patients will have liver disease, and to what extent, potential, preliminary screenings may prove useful to determine how to proactively treat susceptible patients. Though this solution will take a substantial amount of time and resources to come to fruition, it may be the best option.

10.4 Specific Aim 2B (Mechanical circulatory support)

10.4.1 Limitations

Though frequently used, in vitro modeling cannot perfectly represent the human body. The use of lumped compliance and resistance modules will cause the performance of the loop to deviate somewhat from physiologic behavior. For example, the use of a piston pump cannot perfectly mimic the complex systolic and diastolic function of the single ventricle, which necessitates the simplified adaptation modeling as described and used in this study. In addition, the Fontan circulatory loop employed in this study is not validated for all failing Fontan physiologies. In particular, the mock circulation used in this study is representative of failing Fontan patients suffering from chronic Fontan failure: right-sided flow congestion and elevated central venous pressures in the presence of a functioning single ventricle capable of increasing cardiac output. Current efforts are underway to include a detailed ventricle module in the mock circulation that allows for variations in failing Fontan type as well as improved adaptation modeling. Finally, the use of an extracorporeal device is not ideal as a long-term solution, as it severely limits the freedom of a patient. However, the purpose of this study is to focus on MCS as a bridge-to-transplant which allows for relatively "short-term" dependence on the device. Limited patient freedom may be a justifiable cost to preserve organ function while awaiting a heart transplant.

10.4.2 Future Directions

An important next step to improve *in vitro* modeling of the cardiovascular system is to more accurately model the heart. As stated earlier, a piston pump cannot replicate the complex, load dependent functioning of the heart, or naturally adapt to changes in the cardiovascular system. Therefore, future efforts should focus on this modeling component. This could be accomplished through the use of more advanced, artificial hearts whose output is a function of hemodynamic conditions with some level of adaptation, or may benefit from an ex vivo strategy where an actual heart is resuscitated and performs its usual pumping function. The use of a mechanical artificial heart is the more likely solution due to cost and logistics.

To move forward with the pumps that were found to be successful candidates, both hemolysis and animal testing are important next steps. Each pump included in this thesis has previously passed hemolysis testing for their intended uses. However, in the Fontan assist scenario hemodynamics and flow rates are much different than those in cardiac failure for which these devices have been tested. Therefore, hemolysis testing is a necessary requirement. As with most medical devices, the use of an appropriate animal model for further testing before human use may provide additional insights into device efficacy. Unfortunately, no Fontan animal model exists. At best, single ventricle animal models have only lasted several hours and the severe shock and extreme adaptation of the animal to this new physiology may not allow for useful results. This shortcoming is a major barrier to the testing of devices for Fontan use.

Finally, the real validation for *in vitro* testing will only come once one of these pumps are implemented in an actual Fontan patient. This will most likely happen in a “compassionate use” circumstance where there are no alternative options and the patient is failing. It is difficult for a

device to be “successful” in this scenario since the patients is already failing, but this may be the only path to implementation of a Fontan assist device in a human.

11. CONCLUSIONS

From the many modes of Fontan failure, this thesis investigated potential solutions for pulmonary arteriovenous malformations and liver disease. These two specific complictions were chosen because (1) they are very common in the Fontan population, (2) they are thought to be hemodynamic driven and (3) through our clinical collaborations we have access to unique data sets that allow for a thorough analysis of these complications. Two potential solutions for each of these complications were evaluated. The use of surgical planning and Y-grafts were investigated as potential methods to balance HFD and correct/prevent pulmonary arteriovenous malformations, and improving TCPC efficiency and the use of mechanical circulatory support devices were investigated as methods to decrease hepatic congestion and reduce liver disease progression. A brief conclusion for each proposed solution is given below.

11.1 Surgical planning

Fontan surgical planning can provide accurate predictions of hepatic flow distribution, but prediction accuracy varies with graft type. Even with its limitations, surgical planning can provide important insights into surgical decision making which can result in more balanced hepatic flow distrubtion and therefore less risk of PAVMs. Surgical planning was successfully used in Fontan revision cases to “fix” unbalanced HFD and casue PAVMs to regress. Anatomical prediction was found to be a key methodological shortcoming in the surgical planning process. With continued improvements, surgical planning may be a useful tool to avoid pulmonary arteriovenous malformations in Fontan patients.

11.2 Y-grafts

While we observed no difference in HFD during the immediate post-operative state, Y-grafts showed significantly more balanced hepatic flow distribution than traditional connections at a ~3 year follow up. In addition, Y-grafts had similar TCPC resistance to traditional connections, showing no inherenet disadvantages to Y-graft use. Y-grafts have been shown to be a feasible clinical option and therefore this data suggests that Y-grafts will provide more balanced hepatic flow distrubtion and may reduce the risk of pulmonar arteriovenous malformations.

11.3 Effect of TCPC design on liver disease

No relationships were observed between TCPC efficiency and the extent of liver disease at the time of biopsy. However, significant relationships were seen between TCPC efficiency and LPA stenosis at a time point approximately 7 years prior to liver biopsy. Furthermore, the change in IVC flow rate over time was a strong predictor of the extent of liver fibrosis. These findings suggest that an inefficient TCPC design and vessel stenosis may result in increased hepatic congestion, contributing to the progression of liver fibrosis. In addition, the progression of liver disease may lead to hepatic arterialization which decreases resistance to flow through the liver and leads to increases in IVC flow rate. The finding that Fontan metrics are associated with liver fibrosis encourages the consideration of pre-procedural planning and interventional strategies to improve TCPC performance and reduce vessel stenosis.

11.4 Mechanical circulatory support to reduce hepatic congestion

Mechanical circulatory support devices were found to be a successful option to provide failing Fontan support by increasing cardiac output and reducing IVC pressure. This combination of hemodynamic changes would reduce hepatic congestion and potentially delay or stop the progression of liver disease. The ability to provide successful support was highly dependent upon which device was used. We found that more powerful pumps alleviate the need for Fontan pathway banding and produce the most beneficial hemodynamic changes. Advanced banding and cannulation strategies did not significantly effect the hemodynamic changes associated with various devices and are therefore not worth the added complexity. Though successful support was achieved in this benchtop setting, further testing in vivo is needed to evaluate the true efficacy of these devices.

12. FUNDING SOURCES

This work was funded in part by an NIH R01 grant (HL098252) focused on investigating the effect of Fontan hemodynamics on patient outcomes. Specific Aim 2B was also funded by the Michael P. Fisher Cardiac ICU research fund (Children's Healthcare of Atlanta). Finally, the work in Specific Aim 2A and 2B were specifically funded by an American Heart Association Predoctoral Fellowship 17PRE33630117.

APPENDIX A – COMPUTATIONAL METHODS

Appendix A is separated into 6 sections describing the various computational methods used in this thesis. The sections are as follows: Mesh generation and CFD simulation set-up, Blood waveform processing, Flow field visualization, Anatomy characterization, CFD simulation post-processing and anatomy comparison.

Mesh generation and CFD simulation set-up

This appendix contains the protocol for adding flow extensions, generating a mesh and CFD simulation set-up. All of these components are completed using various modules in ANSYS Workbench.

Credit: Dr. Alan Wei

Flow Extensions

In this tutorial, the ANSYS workbench is used. Major modules involved are:

- ANSYS Design Module -- geometry;
- ANSYS Meshing Module -- mesh;
- FLUENT – simulation;

Some Tips:

- Anytime you see the lighting mark on any module, you may want to right-click to "Update" or "Generate" for the sake of proceeding.

ANSYS Design Module – Geometry

Firstly, open the ANSYS Workbench under the ANSYS folder

Drag the “Geometry” module to the workbench following the instruction in Figure 0-1.

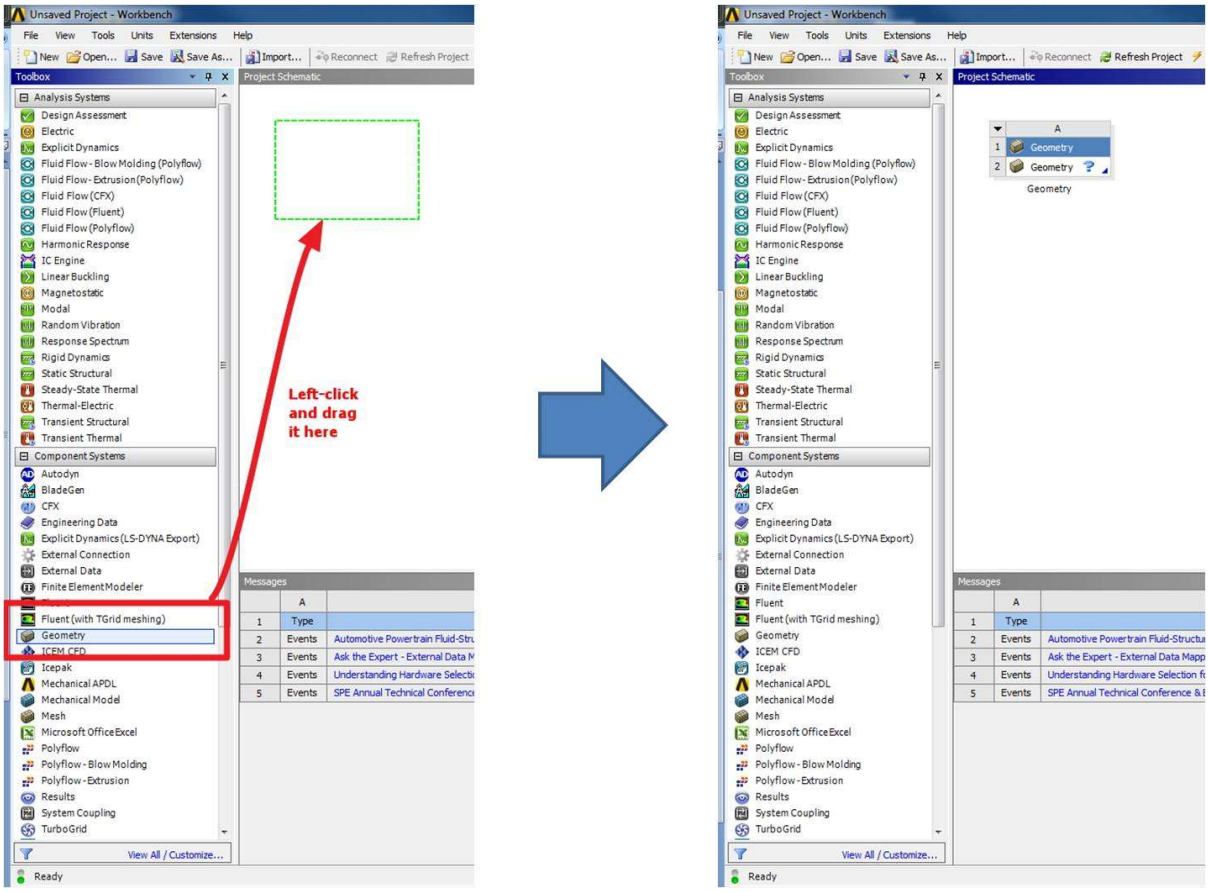

Figure 0-1 ANSYS workbench.

Double-click the question mark next to the “Geometry” to open the ANSYS Design Module.

After the “Geometry” window is on, import the geometry file by clicking the button shown in Figure 0-2 under “File” button of the menu bar,

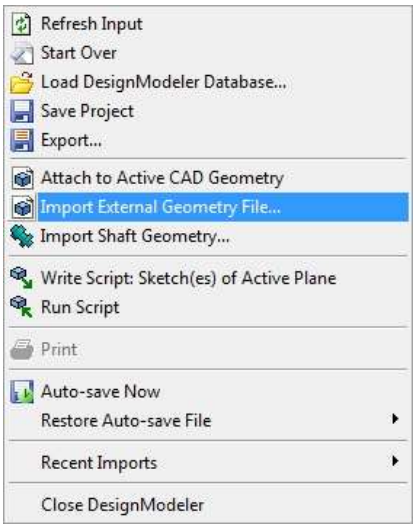

Figure 0-2 Menu bar.

Usually, the geometry should be IGES files. The module will ask about the metric unit; choose 'millimeter' as usual.

Make sure change the "Operation" to "Add Frozen", and then "Generate" the geometry. The geometry will show on the screen, as shown in Fig.3.

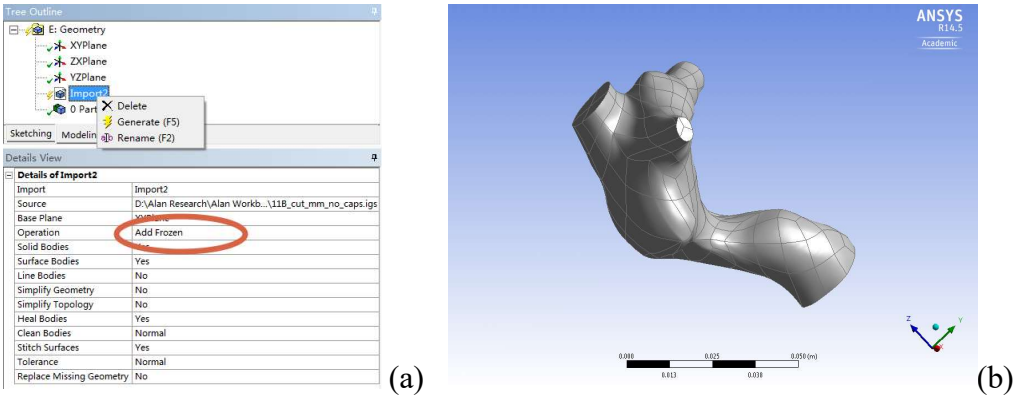

(a) (b)

Figure 0-3 Add frozen operation.

On the screen shown in Figure 0-3 (b) (which will be referred as 'working screen' in the following context), you can use your mouse to adjust the perspective of view. If you had any trouble and need to reset the view, the following buttons in the tool bar may help. (In the software, you can see the tips by moving your mouse on top of the button and keeping it still.)

Figure 0-4 Menu selection.

Now, you need to create the extension for all vessels. Get into "Create" and find "Extrude", make sure:

1. Your "Selection Filter: Faces" on the tool bar is enabled:

Figure 0-5 Selection filters.

2. Select all "faces" on the boundary of a vessel end, i.e.:

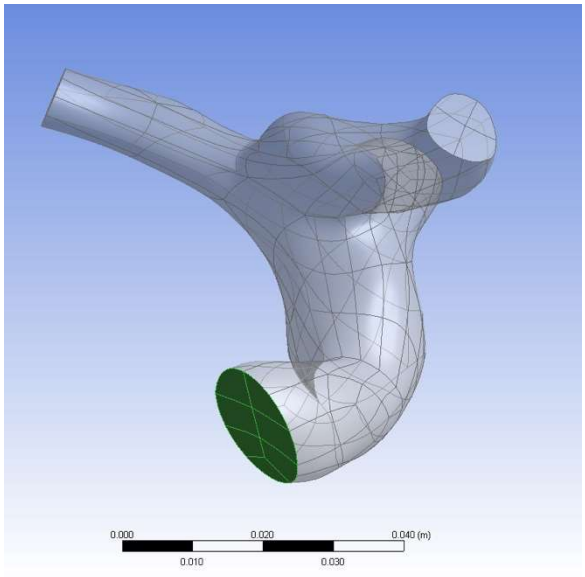

Figure 0-6 Face selection.

3. "Operation" = "Add Frozen";
4. In order to get "Face Normal" for "Direction Vector", you need to again enable "Selection Filter: Faces" mode and pick any face on the surface of certain boundary, as shown in Figure 0-7. When you click the "Direction Vector", the software will automatically reset the "Selection Filter" to "Edges", you may need to manually switch it to "Faces" as the Figure 0-5 illustrated.

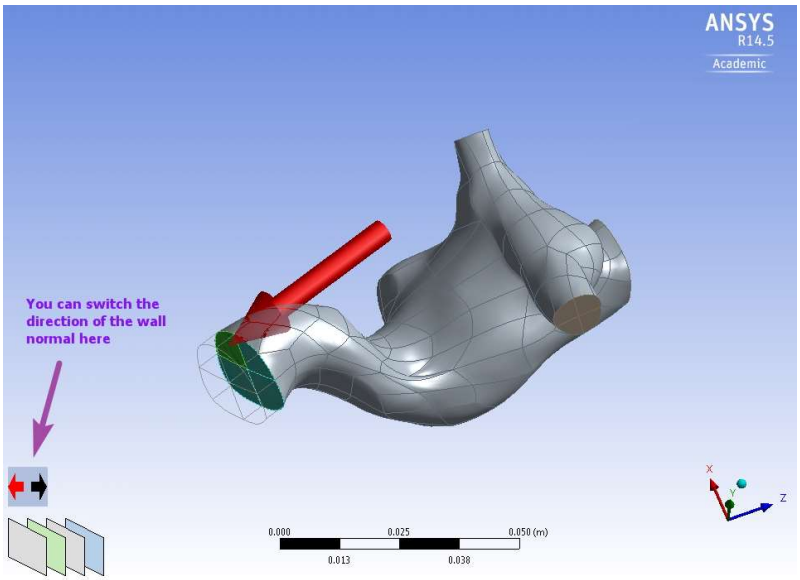

Figure 0-7 Vessel extensions.

5. "Depth" for CFD simulations are:
    a. 10 times the diameter of the vessel
    b. The vessel diameter is equal to $2 * \sqrt{(\frac{A_{vessel}}{\pi})}$ where A_{vessel} is the cross sectional area of the vessel.
    c. Once you generate a set of extensions, you can modify their length arbitrarily. Also, you can right-click and suppress them if you do not need them in the simulations.
6. Finally, change the name and click "Generate", i.e.:

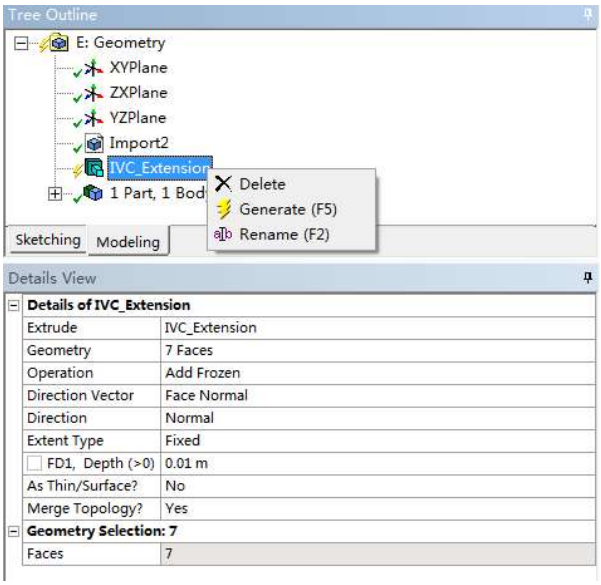

Figure 0-8 Generate part.

As long as an extension is created, a new body under the tree outline of "Parts" should be generated. After **extensions for all vessel ends** are created, remember to change the names for all bodies:

Figure 0-9 Rename parts.

Highlight all of vessel parts (TCPC, IVC, LPA, RPA, RSVC, etc.), right click and "Form a new part":

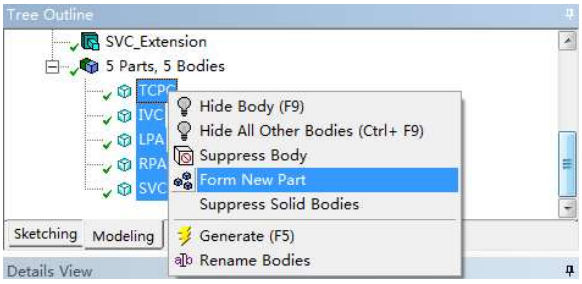

Figure 0-10 Form new part.

You can change the name of the new part to "CFD", and **switch its material property to "Fluid"**:

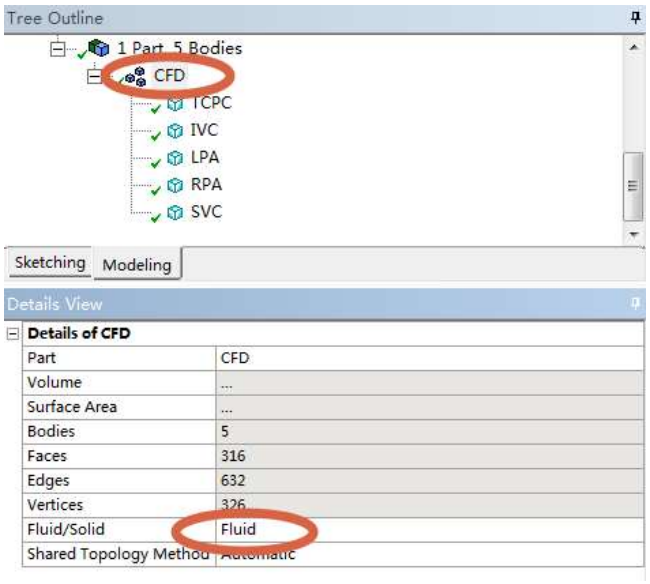

Figure 0-11 Make fluid domain.

So far, you finished all steps for “Geometry”. You can close the “Geometry” module window and save the project.

Mesh generation

ANSYS Meshing Module - Mesh

Go back to the ANSYS Workbench main panel and add a “Mesh” into the working flow. Follow the Figure 0-12 to connect the existing geometry to the meshing module. Then, double-click to open the meshing module.

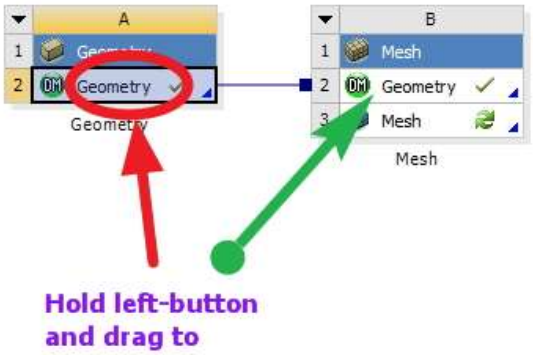

Figure 0-12 Connect to mesh module.

First, you need create "Named Selections". "Named Selections" are the components that will eventually be converted into FLUENT as boundary conditions. Notice that any suppressed components will not be passed to FLUENT, though hidden ones will. In order to create the "Named Selection", right click the "Model" on very top of the project outline:

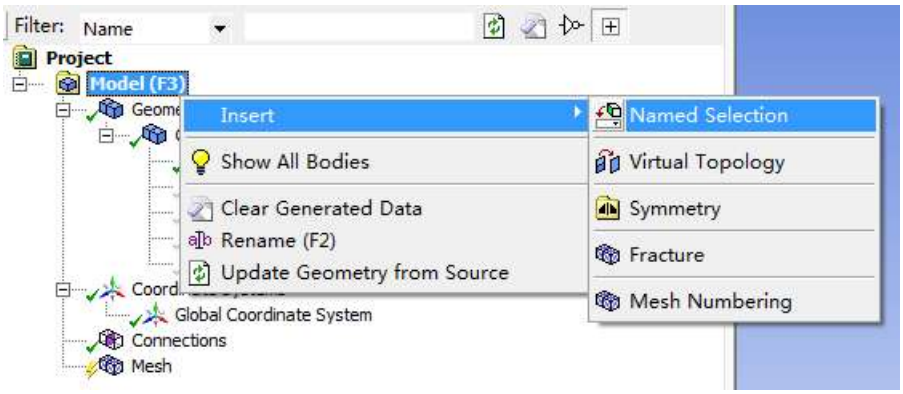

Figure 0-13 Create named selections.

It is always better to identify the body surface of the TCPC first. Right click all OTHER vessels and hide all of them.

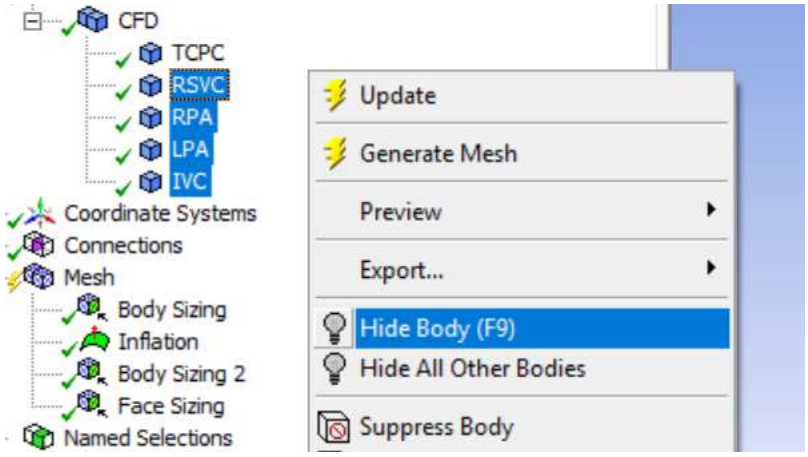

Figure 0-14 Viewing options.

Then, you need to use the "Box select". It is on the tool bar. (By default, it should be just the row under the menu bar and located in the nearly middle of your screen)

Figure 0-15 Selction options.

Now, you can hold the left button and draw a box on the working screen to include everything. And then switch to the "Single Select" and de-select (by holding "Ctrl") boundaries that are not belonging to the body surface.

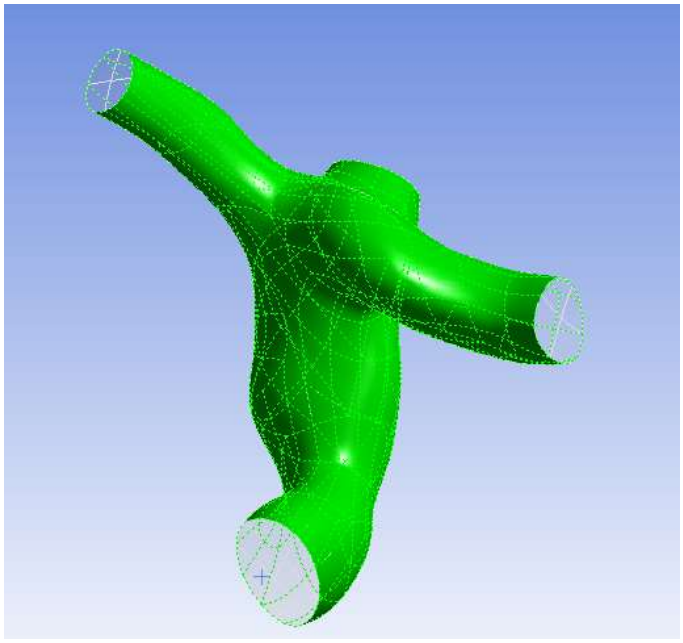

Figure 0-16 Select wall faces.

Then, right click the highlighted surface, and find “Create Named Selection”:

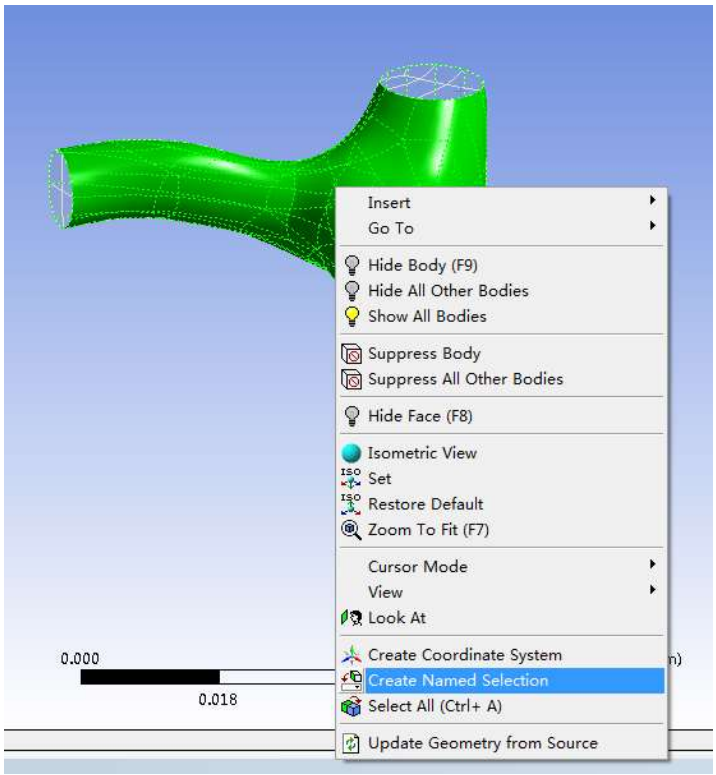

Figure 0-17

You need to create “Name Selection” for

1. Original TCPC Body Wall, i.e. Figure 0-18 (a).
    a. Name = “tcpc_wall”
2. All original TCPC vessel ends, i.e. Figure 0-18 (b). When you do these original vessel ends, you may still want to hide all extension bodies.
    a. Ex. “rsvc”,”ivc”
3. Sidewalls of all vessel extensions, i.e. Figure 0-18 (c).
    a. Ex. “rsvc_ext_wall”,”ivc_ext_wall”
4. Ends of all vessel extensions, i.e. Figure 0-18 (d).
    a. Ex. “rsvc_ext_end”,”ivc_ext_end”

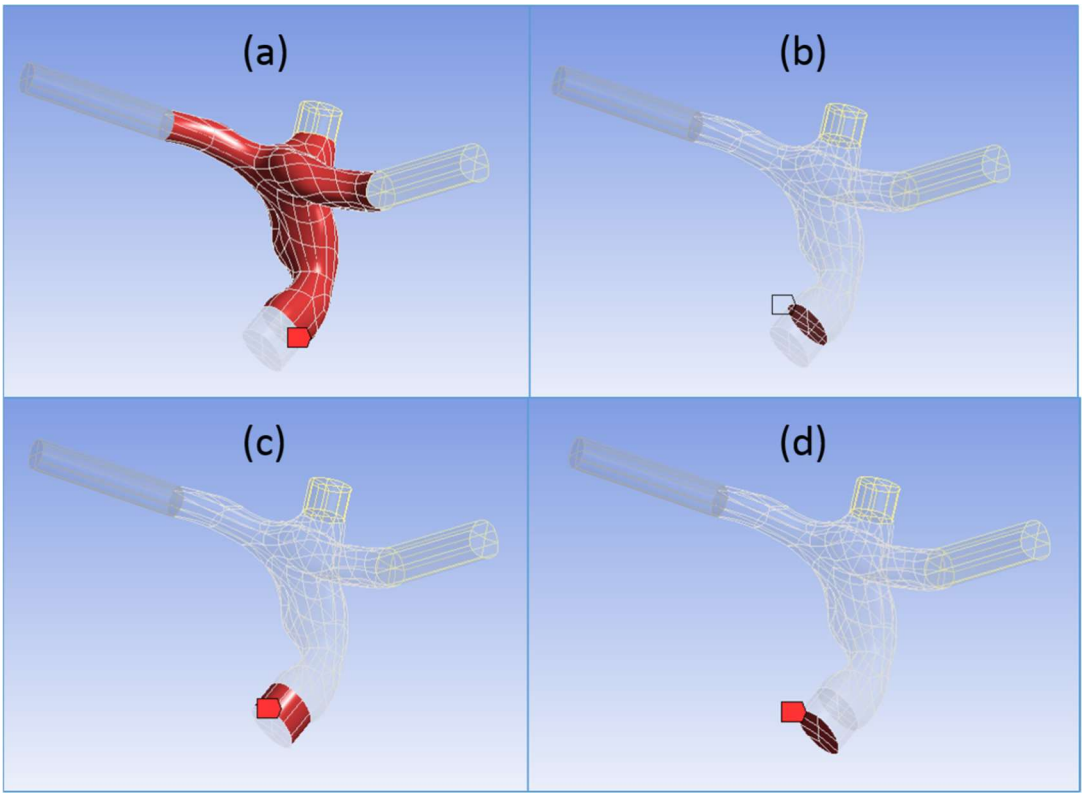

Figure 0-18

You can use the name convention illustrated in Figure 0-19. Make sure that svc and associated features are named “rsvc” or “rsvc_...” in named selections.

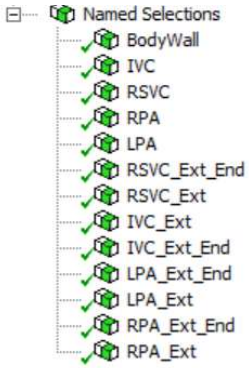

Figure 0-19

Now, click the "Mesh" in the project outline and make sure:

1. "Physical Preference = CFD";

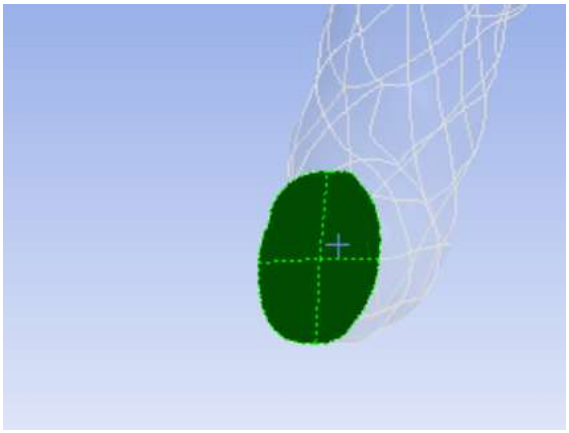

Figure 0-20

Figure 0-21

2. Modify Sizing
    a. Select all the vessel ends and divide them by 4 to get the average area.
    b. Use Matlab or Excel to calculate the average diameter by inserting the average area in the equation derived above.
    c. Go to "Mesh" → "Sizing"
    d. Set "Max Size" and "Max Face Size" as approximately $d_{average}/4$; also, set "Min Size" as $d_{average}/40$. **Please approximate to the nearest number that can be divided by 3.** In the above case, "Max Size" would be 0.0009 (m) and "Min Size" would be 0.009 (m). Type equation here.

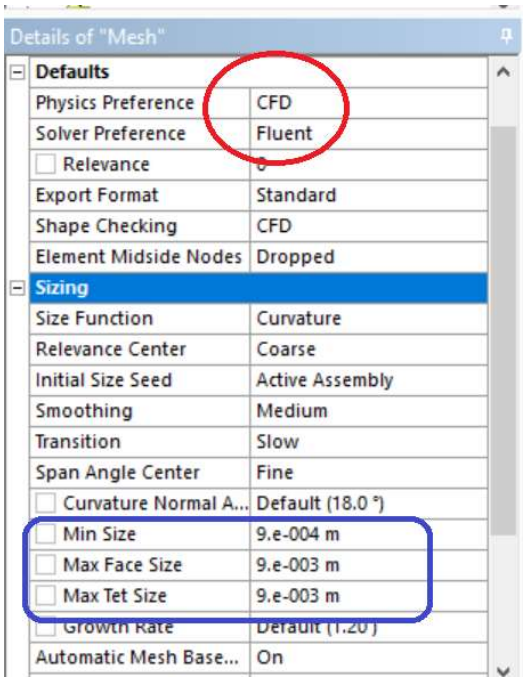

Figure 0-22

3. Next, Right Click "Mesh" and "Insert → Sizing".

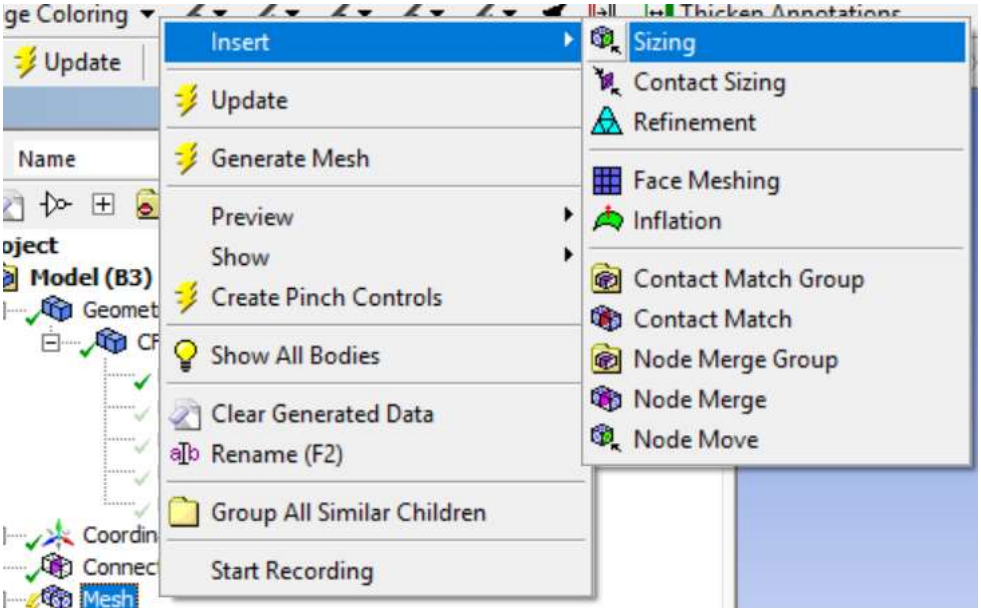

Figure 0-12

a. For Geometry, use the Body Select Tool to select the TCPC Body.

b. Change “Element Size” to $d_{average}$ /40

Details of "Body Sizing" - Sizing	
Scope	
Scoping Method	Geometry Selection
Geometry	1 Body
Definition	
Suppressed	No
Type	Element Size
Element Size	9.e-004 m
Behavior	Soft
Curvature Normal Angle	Default
Growth Rate	Default
Local Min Size	Default (9.e-004 m)

Figure 0-13

4. Right Click “Mesh” and “Insert → Inflation”.

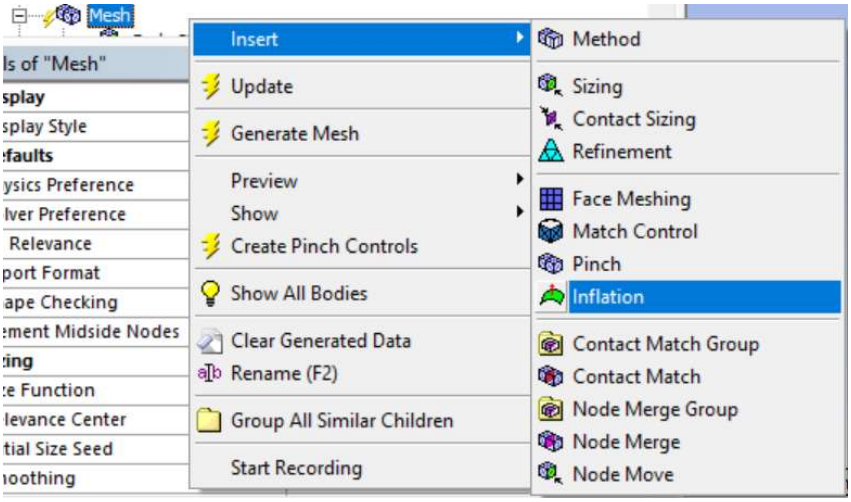

Figure 0-14

a. For ”Geometry”: Use the Body Select Tool to select the TCPC body as above.

b. For “Boundary”: Use Face selecting tool to select the TCPC surface **excluding** vessel ends. You can Press Ctrl + A to select all surfaces and then de-select vessel boundaries with the Face Select Tool.

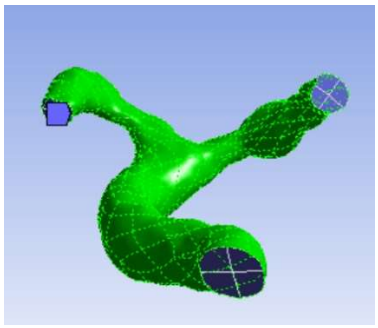

Figure 0-15

c. For “Inflation Option”, select “Total Thickness”. Change “Number of Layers” to 10 and change “Growth Rate” to 1.05

Details of "Inflation" - Inflation

Scope	
Scoping Method	Geometry Selection
Geometry	1 Body
Definition	
Suppressed	No
Boundary Scoping Method	Geometry Selection
Boundary	230 Faces
Inflation Option	Total Thickness
Number of Layers	3
Growth Rate	1
Maximum Thickness	9.e-004 m
Inflation Algorithm	Pre

Figure 0-16

d. Set “Maximum thickness” to $d_{average}$ /40 otherwise

5. Right click “Mesh” and “Insert → Sizing” again

a. Use the Body Select Tool to select all the extrusion bodies

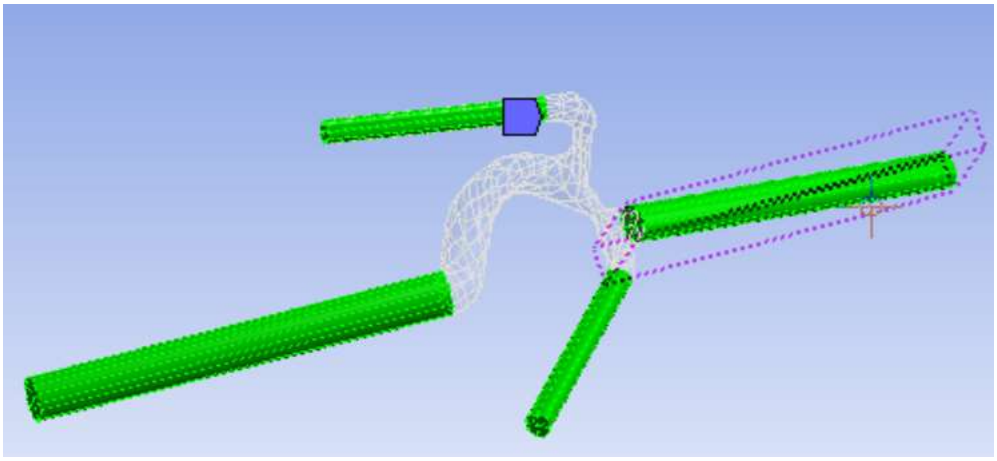

Figure 0-17

b. For “Element Size”, use $d_{average}$ /4

Scope	
Scoping Method	Geometry Selection
Geometry	4 Bodies
Definition	
Suppressed	No
Type	Element Size
Element Size	9.e-003 m
Behavior	Soft
Curvature Normal Angle	Default
Growth Rate	Default
Local Min Size	Default (9.e-004 m)

Figure 0-18

6. Right click “Mesh” and “Insert → Sizing”
    a. Use the Face Select Tool to select all the extrusion ends

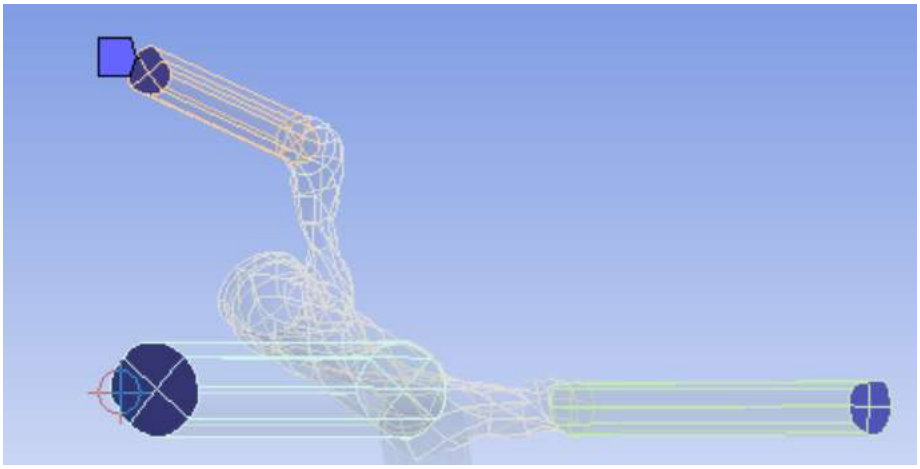

Figure 0-19

b. For “Element Size”, use $d_{average}$ /4

c. Change “Behavior” to “Hard”

Details of "Face Sizing" - Sizing	
Scope	
Scoping Method	Geometry Selection
Geometry	16 Faces
Definition	
Suppressed	No
Type	Element Size
Element Size	9.e-003 m
Behavior	Hard

Figure 0-19

7. Right click “Mesh” and “Insert → Method”
    a. For “Geometry”, use Ctrl-A to select all of the bodies in the domain
    b. Change “Method” to “Tetrahedrons”
    c. [Optional, ask Alan before you do it] Change “Algorithm” to “Patch Independent”
8. Then, right-click the “Mesh” and “Generate” (or “Update”).

So far, you finished all steps for “Meshing”. Close the module and save the project.

Computational Fluid Dynamic simulation set-up

Fluent - Simulation

Go back to the ANSYS Workbench main panel and add a “FLUENT” into the working flow. Connect “Mesh” to “Setup” under “Fluent” icon, shown in Figure 0-23. After the connection, a lighting mark may appear next to the “Mesh”. Just right click, “Update”, and wait.

Figure 0-23

If everything goes fine, a check mark should appear. Now, double-click the “Setup” under “Fluent”. The Fluent start-up dialog should be pop-up. You can either select “Serial” mode (Figure 0-24 (a)), which will run the simulation with single CPU, or “Parallel” mode (Figure 0-24 (b)), where **you need to make sure you do not overestimate the total number of CPUs you have!!**

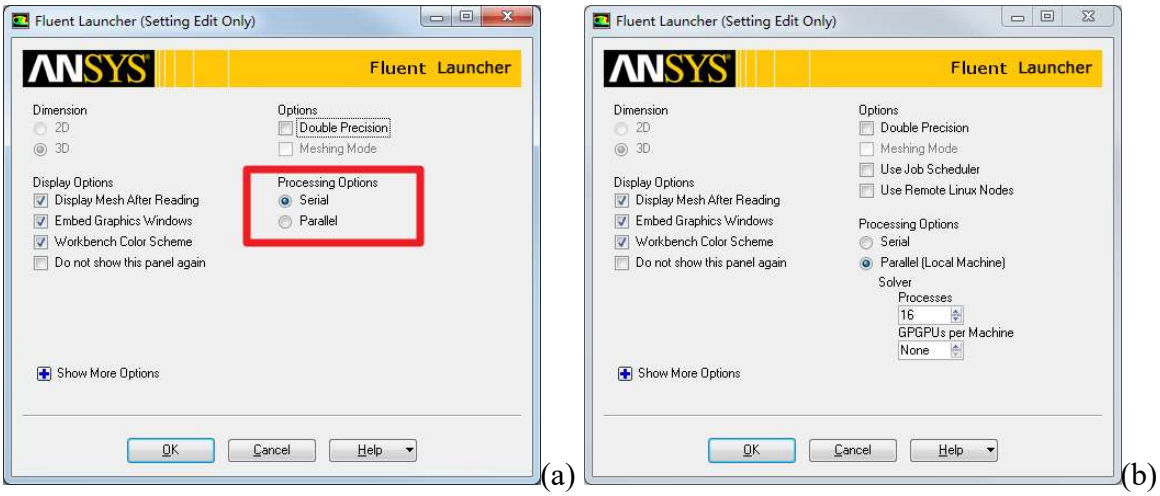

Figure 0-24

In Fluent main window, find the options bar on very left of the screen:

1. "General" → "Time" → "Transient"

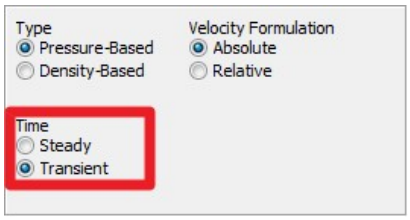

Figure 0-25

2. "Setting Up Domain" -> "Make Polyhedra"

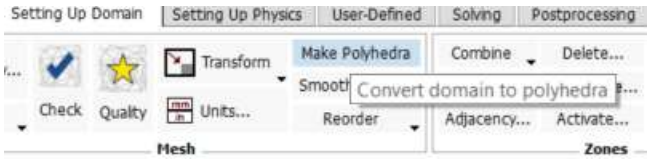

Figure 0-4

a. After finished making polyhedra mesh, "Smooth/Swap". Use default setting and click "Smooth". Smooth for 1-2 times.

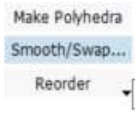

Figure 0-5

b. Check "Quality"

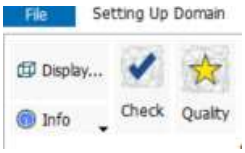

Figure 0-6

i. Make sure that the "Minimum Orthogonal Quality" is greater than 0.3.

ii. Make sure that "Maximum Ortho Skew" is less than 0.7.

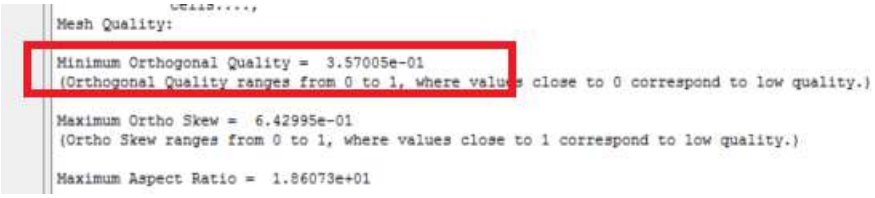

Figure 0-7

c. Then, click "Reorder" -> "Domain"

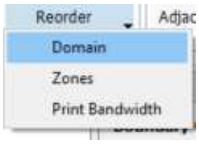

Figure 0-8

3. "User-Defined" → "Scalars"

Figure 0-9

a. Increase the "Number of User-Defined Scalars" to 1

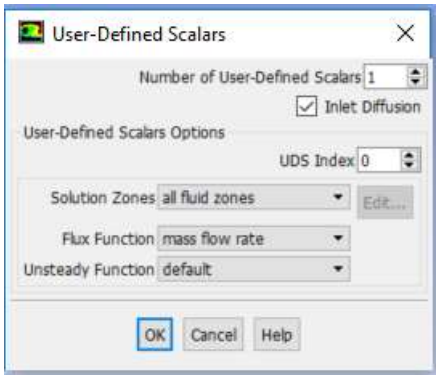

Figure 0-10

4. “Material” → “air” → “Create/Edit”

Figure 0-11

a. Change “Name” to “blood”
b. In the “Properties” section, change the density and viscosity to blood properties:
    i. Blood density = 1060 kg/m3
    ii. Blood viscosity = 0.0034 kg/m*s

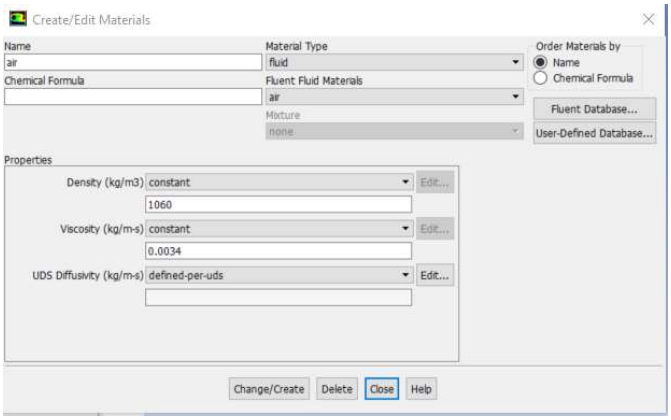

Figure 0-12

c. Click “Edit” After “UDS Diffusivity”
    i. Ensure that the Coefficient = 0

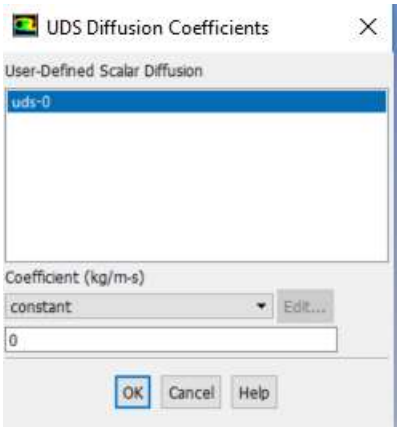

Figure 0-13

d. Click the “Change/Edit” and, then, “Close”.

e. For “Solution Methods”, use settings as shown below, change the Momentum to third order

third-ordered MUSCL

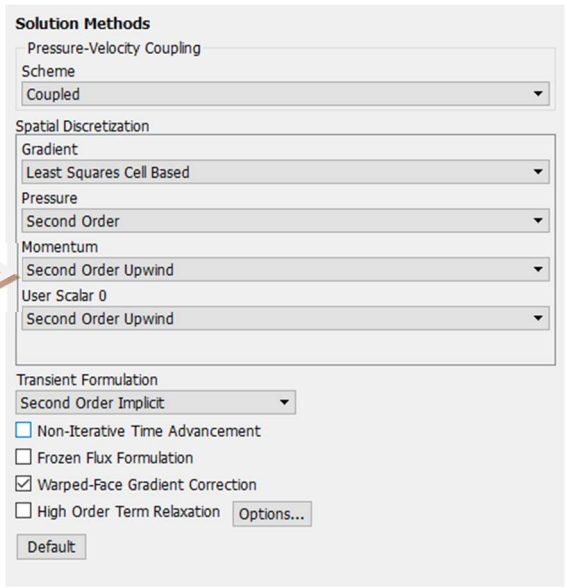

Figure 0-21

f. "Solution Controls": Change the "Flow Courant Number" to 1*10^6 and then click "Advanced."

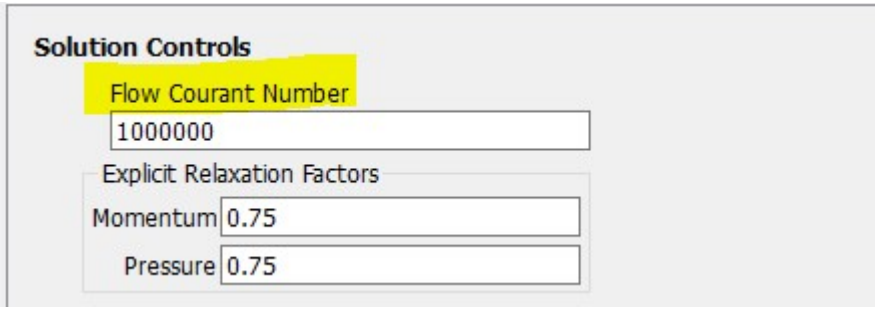

Figure 0-21

g. Make changes according to the figure below.

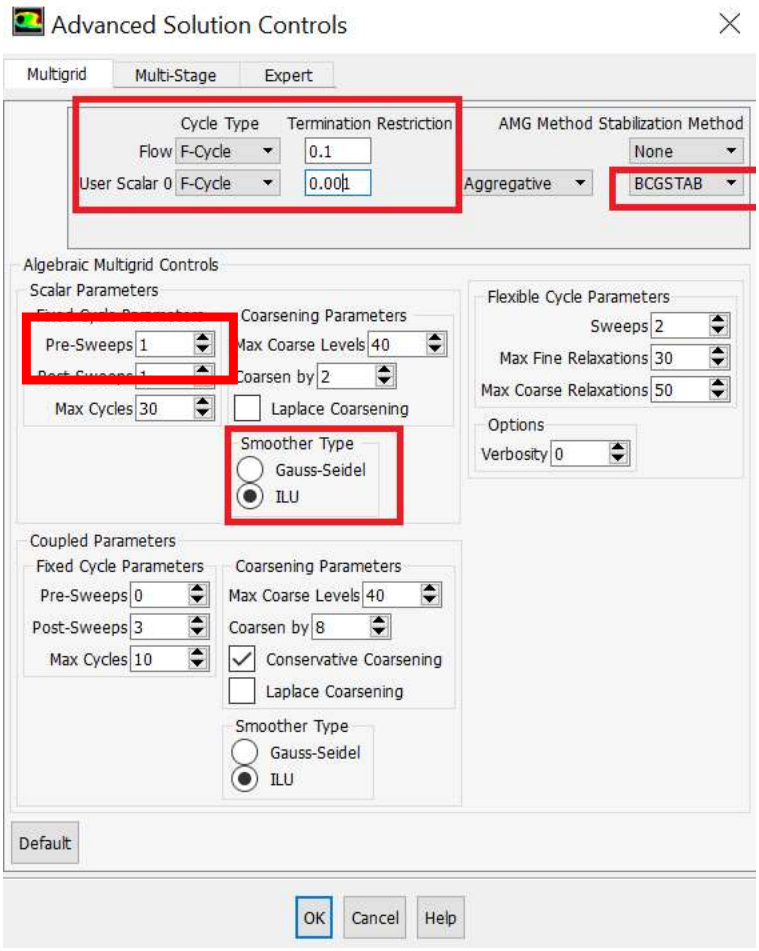

Figure 0-22

h. “Monitors” → “Residuals-Print, Plot” → “Edit”: change all “Absolute Criteria” to 0.0001 except for “continuity”.

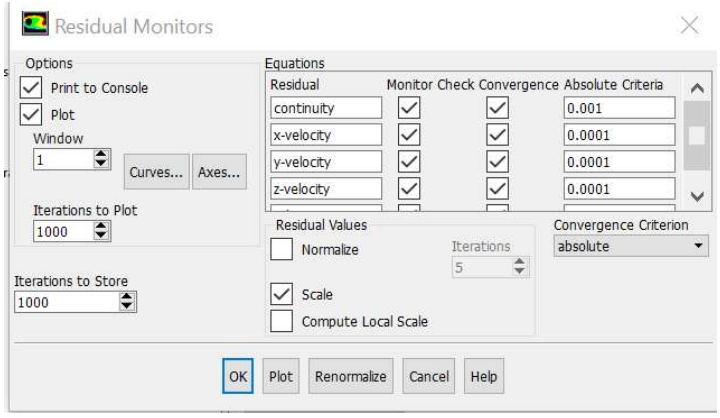

Figure 0-23

i. “Solution Initialization”: enable the “Hybrid Initialization”, but do not click “Initialize”! And wait.

Figure 0-24

5. Save the case to “Setup.cas” in patient case folder (i.e. CHOP128A/)

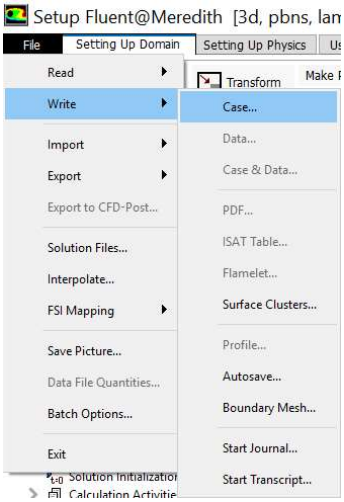

Figure 0-24

Modifying UDF files

1. The Setup Process is complete. Now, Open UDF folder and you should see the following list of files.

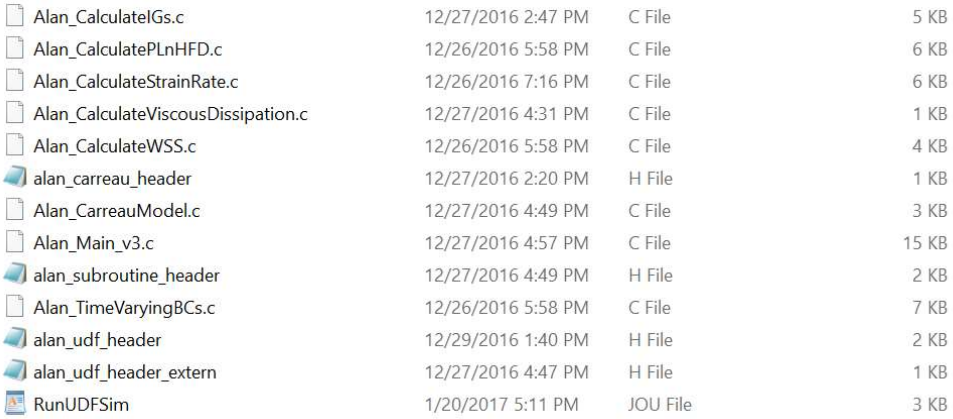

Alan_CalculateIGs.c	12/27/2016 2:47 PM	C File	5 KB
Alan_CalculatePLnHFD.c	12/26/2016 5:58 PM	C File	6 KB
Alan_CalculateStrainRate.c	12/26/2016 7:16 PM	C File	6 KB
Alan_CalculateViscousDissipation.c	12/27/2016 4:31 PM	C File	1 KB
Alan_CalculateWSS.c	12/26/2016 5:58 PM	C File	4 KB
alan_carreau_header	12/27/2016 2:20 PM	H File	1 KB
Alan_CarreauModel.c	12/27/2016 4:49 PM	C File	3 KB
Alan_Main_v3.c	12/27/2016 4:57 PM	C File	15 KB
alan_subroutine_header	12/27/2016 4:49 PM	H File	2 KB
Alan_TimeVaryingBCs.c	12/26/2016 5:58 PM	C File	7 KB
alan_udf_header	12/29/2016 1:40 PM	H File	2 KB
alan_udf_header_extern	12/27/2016 4:47 PM	H File	1 KB
RunUDFSim	1/20/2017 5:11 PM	JOU File	3 KB

Figure 4-1

2. Open the “alan_udf_header.h”

```
*/
int numVessel = 4;
char VesselName[4][20] = {"ivc","lpa","rpa","rsvc"};
int VesselID[4] = {6,9,8,7};
int OutletVessel[4] = {0,1,1,0};

int lpaID = 9;
int TCPC_VolID = 10;
int TCPC_SurfID = 17;
```

Figure 4-2

a. Check Vessel Name and the number of vessels in the format of “VesselName[numVessel][20]” (Figure 4-2).

b. Modify “VesselID” according to the format of “VesselID[numVessel]” and make sure the numbers correspond to the “ID” of original vessel in the “Boundary Conditions” section in Fluent (Figure 4-2, Figure 4-3). For example, the “ID” of IVC is 6, which corresponds to the first value of “VesselID”. Note that these IDs are **not** the IDs of the extrusion ends.

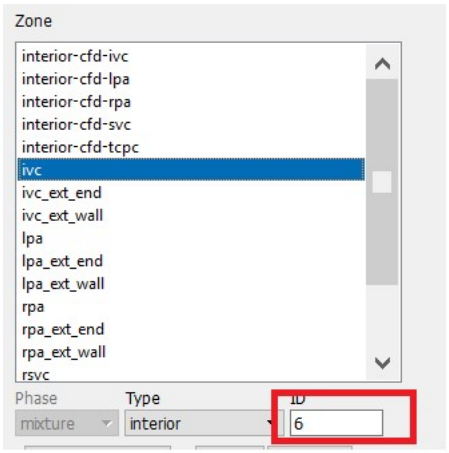

Figure 4-3

c. Check "OutletVessel" variable so that the value matches vessel name.
    i. 1 means the corresponding vessel is outlet
    ii. 0 means the corresponding vessel is inlet

d. Modify "lpaID", and "TCPC_SurfID" according to "ID" of original LPA end and TCPC surface body in the "Boundary Conditions" section in Fluent. (Figure 4-4)

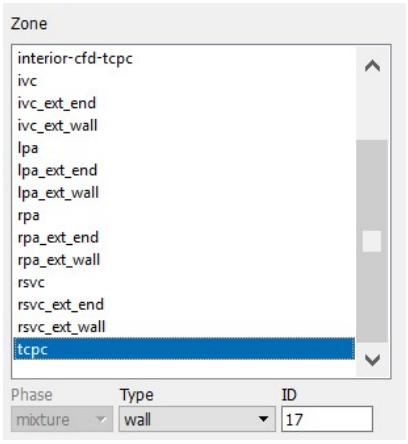

Figure 4-4

e. Modify "TCPC_VolID" according to the ID of Body Wall (TCPC) in the "Cell Zone Conditions" section in Fluent. (Figure 4-5)

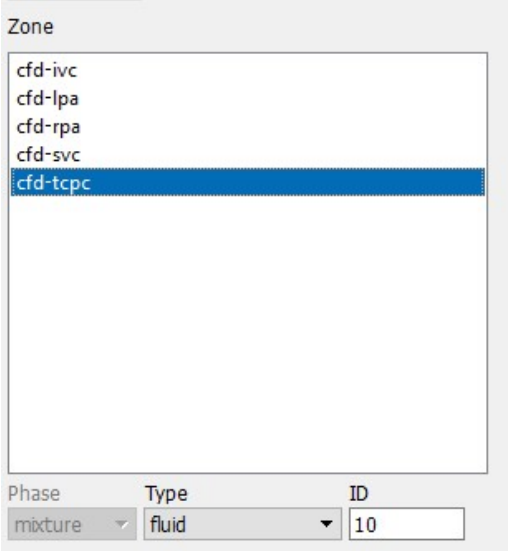

Figure 4-5

3. Open "alan_udf_header_extern.h"
    a. Check and if necessary, modify "VesselName" and the number of vessels in the format of "VesselName[numVessel][20]".
    b. Modify "VesselID" according to the format of "VesselID[numVessel]".

```
extern char VesselName[4][20];
extern int numVessel, VesselID[4], OutletVessel[4];
extern int lpaID, TCPC_VolID, TCPC_SurfID;
```

Figure 4-6

4. Open "RunUDFSim.jou"
    a. First line: change "rcd" to "rc".
    b. Change the name of the case file to the name of your Fluent case file.
        i. For example, if you name your case "Setup.cas", change the name appropriately in the journal file.
    c. In the second section, "define boundary conditions", uncomment additional boundary conditions if these BCs are present in your case. (Figure 4-7)
        i. You can uncomment a line by removing the semicolon in front of it.
        ii. Do not uncomment the RPA line if you are not using the RPA as a velocity inlet.
    d. At the end of the journal file, change the value to the right of /solve/dual-time-iterate to be 10,000 * full cycle time. (Figure 4-8)

i. For example, if the full cardiac cycle in your case is 0.9 seconds, change the value to 9000.

```
-------------------------
;====> define boundary conditions
/define/boundary-conditions/velocity-inlet ivc_ext_end no no yes
yes yes yes udf ivc_udf_vel::libudf no 0 no yes no 1000
/define/boundary-conditions/velocity-inlet rsvc_ext_end no no yes
yes yes yes udf rsvc_udf_vel::libudf no 0 no yes no 0
;/define/boundary-conditions/velocity-inlet rsvc_ext_end no no yes
yes yes yes udf rsvc_udf_vel::libudf no 0 no yes no 1
;/define/boundary-conditions/velocity-inlet lsvc_ext_end no no yes
yes yes yes udf lsvc_udf_vel::libudf no 0 yes no 0
;/define/boundary-conditions/velocity-inlet az_ext_end no no yes
yes yes yes udf az_udf_vel::libudf no 0 yes no 0
/define/boundary-conditions/velocity-inlet lpa_ext_end no no yes
yes yes yes udf lpa_udf_vel::libudf no 0 yes no 0
;/define/boundary-conditions/velocity-inlet rpa_ext_end no no yes
yes yes yes udf rpa_udf_vel::libudf no 0 yes no 0
;/define/boundary-conditions/velocity-inlet rupa_ext_end no no yes
yes yes yes udf rupa_udf_vel::libudf no 0 yes no 0
```

Figure 4-7

```
--
/solve/set/time-step 0.001
/solve/monitors/residual/convergence-criteria 0.001 0.0001 0.0001 0.0001 0.0001
/solve/initialize/hyb-initialization yes
/solve/dual-time-iterate 9000 100
wcd "Final.cas"
exit
```

Figure 4-8

5. Copy all files into patient case folder (i.e. CHOP128A/).

Blood waveform processing

This appendix includes the custom MATLAB scripts for waveform processing including (i) scaling the waveforms and (ii) using FFT analysis to create the boundary condition file for CFD simulation. The FFT_FittedCurves.m script will call the other 2 functions.

Waveform scaling

```
%%code to convert matrix of time/flows from ml/s to kg/m3 and then scale outlets
%%appropariately to maintain appropriate flow split
%Also converts time to seconds and scales as needed to get integer number
%of milliseconds.

%%%this version scales each phase individually

%%based on matrix with the following columns: (time is in milliseconds and
%%flows are in mL/s)
%% time ivc rsvc lsvc az lpa rpa rupa

prompt = 'matrix of time/flows= ';
mat = input(prompt);

%convert units
mat(:,2:8)=mat(:,2:8)*0.00106;

%%calculate sum of inlets and outlets

for i=1:length(mat)
   inlets=sum(mat(i,2:5));
   outlets=sum(mat(i,6:8));
   factor=inlets/outlets;

   %%scale outlets so total inlet equals total outlet FOR EACH PHASE
   mat(i,6)=mat(i,6)*factor;
   mat(i,7)=mat(i,7)*factor;
   mat(i,8)=mat(i,8)*factor;
end


%deal with time column

%check if integer multiple, if not then scale
```

```
finalTime=2*mat(end,1)-mat(end-1,1);
ideal=round(finalTime);

%to get to an integer multiply by the following factor
factor2=ideal/finalTime;

mat(:,1)=mat(:,1)*factor2;

%convert to seconds
mat(:,1)=mat(:,1)/1000;
```

FFT analysis and creation of boundary condition file for simulations

This task requires 3 MATLAB files: (i) FFT_FittedCurves.m, (ii) fscreate.m and (iii) GetWaveform.m.

FFT_FittedCurves.m

```
clear all

fft_num = 30;
dt = 0.001;

interp_enable = 1;
interp_fft_number = 1024; %use how many points to interpolate the original curve. Better to make it 2^n
interp_type = 'spline'; % spline is usually good. pchip is cubic interpolation; sometimes, it over smoothed the curve

fft_plot_cycle = 2; %define how many cycles you want to plot for the fft curves

% make sure ftime is NOT a full cycle!
%       Vessel ID:
%       Column    1           2               3           4           5           6       7
8
%         flow_time  IVC      RSVC/SVC   LSVC          AZ          LPA          RPA
        RUPA
%
%   Unit: flow_time in second, IVC ... are mass flow rates in kg/s
ftime = [
Output from waveform scaling code.
];

%   Below is for developers!
```

```
vname = {'ivc','rsvc','lsvc','az','lpa','rpa','rupa'};
Vessel_Good = mean(ftime);
sizeftime = size(ftime);
nd = sizeftime(1,1);
vesselnum = sizeftime(1,2)-1;

ftime(nd+1,1) = ftime(nd,1)+ftime(nd,1)-ftime(nd-1,1);
vesselnum_good = 0;
for i = 1:vesselnum;
   ftime(nd+1,i+1) = ftime(1,i+1);
   if Vessel_Good(i+1) ~= 0
      vesselnum_good = vesselnum_good + 1;
   else
      vesselnum_good = vesselnum_good;
   end
end


nd = nd+1;

ff = ftime(nd,1);

for t = 1:interp_fft_number+1
   newtime(t) = ftime(nd,1)/interp_fft_number*(t-1);
end

plot_loc = 1;

for vesselID = 1:vesselnum
   timecheck = ftime(:,1);
   vfrcheck(:,vesselID) = ftime(:,vesselID+1);

   % newvfr = spline(ftime(:,1),ftime(:,2),newtime);
   newvfr(:,vesselID) = interp1(ftime(:,1),ftime(:,vesselID+1),newtime, interp_type);

   FSfun_vfr(:) = newvfr(:,vesselID);

%%%%%%%%%%%%%%%%%%%%%%%%%%%%%%%%%%%%%%%%%%%%%%
%%%%%%%%%%%%%%%%%%%%%%%%%%%%%%%%%%
   if interp_enable
      FSfun = fscreate(newtime,FSfun_vfr,fft_num);
   else
      FSfun = fscreate(ftime(:,1),ftime(:,vesselID+1),fft_num);
   end
```

```
   MeanValue(vesselID) = FSfun('avg');
   cosfun1 = FSfun('cosine');
   sinfun1 = FSfun('sine');
   for i = 1:fft_num
      cosfun(i,vesselID) = cosfun1(i);
      sinfun(i,vesselID) = sinfun1(i);
   end


   for t = 1:fft_plot_cycle*interp_fft_number+1
      time_fft(t) = ftime(nd,1)/interp_fft_number*(t-1);
      vfr_fft(t,vesselID) = MeanValue(vesselID);
      for i = 1:fft_num
         vfr_fft(t,vesselID) = vfr_fft(t,vesselID) + cosfun(i,vesselID)*cos(2*pi*i/ff*time_fft(t)) +
sinfun(i,vesselID)*sin(2*pi*i/ff*time_fft(t));
      end
   end

   if interp_enable
      SStot = 0.0;
      SSres = 0.0;
      for i = 1:interp_fft_number
         SStot = SStot + (newvfr(i,vesselID)-MeanValue(vesselID))^2;
         SSres = SSres + (newvfr(i,vesselID)-vfr_fft(i,vesselID))^2;
      end
      alan_r_squared(vesselID) = 1- SSres/SStot;
   else
      warning('interp_enable is diabled. no R^2, i.e. R^2 = 0\n');
      alan_r_squared(vesselID) = 0.0;
   end



   % calculate derivatives
   d_vfr_fft = diff(vfr_fft(:,vesselID));
   d_time_fft = diff(time_fft);
   for t = 1:fft_plot_cycle*interp_fft_number
      d_vfr(t,vesselID) = d_vfr_fft(t)/d_time_fft(t);
   end
   d_vfr(fft_plot_cycle*interp_fft_number+1,vesselID) = d_vfr(1,vesselID);



   % plots

   if Vessel_Good(vesselID+1) ~= 0
```

```
        subplot(vesselnum_good,2,plot_loc);
        plot_loc = plot_loc+1;
        scatter(newtime,newvfr(:,vesselID));
        hold on;
        scatter(ftime(:,1),ftime(:,vesselID+1),'filled','d');
        hold on;
        plot(time_fft, vfr_fft(:,vesselID));
        hold off;
        titlename = sprintf('%s Curves, R^2 = %f',vname{vesselID},alan_r_squared(vesselID));
        title(titlename);
        subplot(vesselnum_good,2,plot_loc);
        plot_loc = plot_loc+1;
        scatter(time_fft, d_vfr(:,vesselID));
        titlename = sprintf('%s Derivative',vname{vesselID});
        title(titlename);
    end
end

fname = sprintf('alan_FFT_BCs_header.h');
FFT_header = fopen(fname,'w');
fprintf(FFT_header,'#ifndef _ALAN_FFTBCs_HEADER_H_\n');
fprintf(FFT_header,'#define _ALAN_FFTBCs_HEADER_H_ 1\n');

fprintf(FFT_header,'/* ');
for i = 1:vesselnum
    fprintf(FFT_header,'%i: %s;',i,vname{i});
end
fprintf('\n');
fprintf(FFT_header,'*/ \n');

fprintf(FFT_header,'double alan_FFT_mean[%i] = {',vesselnum);
for i = 1:vesselnum
    if i ~= vesselnum
        fprintf(FFT_header,'%f,',MeanValue(i));
    else
        fprintf(FFT_header,'%f};\n',MeanValue(i));
    end
end

fprintf(FFT_header,'int fft_num = %i;\n',fft_num);
fprintf(FFT_header,'double samplef = %f;\n',ftime(nd,1));


fprintf(FFT_header,'struct alan_FFT_const {\n\tdouble cos[%i];\n\tdouble
sin[%i];\n};\n\n',fft_num, fft_num);
  fprintf(FFT_header,'struct alan_FFT_const alan_FFT[%i] = {\n',vesselnum);
```

```
for i = 1:vesselnum
   fprintf(FFT_header,'\t{\n');
   fprintf(FFT_header,'\t\t{');
   for j=1:fft_num
      if j ~= fft_num
         fprintf(FFT_header,'%e, ',cosfun(j, i));
      else
         fprintf(FFT_header,'%e},\n',cosfun(j, i));
      end
   end
   fprintf(FFT_header,'\t\t{');
   for j=1:fft_num
      if j ~= fft_num
         fprintf(FFT_header,'%e, ',sinfun(j, i));
      else
         fprintf(FFT_header,'%e}\n',sinfun(j, i));
      end
   end
   if i ~= vesselnum
   fprintf(FFT_header,'\t},\n');
   else
      fprintf(FFT_header,'\t}\n');
      fprintf(FFT_header,'};\n');
   end

end

fprintf(FFT_header,'#endif /* _ALAN_FFTBCs_HEADER_H_ */ \n');

fclose(FFT_header);
fclose('all');
```

fscreate.m

```
function [FSfun,Kn]=fscreate(varargin)
N=64;
FSData.tag='';
narg=nargin;
if narg<2
  error('At Least Two Input Arguments Required.')
end
if narg>2 && ischar(varargin{end}) && ...
      ~any(strcmpi(varargin{end},{'odd','even'})) && ...
      ~any(strcmpi(varargin{end},{'foh','zoh'})) && ...
      (ischar(varargin{end-1}) && ~isequal(lower(varargin{end-1}),'tag'))
  FSData.tag=varargin{end}; % grab tag provided
  varargin(end)=[];         % strip tag from input
  narg=narg-1;
end
switch class(varargin{1}) % find class of first input argument
case {'double' 'single'}
  if isequal(numel(varargin{1}),numel(varargin{2})) % fscreate(t,f,N,TYPE)
    t=varargin{1}(:);
    f=varargin{2}(:);
    if narg>=3 && isnumeric(varargin{3})
      N=varargin{3};
      if fix(N)~=N || abs(N)~=N || N<1
        error('FSCREATE:InputError','N Must be a Positive Integer.')
      end
    end
    if ischar(varargin{end}) % Type is specified
      Tref={'foh' 'zoh'};
      idx=strncmpi(varargin{end},Tref,1);
      Type=char(Tref(idx));
      if isempty(Type)
        error('FSCREATE:InputError','Unknown TYPE Argument.')
      end
    else
      Type='foh';
    end
    Kn=local_getFS(t,f,N,Type);
    FSData.Kn=Kn;
    FSData.T=t(end)-t(1);
    FSfun=@(t) FourierSeries(FSData,t);
  else                                  % fscreate(Kn,T)
    Kn=varargin{1}(:).';
    N=(length(Kn)-1)/2;
    if N~=fix(N) || max(abs(conj(Kn(N:-1:1))-Kn(N+2:end)))>sqrt(eps)
```

```
        error('FSCREATE:InputError', ...
          ['First Input Argument must be a valid Fourier Series\n', ...
           'vector containing the complex exponential series\n', ...
           'coefficients in increasing harmonic order with\n', ...
           'K(-n)=conj(K(n)) where n is the harmonic number.']);
      end
      T=varargin{2};
      if numel(T)~=1 || T<=0 || ~isreal(T)
        error('Second Input Argument Must be the Positive Scalar Period.')
      end
      FSData.Kn=Kn;
      FSData.T=T;
      FSfun=@(t) FourierSeries(FSData,t);
    end
  case 'char'                              % fscreate('WAVE',T,N,P)
    wave=varargin{1};
    T=varargin{2};
    if narg==4
      P=varargin{4};
    else
      P=[];
    end
    if narg>=3 && ~isempty(varargin{3})
      N=varargin{3};
      if fix(N)~=N || abs(N)~=N || N<1
          error('FSCREATE:InputError','N Must be a Positive Integer.')
      end
    end
    Kn=local_getwave(wave,T,N,P);
    FSData.Kn=Kn;
    FSData.T=T;
    FSfun=@(t) FourierSeries(FSData,t);
  case 'function_handle'
    if ~ischar(varargin{2})
      error('FSCREATE:InputError','Second Input Argument Must be a String.')
    end
    if narg==3 && ...
      isa(varargin{3},'function_handle')     % fscreate(FSfunA,'Op',FSfunB)

      FSfunA=varargin{1};
      NA=FSfunA('size');
      KnA=FSfunA('coef');
      FSData.T=FSfunA('period');

      FSfunB=varargin{3};
      NB=FSfunB('size');
```

```
  KnB=FSfunB('coef');

  zAB=zeros(1,NA-NB);
  zBA=zeros(1,NB-NA);
  switch lower(varargin{2})
  case '+'
    Kn=[zBA KnA zBA]+[zAB KnB zAB];
  case '-'
    Kn=[zBA KnA zBA]-[zAB KnB zAB];
  case '*'
    Kn=conv(KnA,KnB);
    iDC=(length(Kn)+1)/2;
    N=max(NA,NB);
    Kn=Kn(iDC-N:iDC+N);
  otherwise
    error('FSCREATE:InputError','Unknown Mathematical Operator.')
  end
  FSData.Kn=Kn;
  FSfun=@(t) FourierSeries(FSData,t);

else                % fscreate(FSfun,'Op') or fscreate(FSfun,'Op',P)
  FSfun=varargin{1};
  Kn=FSfun('coef');
  N=(length(Kn)-1)/2;
  iDC=N+1;
  T=FSfun('period');
  wo=2*pi/T;
  if narg==3
    P=varargin{3};
  end
  switch lower(varargin{2}(1:min(2,length(varargin{2}))))
  case 'ta'                     % tag
    if ischar(P)
      FSData.tag=P;
    else
      error('FSCREATE:InputError','Character String Tag Required.')
    end
  case 'di'                     % differentiate
    Kn=1j*wo*(-N:N).*Kn;
  case 'in'                     % integrate
    nn=-N:N;
    idx=nn~=0;
    iKn=zeros(size(Kn));
    iKn(idx)=Kn(idx)./(nn(idx)*wo*1i);
    iKn(iDC)=0;
    Kn=iKn;
```

```
case 'mi'                       % time mirror
  Kn=Kn(end:-1:1);
case 'sm'                       % Exact Blackman smoothing
  m=linspace(-pi,pi,length(Kn));
  Kn=Kn.*(7938 + 9240*cos(m) + 1430*cos(2*m))/18608;
case 'tr'                       % trim negigible elements
  tol=sqrt(eps);
  mKn=abs(Kn);
  rKn=abs(real(Kn));
  iKn=abs(imag(Kn));
  b=mKn<tol*max(mKn);
  Kn(b)=0;            % elements with small magnitude
  b=rKn<tol*max(rKn) | rKn<tol*iKn;
  Kn(b)=1i*imag(Kn(b)); % elements with small real part
  b=iKn<tol*max(iKn) | iKn<tol*rKn;
  Kn(b)=real(Kn(b));    % elements with small imaginary part
case 'ev'                       % Even part
  Kn=real(Kn);
case 'od'                       % Odd part
  Kn=1i*imag(Kn);
case 'ha'                       % Halfwave part
  idx=rem(N,2)+1:2:length(Kn);
  Kn(idx)=0;
case 'no'                       % no DC part
  Kn(iDC)=0;
case 'dc'                       % set DC value
  if narg==2 || numel(varargin{3})>1
    error('FSCREATE:InputError','Scalar Third Argument P Required.')
  end
  Kn(iDC)=real(P);
case 'ad'                       % set DC value
  if narg==2 || numel(varargin{3})>1
    error('FSCREATE:InputError','Scalar Third Argument P Required.')
  end
  Kn(iDC)=Kn(iDC)+real(P);
case 'de'                       % delay
  if narg==2
    error('FSCREATE:InputError','Third Argument P Required.')
  end
  if ischar(P)
    a1=angle(Kn(iDC+1))/(2*pi);
    switch lower(P(1))
    case 'o'
      d=a1+1/4;
    case 'e'
      d=a1;
```

```
        otherwise
          error('FSCREATE:InputError','Unknown Delay Requested.')
        end
      else
        d=P(1);
      end
      Kn=exp(-2j*pi*(-N:N)*d).*Kn;
    case 'sc'                       % scale amplitude
      if narg==2 || numel(varargin{3})>1
        error('FSCREATE:InputError','Scalar Third Argument P Required.')
      end
      Kn=P*Kn;
    case 'pe'                       % set period
      if narg==2 || numel(varargin{3})>1
        error('FSCREATE:InputError','Scalar Third Argument P Required.')
      end
      T=varargin{3};
    case 're'                       % resize
      if narg==2 || numel(varargin{3})>1
        error('FSCREATE:InputError','Scalar Third Argument P Required.')
      elseif fix(P)~=P || abs(P)~=P || P<1
        error('FSCREATE:InputError','P Must be a Positive Integer.')
      end
      if P>N     % pad with zeros
        zpadd=zeros(1,P-N);
        Kn=[zpadd Kn zpadd];
      elseif P<N % delete excess terms
        Kn=Kn(iDC-P:iDC+P);
      else % P=N no work
        return
      end
    otherwise
      error('FSCREATE:InputError','Unknown Operation Requested.')
    end
    FSData.Kn=Kn;
    FSData.T=T;
    FSfun=@(t) FourierSeries(FSData,t);
  end
otherwise
  error('Unknown First Input Argument.')
end % END of Primary Function
%---------------------------------------------------------------------------
%---------------------------------------------------------------------------
function Kn=local_getFS(t,f,N,type)      % fscreate(t,f,N,type) Subfunction
T=t(end)-t(1);
if T<=0
```

```
  error('Period Must be Positive.')
end
if ~isreal(f)
  error('Input Must be Real-Valued.')
end
if abs(f(1)-f(end))> eps*(1+abs(max(f)-min(f)))
  error('Input Must Describe Exactly One Period of the Function.')
end
t=t/T;
wo=2*pi;
df=diff(f);
dt=diff(t);
if any(dt<0)
  error('Time Points Must be Nondecreasing.')
end
switch type
case 'foh'
  Nl=length(f)-1;
  idx=dt~=0;
  m=zeros(Nl,1);
  m(idx)=df(idx)./dt(idx);
  b=f(1:end-1)-m.*t(1:end-1);
  n=1:N;
  mm=repmat(m,1,N);
  bb=repmat(b,1,N);
  t1=repmat(t(1:end-1),1,N);
  t2=repmat(t(2:end),1,N);
  nn=repmat(n,Nl,1);
  Fp=sum((1j*(mm.*t2+bb)./(nn*wo)+mm./(nn*wo).^2).*exp(-1j*nn*wo.*t2) - ...
       (1j*(mm.*t1+bb)./(nn*wo)+mm./(nn*wo).^2).*exp(-1j*nn*wo.*t1));
  Kn=[conj(Fp(end:-1:1)) trapz(t,f) Fp];
case 'zoh'
  n=1:N;
  Ni=length(f)-1;
  ff=repmat(f(1:end-1),1,N);
  t1=repmat(t(1:end-1),1,N);
  t2=repmat(t(2:end),1,N);
  nn=repmat(n,Ni,1);

  Fp=sum(1j*ff./(nn*wo).*(exp(-1j*nn*wo.*t2) - exp(-1j*nn*wo.*t1)));
  Kn=[conj(Fp(end:-1:1)) trapz(t,f) Fp];
end
%--------------------------------------------------------------------------
function Kn=local_getwave(wave,T,N,P) % fscreate('WAVE',T,N,P) Subfunction
lenP=length(P);
lkn=2*N+1;
```

```
Kn=zeros(1,lkn);

switch lower(wave(1:min(3,length(wave))))
case 'squ'                                  % squarewave
  Kn(N+2:2:lkn)=-2j*(((1:2:N)*pi).^(-1));
  Kn(1:N)=conj(Kn(lkn:-1:N+2));
case 'tri'                                  % triangle
  Kn(N+2:2:lkn)=4*(((1:2:N)*pi).^(-2));
  Kn(1:N)=conj(Kn(lkn:-1:N+2));
case 'ful'                                  % fullwave rectified sine
  Kn(N+1)=2/pi;
  n=2:2:N;
  Kn(N+3:2:lkn)=2./(pi*(1-n.^2));
  Kn(1:N)=conj(Kn(lkn:-1:N+2));
case 'hal'                                  % halfwave rectified sine
  Kn(N+1)=1/pi;
  Kn(N+2)=-j/4;
  n=2:2:N;
  Kn(N+3:2:lkn)=1./(pi*(1-n.^2));
  Kn(1:N)=conj(Kn(lkn:-1:N+2));
case 'dc'                                   % dc or constant
  Kn(N+1)=1;
case 'sin'                                  % sine wave
  if lenP==1
    n=P;
  else
    n=1;
  end
  if fix(n)~=n || n<1 || n>N
    error('Harmonic Number Must be an Integer Between 1 and N.')
  end
  Kn=zeros(1,N);
  Kn(n)=-1i/2;
  Kn=[conj(Kn(end:-1:1)) 0 Kn];
case 'cos'                                  % cosine wave
  if lenP==1
    n=P;
  else
    n=1;
  end
  if fix(n)~=n || n<1 || n>N
    error('Harmonic Number Must be an Integer Between 1 and N.')
  end
  Kn=zeros(1,N);
  Kn(n)=1/2;
  Kn=[Kn(end:-1:1) 0 Kn];
```

```
case 'saw'                                          % sawtooth
  if lenP==0                          % ideal sawtooth
    Kn(N+2:lkn)=2j*(((1:N)*2*pi).^(-1));
    Kn(1:N)=conj(Kn(lkn:-1:N+2));
  else                                % finite fall time sawtooth
    a=min(.4999,P(1));
    if a~=P(1)
      warning('FSCREATE:InputError',...
            'Requested Fall Time Must be Less Than 1/2.')
    end
    t=[0 a .5 1-a 1];
    f=[0 -1 0  1  0];
    [dum,Kn]=fscreate(t,f,N);
  end
case 'rsa'                                        % reverse sawtooth
  [dum,Kn]=fscreate('saw',T,N,P);
  Kn=Kn(end:-1:1);
case 'tra'                                          % trapezoid
  if lenP==0
    p=2/3;
  else
    p=min(abs(P(1)),.999);
  end
  if lenP>0 && p~=P(1)
    warning('FSCREATE:InputError',...
          'Requested Duty Cycle Must Be Less Than 1.')
  end
  a=(1-p)/2;
  b=1-a;
  npi=(1:2:N)*pi;
  jnpia=1j*a*npi;
  jnpib=1j*b*npi;
  Kn(N+2:2:lkn)=(( (1+1j*a*npi).*exp(-jnpia)...
    - (1+jnpib).*exp(jnpia)...
    + 1j*npi).*(npi.^(-2))./a...
    + ( (1/a-1)*exp(jnpia)...
    - exp(-jnpia) -1/a)*1j./npi);
  Kn(1:N)=conj(Kn(lkn:-1:N+2));
case 'pul'                                          % Pulsetrain
  if lenP==0
    p=1/2;
  else
    p=min(abs(P(1)),.999);
  end
  if lenP>0 && p~=P(1)
    warning('FSCREATE:InputError',...
```

```
            'Requested Duty Cycle Must Be Less Than 1.')
    end
    if lenP<2 || P(2)==0                % ideal zero rise time pulse
      Kn(N+1)=p;
      arg=pi*p*(1:N);
      Kn(N+2:lkn)=p*sin(arg)./(arg+eps);
      Kn(1:N)=conj(Kn(lkn:-1:N+2));
    else                                % finite rise time pulse
      r=min((1-p)/2-10*eps,abs(P(2)));
      if r~=P(2)
        warning('FSCREATE:InputError',...
              'Requested Rise Time Too Long.')
      end
      a=p/2;
      t=[0 a a+r 0.5 1-a-r 1-a 1];
      f=[1 1  0   0    0    1  1];
      [dum,Kn]=fscreate(t,f,N);
    end
  case 'bip'                                % Bipolar Pulsetrain
    if lenP==0
      p=2/3;
    else
      p=min(abs(P(1)),.999);
    end
    if lenP>0 && p~=P(1)
      warning('FSCREATE:InputError',...
            'Requested Duty Cycle Must Be Less Than 1.')
    end
    if lenP<2 || P(2)==0                % ideal zero rise time pulsetrain
      a=(1-p)/2; b=1-a;
      jnpi=(1:2:N)*pi*1j;
      Kn(N+2:2:lkn)=(exp(-jnpi*b)-exp(-jnpi*a))./(-jnpi);
      Kn(1:N)=conj(Kn(lkn:-1:N+2));
    else                                % finite rise time pulse
      r=min((1-p)/4-10*eps,abs(P(2)));
      if r~=P(2)
        warning('FSCREATE:InputError',...
              'Requested Rise Time Too Long.')
      end
      a=p/4;
      b=.25;
      c=.75;
      t=[0 b-a-r b-a b+a b+a+r 0.5 c-a-r c-a c+a c+a+r 1];
      f=[0   0    1   1    0    0    0    -1  -1   0   0];
      [dum,Kn]=fscreate(t,f,N);
    end
```

```
case 's2s'                                  % sine to square morph
  if lenP==0
    p=1/2;
  else
    p=P(1);
  end
  if p<0 || p>1
    error('FSCREATE:InputError',...
        'Morphing Parameter Must be Between 0 and 1.')
  end
  if p==0                          % sine wave
    Kn=zeros(1,N);
    Kn(1)=-1i/2;
    Kn=[conj(Kn(end:-1:1)) 0 Kn];
  elseif p==1                       % square wave
    Kn(N+2:2:lkn)=-2j*(((1:2:N)*pi).^(-1));
    Kn(1:N)=conj(Kn(lkn:-1:N+2));
  else                             % morph between sine and square
    kp=zeros(1,N);
    b=(1-p)/2;
    m=1:2:N;
    bm=b*m;
                kp(m)=(2*b/pi)*( 2i*bm.*exp(-1i*bm*pi)-1 )./(4*bm.^2-1)...
        - 2i*cos(bm*pi)./(m*pi)...
        + (2*b/pi)*( 1+ 2i*bm.*exp(1i*bm*pi))./(4*bm.^2-1);
                Kn=[conj(kp(end:-1:1)) 0 kp];
  end
otherwise
    error('FSCREATE:InputError','Unknown Waveform Input.')
end
%--------------------------------------------------------------------------
% Fourier Series Function
%--------------------------------------------------------------------------
function y=FourierSeries(FSData,t)
% Fourier Series Evaluation and Manipulation using function handles
%
% This function gets called when FSfun(...) is issued where FSfun is a
% function handle as returned by FSCREATE.

Kn=FSData.Kn;          % FS coefficient vector
wo=2*pi/FSData.T;      % fundamental frequency
N=(length(Kn)-1)/2;    % highest harmonic
iDC=N+1;              % index of dc component

if isnumeric(t)                          % Evaluate Fourier Series
  nwo=wo*(1:N);                  % positive harmonic indices
```

```
  ko=real(Kn(iDC));      % average value
  tsize=size(t);
  Knp=Kn(iDC+1:end).';          % positive frequency coefs
  y=ko+2*(real(exp(1j*t(:)*nwo)*Knp))';
  y=reshape(y,tsize);
elseif ~ischar(t)
  error('Unknown Input Argument.')
else                                        % FSfun('string')
  switch lower(t(1:min(3,length(t))))
  case 'tag'
    y=FSData.tag;
  case {'coe' 'kn'}                          % coefficient vector
    y=Kn;
  case {'per' 't'}                                % period
    y=FSData.T;
  case 'siz'                          % size or highest harmonic
    y=N;
  case {'dc' 'ave' 'avg'}                     % dc or average value
    y=Kn(iDC);
  case 'msv'                                 % mean square value
    y=real(Kn*Kn');
  case 'thd'                          % total harmonic distortion
    idx=iDC+[-1 1];
    fn=Kn(idx);
    Kn(idx)=[];
    y=sqrt(real(Kn*Kn')/real(fn*fn'));
  case 'one'                       % one-sided line amplitude spectra
    y=abs([Kn(iDC) 2*Kn(iDC+1:end)]);
  case 'pha'                         % one-sided line phase spectra
    y=angle(Kn(iDC:end))*180/pi;
  case 'sin'                           % trig sine coefficients
    y=-2*imag(Kn(iDC+1:end));
  case 'cos'                           % trig cosine coefficients
    y=2*real(Kn(iDC+1:end));
  case 'all'                       % return all data in a structure
    y.tag=FSData.tag;
    y.coef=Kn;
    y.period=FSData.T;
    y.size=N;
    y.avg=Kn(iDC);
    y.msv=real(Kn*Kn');
    idx=iDC+[-1 1];
    fn=Kn(idx);
    Kn(idx)=[];
    y.thd=sqrt(real(Kn*Kn')/real(fn*fn'));
    y.one=abs([Kn(iDC) 2*Kn(iDC+1:end)]);
```

```
    y.phase=angle(Kn(iDC:end))*180/pi;
    y.sine=-2*imag(Kn(iDC+1:end));
    y.cosine=2*real(Kn(iDC+1:end));
  case {'spe' 'ste'}                          % create stem plot
    xdata=0:N;
    subplot(2,1,1)
    ydata=abs([Kn(iDC) 2*Kn(iDC+1:end)]);
    stem(xdata,ydata)
    ylabel('Amplitude')
    xlabel('Harmonic Index')
    title('Fourier Series Line Spectra Plot')
    ydata=angle(Kn(iDC:end))*180/pi;
    subplot(2,1,2)
    stem(xdata,ydata)
    ylabel('Phase')
    xlabel('Harmonic Index')
  case 'plo'                                  % create time plot
    t=linspace(0,FSData.T,min(max(5*N,100),500));
    nwo=wo*(1:N);
    ko=real(Kn(iDC));
    Knp=Kn(iDC+1:end).';
    ydata=ko+2*(real(exp(1j*t(:)*nwo)*Knp))';
    plot(t,ydata)
    title('Fourier Series Plot.')
  otherwise
    error('Uknown Input Argument.')
  end
end
%--------------------------------------------------------------------------
```

GetWaveform.m

```
function GetWaveform(picturename)

%%%%%%%%%%%%%%%%%%%%%%%%%%%%%%%%%%%%%%%%%%%%%%%%%%
%%%%%%%%%%%%%%%%%%%%%%%%
% clear;clc
pname = 'C.jpg';
a=imread(pname); % name of the image
image(a);
hold on
DataX=[];
DataY=[];

disp(['The x axis range is the period length of one cardiac cycle in seconds: Tcycle']);
x_range =input('Type in the range of x axis -- Tcycle=');
disp(['Then click on the x axis where x=0 and x=Tcycle']);
for i=1:2
X=ginput(1);
plot(X(1),X(2),'+r');
hold on
DataX=[DataX; X];
end

disp(['Choose one of the value markers shown on the y axis: Yvalue']);
y_range =input('Type in the range of y axis -- Yvalue=');
disp(['Then click on the y axis where y=0 and y=Yvalue']);
for i=1:2
Y=ginput(1);
plot(Y(1),Y(2),'+r');
hold on
DataY=[DataY; Y];
end

X_L=abs(DataX(1,1)-DataX(2,1));
m=2;
X_Step=X_L/m;
for i=1:m+1
X_Data(i)=DataX(1,1)+X_Step*(i-1);
line([X_Data(i),X_Data(i)],[0,14000]);
end
%disp(['X axis length is ',num2str(X_L)]);

Point=[];
for i=1:m+1
P=ginput(1);
plot(P(1),P(2),'*g');
```

```
hold on
Point=[Point; P];
end
disp(['Points have been done']);

Y_Length=abs(DataY(2,2)-DataY(1,2));
Y_Step=Y_Length/y_range;

for i=1:m+1
   Point(i,2)=(DataY(1,2)-Point(i,2))/Y_Step;
   Point(i,1)=Point(i,1)-DataY(1,1);
end

figure;
X_Length=abs(Point(1,1)-Point(m+1,1));
zz=Point(1,1);
for i=1:m+1
   Point(i,1)=(Point(i,1)-zz)*x_range/X_Length;
end

t=Point(:,1);
f=Point(:,2);
f(m+1)=f(1);
FSfun = fscreate(t,f,25); %30 coefficients
FSfun('plot');
hold on;
plot(t,f,'g');
MeanValue = FSfun('avg');
a = FSfun('cosine');
b = FSfun('sine');
save Waveform MeanValue a b
disp(['Job done !']);
```

Flow field visualization – streamline coloring

This appendix includes the protocol to color streamlines by outlet vessel. It involves MATLAB and Tecplot. Content includes (i) general protocol, (ii) MATLAB script and (iii) Tecplot macro.

General protocol

1. Create a cross section near the bottom of the IVC
2. Create streamlines from that cross section.
3. Using the slice from plane tool, determine some threshold to determine what streamlines are exiting through one of the PAs. For example, if streamlines going to the lpa all have x vales greater than 0.028 at some point on the streamline, you can use that as your threshold.
4. Data - Extract – Streamtraces (do NOT concatenate into one zone)
5. File – write data file – point data, asci
    a. Select all streamlines, and only the x/z/y coordinate you are using as your threshold to write to the data file.
6. Drag and drop the data file into the workspace in matlab. Matlab will open up an import GUI, just select all and click import.
7. Run matlab code (VesselStreamlines.m)
    a. Will produce a variable called “allOneString”
8. Make a TecPlot macro that changes the color of a streamline. Copy and paste the “allOneString” variable into the macro where it specifies which zone changes color.
9. When the macro runs, it will change every zone number included in “allOneString” to whatever color you have specified. This will include all the streamlines that exit either the LPA or RPA if your threshold was set appropriately.

MATLAB script

```
%% code to determine which streamlines to go either the LPA/RPA.
% Outputs a variable called StreamLines that gives the steamline IDs of the
% streamlines that go to whichever vessel you specified.

%%Must load in streamline data from Tecplot:
%     1. Create streamlines from IVC
```

```
%     2. Write data file (ascii, point).  Write only one variable
%      (whichever variable you are using as the threshold.
%     3. Drag and drop data file into matlab workspace.
%     4. Import window opens in matlab.  Select all...import selection.
%     5. Change name of variable to data.

%%To run code:
%     1. fill out the following two lines of code (number of streamlines and threshold, then run.

NumberOfStreamlines=500;  %number of streamlines you exported from Tecplot
threshold=.0166;  %%set this number based on vessel, you can use any x/y/z threshold

streamlineList=[];  %%initialize vector for list of streamlines

vesselID = data(11);  %11
datalength=data(12); %12
start=15; %15
finish=start+datalength-1; %14 used to be 15

for in=1:NumberOfStreamlines;
   for i=start:finish;
      %vesselID=4+in;  %%added this
      if data(i)>threshold
         streamlineList=[streamlineList vesselID];
      end
   end

   if in<NumberOfStreamlines
      vesselID=data(i+2);
      datalength=data(i+3);
      start=i+6;
      finish=i+6+datalength-1;
      %in=in+1;
   end
end

StreamLines = unique(streamlineList);

StreamsCommas = StreamLines;
allOneString = sprintf('%.0f,' , StreamsCommas);
allOneString = allOneString(1:end-1);% strip final comma

HFD = length(StreamLines)/NumberOfStreamlines*100
```

Tecplot macro

```
#!MC 1400
# Created by Tecplot 360 build 14.0.2.35002
$!VarSet |MFBD| = 'C:\Users\Phillip\Documents'
$!FIELDMAP ['allOneString' - output from MATLAB]  SCATTER{COLOR = RED}
$!RemoveVar |MFBD|
```

Anatomy characterization

The following protocol is used to measure vessel dimensions using vascular modeling toolkit (VMTK) and MATLAB. A custom MATLAB script is included below (VesselMeasurements_v3) which analyzes the output from VMTK and calculates the average, minimum and maximum vessel diameters, as well as percent stenosis for each vessel. This appendix includes (i) the protocol, (ii) custom VMTK script, and (iii) custom MATLAB code.

Protocol

1. Prepare anatomy file (Geomagic)
    a. Load .igs file, convert to polygons (menu button)
    b. Remove boundaries and subdivision points
    c. Decimate - 40,000 triangles
    d. Cut off vessel ends to make hollow
    e. Save as .stl file (name as Patient1_hollow.stl)
2. Open VMTK code (VesselMeasurements_v3)
3. Change path/filename of the .stl file in the VMTK code (line 1)
4. Change path of where to store the temporary .stl file (surface.stl)
5. Change paths of where to store the output files (there are 4 of these)
6. Run the VMTK code
    a. VMTK will ask you to specify inlets and outlets, you must go in this order (each has one inlet and 2 outlets):
        i. IVC to LPA and RPA
        ii. SVC to LPA and RPA
        iii. LPA to IVC and SVC
        iv. RPA to IVC and SVC
    b. VMTK will output .dat files named IVCtoPAs, SVCtoPAs, LPAtoVCs and RPAtoVCs (these are the files that matlab will read)
7. Open MATLAB script (ComputeVessel_sizes_v3.m). This script needs to be in the same directory as the outputted VMTK files.
8. Change name in MATLAB file (line 17).
9. Run the code. Code will spit out a warning if the number of cross sections used to calculate vessel dimensions was less than 50. This can happen either because the vessel is very short, or because there is a problem. Always check which of these is the case if you get a warning (ex: “IVC indices are low!”)
10. Matlab will output a file (in the same directory as the code and VMTK outputs) that gives the vessel measurements (ex: LB03_vessel_measurements.txt)

**NOTE: this code is currently set up to only deal with 4 vessel cases. If there are more than 4 vessels, this code can still be used the same way to get measurements for the 4 vessels, but cannot measure additional vessels.

VMTK script

##Must go in correct order!!!
##IVC to PAs, SVC to PAs, LPA to VCs, RPA to VCs

vmtksurfacereader -ifile C:/Users/Phillip/Desktop/vmtk_trial/new/version_v3/LB05_hollow.stl -ofile C:/Users/Phillip/Desktop/vmtk_trial/new/version_v3/surface.stl

vmtksurfacereader -ifile C:/Users/Phillip/Desktop/vmtk_trial/new/version_v3/surface.stl --pipe vmtkcenterlines -seedselector openprofiles --pipe vmtkcenterlineresampling -length 0.1 --pipe vmtkcenterlinesections -ocenterlinesfile C:/Users/Phillip/Desktop/vmtk_trial/new/version_v3/IVCtoPAs.dat

vmtksurfacereader -ifile C:/Users/Phillip/Desktop/vmtk_trial/new/version_v3/surface.stl --pipe vmtkcenterlines -seedselector openprofiles --pipe vmtkcenterlineresampling -length 0.1 --pipe vmtkcenterlinesections -ocenterlinesfile C:/Users/Phillip/Desktop/vmtk_trial/new/version_v3/SVCtoPAs.dat

vmtksurfacereader -ifile C:/Users/Phillip/Desktop/vmtk_trial/new/version_v3/surface.stl --pipe vmtkcenterlines -seedselector openprofiles --pipe vmtkcenterlineresampling -length 0.1 --pipe vmtkcenterlinesections -ocenterlinesfile C:/Users/Phillip/Desktop/vmtk_trial/new/version_v3/LPAtoVCs.dat

vmtksurfacereader -ifile C:/Users/Phillip/Desktop/vmtk_trial/new/version_v3/surface.stl --pipe vmtkcenterlines -seedselector openprofiles --pipe vmtkcenterlineresampling -length 0.1 --pipe vmtkcenterlinesections -ocenterlinesfile C:/Users/Phillip/Desktop/vmtk_trial/new/version_v3/RPAtoVCs.dat

MATLAB script

%%%code to read in centerline/area data from vmtk and then gives average,
%%%minimum and maximum vessel sizes, along with stenosis calculations.
%%%Warning will display on screen if using less than 50 cross sections to
%%%calculate dimensions.

```
clear; clc;  close all

%%name case!!
name='CHOP088A';

%tol=.1;  %parameter to decide how far centerlines need to be apart before
%terminating the vessel
tol=.5;

sep=.01;  %parameter to decide when the first centerline stops and the 2nd one begins
%sep=.005;

IVCtoPAs = importdata('IVCtoPAs.dat');
ivcCoor=IVCtoPAs.data(:,1:3);

in=2;
while sqrt( (ivcCoor(in,1)-ivcCoor(1,1))^2+(ivcCoor(in,2)-ivcCoor(1,2))^2+(ivcCoor(in,3)-
ivcCoor(1,3))^2 )>sep;
   in=in+1;
end

ivcLPAsize=IVCtoPAs.data(1:in-1,10);
ivcRPAsize=IVCtoPAs.data(in:end,10);




%%IVC

% ivcLPA = importdata('IVCtoLPA.dat');
% ivcLPAsize=ivcLPA.data(:,10); %gets only vessel size column
%
% ivcRPA = importdata('IVCtoRPA.dat');
% ivcRPAsize=ivcRPA.data(:,10); %gets only vessel size column

ind=1;

while sqrt( (IVCtoPAs.data(ind,1)-IVCtoPAs.data(ind+in-1,1))^2+(IVCtoPAs.data(ind,2)...
      -IVCtoPAs.data(ind+in-1,2))^2+(IVCtoPAs.data(ind,3)-IVCtoPAs.data(ind+in-1,3))^2 ...
      )<tol;   %this specifies that when centerlines are more than 0.1 mm apart that we have left the
IVC
      ind=ind+1;
end
IVCind=ind;
%%calculate metrics
```

```
avgIVCsize=mean(ivcLPAsize(1:ind-1));
minIVCsize=min(ivcLPAsize(1:ind-1));
maxIVCsize=max(ivcLPAsize(1:ind-1));
IVCstenosis = 100-minIVCsize/avgIVCsize*100;
avgIVCdiameter=2*sqrt(avgIVCsize/3.1415);
minIVCdiameter=2*sqrt(minIVCsize/3.1415);

plot3(IVCtoPAs.data(1:ind,1),IVCtoPAs.data(1:ind,2),IVCtoPAs.data(1:ind,3),'o',IVCtoPAs.data
(in:in+ind,1),IVCtoPAs.data(in:in+ind,2),IVCtoPAs.data(in:in+ind,3))
hold on


%%SVC section

SVCtoPAs = importdata('SVCtoPAs.dat');
svcCoor=SVCtoPAs.data(:,1:3);

in=2;
while sqrt( (svcCoor(in,1)-svcCoor(1,1))^2+(svcCoor(in,2)-svcCoor(1,2))^2+(svcCoor(in,3)-
svcCoor(1,3))^2 )>sep;
   in=in+1;
end

svcLPAsize=SVCtoPAs.data(1:in-1,10);
svcRPAsize=SVCtoPAs.data(in:end,10);




%%SVC

% svcLPA = importdata('SVCtoLPA.dat');
% svcLPAsize=svcLPA.data(:,10); %gets only vessel size column
%
% svcRPA = importdata('SVCtoRPA.dat');
% svcRPAsize=svcRPA.data(:,10); %gets only vessel size column

ind=1;

while sqrt( (SVCtoPAs.data(ind,1)-SVCtoPAs.data(ind+in-1,1))^2+(SVCtoPAs.data(ind,2)...
      -SVCtoPAs.data(ind+in-1,2))^2+(SVCtoPAs.data(ind,3)-SVCtoPAs.data(ind+in-1,3))^2 ...
      )<tol;   %this specifies that when centerlines are more than 0.1 mm apart that we have left the
SVC
      ind=ind+1;
end
SVCind=ind;
```

```
%%calculate metrics
avgSVCsize=mean(svcLPAsize(1:ind-1));
minSVCsize=min(svcLPAsize(1:ind-1));
maxSVCsize=max(svcLPAsize(1:ind-1));
SVCstenosis = 100-minSVCsize/avgSVCsize*100;
avgSVCdiameter=2*sqrt(avgSVCsize/3.1415);
minSVCdiameter=2*sqrt(minSVCsize/3.1415);

plot3(SVCtoPAs.data(1:ind,1),SVCtoPAs.data(1:ind,2),SVCtoPAs.data(1:ind,3),'o',SVCtoPAs.d
ata(in:in+ind,1),SVCtoPAs.data(in:in+ind,2),SVCtoPAs.data(in:in+ind,3))
hold on



%%LPA section
% lpaIVC = importdata('LPAtoIVC.dat');
% lpaIVCsize=lpaIVC.data(:,10); %gets only vessel size column
%
% lpaSVC = importdata('LPAtoSVC.dat');
% lpaSVCsize=lpaSVC.data(:,10); %gets only vessel size column

LPAtoVCs = importdata('LPAtoVCs.dat');
lpaCoor=LPAtoVCs.data(:,1:3);

in=2;
while sqrt( (lpaCoor(in,1)-lpaCoor(1,1))^2+(lpaCoor(in,2)-lpaCoor(1,2))^2+(lpaCoor(in,3)-
lpaCoor(1,3))^2 )>sep;
   in=in+1;
end

lpaIVCsize=LPAtoVCs.data(1:in-1,10);
lpaSVCsize=LPAtoVCs.data(in:end,10);



ind=1;

while sqrt( (LPAtoVCs.data(ind,1)-LPAtoVCs.data(ind+in-1,1))^2+(LPAtoVCs.data(ind,2)...
      -LPAtoVCs.data(ind+in-1,2))^2+(LPAtoVCs.data(ind,3)-LPAtoVCs.data(ind+in-1,3))^2 ...
      )<tol;   %this specifies that when centerlines are more than 0.1 mm apart that we have left the
LPA
      ind=ind+1;
end
LPAind=ind;
%%calculate metrics
avgLPAsize=mean(lpaIVCsize(1:ind-1));
```

```
minLPAsize=min(lpaIVCsize(1:ind-1));
maxLPAsize=max(lpaIVCsize(1:ind-1));
LPAstenosis =100- minLPAsize/avgLPAsize*100;
avgLPAdiameter=2*sqrt(avgLPAsize/3.1415);
minLPAdiameter=2*sqrt(minLPAsize/3.1415);

plot3(LPAtoVCs.data(1:ind,1),LPAtoVCs.data(1:ind,2),LPAtoVCs.data(1:ind,3),'o',LPAtoVCs.d
ata(in:in+ind,1),LPAtoVCs.data(in:in+ind,2),LPAtoVCs.data(in:in+ind,3))
hold on

%%RPA section


RPAtoVCs = importdata('RPAtoVCs.dat');
rpaCoor=RPAtoVCs.data(:,1:3);

in=2;
while sqrt( (rpaCoor(in,1)-rpaCoor(1,1))^2+(rpaCoor(in,2)-rpaCoor(1,2))^2+(rpaCoor(in,3)-
rpaCoor(1,3))^2 )>sep;
   in=in+1;
end

rpaIVCsize=RPAtoVCs.data(1:in-1,10);
rpaSVCsize=RPAtoVCs.data(in:end,10);



ind=1;

while sqrt( (RPAtoVCs.data(ind,1)-RPAtoVCs.data(ind+in-1,1))^2+(RPAtoVCs.data(ind,2)...
      -RPAtoVCs.data(ind+in-1,2))^2+(RPAtoVCs.data(ind,3)-RPAtoVCs.data(ind+in-1,3))^2 ...
      )<tol;   %this specifies that when centerlines are more than 0.1 mm apart that we have left the
RPA
      ind=ind+1;
end
RPAind=ind;
%%calculate metrics
avgRPAsize=mean(rpaIVCsize(1:ind-1));
minRPAsize=min(rpaIVCsize(1:ind-1));
maxRPAsize=max(rpaIVCsize(1:ind-1));
RPAstenosis =100- minRPAsize/avgRPAsize*100;
avgRPAdiameter=2*sqrt(avgRPAsize/3.1415);
minRPAdiameter=2*sqrt(minRPAsize/3.1415);

plot3(RPAtoVCs.data(1:ind,1),RPAtoVCs.data(1:ind,2),RPAtoVCs.data(1:ind,3),'o',RPAtoVCs.
data(in:in+ind,1),RPAtoVCs.data(in:in+ind,2),RPAtoVCs.data(in:in+ind,3))
```

```
hold on



OverallStenosis =100- (minLPAsize+minRPAsize+minIVCsize)/(avgLPAsize
+avgRPAsize+avgIVCsize)*100;

if IVCind <50
   %disp('IVC Indices are Low!')
   warndlg(sprintf('IVC indices are low!'))
end

if SVCind <50
   %disp('SVC Indices are Low!')
   warndlg(sprintf('SVC indices are low!'))
end

if LPAind <50
   %disp('LPA Indices are Low!')
   warndlg(sprintf('LPA indices are low!'))
end

if RPAind <50
   %disp('RPA Indices are Low!')
   warndlg(sprintf('RPA indices are low!'))
end


%%write text file
fileID = fopen(sprintf('%s_vessel_measurements.txt',name),'w');
fprintf(fileID, 'Vessel sizes (mm)');
fprintf(fileID, ['\n' '\n']);
fprintf(fileID,['IVC_d_avg' '\t' 'IVC_d_min' '\t' 'SVC_d_avg' '\t' 'SVC_d_min' '\t' 'LPA_d_avg' '\t'
'LPA_d_min' '\t' 'RPA_d_avg' '\t' 'RPA_d_min']);
fprintf(fileID, ['\n' '\n']);

formatSpec = ['%5.2f' '\t' '%5.2f' '\t' '%5.2f' '\t' '%5.2f' '\t' '%5.2f' '\t' '%5.2f' '\t' '%5.2f' '\t' '%5.2f'
'\t'];
fprintf(fileID,
formatSpec,avgIVCdiameter,minIVCdiameter,avgSVCdiameter,minSVCdiameter,avgLPAdiame
ter,minLPAdiameter,avgRPAdiameter,minRPAdiameter);

fprintf(fileID, ['\n' '\n' '\n' '\n']);
```

```
fprintf(fileID, ['Stenosis (percent)']);
fprintf(fileID, ['\n' '\n']);
fprintf(fileID, ['IVC_stenosis' '\t' 'SVC_stenosis' '\t' 'LPA_stenosis' '\t' 'RPA_stenosis' '\t' 'Overall
Stenosis']);
fprintf(fileID, ['\n' '\n' ]);

formatSpec = ['%5.2f' '\t' '%5.2f' '\t' '%5.2f' '\t' '%5.2f' '\t' '%5.2f'];
fprintf(fileID, formatSpec,IVCstenosis, SVCstenosis,LPAstenosis,RPAstenosis,OverallStenosis);


fprintf(fileID, ['\n' '\n' '\n' '\n']);
fprintf(fileID, 'Smallest IVC area (cm2)= ');

formatSpec = ['%5.2f'];
fprintf(fileID, formatSpec,minIVCsize/100);


fprintf(fileID, ['\n' '\n' '\n' '\n']);
fprintf(fileID, 'Number of cross sections to determine dimensions= ');

fprintf(fileID, ['\n' '\n']);
fprintf(fileID, ['IVC #' '\t' 'SVC #' '\t' 'LPA #' '\t' 'RPA #' ]);
fprintf(fileID, ['\n' '\n' ]);

formatSpec = ['%5.0f' '\t' '%5.0f' '\t' '%5.0f' '\t' '%5.0f' ];
fprintf(fileID, formatSpec,IVCind, SVCind,LPAind,RPAind);

values                                                                                                  =
[avgIVCdiameter,minIVCdiameter,avgSVCdiameter,minSVCdiameter,avgLPAdiameter,minLP
Adiameter,avgRPAdiameter,minRPAdiameter,IVCstenosis,
SVCstenosis,LPAstenosis,RPAstenosis,OverallStenosis,minIVCsize/100]
indices = [IVCind SVCind LPAind RPAind]
save(name)
```

CFD simulation post-processing

The following appendix includes the post-processing MATLAB code used to calculate power loss, index power loss, resistance and hepatic flow distribution. This code was also used to check the convergence of these metrics over multiple cardiac cycles. This code must be in the same directory as the PLnHFD files outputted from Fluent. Instructions are given within the first several lines of code.

```
%%code that does post-processing on PLnHFD output files from Fluent. Checks
%%HFD convergence, calculates and checks power loss convergence, calculates
%%iPL, pressure drop,and resistance.  Also gives flow rates (L/min) to
%%make sure they are correct.

%Instructions:
%     (1) drag and drop all PLnHFD output files into same directory as code
%     (2) delete last cycle output file (it should be an empty file
%     (3) Need to have patient's BSA, know which vessels the patient has
%     (4) Name patient
%     (5) Run code

clc
clear
close all

%%name case!!
name='test';

%%output file column numbers differ based on how many vessels
prompt = 'What type of case is this? 1: 4 vessel,2: lsvc, 3: az, 4:lsvc and az, 5:rupa, 6:rupa and lsvc
';
option = input(prompt);

prompt = 'Patient BSA =  ';
BSA = input(prompt);


fnames = dir('*.out');
numfids = length(fnames);
vals = cell(1,numfids);
[~,index] = sortrows({fnames.date}.'); fnames = fnames(index); clear index
```

```
for K = 1:numfids
  vals{K} = importdata(fnames(K).name);
end


%%%%%%%%%%%%%%%%%%%%%%%%%%%%%%%%%%%%%%%%%%%%%%%%%%%%
%%%%%%%%%%%%%%%%%%%%%%%%%%%%%%%%
%%PL/resistance/pressure/drop section

%%specify which columns have the various flows/PL (depends on what vessels
%%are present (determined by user input to prompt). Also calculate flow
%%rates, Qs, outlet flow splits for comparison.

w=vals{1,numfids}.data;

if option==1
   %%option 1: standard 4 vessel case
   QivcCol=2; QsvcCol=5; QlpaCol=3; QrpaCol=4; PLcol=20;

   Qivc = -mean(w(:,QivcCol))*60*1000;Qsvc = -mean(w(:,QsvcCol))*60*1000;Qlpa = mean(w(:,QlpaCol))*60*1000;Qrpa = mean(w(:,QrpaCol))*60*1000;  %%in L/min
   Qs=Qivc+Qsvc;
   FlowRates=[Qivc Qsvc 0 0 Qlpa Qrpa 0]
   OutletFlowSplit=[Qlpa/Qs Qrpa/Qs 0]
   if Qivc<0 || Qsvc<0 || Qlpa<0 || Qrpa<0
      warndlg(sprintf('Check Normal Vector Directions!!'))
   end

elseif option==2
   %%option 2: lsvc
   QivcCol=2; QsvcCol=5; QlpaCol=3; QrpaCol=4; QlsvcCol=6; PLcol=24;

   Qivc = -mean(w(:,QivcCol))*60*1000;Qsvc = -mean(w(:,QsvcCol))*60*1000;Qlpa = mean(w(:,QlpaCol))*60*1000;Qrpa = mean(w(:,QrpaCol))*60*1000;  %%in L/min
   Qlsvc = -mean(w(:,QlsvcCol))*60*1000;
   Qs=Qivc+Qsvc+Qlsvc;
   FlowRates=[Qivc Qsvc Qlsvc 0 Qlpa Qrpa 0]
   OutletFlowSplit=[Qlpa/Qs Qrpa/Qs 0]

   if Qivc<0 || Qsvc<0 || Qlpa<0 || Qrpa<0 ||Qlsvc<0
      warndlg(sprintf('Check Normal Vector Directions!!'))
   end

elseif option==3
   %%option 3: az
   QivcCol=2; QsvcCol=5; QlpaCol=3; QrpaCol=4; QazCol=6; PLcol=24;
```

```
   Qivc = -mean(w(:,QivcCol))*60*1000;Qsvc = -mean(w(:,QsvcCol))*60*1000;Qlpa =
mean(w(:,QlpaCol))*60*1000;Qrpa = mean(w(:,QrpaCol))*60*1000;  %%in L/min
   Qaz = -mean(w(:,QazCol))*60*1000;
   Qs=Qivc+Qsvc+Qaz;
   FlowRates=[Qivc Qsvc 0 Qaz Qlpa Qrpa 0]
   OutletFlowSplit=[Qlpa/Qs Qrpa/Qs 0]

   if Qivc<0 || Qsvc<0 || Qlpa<0 || Qrpa<0 ||Qaz<0
      warndlg(sprintf('Check Normal Vector Directions!!'))
   end

elseif option==4
   %%option 4: lsvc and az
   QivcCol=2; QsvcCol=5; QlpaCol=3; QrpaCol=4; QlsvcCol=6; QazCol=7; PLcol=28;
   Qivc = -mean(w(:,QivcCol))*60*1000;Qsvc = -mean(w(:,QsvcCol))*60*1000;Qlpa =
mean(w(:,QlpaCol))*60*1000;Qrpa = mean(w(:,QrpaCol))*60*1000;  %%in L/min
   Qlsvc = -mean(w(:,QlsvcCol))*60*1000;   Qaz = -mean(w(:,QazCol))*60*1000;
   Qs=Qivc+Qsvc+Qaz+Qlsvc;
   FlowRates=[Qivc Qsvc Qlsvc Qaz Qlpa Qrpa 0]
   OutletFlowSplit=[Qlpa/Qs Qrpa/Qs 0]

   if Qivc<0 || Qsvc<0 || Qlpa<0 || Qrpa<0 || Qlsvc<0 || Qaz<0
      warndlg(sprintf('Check Normal Vector Directions!!'))
   end

elseif option==5
   %%option 5: rupa
   QivcCol=2; QsvcCol=5; QlpaCol=3; QrpaCol=4; QrupaCol=6; PLcol=24;
   Qivc = -mean(w(:,QivcCol))*60*1000;Qsvc = -mean(w(:,QsvcCol))*60*1000;Qlpa =
mean(w(:,QlpaCol))*60*1000;Qrpa = mean(w(:,QrpaCol))*60*1000;  %%in L/min
   Qrupa = mean(w(:,QrupaCol))*60*1000;
   FlowRates=[Qivc Qsvc 0 0 Qlpa Qrpa Qrupa]
   Qs=Qivc+Qsvc;
   OutletFlowSplit=[Qlpa/Qs Qrpa/Qs Qrupa/Qs]

   if Qivc<0 || Qsvc<0 || Qlpa<0 || Qrpa<0 || Qrupa<0
      warndlg(sprintf('Check Normal Vector Directions!!'))
   end

elseif option==6  %%put all column 1 for now
   %%option 6: rupa and lsvc
   QivcCol=1; QsvcCol=1; QlpaCol=1; QrpaCol=1; QlsvcCol=1; QrupaCol=1; PLcol=1;
   Qivc = -mean(w(:,QivcCol))*60*1000;Qsvc = -mean(w(:,QsvcCol))*60*1000;Qlpa =
mean(w(:,QlpaCol))*60*1000;Qrpa = mean(w(:,QrpaCol))*60*1000;  %%in L/min
   Qlsvc = -mean(w(:,QlsvcCol))*60*1000;    Qrupa = mean(QrupaCol)*60*1000;
   Qs=Qivc+Qsvc+Qlsvc;
```

```
    FlowRates=[Qivc Qsvc Qlsvc 0 Qlpa Qrpa Qrupa]
    OutletFlowSplit=[Qlpa/Qs Qrpa/Qs Qrupa/Qs]

    if Qivc<0 || Qsvc<0 || Qlpa<0 || Qrpa<0 || Qlsvc<0 || Qrupa<0
        warndlg(sprintf('Check Normal Vector Directions!!'))
    end

end

PL=[];
for K=1:numfids
    a=vals{1,K}.data;
    PL_temp=-1000*mean(a(:,PLcol)); %multiply by 1000 to get mW
    PL = [PL PL_temp];
end



subplot(2,2,3)
plot(PL)
xlabel('Cycles')
ylabel('PL')
title('Power Loss')

subplot(2,2,4) %plot percentage change over the final 5 cycles
convValuesPL = [];
for i=fliplr(0:5)
    d=(PL(end-i)-PL(end-i-1))/PL(end-i-1)*100;
    convValuesPL=[convValuesPL d];
end
plot(convValuesPL)
xlabel('final 6 cycles')
ylabel('PL Convergence')
title('PL Convergence')


%%%%%%%%%%%%%%%%%%%%%%%%%%%%%%%%%%%%%%%%%%%%%%%%%
%%%%%%%%%%%%%%%%%%%%%%%%%%%%%%
%%HFD section

HFD=[];



for K=1:numfids
    a=vals{1,K}.data;
```

```
if option==1||2||3||4;

[rows,columns]=size(a);
flux_it_LPA_temp=[];
flux_it_RPA_temp=[];
for count=1:rows
   %calculate total flux of scalar for LPA
   flux_it_lpa= a(count,end-2)*a(count,3);
   flux_it_LPA_temp=[flux_it_LPA_temp flux_it_lpa];


   %calculate total flux of scalar for RPA
   flux_it_rpa= a(count,end-1)*a(count,4);
   flux_it_RPA_temp=[flux_it_RPA_temp flux_it_rpa];

end

total_flux_LPA = sum(flux_it_LPA_temp);
total_flux_RPA = sum(flux_it_RPA_temp);

%calculate HFD by calculating ratio of LPA to total fluxes
   hfd_temp = round(100*total_flux_LPA/(total_flux_LPA+total_flux_RPA));



HFD = [HFD hfd_temp];

elseif option==5   %%%%%for rupa and 2 inlets

[rows,columns]=size(a);
flux_it_LPA_temp=[];
flux_it_RPA_temp=[];
flux_it_RUPA_temp=[];
for count=1:rows
   %calculate total flux of scalar for LPA
   flux_it_lpa= a(count,end-3)*a(count,3);
   flux_it_LPA_temp=[flux_it_LPA_temp flux_it_lpa];


   %calculate total flux of scalar for RPA
   flux_it_rpa= a(count,end-2)*a(count,4);
   flux_it_RPA_temp=[flux_it_RPA_temp flux_it_rpa];

   %calculate total flux of scalar for RUPA
   flux_it_rupa= a(count,end-1)*a(count,6);
```

```
        flux_it_RUPA_temp=[flux_it_RUPA_temp flux_it_rupa];

    end

    total_flux_LPA = sum(flux_it_LPA_temp);
    total_flux_RPA = sum(flux_it_RPA_temp);
    total_flux_RUPA = sum(flux_it_RUPA_temp);

    %calculate HFD by calculating ratio of LPA to total fluxes
        hfd_temp                                                                    =
round(100*total_flux_LPA/(total_flux_LPA+total_flux_RPA+total_flux_RUPA));



    HFD = [HFD hfd_temp];


    end

end

subplot(2,2,1)
plot(HFD)
xlabel('Cycles')
ylabel('HFD')
title('HFD')

subplot(2,2,2) %plot percentage change over the final 5 cycles
convValues = [];
for i=fliplr(0:5)
    c=(HFD(end-i)-HFD(end-i-1))/HFD(end-i-1)*100;
    convValues=[convValues c];
end
plot(convValues)
xlabel('final 6 cycles')
ylabel('HFD Convergence')
title('HFD Convergence')

hfd=HFD(end);
Convergence = (HFD(end)-HFD(end-1))/HFD(end-1)*100;
HFD
```

```
%%%%%%%%%%%%%%%%%%%%%%%%%%%%%%%%%%%%%%%%%%%%%%%%%%%%%%%%%%
%%%%%%%%%%%%%%%%%%%%%%%%%%%%%%%
%%CFD metrics
PL_final = PL(end);
PL;
iPL=PL_final/(1060*1000*((Qs/60)^3))*BSA^2;
Resistance=PL_final/Qs/Qs*.45;
pressureDrop=Resistance*Qs;

CFDmetrics = [PL_final iPL Resistance pressureDrop]


%%%%%%%%%%%%%%%%%%%%%%%%%%%%%%%%%%%%%%%%%%%%%%%%%%%%%%%%%%
%%%%%%%%%%%%%%%%%%%%%%%%%%%%%%%%
%%write text file
fileID = fopen(sprintf('%s_PostProcess.txt',name),'w');
fprintf(fileID,name);
fprintf(fileID, ['\n' '\n']);

fprintf(fileID, '------------Hepatic Flow Distribution------------');
fprintf(fileID, ['\n' '\n']);
fprintf(fileID,['HFD for last 10 cycles']);
fprintf(fileID, ['\n' '\n']);

formatSpec = ['%5.0f'];
fprintf(fileID, formatSpec,HFD(end-8:end));  %%write HFD values for final 9 or 10 cycles



fprintf(fileID, ['\n' '\n' ]);
fprintf(fileID, ['HFD convergence (percent)']);
fprintf(fileID, ['\n']);

formatSpec = ['%5.2f'];
fprintf(fileID, formatSpec,convValues);  %%write HFD convergence values


fprintf(fileID, ['\n' '\n' '\n' '\n']);
fprintf(fileID, '-------------------Power Loss-------------------');
fprintf(fileID, ['\n' '\n']);
fprintf(fileID,['Power Loss for last 10 cycles']);
fprintf(fileID, ['\n' '\n']);

formatSpec = ['%5.2f'];
fprintf(fileID, formatSpec,PL(end-8:end));  %%write PL values for final 9 or 10 cycles
```

```
fprintf(fileID, ['\n' '\n']);
fprintf(fileID, ['PL convergence (percent)']);
fprintf(fileID, ['\n']);

formatSpec = ['%5.1f'];
fprintf(fileID, formatSpec,convValuesPL);  %%write PL convergence values



fprintf(fileID, ['\n' '\n' '\n' '\n']);
fprintf(fileID, ['---------------Flow Rates (L/min)---------------']);
fprintf(fileID, ['\n' '\n']);

fprintf(fileID, ['IVC' '\t' 'RSVC' '\t' 'LSVC' '\t' 'AZ' '\t' 'LPA' '\t' 'RPA' '\t' 'RUPA']);
fprintf(fileID, ['\n' '\n' ]);

formatSpec = ['%5.2f' ];
fprintf(fileID, formatSpec,FlowRates);


fprintf(fileID, ['\n' '\n' '\n'  ]);
fprintf(fileID, ['---------------Outlet Flow Split---------------']);
fprintf(fileID, ['\n' '\n']);
fprintf(fileID, ['LPA'  '\t' 'RPA'  '\t' 'RUPA' ]);
fprintf(fileID, ['\n' '\n']);

formatSpec = ['%5.2f'];
fprintf(fileID, formatSpec,OutletFlowSplit);  %%write outlet Flow splits
```

Anatomy Comparison

This appendix describes the protocol to compare differences between two TCPCs. This could be used for two different patients, for one patient at two different time points, or for a comparison between a surgical planning prediction and actual post-operative anatomy.

Protocol:

1. Open the two anatomies for comparison in Geomagic.

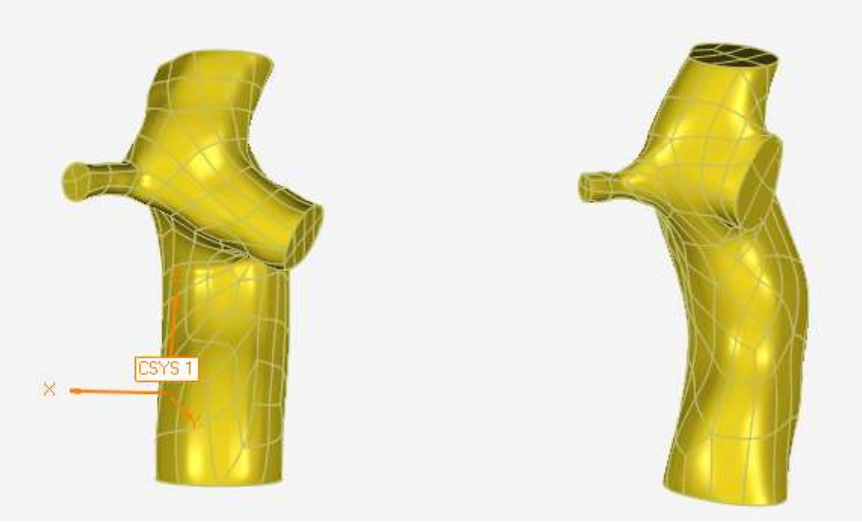

2. Use the “Best-fit alignment” feature to allow Geomagic to register the two anatomies. (This is an important step to account for differences in coordinate systems between various image acquisitions.)

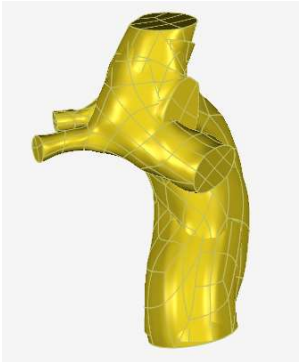

3. Using the “trim” feature in Geomagic, trim all vessels to end at the same location for both anatomies.

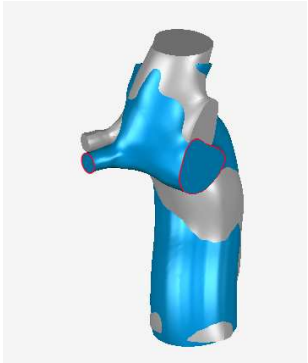

4. Decimate to approximately 20,000 triangles for each anatomy. (A higher number of triangles is unnecessary and slows down the Cloud Compare calculations.)
5. Delete the coordinate systems for each anatomy. (CSYS 1)

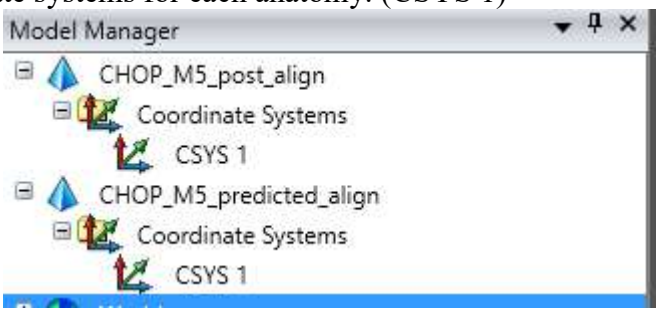

6. Export each anatomy as a .stl file.
7. To compare the grafts by themselves, “trim” the graft from the TCPC of each anatomy and save the graft as a .stl. (DO NOT register the grafts to one another, this would “erase” important positioning differences between the two TCPCs.

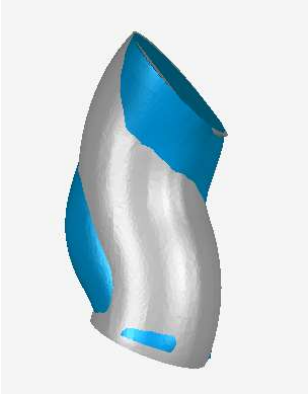

8. Open Cloud Compare.
9. Open the two .stl files (either both TCPCs or both grafts).
10. Select the “wrap” item under each file.

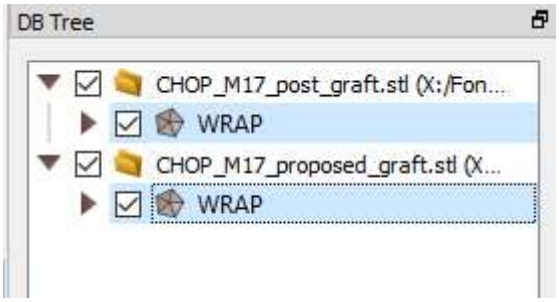

11. Click the “Compute cloud/mesh distance” button.

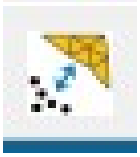

12. The program will make several estimations. Uncheck the “signed differences” option. Click “Compute”.

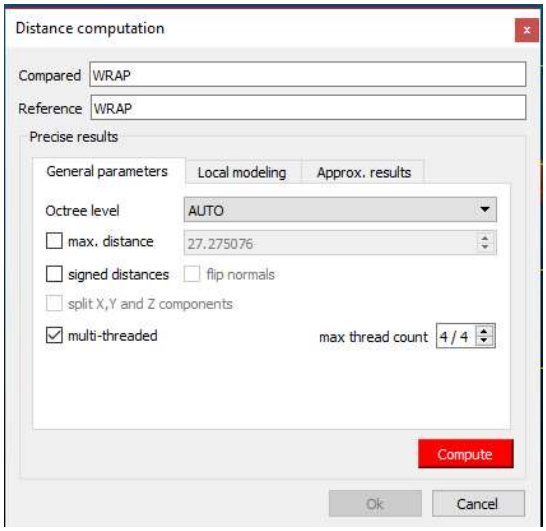

13. View results in the “approximate results” tab.

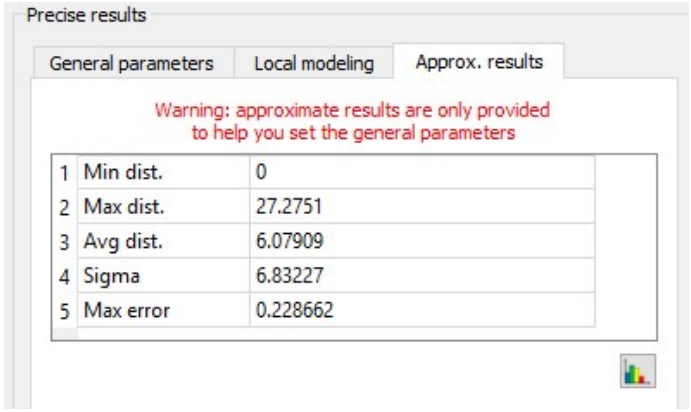

14. The “trace a polyline by point-clicking” option can be used to make manual measurements. Simply click the two points you want to measure the distance between, then right click and press enter. The polyline now shows up in the “Tree” menu. Click on it to view coordinates, length etc.

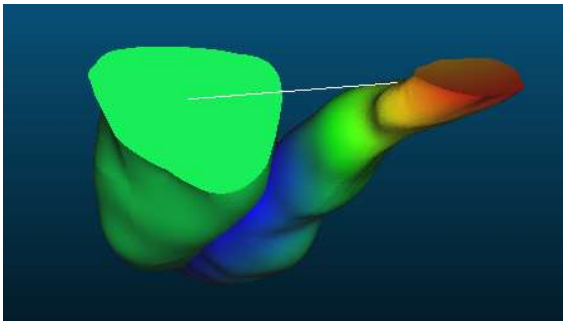

Figure 0-26 Comparison of grafts. Distance apart is indicated by color. The white line shows a manual measurement between the two insertion points.

APPENDIX B – EXPERIMENTAL METHODS

LabVIEW virtual instrument

The LabVIEW virtual instrument used to control the pulsatile piston pump, trigger imaging systems, and record pressure and flow measurements was composed of an active waveform display on the left-hand side and various control panels on the right with different display, calculations, calibration, and output settings. Figure 0-1 shows the panel with display settings. Figure 0-2 shows the panel with calculations settings. Figure 0-3 shows the panel with calibration settings. Figure 0-4 shows the panel with output settings.

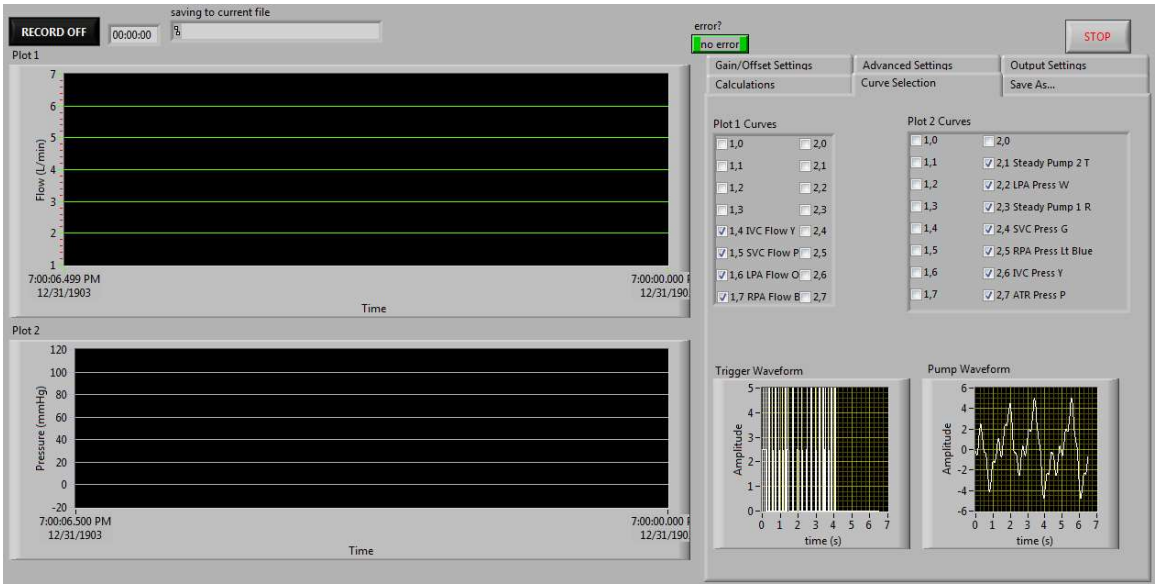

Figure 0-1 LabVIEW virtual instrument with plot display settings panel. The Plot 1 and Plot 2 curves settings are used to display different channels in the plots on the left. The two plots in the lower right display the analog output signals generated by the virtual instrument.

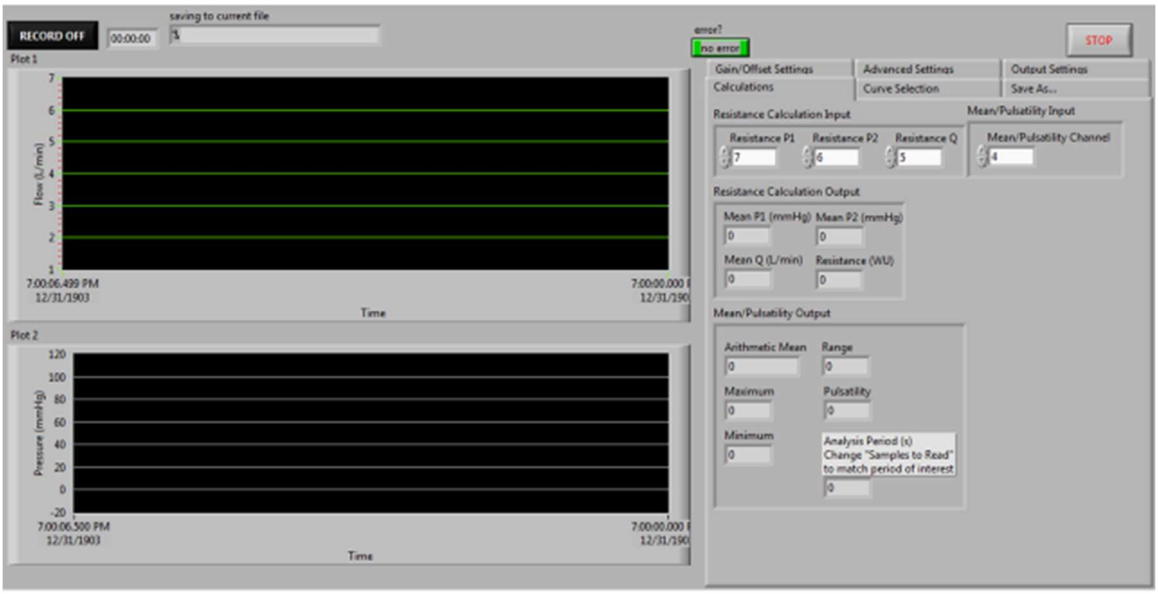

Figure 0-2 LabVIEW virtual instrument with calculations settings panel. The Resistance Calculation Input and Mean/Pulsatility Channel boxes are used to specify the input channel number (0-15) for the calculations displayed below. The analysis period displays the time, in seconds, over which the calculated numbers take place.

Figure 0-3 LabVIEW virtual instrument with calibration settings panel. This panel is used to specify the linear relationship between the analog input signal (V) and its respective metric value (L/min or mmHg) using a gain (G) and offset (O) for each channel. The DO Force Null? button

can be used to force all readings to zero by modification of their respective offset values. All values can also be altered manually.

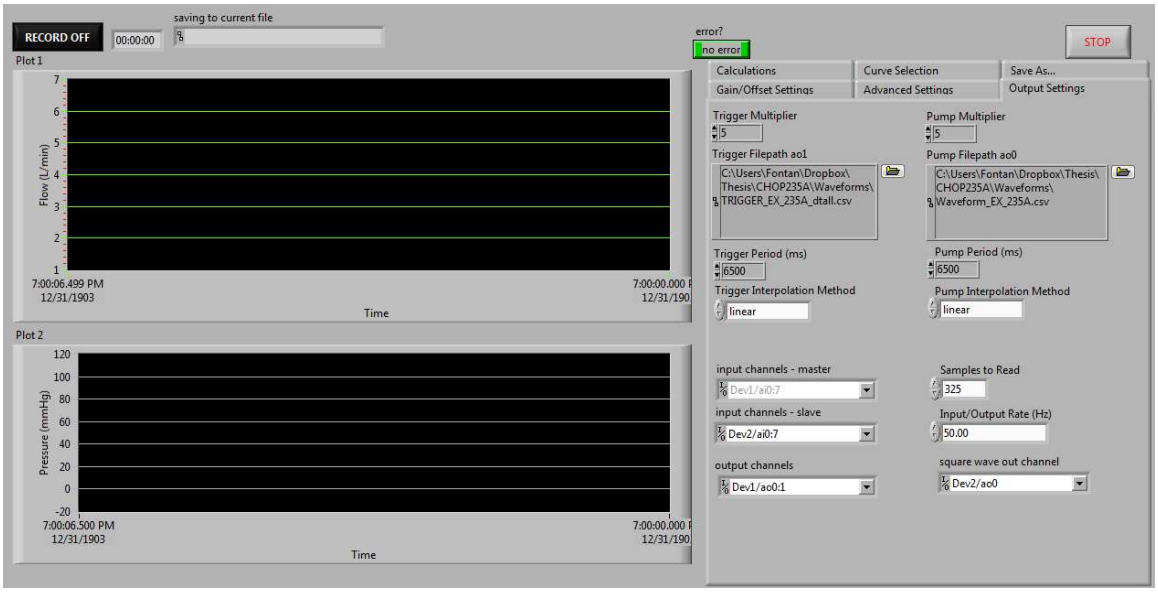

Figure 0-4 LabVIEW virtual instrument with output settings panel. The trigger and pump filepath boxes specify the custom waveform file location (.csv format) on the computer hard drive. The multiplier and period boxes (above and below) specify the custom waveform amplitude gain and time period, respectively. The input and output channels boxes specify the DAQ devices and channels used. The Input/Output Rate box specifiys the data sampling and created waveform frequency. The Samples to Read box specifies the number of samples (at the Input/Output Rate box frequency) to use when calculating metrics and displaying plots on the left.

APPENDIX C – SPECIFIC AIM 1A PATIENT DATA

This appendix contains all raw data (flow rates, birth and surgery dates, HFD prediction errors etc) for all patients included in Specific Aim 1A. The Georgia Tech patient IDs are also given for internal reference.

Patient ID	GT ID	Surgical option	Diagnosis	Patient initials	Date of birth	Gender	Fenestrated	Surgery type	PulseOx	PulseOx date
Patient 1	CHOP_M1	hep to AZ	heterotaxy, pulmonary atresia	AM	6/8/2003	female	no	revision	92	11/27/2017
Patient 2	CHOA_M2 (Y1)	Ygraft	Heterotaxy	BS	9/1/1991	female	no	revision	83	4/1/2018
Patient 3	CHOP_M7	hep to AZ	heterotaxy with detrocardia	JP	8/5/1998	male	no	revision	93	10/27/2016
Patient 4	CHOA_M5 (Y11)	Ygraft	Unbal canal	AM	8/1/1999	female	no	revision	90	5/16/2018
Patient 5	CHOP_M17	ECC	heterotaxy, levocardia, pulmonary atresia	MS	2/2/1998	male	no	revision	100	3/6/2018
Patient 6	CHOP_M5	ECC	4 vessel, LPA stenosis,	MP	1/24/2008	male	no	Stage 2-3	96	5/6/2018
Patient 7	CHOP_M9	Ygraft	HLHS with heterotaxy	AH	6/4/2008	male	no	Stage 2-3	95	8/6/2018
Patient 8	CHOP_M10	Ygraft	pulmonary atresia, VSD, tricuspid hypoplasia	AR	12/29/2007	female	no	Stage 2-3	93	6/6/2018
Patient 9	CHOP_M12	ECC	DILV with pulmonary atresia	DC	1/14/2009	male	no	Stage 2-3	97	3/29/2018
Patient 10	CHOP_M19	hep to AZ	common AV canal, heterotaxy	AM	3/16/2012	female	no	Stage 2-3	97	7/19/2018
Patient 11	CHOP_M24	hep to AZ	heterotaxy, common AV canal, DORV	BB	6/25/2012	female	no	Stage 2-3	90	9/1/2016
Patient 12	CHOP_M25	hep to inn.	heteotaxy, HLHS	DW	3/10/2016	female	no	Stage 2-3	99	12/8/2017

Patient ID	GT ID	Delta_T (follow up MRI and PulseOx) days	Delta_T (follow up MRI and PulseOx) years	BSA pre	BSA post	Surgery age	Follow up age	pre_op_MRI _date	surgery_date
Patient 1	CHOP_M1	612	1.7	0.606	1.16	4.65	12.81	10/9/2007	2/1/2008
Patient 2	CHOA_M2 (Y1)	2771	7.6	1.48	1.48	18.98	19.01	7/12/2010	8/20/2010
Patient 3	CHOP_M7	1186	3.2	1.22	1.73	11.62	14.99	9/18/2009	3/18/2010
Patient 4	CHOA_M5 (Y11)	2189	6.0	1.4	1.40	12.67	12.81	12/8/2011	3/29/2012
Patient 5	CHOP_M17	665	1.8	1.46	1.66	17.53	18.28	12/1/2013	8/11/2015
Patient 6	CHOP_M5	2179	6.0	0.467	0.56	1.32	4.32	5/13/2009	5/21/2009
Patient 7	CHOP_M9	2771	7.6	0.57	0.58	2.57	2.59	9/22/2010	12/29/2010
Patient 8	CHOP_M10	770	2.1	0.59	0.60	3.03	8.33	10/28/2010	1/7/2011
Patient 9	CHOP_M12	2541	7.0	0.51	0.54	2.22	2.25	3/22/2011	4/4/2011
Patient 10	CHOP_M19	1918	5.3	0.42	0.42	1.07	1.09	4/4/2013	4/10/2013
Patient 11	CHOP_M24	1	0.0	0.58	0.72	3.21	4.19	6/5/2015	9/9/2015
Patient 12	CHOP_M25	80	0.2	0.433	0.48	1.36	1.53	5/22/2017	7/18/2017

Patient ID	GT ID	Delta_T (pre-op MRI and surgery) months	Follow up date	FU_time_months	HFD_pre	HFD_predicted	HFD_post	HFD prediction (improved anatomy)	HFD prediction (improved flow)	HFD Error current
Patient 1	CHOP_M1	3.83	3/25/2016	97.81	34	60	56	62	67	-4
Patient 2	CHOA_M2 (Y1)	1.30	8/30/2010	0.33	17	38	45	32	46	7
Patient 3	CHOP_M7	6.03	7/29/2013	40.41	100	100	100	100	100	0
Patient 4	CHOA_M5 (Y11)	3.73	5/18/2012	1.64	65	53	32	42	61	-21
Patient 5	CHOP_M17	20.60	5/10/2016	8.98	0	26	71	87	13	45
Patient 6	CHOP_M5	0.27	5/18/2012	35.93	-	17	51	33	34	34
Patient 7	CHOP_M9	3.27	1/4/2011	0.20	-	27	48	55	10	21
Patient 8	CHOP_M10	2.37	4/27/2016	63.68	-	60	77	83	63	17
Patient 9	CHOP_M12	0.43	4/14/2011	0.33	-	73	80	67	85	7
Patient 10	CHOP_M19	0.20	4/18/2013	0.26	-	51	56	54	53	5
Patient 11	CHOP_M24	3.20	8/31/2016	11.74	-	71	87	90	64	16
Patient 12	CHOP_M25	1.90	9/19/2017	2.07	-	48	25	43	12	-23

Patient ID	GT ID	HFD Error current	Error improved Anatomy	Error improved Flow	Error current abs	Error improved Anatomy abs	Error improved Flow abs
Patient 1	CHOP_M1	-4	-6	-11	4	6	11
Patient 2	CHOA_M2 (Y1)	7	13	-1	7	13	1
Patient 3	CHOP_M7	0	0	0	0	0	0
Patient 4	CHOA_M5 (Y11)	-21	-10	-29	21	10	29
Patient 5	CHOP_M17	45	-16	58	45	16	58
Patient 6	CHOP_M5	34	18	17	34	18	17
Patient 7	CHOP_M9	21	-7	38	21	7	38
Patient 8	CHOP_M10	17	-6	14	17	6	14
Patient 9	CHOP_M12	7	13	-5	7	13	5
Patient 10	CHOP_M19	5	2	3	5	2	3
Patient 11	CHOP_M24	16	-3	23	21	3	23
Patient 12	CHOP_M25	-23	-18	13	23	18	13

Patient ID	GT ID	IVC_pre	SVC_pre	LSVC_pre	AZ_pre	LPA_pre	RPA_pre	IVC_pre ind	SVC_pre ind	LSVC_pre ind	AZ_pre ind	LPA_pre ind	RPA_pre ind
Patient 1	CHOP_M1	0.57	1.13	0.72	0.71	2.22	0.91	0.94	1.86	1.19	1.17	3.66	1.50
Patient 2	CHOA_M2 (Y1)	0.56	0.7		1.6	0.97	3.3	0.38	0.47	0.00	1.08	0.66	2.23
Patient 3	CHOP_M7	0.42	1.54	0.64	1.23	2.14	0.41	0.34	1.26	0.52	1.01	1.75	0.34
Patient 4	CHOA_M5 (Y11)	1.11	0.96			1.33	1.66	0.79	0.69			0.95	1.19
Patient 5	CHOP_M17	0.34	1.1		1.27	1.9	0.81	0.23	0.75		0.87	1.30	0.55
Patient 6	CHOP_M5	0.84	0.93			0.26	0.62	1.80	1.99			0.56	1.33
Patient 7	CHOP_M9	0.47	1.25		0.68	0.54	0.94	0.82	2.19		1.19	0.95	1.65
Patient 8	CHOP_M10	0.47	0.97		0.46	1.28	0.39	0.80	1.64		0.78	2.17	0.66
Patient 9	CHOP_M12	1.13	0.57	0.39		1.73	0.37	2.22	1.12	0.76		3.39	0.73
Patient 10	CHOP_M19	0.42	1.09		0.37	0.58	1	1.00	2.60	0.00	0.88	1.38	2.38
Patient 11	CHOP_M24	0.55	0.54	0.98	0.29	1.1	0.84	0.95	0.93	1.69	0.50	1.90	1.45
Patient 12	CHOP_M25	0.27	0.68		0.42	0.65	0.6	0.62	1.57	0.00	0.97	1.50	1.39

Patient ID	GT ID	IVC_post	SVC_post	LSVC_post	AZ_post	LPA_post	RPA_post	IVC_post_ind	SVC_post_ind	LSVC_post_ind	AZ_post_ind	LPA_post_ind	RPA_post_ind
Patient 1	CHOP_M1	0.6	0.73	0.79	1	1.7	1.1	0.52	0.63	0.68	0.86	1.47	0.95
Patient 2	CHOA_M2 (Y1)	0.68	1.16		0.63	0.4	1.68	0.46	0.78		0.43	0.27	1.14
Patient 3	CHOP_M7	0.57	1.27	0.78	2.25	2.78	0.64	0.33	0.73	0.45	1.30	1.61	0.37
Patient 4	CHOA_M5 (Y11)	0.72	1.41			0.5	0.75	0.51	1.01			0.36	0.54
Patient 5	CHOP_M17	0.73	0.94		1.42	1.6	1.86	0.44	0.57		0.86	0.97	1.12
Patient 6	CHOP_M5	0.57	0.78			0.58	0.5	1.03	1.41			1.05	0.90
Patient 7	CHOP_M9	0.32	0.54		0.25	0.17	0.67	0.55	0.93		0.43	0.29	1.16
Patient 8	CHOP_M10	0.45	1.9		0.76	2.18	1	0.75	3.17		1.27	3.64	1.67
Patient 9	CHOP_M12	0.59	0.23	0.2		0.62	0.37	1.09	0.43	0.37		1.15	0.69
Patient 10	CHOP_M19	0.3	0.52		0.28	0.48	0.51	0.71	1.24	0.00	0.67	1.14	1.21
Patient 11	CHOP_M24	0.1	0.59	1.09	0.29	0.75	0.98	0.14	0.82	1.51	0.40	1.04	1.36
Patient 12	CHOP_M25	0.1	0.98		0.22	0.42	0.5	0.21	2.04		0.46	0.88	1.04

Patient ID	GT ID	IVC_change	SVC_change	LSVC_change	AZ_change	LPA_change	RPA_change	IVC_change_percent	SVC_change_percent	LSVC_change_percent	AZ_change_percent	LPA_change_percent	RPA_change_percent
Patient 1	CHOP_M1	0.03	-0.4	0.07	0.29	-0.52	0.19	0.05	-0.35	0.10	0.41	-0.23	0.21
Patient 2	CHOA_M2 (Y1)	0.12	0.46		-0.97	-0.57	-1.62	0.21	0.66		-0.61	-0.59	-0.49
Patient 3	CHOP_M7	0.15	-0.27	0.14	1.02	0.64	0.23	0.36	-0.18	0.22	0.83	0.30	0.56
Patient 4	CHOA_M5 (Y11)	-0.39	0.45			-0.83	-0.91	-0.35	0.47			-0.62	-0.55
Patient 5	CHOP_M17	0.39	-0.16		0.15	-0.3	1.05	1.15	-0.15		0.12	-0.16	1.30
Patient 6	CHOP_M5	-0.27	-0.15			0.32	-0.12	-0.32	-0.16			1.23	-0.19
Patient 7	CHOP_M9	-0.15	-0.71		-0.43	-0.37	-0.27	-0.32	-0.57		-0.63	-0.69	-0.29
Patient 8	CHOP_M10	-0.02	0.93		0.3	0.9	0.61	-0.04	0.96		0.65	0.70	1.56
Patient 9	CHOP_M12	-0.54	-0.34	-0.19		-1.11	0	-0.48	-0.60	-0.49		-0.64	0.00
Patient 10	CHOP_M19	-0.12	-0.57		-0.09	-0.1	-0.49	-0.29	-0.52		-0.24	-0.17	-0.49
Patient 11	CHOP_M24	-0.45	0.05	0.11	0	-0.35	0.14	-0.82	0.09	0.11	0.00	-0.32	0.17
Patient 12	CHOP_M25	-0.17	0.3		-0.2	-0.23	-0.1	-0.63	0.44		-0.48	-0.35	-0.17

Patient ID	GT ID	PFD_pre	PFD_post	PFD_change	TCPC_deviation_avg	TCPC_deviation_stdev	TCPC_deviation_max	Graft_deviation_avg	Graft_deviation_stdev	Graft_maxDeviation	Graft_insertion_offset
Patient 1	CHOP_M1	70.93	60.71	-10.21	2.63	2.15	16.26	6.25	4.1	15.5	15.03
Patient 2	CHOA_M2 (Y1)	22.72	19.23	-3.49	2.97	2.42	14.8	2.37	1.63	8.9	2.87
Patient 3	CHOP_M7	83.92	81.29	-2.64	3.63	3.46	18.97	3.49	2.94	13.28	20.7
Patient 4	CHOA_M5 (Y11)	44.48	40.00	-4.48	4.43	3.94	19.11	6.53	4.43	19.1	7.15
Patient 5	CHOP_M17	70.11	46.24	-23.87	2.69	3.19	18.97	9.53	4.81	19.62	21.58
Patient 6	CHOP_M5	29.55	53.70	24.16	1.15	1.11	5.94	0.71	0.65	2.81	0
Patient 7	CHOP_M9	36.49	20.24	-16.25	1.14	1.07	5.84	2.39	1.78	7.71	7.47
Patient 8	CHOP_M10	76.65	68.55	-8.09	1.59	1.61	9.42	2.69	2.2	9.39	6.5
Patient 9	CHOP_M12	82.38	62.63	-19.75	1.16	1.12	6.66	0.86	1.01	6.23	0
Patient 10	CHOP_M19	36.71	48.48	11.78	1.5	1.74	10.08	3.85	3.19	12.42	12.86
Patient 11	CHOP_M24	56.70	43.35	-13.35	2.08	1.47	9.84	3.11	2.19	9.75	6.78
Patient 12	CHOP_M25	52.00	45.65	-6.35	2.52	3.23	16.55	6.14	4.89	16.89	6.76

APPENDIX D – SPECIFIC AIM 1B CROSS-SECTIONAL PATIENT DATA

This appendix contains all data for all patients included in the cross-sectional portion of Specific Aim 1B (30 Y-graft and 30 LT/ECC patients). The posterior views for a variety of the Y-graft patients are shown below:

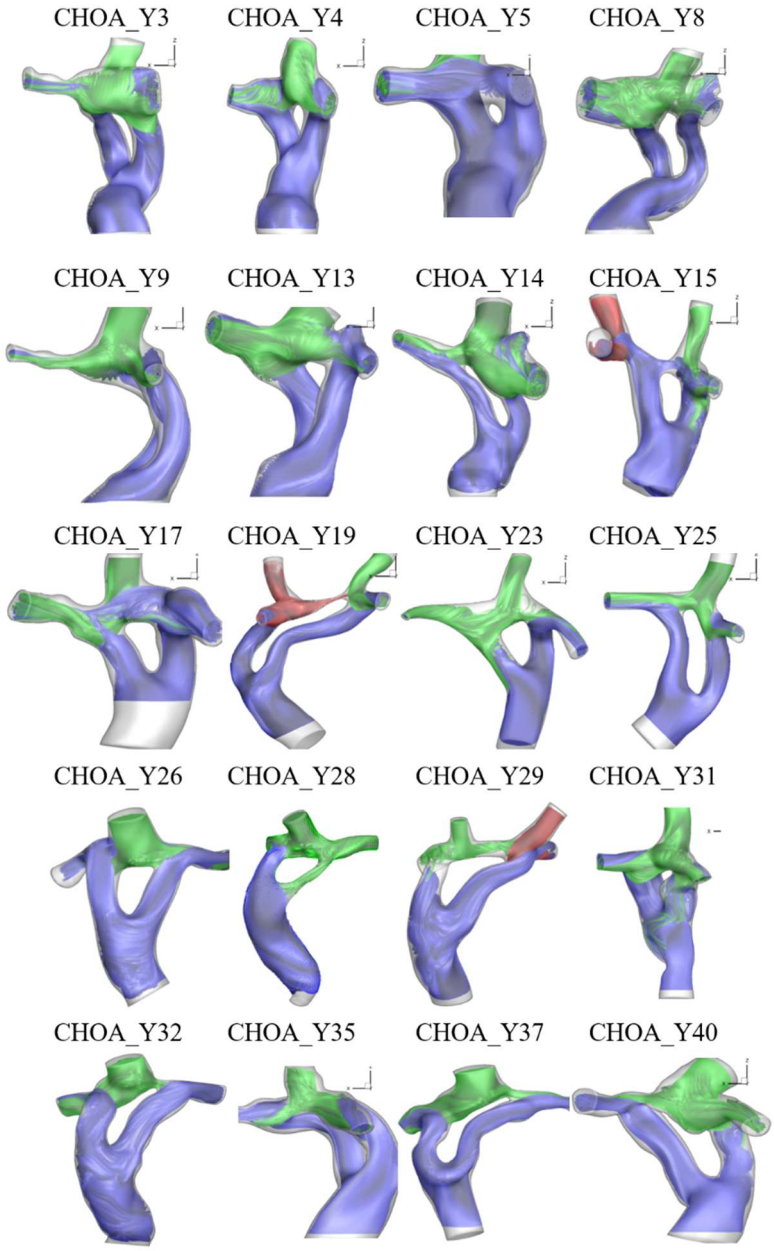

	Graft type	Age (yrs)	Gender	Power loss (mW)	Total Return (L/min)	BSA (m2)	iPL
CHOA_Y2B	ygraft	9	F	4.9798	3.08	0.899	0.02807
CHOA_Y3	ygraft	2	M	5.6085	0.79	0.53	0.65113
CHOA_Y4	ygraft	3	M	0.7201	1.448	0.73	0.02576
CHOA_Y4B	ygraft	6	M	2.1768	1.438	0.935	0.13041
CHOA_Y5	ygraft	2	F	1.3269	0.85	0.5	0.11007
CHOA_Y8	ygraft	14	M	3.525	3.2509	1.523	0.04849
CHIOA_Y9	ygraft	3	M	4.8748	1.38	0.512	0.09908
CHOA_Y10	ygraft	2	F	5.8903	1.39	0.554	0.13717
CHOA_Y13	ygraft	3	M	0.479	1.27	0.598	0.01704
CHOA_Y14	ygraft	1.5	M	2.8018	1.59	0.562	0.04486
CHOA_Y15	ygraft	2	F	25.9811	1.58	0.503	0.3396
CHOA_Y17	ygraft	2	F	0.4464	1.76	0.521	0.00453
CHOA_Y19	ygraft	4	M	7.9623	1.47	0.709	0.25676
CHOA_Y21	ygraft	3	F	0.9444	0.7026	0.54	0.1618
CHOA_Y22	ygraft	2	F	3.0074	1.8598	0.57	0.03095
CHOA_Y23	ygraft	3	F	8.1206	0.9711	0.553	0.55258
CHOA_Y24	ygraft	2	M	0.0147	1.994	0.539	0.00049
CHOA_Y25	ygraft	3	F	0.1116	1.413	0.553	0.00247
CHOA_Y26	ygraft	3	M	16.9388	1.5912	0.591	0.299
CHOA_Y27	ygraft	4	F	24.2854	1.7596	0.66	0.39568
CHOA_Y28	ygraft	2	M	6.96	0.8738	0.544	0.629
CHOA_Y29	ygraft	4	M	17.8996	1.9376	0.651	0.2125
CHOA_Y30	ygraft	5	M	8.9636	2.088	0.65	0.08477
CHOA_Y31	ygraft	3	M	0.1672	0.623	0.61	0.05243
CHOA_Y32	ygraft	4	M	11.9254	1.6	0.751	0.33461
CHOA_Y34	ygraft	6	M	2.6768	1.7946	0.895	0.0756
CHOA_Y35	ygraft	3	F	27.4868	1.656	0.626	0.48333
CHOA_Y36	ygraft	4	F	7.3748	2.22	0.768	0.08101
CHOA_Y37	ygraft	3	F	5.8173	1.42	0.647	0.17331
CHOA_Y40	ygraft	3	F	8.1884	1.3795	0.6	0.2285

	Graft type	Age (yrs)	Gender	Power loss (mW)	Total Return (L/min)	BSA (m2)	iPL
SVC033	ECC	4	M	4.5606	2.6177	0.81	0.03399
SVC040	LT	3	M	1.2396	1.4598	0.62	0.03121
SVC043	ECC	4	M	3.3148	1.9872	0.69	0.04098
SVC047	ECC	4	M	10.3004	2.138	0.61	0.07992
SVC051	ECC	3	M	1.98	1.9709	0.64	0.02159
SVC057	LT	3	M	0.7987	1.6684	0.61	0.01304
SVC058	ECC	3	M	3.1517	2.5939	0.59	0.01281
SVC059	ECC	4	M	9.2832	1.7594	0.75	0.19538
SVC062	ECC	4.5	M	1.6099	1.7568	0.71	0.0305
SVC063	ECC	2	F	1.2165	1.3881	0.65	0.03916
SVC070	ECC	3	M	4.1322	2.3678	0.51	0.0165
SVC075	LT	2	F	2.2418	2.6856	0.58	0.00793
SVC078	ECC	2	M	2.2371	2.2557	0.56	0.01246
SVC079	ECC	3	M	4.2784	2.4183	0.91	0.05105
SVC083	ECC	5	M	2.8171	2.0857	0.62	0.02432
SVC085	ECC	4	M	1.602	1.6998	0.62	0.02555
SVC093	ECC	3	M	3.6621	3.0816	0.71	0.01285
SVC100	LT	3	F	13.2363	2.7563	0.69	0.06132
SVC112	ECC	3	M	5.0149	2.8064	0.63	0.01835
CHOP042B	ECC	3	F	3.0329	1	0.62	0.23757
CHOP051B	ECC	4	M	1.8381	1.4743	0.63	0.04639
CHOP054A	LT	4	F	0.6955	2.0442	0.46	0.00351
CHOP081A	ECC	3	F	9.0232	1.5345	0.54	0.14839
CHOP085A	LT	2	M	2.2176	1.2016	0.5	0.06512
CHOP086A	ECC	6	F	32.3467	3.7103	0.81	0.08467
CHOP087A	LT	5	M	19.2336	1.9333	0.81	0.35586
CHOP109B	ECC	4	M	6.4896	2.6612	0.65	0.02965
CHOP064A	LT	6	F	0.4898	1.2614	0.94	0.04394
CHOP148A	LT	4	M	7.0043	1.7705	0.73	0.13705
CHOP026A	LT	6	F	5	2.08	0.83	0.078

	GFD (% LPA)	GFD deviation from 50	HFD (%LPA)	HFD Deviation from 50	Resistance (WU)	CO (L/min)	CI (L/min/m2)
CHOA_Y2B	38	12	66	16	0.47192	2.15	2.39
CHOA_Y3	33	17	18	32	4.76287	2.03	3.83
CHOA_Y4	34	16	55	5	0.25071	2.50	3.42
CHOA_Y4B	36	14	78	28	0.98427	3.20	3.43
CHOA_Y5	74	24	38	12	0.91827	1.44	2.88
CHOA_Y8	49	1	38	12	0.50799	4.14	2.72
CHIOA_Y9	30	20	5	45	1.3106	1.46	2.85
CHOA_Y10	35	15	25	25	1.68895	1.50	2.71
CHOA_Y13	80	30	37	13	0.17759	0.92	1.54
CHOA_Y14	46	4	47	3	0.62284	1.84	3.27
CHOA_Y15	64	14	64	14	5.23494	2.23	4.44
CHOA_Y17	55	5	12	38	0.07508	1.35	2.59
CHOA_Y19	52	2	37	13	2.61246	1.78	2.51
CHOA_Y21	7	43	77	27	1.03308	1.07	1.98
CHOA_Y22	25	25	0	50	0.4956	1.74	3.05
CHOA_Y23	44	6	6	44	4.76196	1.72	3.12
CHOA_Y24	56	6	48	2	0.00199	1.95	3.61
CHOA_Y25	48	2	72	22	0.03091	1.41	2.56
CHOA_Y26	60	10	65	15	3.95385	2.16	3.66
CHOA_Y27	32	18	29	21	5.1768	1.55	2.35
CHOA_Y28	51	1	1	49	4.95889	1.08	1.98
CHOA_Y29	47	3	92	42	3.10382	2.14	3.29
CHOA_Y30	49	1	89	39	1.33639	1.63	2.50
CHOA_Y31	84	34	99	49	0.26278	0.66	1.08
CHOA_Y32	65	15	81	31	3.49843	2.60	3.46
CHOA_Y34	41	9	86	36	0.74388	1.75	1.96
CHOA_Y35	40	10	83	33	6.27448	1.74	2.78
CHOA_Y36	38	12	69	19	1.14923	2.12	2.76
CHOA_Y37	24	26	48	2	1.86659	1.20	1.85
CHOA_Y40	43	7	91	41	2.58171	1.34	2.23

	GFD (% LPA)	GFD deviation from 50	HFD (%LPA)	HFD Deviation from 50	Resistance (WU)	CO (L/min)	CI (L/min/m2)
SVC033	45	5	19	31	0.5391	4.38	5.40
SVC040	28	22	40	10	0.36065	2.04	3.29
SVC043	69	19	72	22	0.57919	2.42	3.51
SVC047	58	8	40	10	1.37458	3.17	5.20
SVC051	31	19	43	7	0.32622	2.92	4.56
SVC057	44	6	51	1	0.17503	2.12	3.47
SVC058	35	15	21	29	0.27637	3.20	5.43
SVC059	38	12	70	20	2.24921	3.33	4.45
SVC062	71	21	45	5	0.37035	2.13	3.00
SVC063	24	26	1	49	0.41038	3.03	4.66
SVC070	40	10	15	35	0.37589	1.86	3.66
SVC075	58	8	63	13	0.18028	2.69	4.63
SVC078	55	5	29	21	0.24621	2.26	4.03
SVC079	60	10	23	27	0.66574	2.59	2.85
SVC083	32	18	6	44	0.4015	4.38	7.06
SVC085	45	5	28	22	0.34376	2.82	4.54
SVC093	44	6	7	43	0.2738	3.80	5.35
SVC100	41	9	45	5	1.20216	2.72	3.95
SVC112	55	5	26	24	0.40115	3.26	5.17
CHOP042B	77	27	48	2	1.8804	2.08	3.35
CHOP051B	79	29	61	11	0.53277	1.95	3.09
CHOP054A	21	29	19	31	0.07656	2.05	4.45
CHOP081A	38	12	18	32	2.06929	3.88	7.18
CHOP085A	35	15	40	10	0.76795	1.60	3.20
CHOP086A	36	14	33	17	1.90325	2.83	3.50
CHOP087A	35	15	69	19	4.16819	2.69	3.32
CHOP109B	51	1	14	36	0.59563	2.63	4.04
CHOP064A	55	5	77	27	0.28936	1.61	1.72
CHOP148A	42	8	43	7	1.63116	2.47	3.39
CHOP026A	40	10	76	26	0.95923	3.10	3.74

	LPA mean Diameter (mm)	LPA min Diameter (mm)	RPA mean Diameter (mm)	RPA min Diameter (mm)	Nakata Index mean	Nakata Index min	stenosis LPA	stenosis RPA
CHOA_Y2B	9.78	9.36	10.89	10.18	187.21	167.11	8.42	12.61
CHOA_Y3	5.91	3.19	8.82	8.05	167.02	111.23	70.75	16.64
CHOA_Y4	7.71	6.57	9.02	8.45	151.47	123.20	27.45	12.25
CHOA_Y4B	10.28	9.23	9.44	7.59	163.64	119.94	19.46	35.30
CHOA_Y5	8.50	7.05	7.94	7.21	212.50	159.69	31.19	17.58
CHOA_Y8	18.29	16.88	13.17	12.91	261.87	232.75	14.85	3.92
CHIOA_Y9	5.70	3.74	6.78	5.81	120.24	73.23	56.84	26.57
CHOA_Y10	5.10	4.19	7.90	7.19	125.49	98.17	32.75	17.19
CHOA_Y13	7.59	6.96	7.22	6.20	144.06	114.12	15.93	26.15
CHOA_Y14	6.06	4.81	10.03	9.25	191.96	151.76	37.14	15.02
CHOA_Y15	6.85	5.35	5.73	4.75	124.51	79.88	38.96	31.40
CHOA_Y17	8.71	7.75	7.28	6.63	194.15	156.63	20.88	17.09
CHOA_Y19	6.66	5.28	7.22	6.36	106.98	75.67	37.23	22.49
CHOA_Y21	5.36	4.19	10.65	10.47	206.59	184.97	38.96	3.25
CHOA_Y22	4.01	3.12	6.15	5.18	74.21	50.46	39.27	28.90
CHOA_Y23	4.28	2.54	5.77	4.32	73.36	35.74	64.71	43.91
CHOA_Y24	5.67	4.30	5.86	5.34	96.79	68.52	42.50	16.78
CHOA_Y25	6.03	5.34	4.48	4.08	80.16	64.13	21.60	17.11
CHOA_Y26	5.44	4.52	6.52	4.52	95.80	54.31	31.12	51.81
CHOA_Y27	4.22	3.16	7.07	6.55	80.65	62.95	43.76	14.18
CHOA_Y28	5.08	2.84	3.32	3.04	53.16	24.91	68.85	16.31
CHOA_Y29	7.00	6.27	5.64	4.92	97.51	76.60	19.78	24.00
CHOA_Y30	6.86	5.70	6.49	6.11	107.75	84.41	30.90	11.32
CHOA_Y31	7.93	5.97	7.07	5.87	145.33	90.27	43.33	31.04
CHOA_Y32	6.10	5.39	7.21	6.88	93.37	79.88	22.11	8.97
CHOA_Y34	7.06	6.36	9.37	7.87	120.86	89.86	18.99	29.43
CHOA_Y35	5.94	4.83	7.65	6.64	117.79	84.51	33.94	24.83
CHOA_Y36	8.61	7.88	6.17	4.89	114.70	87.87	16.32	37.19
CHOA_Y37	4.22	3.55	6.33	5.47	70.26	51.61	29.19	25.38
CHOA_Y40	6.35	5.10	6.38	5.43	106.21	72.71	35.52	27.61

	LPA mean Diameter (mm)	LPA min Diameter (mm)	RPA mean Diameter (mm)	RPA min Diameter (mm)	Nakata Index mean	Nakata Index min	stenosis LPA	stenosis RPA
SVC033	8.48	5.53	10.20	9.13	170.50	110.46	57.48	19.83
SVC040	9.21	5.85	9.43	7.42	219.93	113.13	59.59	38.04
SVC043	10.21	7.63	9.25	8.81	215.97	154.69	44.10	9.19
SVC047	6.26	5.02	7.93	7.83	131.55	111.39	35.74	2.61
SVC051	7.54	5.74	10.49	9.67	204.86	155.32	42.01	14.97
SVC057	12.43	9.10	10.01	7.20	327.97	173.32	46.36	48.37
SVC058	8.65	5.90	10.62	9.61	249.95	169.25	53.48	18.23
SVC059	9.01	6.91	8.26	7.17	156.59	103.89	41.21	24.68
SVC062	9.76	9.02	11.40	8.94	248.94	178.41	14.43	38.52
SVC063	7.59	6.74	7.47	6.97	137.16	113.57	21.17	13.11
SVC070	6.94	5.29	9.11	7.18	201.81	122.53	41.88	37.78
SVC075	8.08	5.55	10.81	9.47	246.55	163.24	52.74	23.20
SVC078	9.78	9.35	8.72	7.79	240.71	207.64	8.65	20.15
SVC079	9.23	8.98	8.64	6.52	137.89	106.25	5.36	43.01
SVC083	8.21	6.40	8.65	8.36	180.17	140.57	39.13	6.54
SVC085	9.17	8.52	9.38	8.51	217.87	183.79	13.67	17.53
SVC093	10.87	9.00	9.00	8.83	220.30	175.79	31.45	3.82
SVC100	9.61	4.77	9.84	7.62	215.25	92.03	75.36	39.96
SVC112	9.27	7.35	10.21	8.13	237.30	149.68	37.19	36.70
CHOP042B	9.82	5.97	4.37	4.27	146.33	68.33	63.02	4.16
CHOP051B	9.24	8.01	8.30	7.02	192.29	141.52	24.74	28.46
CHOP054A	12.20	8.58	13.67	10.07	573.09	298.72	50.61	45.69
CHOP081A	8.90	6.45	12.69	10.58	349.38	223.34	47.57	30.41
CHOP085A	7.07	4.05	7.95	7.35	177.65	110.72	67.15	14.35
CHOP086A	7.67	6.47	11.28	10.39	180.39	145.31	28.82	15.12
CHOP087A	10.38	5.91	15.25	12.62	329.93	188.24	67.51	31.58
CHOP109B	9.47	7.21	9.00	6.47	206.14	113.41	42.00	48.28
CHOP064A	10.35	6.39	10.08	8.32	174.29	91.88	61.92	31.84
CHOP148A	7.80	6.14	7.77	6.14	130.37	81.08	38.00	37.61
CHOP026A	9.38	4.47	9.25	7.75	164.08	75.72	77.30	29.74

	Overall stenosis	Average PRT (s)	Minimum PRT (s)	Maximum PRT (s)	Mode PRT (s)	PI_IVC (%)	PI_SVC (%)	wPI (%)
CHOA_Y2B	10.74	0.53	0.18	2.68	0.35	0.51	0.28	39.36
CHOA_Y3	33.40	1.60	0.82	2.82	1.46	1.08	0.40	73.98
CHOA_Y4	18.67	1.41	0.74	3.08	0.85	0.16	0.19	17.45
CHOA_Y4B	26.70	2.46	1.84	2.86	2.49	2.64	0.31	147.62
CHOA_Y5	24.85	1.43	0.72	2.87	1.01	1.05	0.31	68.03
CHOA_Y8	11.12	1.04	0.37	3.46	0.65	0.27	0.40	33.59
CHIOA_Y9	39.10	1.19	0.38	3.55	0.56	0.61	0.51	55.95
CHOA_Y10	21.77	0.84	0.33	2.26	0.67	0.57	0.39	48.14
CHOA_Y13	20.79	1.38	0.85	2.34	0.91	0.24	0.42	33.05
CHOA_Y14	20.94	1.21	0.34	2.97	0.91	0.73	0.29	50.81
CHOA_Y15	35.84	1.13	0.41	2.74	0.74	2.31	0.46	138.24
CHOA_Y17	19.32	0.91	0.04	2.57	0.60	2.40	0.31	135.17
CHOA_Y19	29.27	1.35	0.42	3.76	0.98	1.16	0.62	89.19
CHOA_Y21	10.47	1.17	0.08	3.23	0.65	1.19	0.83	101.06
CHOA_Y22	31.99	0.24	0.13	0.29	0.27	0.25	0.46	35.80
CHOA_Y23	51.28	1.03	0.45	2.26	0.53	0.67	0.33	50.21
CHOA_Y24	29.21	2.88	0.91	8.87	1.95	1.19	0.52	85.39
CHOA_Y25	20.00	0.81	0.37	2.58	0.45	0.33	0.64	48.28
CHOA_Y26	43.30	0.73	0.27	2.41	0.35	0.35	0.25	29.76
CHOA_Y27	21.94	1.03	0.09	1.97	0.84	1.47	0.28	87.74
CHOA_Y28	53.13					2.29	0.52	140.28
CHOA_Y29	21.44	0.75	0.38	1.81	0.48	0.33	0.34	33.65
CHOA_Y30	21.66	0.94	0.19	2.93	0.78	0.64	0.45	54.55
CHOA_Y31	37.88	1.68	0.88	2.81	1.16	0.80	0.90	85.00
CHOA_Y32	14.45	1.40	0.45	3.02	0.89	0.37	0.28	32.51
CHOA_Y34	25.65					0.38	0.53	45.59
CHOA_Y35	28.25	1.39	0.65	2.88	0.68	1.56	0.23	89.67
CHOA_Y36	23.39	0.99	0.34	4.04	0.43	0.24	0.31	27.41
CHOA_Y37	26.55	0.58	0.14	2.35	0.43	0.51	0.45	47.90
CHOA_Y40	31.54	0.86	0.26	2.85	0.45	1.49	0.53	101.11

	Overall stenosis	Average PRT (s)	Minimum PRT (s)	Maximum PRT (s)	Mode PRT (s)	PI_IVC (%)	PI_SVC (%)	wPI (%)
SVC033	35.21	0.77	0.24	3.06	0.38	0.32	0.34	32.78
SVC040	48.56	0.96	0.37	2.35	0.48	0.68	0.45	56.51
SVC043	28.37	1.16	0.44	2.80	0.73	0.17	0.35	26.18
SVC047	15.32	0.76	0.00	2.48	0.11	0.20	0.19	19.63
SVC051	24.18	0.87	0.24	3.87	0.38	0.41	0.66	53.57
SVC057	47.15	1.11	0.32	2.59	0.83	0.59	0.53	56.04
SVC058	32.29	0.99	0.32	3.00	0.40	0.50	0.34	41.74
SVC059	33.66	0.64	0.18	2.53	0.25	1.06	0.38	71.75
SVC062	28.33	1.59	0.65	3.01	1.67	0.81	0.50	65.06
SVC063	17.20	0.94	0.35	2.49	0.45	0.40	0.54	47.00
SVC070	39.29	0.79	0.26	2.78	0.35	0.25	0.33	28.91
SVC075	33.79	1.33	0.33	3.24	0.41	0.69	2.94	181.50
SVC078	13.73	0.93	0.35	2.15	0.41	0.45	0.34	39.59
SVC079	22.95	0.77	0.38	2.34	0.48	0.25	0.35	29.93
SVC083	21.97	1.16	0.54	2.64	0.60	0.57	0.27	42.08
SVC085	15.64	1.29	0.55	2.80	0.89	0.70	0.29	49.91
SVC093	20.20	0.81	0.31	2.34	0.38	0.29	0.37	33.13
SVC100	57.24	0.83	0.23	3.68	0.37	0.64	0.55	59.60
SVC112	36.92	0.93	0.30	3.19	0.42	0.47	0.15	31.16
CHOP042B	53.30	1.82	0.14	4.60	1.50	2.29	0.44	136.76
CHOP051B	26.40	1.19	0.57	2.79	0.66	0.29	0.91	60.22
CHOP054A	47.88	1.32	0.48	3.59	0.53	0.44	0.37	40.75
CHOP081A	36.07	1.51	0.53	2.76	0.86	3.41	0.21	180.92
CHOP085A	37.67	1.00	0.63	2.83	0.74	0.62	0.42	52.13
CHOP086A	19.45	0.68	0.17	3.15	0.35	0.40	1.16	78.07
CHOP087A	42.94	1.27	0.47	3.87	0.66	0.44	0.37	40.51
CHOP109B	44.98	0.79	0.28	2.82	0.36	0.70	0.24	47.02
CHOP064A	47.28	1.48	0.66	4.30	0.90	0.30	0.59	44.26
CHOP148A	37.81	1.20	0.28	3.80	0.59	1.05	0.52	78.37
CHOP026A	53.85	1.07	0.52	3.86	0.69	0.41	0.35	37.91

	HFD deviation	0-10	11-20	21-30	31-40	41-50
Number of patients	Ygraft	4	8	5	6	7
	LT/ECC	9	5	8	5	3
	TCPC resistance (WU)	0-1	1-2	2-3	3-4	4-5
Number of patients	Ygraft	13	7	2	3	5
	LT/ECC	23	5	2	0	0

Data used to make Figure 6-2 and 6-4.

APPENDIX E – SPECIFIC AIM 1B LONGITUDINAL PATIENT DATA

This appendix contains all data for all patients included in the longitudinal portion of Specific Aim 1B. This includes 10 Y-graft patients with two serial time points, as well as three unique ECC control groups which each have 10 unique patients. The Y-graft data are presented first, follow by the three control groups.

Patient ID	GT ID	FU_time	FU_time_months	gender (M=1, F=2)	morphology (HLHS=1, other=2)	fenestration (Yes=1)	BSA1	FU timepoint 1	FU timepoint 1 (years)
Y1	CHOA_Y5	3.51	42.14	2	1	1	0.5	6 days	0.016
Y2	CHOA_Y13	3.23	38.70	1	2	1	0.6	12 days	0.032
Y3	CHOA_Y14	3.75	45.04	1	2	1	0.59	45 days	0.123
Y4	CHOA_Y26	3.24	38.83	1	2	1	0.62	14 days	0.038
Y5	CHOA_Y27	3.01	36.13	2	1	1	0.62	7 days	0.019
Y6	CHOA_Y32	2.44	29.26	2	2	1	0.75	23 days	0.063
Y7	CHOA_Y36	1.22	14.59	2	2	1	0.8	7 days	0.019
Y8	CHOA_Y37	0.32	3.82	2	1	2	0.65	9 days	0.0246
Y9	CHOA_Y40	3.02	36.24	2	2	1	0.6	7 days	0.019
Y10	CHOA_Y42	2.50	30.00	1	2	1	0.81	30 days	0.082

Patient ID	GT ID	MRIdate1	Age At MRI1 (yrs)	Power loss 1 (mW)	iPL1	resistance1 (WU)	PressureDrop 1 (mmHg)	HFD1 (%LPA)	HFDdeviation1
Y1	CHOA_Y5	12/9/2010	2	0.118	0.008	0.064	0.058	14	36
Y2	CHOA_Y13	5/1/2012	3	0.27	0.015	0.103	0.112	54	4
Y3	CHOA_Y14	5/10/2012	1.6	0.964	0.025	0.221	0.309	68	18
Y4	CHOA_Y26	8/22/2013	3	4.147	0.075	0.703	1.146	63	13
Y5	CHOA_Y27	10/10/2013	4	1.215	0.11	0.604	0.575	48	2
Y6	CHOA_Y32	3/17/2014	4	0.73	0.035	0.184	0.246	92	42
Y7	CHOA_Y36	7/29/2014	4	2.935	0.043	0.307	0.636	68	18
Y8	CHOA_Y37	8/14/2014	3	1.087	0.055	0.343	0.41	37	13
Y9	CHOA_Y40	10/2/2014	3	0.937	0.053	0.352	0.385	44	6
Y10	CHOA_Y42	7/28/2015	5	0.572	0.038	0.121	0.177	78	28

Patient ID	GT ID	CO1 (L/min)	CI1 (L/min/m2)	IVC flow1	SVC flow1	LPA flow1	RPA flow1	PFD1	PFDdeviation1	Qs1	Collateral flow1
Y1	CHOA_Y5	1.53	3.06	0.45	0.556	0.638	0.19	77	27	1.006	0.524
Y2	CHOA_Y13	3.28	5.467	0.37	0.61	0.732	0.183	80	30	0.98	2.3
Y3	CHOA_Y14	1.84	3.119	0.39	0.72	0.37	0.37	50	0	1.11	0.73
Y4	CHOA_Y26	2.4	3.871	0.55	0.97	0.85	0.61	58	8	1.52	0.88
Y5	CHOA_Y27	2.36	3.806	0.255	0.44	0.27	0.44	38	12	0.695	1.665
Y6	CHOA_Y32	2.6	3.467	0.39	0.8	0.59	0.88	40	10	1.19	1.41
Y7	CHOA_Y36	2.26	2.825	0.2	1.25	0.83	1.14	42	8	1.45	0.81
Y8	CHOA_Y37	1.7	2.615	0.6	0.6	0.3	0.9	25	25	1.2	0.5
Y9	CHOA_Y40	1.34	2.23	0.28	0.82	0.44	0.57	44	6	1.1	0.24
Y10	CHOA_Y42	2.3	2.84	0.4	1.1	0.7	0.7	50	0	1.5	0.8

Patient ID	GT ID	IVC_davg1	IVC_dmin1	SVC_davg1	SVC_dmin1	LPA_davg1	LPA_dmin1	RPA_davg1	RPA_dmin1
Y1	CHOA_Y5	18.293	18.09	13.12	13.12	9.076	7.785	8.59	8.59
Y2	CHOA_Y13	24.453	23.627	19.727	17.969	9.424	9.336	9.464	8.456
Y3	CHOA_Y14	16.028	15.411	12.356	12.208	6.683	6.18	11.5	11.5
Y4	CHOA_Y26	17.385	17.139	13.406	13.201	5.871	5.46	7.534	5.019
Y5	CHOA_Y27	15.568	8.103	10.36	9.713	4.355	3.701	7.379	6.911
Y6	CHOA_Y32	19.634	17.318	17.692	16.985	7.056	6.561	8.021	7.791
Y7	CHOA_Y36	16.404	15.297	11.011	10.107	9.488	8.917	7	6.6
Y8	CHOA_Y37	12.118	11.88	12	12	4.729	3.774	7.635	6.988
Y9	CHOA_Y40	20.575	19.110	15.409	13.193	6.905	6.104	6.760	6.284
Y10	CHOA_Y42	16.291	16.201	17.279	16.124	8.465	8.164	13.266	8.785

Patient ID	GT ID	IVC stenosis1	SVC stenosis1	LPA stenosis1	RPA stenosis1	Overall PA stenosis1	Overall stenosis 1
Y1	CHOA_Y5	2.208	0	26.436	0	13.946	13.946
Y2	CHOA_Y13	6.643	17.028	1.861	20.172	11.056	11.056
Y3	CHOA_Y14	7.547	2.368	14.467	0	3.652	3.652
Y4	CHOA_Y26	2.813	3.028	13.486	55.635	39.713	39.713
Y5	CHOA_Y27	72.91	12.104	27.772	12.278	16.281	16.281
Y6	CHOA_Y32	22.194	7.837	13.551	5.661	9.103	9.103
Y7	CHOA_Y36	13.047	15.745	11.678	10	11.475	11.475
Y8	CHOA_Y37	3.889	0	36.3	16.223	21.79	21.79
Y9	CHOA_Y40	13.733	26.698	21.862	13.576	18	14.46
Y10	CHOA_Y42	1.101	12.925	6.988	56.145	42	20.8

Patient ID	GT ID	BSA2 (m2)	MRIdate2	AgeAtMRI2 (yrs)	Power loss 2 (mW)	iPL2	resistance2 (WU)	PressureDrop 2 (mmHg)	HFD2 (%LPA)	HFDdeviation2
Y1	CHOA_Y5	0.78	6/13/2014	5	1.784	0.058	0.328	0.513	28	22
Y2	CHOA_Y13	0.81	7/22/2015	6	1.124	0.023	0.146	0.271	49	1
Y3	CHOA_Y14	0.98	2/9/2016	5	2.067	0.024	0.143	0.364	49	1
Y4	CHOA_Y26	0.87	11/15/2016	6	0.73	0.022	0.111	0.191	52	2
Y5	CHOA_Y27	0.7	10/13/2016	7	0.618	0.033	0.183	0.226	65	15
Y6	CHOA_Y32	1.01	8/23/2016	6	3.547	0.017	0.127	0.451	71	21
Y7	CHOA_Y36	0.88	10/16/2015	5	1.637	0.022	0.144	0.326	52	2
Y8	CHOA_Y37	0.7	12/8/2014	3	0.822	0.04	0.23	0.292	43	7
Y9	CHOA_Y40	0.86	10/10/2017	6	1.290	0.042	0.171	0.315	53	3
Y10	CHOA_Y42	1.05	1/25/2018	7.5	1.970	0.020	0.114	0.318	58	8

Patient ID	GT ID	CO2 (L/min)	CI2 (L/min/m2)	IVC_flow2	SVC_flow2	LPA_flow2	RPA_flow2	PFD2 (%LPA)	PFD deviation2	Qs2	Percent IVC_flow	collateral_flow2
Y1	CHOA_Y5	4.21	5.40	0.87	0.83	0.79	0.55	59	9	1.70	0.51	2.51
Y2	CHOA_Y13	2.50	3.09	1.09	1.38	1.00	0.60	63	13	2.48	0.44	0.02
Y3	CHOA_Y14	4.00	4.08	1.10	1.60	1.00	1.20	45	5	2.70	0.41	1.30
Y4	CHOA_Y26	2.10	2.41	0.70	1.00	0.80	0.90	47	3	1.70	0.41	0.40
Y5	CHOA_Y27	2.20	3.14	0.40	0.90	0.50	0.60	45	5	1.30	0.31	0.90
Y6	CHOA_Y32	3.60	3.56	1.40	2.00	1.40	1.90	42	8	3.40	0.41	0.20
Y7	CHOA_Y36	2.70	3.07	0.90	1.20	1.00	1.20	45	5	2.10	0.43	0.60
Y8	CHOA_Y37	2.40	3.43	0.56	0.71	0.21	0.74	22	28	1.27	0.44	1.13
Y9	CHOA_Y40	1.70	1.97	0.90	0.89	0.70	0.44	61	11	1.80	0.50	0.00
Y10	CHOA_Y42	3.20	3.05	1.10	1.60	1.30	1.10	52	2	2.70	0.41	0.50

Patient ID	GT ID	IVC_d_avg2	IVC_d_min2	SVC_d_avg2	SVC_d_min2	LPA_d_avg2	LPA_d_min2	RPA_d_avg2	RPA_d_min2	IVC_stenosis2	SVC_stenosis2	LPA_stenosis2	RPA_stenosis2	Overall_PAstenosis2
Y1	CHOA_Y5	17.69	16.89	10.46	10.37	8.75	6.75	7.10	6.90	9	2	40	6	27
Y2	CHOA_Y13	21.32	21.14	21.19	20.75	9.98	9.00	8.99	8.49	2	4	19	11	15
Y3	CHOA_Y14	17.65	16.54	13.51	13.39	10.30	10.07	12.16	12.16	12	2	5	0	2
Y4	CHOA_Y26	21.99	21.61	13.04	12.83	9.33	8.91	11.49	11.24	3	3	9	4	6
Y5	CHOA_Y27	17.95	17.70	13.75	13.39	7.79	7.66	7.81	7.34	3	5	3	12	7
Y6	CHOA_Y32	20.95	20.38	27.36	26.72	9.38	7.80	10.08	8.00	5	5	31	37	34
Y7	CHOA_Y36	18.26	17.85	12.80	12.12	13.15	12.49	10.86	10.10	4	10	10	14	11
Y8	CHOA_Y37	15.50	15.18	15.18	15.17	5.37	4.89	7.80	6.20	4	0	17	37	30
Y9	CHOA_Y40	17.29	16.76	17.05	15.12	10.40	9.85	10.92	10.00	6	21	10	16	13
Y10	CHOA_Y42	16.36	16.21	21.54	16.92	9.55	7.96	14.82	12.33	2	38	30	31	31

PatientID	Comparison group	Source study	Institution	LT:1, ECC:2	FU_time	FU_time_months	gender (M=1)	morphology (HLHS=1, other=2)	fenestration (1=Yes)
SVC043	1	CBF	CHOP	2	0.43	5.19	1	2	1
SVC059	1	CBF	CHOP	2	0.59	7.13	1	2	1
SVC063	1	CBF	CHOP	2	0.67	8.09	2	1	1
SVC075	1	CBF	CHOP	1	0.54	6.48	2	1	1
SVC085	1	CBF	CHOP	2	0.64	7.73	1	2	1
SVC112	1	CBF	CHOP	2	0.72	8.58	1	1	1
CHOP081A	1	R01	CHOP	2	0.46	5.49	2	2	1
LB13_2	1	Serial liver	CHOP	?	0.01	0.12	2	2	2
LB18_2	1	Serial liver	CHOP	2	0.54	6.48	2	1	2
LB23_1	1	Serial liver	CHOP	2	2.15	25.80	2	1	2
CHOP026A	2	R01	CHOP	1	4.48	53.79	2	1	1
CHOP016A	2	R01	CHOP	2	4.62	55.43	1	1	2
CHOP018A	2	R01	CHOP	1	5.38	64.50	1	2	2
CHOP024A	2	R01	CHOP		5.36	64.31	2	2	2
CHOP082A	2	R01	CHOP	2	5.30	63.60	1	2	2
CHOP088A	2	R01	CHOP	2	5.60	67.20	2	2	2
LB19_1	2	Serial liver	CHOP	2	4.35	52.20	2	1	1
LB20_2	2	Serial liver	CHOP	2	5.21	62.52	1	1	2
LB24_1	2	Serial liver	CHOP	2	5.85	70.20	1	1	1
LB25_1	2	Serial liver	CHOP	2	3.86	46.32	1	1	1
LB03_1	3	Serial liver	CHOP	1	16.04	192.48	2	1	2
LB05_1	3	Serial liver	CHOP	2	12.27	147.24	2	1	2
LB06_5	3	Serial liver	CHOP	2	12.64	151.68	1	2	1
LB07_3	3	Serial liver	CHOP	2	11.98	143.76	2	2	1
LB08_1	3	Serial liver	CHOP	2	15.58	186.96	1	2	2
LB09_2	3	Serial liver	CHOP	2	11.76	141.12	2	1	1
LB12_1	3	Serial liver	CHOP	2	16.32	195.84	2	1	2
LB15_2	3	Serial liver	CHOP	2	13.48	161.76	2	1	1
LB21_1	3	Serial liver	CHOP	2	13.11	157.32	1	2	2
MRI1	3	Concurrent liver	CHOP		12.00	144.00	2	2	2

PatientID	Comparison group	BSA2	AgeAtMRI2	PL2 (mW)	iPL2	resistance2 (WU)	Pressure Drop2	HFD2	HFDdeviation2
SVC043	1	0.69	4	2.29	0.0283	0.2610	0.5186	86	36
SVC059	1	0.75	4	9.1	0.1915	1.3229	2.3275	51	1
SVC063	1	0.65	2	0.61	0.0196	0.1425	0.1978	3	47
SVC075	1	0.58	2	0.72	0.0025	0.0449	0.1206	64	14
SVC085	1	0.62	4	0.9	0.0144	0.1402	0.2383	16	34
SVC112	1	0.63	3	2.54	0.0093	0.1451	0.4073	26	24
CHOP081A	1	0.54	3	0.52	0.0086	0.0994	0.1525	12	38
LB13_2	1	0.62	3	3.4	0.0310	0.3651	0.7476	67	17
LB18_2	1	0.58	3	1.04	0.0155	0.1696	0.2824	41	9
LB23_1	1	0.66	5	1.11	0.0278	0.2150	0.3280	33	17
CHOP026A	2	0.83	6	1.91	0.0298	0.1987	0.4132	58	8
CHOP016A	2	0.83	6	2.13	0.0086	0.0896	0.2931	3	47
CHOP018A	2	0.68	7	0.58	0.0030	0.0377	0.0992	51	1
CHOP024A	2	0.74	7	1.15	0.0077	0.0796	0.2029	52	2
CHOP082A	2	0.87	7	0.93	0.0099	0.0703	0.1715	61	11
CHOP088A	2	1.25	8	0.66	0.0160	0.0533	0.1258	28	22
LB19_1	2	0.8	6	1.400893	0.0403	0.2302	0.3810	7	43
LB20_2	2	1	7	4.459021	0.0374	0.2391	0.6927	3	47
LB24_1	2	1	9	1.532863	0.0264	0.1329	0.3027	57	7
LB25_1	2	0.63	6	1.062668	0.0097	0.1119	0.2314	27	23
LB03_1	3	1.53	20	1.627477	0.0198	0.0636	0.2158	57	7
LB05_1	3	1.29	14	5.228602	0.0386	0.1834	0.6569	36	14
LB06_5	3	1.6	14	5.269497	0.0548	0.1743	0.6428	33	17
LB07_3	3	1.57	24	6.914106	0.0571	0.2012	0.7911	66	16
LB08_1	3	1.96	16	7.033888	0.0238	0.0841	0.5159	57	7
LB09_2	3	1.02	15	2.080923	0.0317	0.1617	0.3892	61	11
LB12_1	3	1.48	17	2.581938	0.1105	0.2434	0.5318	37	13
LB15_2	3	1.63	15	7.873656	0.0648	0.2173	0.8775	31	19
LB21_1	3	1.68	15	9.057736	0.0357	0.1470	0.7740	62	12
MRI1	3	1.09	13	9.87	0.1218	0.6110	1.6470	55	5

PatientID	Comparison group	CO 2 (L/min)	CI2 (L/min/m2)	IVC_flow2	SVC_flow2	LPA_flow2	RPA_flow2	PFD2	PFDdeviation2
SVC043	1	2.42	3.51	0.57	1.41	1.36	0.62	69	19
SVC059	1	3.33	4.45	0.88	0.87	0.47	0.76	38	12
SVC063	1	3.03	4.66	0.64	0.75	0.50	1.56	24	26
SVC075	1	2.69	4.63	0.82	1.87	0.67	0.48	58	8
SVC085	1	2.82	4.54	0.52	1.16	0.70	0.85	45	5
SVC112	1	3.26	5.17	0.84	1.96	0.70	0.56	55	5
CHOP081A	1	3.88	7.18	0.32	1.22	0.52	0.85	38	12
LB13_2	1	2.10	3.39	0.53	0.75	1.70	0.40	81	31
LB18_2	1	2.40	4.14	0.94	0.72	0.76	0.64	54	4
LB23_1	1	2.00	3.03	0.74	0.79	0.58	0.92	39	11
CHOP026A	2	3.10	3.74	0.79	0.80	0.64	0.96	40	10
CHOP016A	2	3.27	3.94	2.23	1.71	1.00	2.94	25	25
CHOP018A	2	2.63	3.87	2.03	1.84	1.37	1.87	42	8
CHOP024A	2	2.55	3.45	2.14	1.31	1.15	1.55	43	7
CHOP082A	2	2.47	2.84	1.56	0.88	0.96	1.47	40	10
CHOP088A	2	3.12	2.50	1.47	0.89	1.28	1.09	54	4
LB19_1	2	3.63	4.53	1.05	0.69	0.53	0.91	37	13
LB20_2	2	5.39	5.39	1.16	1.70	0.63	2.40	21	29
LB24_1	2	3.60	3.60	1.10	1.10	1.00	1.10	48	2
LB25_1	2	1.76	2.79	1.17	0.89	0.61	0.67	48	2
LB03_1	3	3.90	2.55	2.52	0.88	1.43	1.79	44	6
LB05_1	3	4.50	3.49	1.68	0.94	1.40	2.20	39	11
LB06_5	3	7.60	4.75	2.50	1.40	1.70	1.30	57	7
LB07_3	3	4.74	3.02	3.04	1.05	1.83	1.78	51	1
LB08_1	3	6.75	3.44	4.30	2.10	3.09	3.29	48	2
LB09_2	3	3.90	3.82	1.43	0.98	1.09	0.75	59	9
LB12_1	3	4.94	3.34	1.84	0.34	0.70	1.48	32	18
LB15_2	3	4.90	3.01	2.77	1.70	1.40	3.40	29	21
LB21_1	3	6.02	3.58	3.46	0.93	2.79	2.47	53	3
MRI1	3	3.60	3.30	1.10	0.90	0.90	1.60	36	14

PatientID	Comparison group	Qs2	Percent_ IVC_flow	collateral_flow2	IVC_d_avg2	IVC_d_min2	SVC_d_avg2	SVC_d_min2	LPA_d_avg2	LPA_d_min2	RPA_d_avg2	RPA_d_min2
SVC043	1	1.99	0.29	0.44	16.67	15.28	11.45	10.42	10.21	7.63	9.25	8.81
SVC059	1	1.76	0.50	2.11	14.37	13.53	13.92	13.00	9.01	6.91	8.26	7.17
SVC063	1	1.39	0.46	0.97	14.53	12.17	11.39	10.78	7.59	6.74	7.47	6.97
SVC075	1	2.69	0.31	1.54	16.95	13.74	11.25	8.80	8.08	5.55	10.81	9.47
SVC085	1	1.70	0.31	1.26	16.38	15.10	9.61	7.01	9.17	8.52	9.38	8.51
SVC112	1	2.81	0.30	1.99	16.31	15.26	13.96	13.34	9.27	7.35	10.21	8.13
CHOP081A	1	1.53	0.21	2.50	20.03	17.97	15.07	14.06	8.90	6.45	12.69	10.58
LB13_2	1	2.10	0.25	0.00	12.80	12.20	7.50	6.90	8.30	8.30	5.30	5.10
LB18_2	1	1.67	0.57	0.74	18.70	18.10	10.70	9.70	10.20	9.80	7.50	7.50
LB23_1	1	1.53	0.48	0.47	18.50	17.20	10.70	10.70	12.90	5.50	11.30	9.40
CHOP026A	2	2.08	0.38	1.50	19.98	18.73	13.80	11.76	9.38	4.47	9.25	7.75
CHOP016A	2	3.27	0.68	0.00	15.73	12.80	14.16	13.47	7.09	4.54	11.59	10.81
CHOP018A	2	2.63	0.77	0.00	17.72	16.71	12.28	11.66	11.60	8.72	10.09	8.60
CHOP024A	2	2.55	0.84	0.00	16.88	14.94	14.96	13.09	10.72	5.80	13.11	8.85
CHOP082A	2	2.44	0.64	0.03	19.86	19.05	15.68	14.92	14.96	10.41	11.83	11.79
CHOP088A	2	2.36	0.62	0.76	18.99	18.49	33.51	28.84	12.53	10.31	25.49	15.97
LB19_1	2	2.17	0.48	1.46	17.20	15.40	9.90	9.20	8.70	5.10	7.20	7.20
LB20_2	2	2.86	0.40	2.54	17.00	15.50	23.50	21.90	6.50	5.10	16.60	10.70
LB24_1	2	2.20	0.50	1.40	20.60	18.30	13.30	13.00	10.70	8.70	17.00	9.60
LB25_1	2	1.76	0.66	0.00	17.90	16.50	14.70	14.50	9.40	8.60	13.10	10.20
LB03_1	3	3.40	0.74	0.51	22.40	15.40	15.30	14.10	13.80	9.90	14.00	13.90
LB05_1	3	2.62	0.64	1.88	16.60	15.10	16.40	16.40	11.70	10.00	11.60	11.60
LB06_5	3	3.90	0.64	3.70	16.20	16.00	13.80	13.10	15.10	13.60	9.30	8.50
LB07_3	3	4.09	0.74	0.65	18.30	14.50	12.70	12.70	13.00	11.20	9.90	9.40
LB08_1	3	6.40	0.67	0.35	20.20	19.60	17.90	17.70	18.60	17.70	13.80	12.50
LB09_2	3	2.41	0.59	1.49	22.30	17.50	15.30	13.10	12.20	9.70	11.50	7.80
LB12_1	3	2.18	0.84	2.76	15.20	13.50	11.00	10.50	9.10	6.80	11.60	10.10
LB15_2	3	4.50	0.62	0.40	19.60	15.80	17.70	16.50	13.10	7.60	10.80	8.90
LB21_1	3	5.00	0.69	1.02	15.70	14.40	16.70	16.70	13.80	13.80	12.90	11.60
MRI1	3	2.70	0.41	0.60	11.29	10.23	9.33	8.07	10.43	8.21	8.56	7.05

PatientID	Comparison group	IVC stenosis 2	SVC stenosis 2	LPA stenosis 2	RPA stenosis 2	Overall PA stenosis 2
SVC043	1	16	17	44	9	28
SVC059	1	11	13	41	25	34
SVC063	1	30	10	21	13	17
SVC075	1	34	39	53	23	34
SVC085	1	15	47	14	18	16
SVC112	1	12	9	37	37	37
CHOP081A	1	20	13	48	30	36
LB13_2	1	9	17	0	8	2
LB18_2	1	6	17	9	0	5
LB23_1	1	13	0	82	31	60
CHOP026A	2	12	27	77	30	54
CHOP016A	2	34	9	59	13	26
CHOP018A	2	11	10	43	27	37
CHOP024A	2	22	23	71	55	61
CHOP082A	2	8	9	52	1	32
CHOP088A	2	5	26	32	61	55
LB19_1	2	20	14	65	0	38
LB20_2	2	17	13	38	58	37
LB24_1	2	21	4	33	68	39
LB25_1	2	16	3	16	40	23
LB03_1	3	53	14	49	1	25
LB05_1	3	17	0	27	0	14
LB06_5	3	3	9	20	16	19
LB07_3	3	37	0	25	10	20
LB08_1	3	6	2	10	18	12
LB09_2	3	39	27	37	54	45
LB12_1	3	21	8	43	24	32
LB15_2	3	35	14	67	32	53
LB21_1	3	16	0	0	20	9
MRI1	3	18	25	38	32	36

APPENDIX F – SPECIFIC AIM 2A CROSS-SECTIONAL PATIENT DATA

This appendix contains data for all patients included in the cross-sectional portion of Specific Aim 2A. This includes data from cardiac MRI, catheterization and anatomic and CFD analysis for 33 patients.

Patient ID	GT ID	siriusRED	morphology (1=HLHS, 2=other)	Fontan duration (yrs)	fenestration (1=yes, 2=no, 3=unknown)	Fontan year	Age (yrs)	Gender (1=Male)	Fontan Type (1=ECC, 2=LT, 3=other)
MRI1	CHOP_F1	17.34	2	12	2	2002	13	2	3
MRI3	CHOP_F3	20.28	1	9	1	2002	12	2	2
MRI4	CHOP_F4	19.13	1	13	1	1998	15	1	2
MRI5	CHOP_F5	20.00	1	5	2	2006	7	1	1
MRI6	CHOP_F6	22.93	2	22	2	1989	26	2	2
MRI7	CHOP_F7	9.36	1	10	3	2002	10	2	2
MRI11	CHOP_F11	36.55	2	14	1	1998	16	1	1
MRI12	CHOP_F12	18.52	2	18	2	1994	22	1	2
MRI14	CHOP_F14	14.04	2	24	2	1988	26	2	2
MRI15	CHOP_F15	18.22	2	17	3	1995	18	1	1
MRI16	CHOP_F16	14.28	2	15	2	1997	17	1	2
MRI17	CHOP_F17	20.14	1	16	1	1996	19	2	2
MRI18	CHOP_F18	49.43	2	17	2	1995	19	2	2
MRI19	CHOP_F19	12.65	1	17	1	1995	18	2	2
MRI20	CHOP_F20	14.92	2	14	3	1998	16	1	1
MRI22	CHOP_F22	22.32	1	20	2	1993	21	1	2
MRI25	CHOP_F25	19.74	2	15	3	1998	18	1	1
MRI27	CHOP_F27	12.09	2	9	2	2004	12	2	1
MRI28	CHOP_F28	12.59	2	11	2	2002	13	1	1
MRI29	CHOP_F29	13.51	1	18	1	1996	18	2	2
MRI31	CHOP_F31	18.25	1	10	1	2003	13	2	1
MRI32	CHOP_F32	22.62	1	18	2	1996	19	1	2
MRI33	CHOP_F33	17.14	2	19	2	1995	20	1	2
MRI34	CHOP_F34	25.69	2	7	2	2007	10	2	1
MRI35	CHOP_F35	18.97	2	15	1	1999	17	2	2
MRI36	CHOP_F36	36.24	2	18	2	1996	20	1	1
MRI39	CHOP_F39	37.78	1	10	2	2005	12	2	1
MRI41	CHOP_F41	32.88	1	11	1	2004	12	2	1
MRI42	CHOP_F42	20.00	1	9	1	2006	10	1	1
MRI44	CHOP_F44	16.38	2	11	3	2004	14	1	1
MRI45	CHOP_F45	26.35	1	12	1	2003	15	1	1
MRI46	CHOP_F46	19.05	1	21	1	1994	24	2	2
MRI47	CHOP_F47	24.24	2	11	1	2004	12	2	2

Patient ID	GT ID	BSA (m2)	Cardiac cycle (s)	TCPC_PL (mW)	TCPC_iPL	total_power (mW)	lowerBody_PL (mW)	Percent of total power lost Lower Body (%)	Percent power lost TCPC (%)	PRT (cardiac cycle)	PRT (s)
MRI1	CHOP_F1	1.09	0.738	9.871	0.1218	549	129	23.56	1.80	1.020	0.753
MRI3	CHOP_F3	0.758	0.719	10.010	0.0963	455	186	40.92	2.20	0.881	0.633
MRI4	CHOP_F4	1.515	0.77	34.000	0.4853	416	214	51.47	8.17	1.039	0.800
MRI5	CHOP_F5	1	0.69	11.903	0.1380	702	234	33.31	1.70	1.067	0.736
MRI6	CHOP_F6	1.58	0.819	4.378	0.0605	613	413	67.42	0.71	1.126	0.922
MRI7	CHOP_F7	0.993	0.565	1.166	0.0387	344	122	35.38	0.34	1.021	0.577
MRI11	CHOP_F11	1.82	0.799	7.428	0.0820	1317	486	36.90	0.56	0.991	0.792
MRI12	CHOP_F12	1.88	0.734	7.767	0.0631	891	414	46.48	0.87	1.200	0.881
MRI14	CHOP_F14	1.59	0.923	6.070	0.1050	633	377	59.49	0.96	0.811	0.749
MRI15	CHOP_F15	1.9	0.828	6.052	0.0317	839	354	42.15	0.72	0.401	0.332
MRI16	CHOP_F16	1.6	0.835	5.260	0.0398	1049	467	44.50	0.50	0.820	0.685
MRI17	CHOP_F17	1.3	0.75	3.119	0.0398	595	277	46.57	0.52	0.920	0.690
MRI18	CHOP_F18	1.66	1	16.1	0.1129	762	351	46.08	2.11	0.181	0.181
MRI19	CHOP_F19	1.28	0.702	8.041	0.1263	593	325	54.80	1.36	1.036	0.727
MRI20	CHOP_F20	2	1.244	22.6	0.3637	253	313	123.56	8.93	0.391	0.486
MRI22	CHOP_F22	1.78	0.951	14.696	0.1106	783	444	56.65	1.88	0.839	0.798
MRI25	CHOP_F25	1.57	1.035	9.917	0.1267	889	500	56.20	1.12	1.010	1.045
MRI27	CHOP_F27	1.19	1.04	10.6	0.0778	456	201	44.15	2.32	0.479	0.498
MRI28	CHOP_F28	1.32	0.905	13.856	0.1147	608	174	28.69	2.28	0.741	0.671
MRI29	CHOP_F29	1.53	1.054	1.28	0.0763	497	224	45.14	0.26	1.058	1.115
MRI31	CHOP_F31	1.35	0.709	6.519	0.0739	531	212	39.99	1.23	0.948	0.672
MRI32	CHOP_F32	2	0.963	39.99	0.0637	1109	875	78.87	3.61	1.020	0.982
MRI33	CHOP_F33	1.92	0.923	5.293	0.0852	735	410	55.76	0.72	0.810	0.748
MRI34	CHOP_F34	1.06	0.687	0.854	0.0579	343	129	37.74	0.25	0.867	0.596
MRI35	CHOP_F35	1.66	0.706	12.559	0.1189	688	445	64.70	1.83	0.971	0.686
MRI36	CHOP_F36	1.856	0.901	7.310	0.0563	782	273	34.97	0.93	0.291	0.262
MRI39	CHOP_F39	1.434	0.803	5.278	0.1415	613	288	46.95	0.86	0.839	0.674
MRI41	CHOP_F41	1.39	0.6	19.900	0.1321	709	317	44.71	2.81	1.246	0.748
MRI42	CHOP_F42	1.369	0.937	49.477	0.3730	784	272	34.70	6.31	0.561	0.526
MRI44	CHOP_F44	1.877	0.772	16.8	0.0909	814	511	62.79	2.06	0.583	0.450
MRI45	CHOP_F45	1.3	1.11	5.100	0.0410	727	318	43.72	0.70	0.661	0.734
MRI46	CHOP_F46	1.99	0.632	6.63	0.0722					1.031	0.651
MRI47	CHOP_F47	1.42	0.811	8.230	0.0860	546	277	50.71	1.51	1.018	0.825

Patient ID	GT ID	IVC Pressure	SVC Pressure	LPA Pressure	RPA Pressure	Dao Pressure _sys	Dao Pressure _dias	Dao Pressure _avg	Ventricle Pressure _sys	Ventricle Pressure dias
MRI1	CHOP_F1	16	16	16	16	67		67	101	8
MRI3	CHOP_F3	14	14	14	14	87	52	70	87	9
MRI4	CHOP_F4	12	12	11	11	80	59	69	80	6
MRI5	CHOP_F5	15	15	13	15	85	50	65	85	9
MRI6	CHOP_F6	14	12	12	12	105	65	80	105	7
MRI7	CHOP_F7	15	15	15	15	82	62	70	84	10
MRI11	CHOP_F11	13	13	13	11	121	50	80	120	9
MRI12	CHOP_F12	12	11	12	12	100	66	80	114	9
MRI14	CHOP_F14	9	9	9	9	105	60	78	104	10
MRI15	CHOP_F15	6	6	6	6	80	53	63	84	7
MRI16	CHOP_F16	13	13	13	9	95	50	65	95	8
MRI17	CHOP_F17	12	12	12	12	85	55	65	85	12
MRI18	CHOP_F18	9	8	7	8	100	60	70	100	4
MRI19	CHOP_F19	12	12	12	12	83	57	69	114	7
MRI20	CHOP_F20	14	14	14	13	94	60	73	100	9
MRI22	CHOP_F22	15	14	14	14	95	55	70	93	10
MRI25	CHOP_F25	16	16	15	15	125	80	95	130	12
MRI27	CHOP_F27	12	12	10	12	85	50	60	85	8
MRI28	CHOP_F28	10	10	10	10	75	50	60	82	7
MRI29	CHOP_F29	11	11		11	85	50	70	88	9
MRI31	CHOP_F31	14	13	13	12	70	44	55	75	9
MRI32	CHOP_F32	10	10	10	10	95	60	72	100	4
MRI33	CHOP_F33	12	12	12	12	110	70	85	110	10
MRI34	CHOP_F34	12	12	12	12	85	54	68	89	11
MRI35	CHOP_F35	8	8	8	8	92	57	70	90	6
MRI36	CHOP_F36	11	11	10	11	90	45	62	100	7
MRI39	CHOP_F39	10	11	10	10	81	55	67	85	7
MRI41	CHOP_F41	9	9	8	9	88	56	70	97	5
MRI42	CHOP_F42	13	13	12	13	91	57	70	92	6
MRI44	CHOP_F44	15	15	17	15	106	70	83	106	12
MRI45	CHOP_F45	15	15	14	14	95	51	67	95	14
MRI46	CHOP_F46	15	15	14	15					
MRI47	CHOP_F47	12	12	9	11	81	47	61	85	5

Patient ID	GT ID	TCPC Resistance (WU)	TCPC pressure drop (mmHg)	PVR (WU)	SVR (WU)	Indexed PVR	Indexed SVR	Total Resistance (WU)	Indexed Total Resistance	Ratio TCPC PVR resistance	Ratio TCPC SVR resistance	Ratio TCPC SVRPVR resistance
MRI1	CHOP_F1	0.611	1.647	1.64	17.44	1.50	16.00	19.69	18.06	0.37	0.04	0.03
MRI3	CHOP_F3	0.852	1.958	1.36	13.80	1.80	18.20	16.01	21.12	0.62	0.06	0.06
MRI4	CHOP_F4	1.494	4.781	1.06	27.27	0.70	18.00	29.82	19.69	1.41	0.05	0.05
MRI5	CHOP_F5	0.792	2.060	1.05	20.90	1.05	20.90	22.74	22.74	0.75	0.04	0.04
MRI6	CHOP_F6	0.178	0.592	2.37	33.02	1.50	20.90	35.57	22.51	0.08	0.01	0.01
MRI7	CHOP_F7	0.158	0.288	2.88	34.26	2.90	34.50	37.30	37.56	0.05	0.00	0.00
MRI11	CHOP_F11	0.215	0.848	1.46	44.41	0.80	24.40	46.08	25.32	0.15	0.00	0.00
MRI12	CHOP_F12	0.176	0.784	1.88	41.36	1.00	22.00	43.42	23.09	0.09	0.00	0.00
MRI14	CHOP_F14	0.284	0.881	1.50	40.70	0.94	25.60	42.49	26.72	0.19	0.01	0.01
MRI15	CHOP_F15	0.101	0.524	1.03	29.22	0.54	15.38	30.35	15.97	0.10	0.00	0.00
MRI16	CHOP_F16	0.141	0.577	1.92	24.80	1.20	15.50	26.86	16.79	0.07	0.01	0.01
MRI17	CHOP_F17	0.156	0.468	2.47	16.90	1.90	13.00	19.53	15.02	0.06	0.01	0.01
MRI18	CHOP_F18	0.390	1.681	2.54	33.20	1.53	20.00	36.13	21.76	0.15	0.01	0.01
MRI19	CHOP_F19	0.472	1.306	2.94	24.32	2.30	19.00	27.74	21.67	0.16	0.02	0.02
MRI20	CHOP_F20	0.743	2.749	3.40	23.50	1.70	11.75	27.64	13.82	0.22	0.03	0.03
MRI22	CHOP_F22	0.340	1.500	2.85	17.91	1.60	10.06	21.10	11.85	0.12	0.02	0.02
MRI25	CHOP_F25	0.386	1.313	2.04	52.91	1.30	33.70	55.34	35.25	0.19	0.01	0.01
MRI27	CHOP_F27	0.413	1.403	3.42	20.87	2.87	17.54	24.70	20.76	0.12	0.02	0.02
MRI28	CHOP_F28	0.509	1.781	2.11	20.57	1.60	15.58	23.19	17.57	0.24	0.02	0.02
MRI29	CHOP_F29	0.144	0.288	0.57	38.25	0.37	25.00	38.96	25.47	0.25	0.00	0.00
MRI31	CHOP_F31	0.286	0.917	1.35	18.90	1.00	14.00	20.54	15.21	0.21	0.02	0.01
MRI32	CHOP_F32	0.281	2.249	2.00	30.00	1.00	15.00	32.28	16.14	0.14	0.01	0.01
MRI33	CHOP_F33	0.184	0.662	1.73	57.60	0.90	30.00	59.51	31.00	0.11	0.00	0.00
MRI34	CHOP_F34	0.171	0.256	0.64	51.33	0.60	48.42	52.14	49.19	0.27	0.00	0.00
MRI35	CHOP_F35	0.372	1.449	2.49	38.18	1.50	23.00	41.04	24.72	0.15	0.01	0.01
MRI36	CHOP_F36	0.162	0.731	3.16	20.00	1.70	10.78	23.32	12.56	0.05	0.01	0.01
MRI39	CHOP_F39	0.380	0.950	2.01	34.42	1.40	24.00	36.80	25.67	0.19	0.01	0.01
MRI41	CHOP_F41	0.589	2.296	1.67	22.24	1.20	16.00	24.50	17.62	0.35	0.03	0.02
MRI42	CHOP_F42	1.626	6.017	1.51	22.70	1.10	16.58	25.83	18.87	1.08	0.07	0.07
MRI44	CHOP_F44	0.291	1.482	3.38	67.57	1.80	36.00	71.24	37.95	0.09	0.00	0.00
MRI45	CHOP_F45	0.187	0.656	1.17	22.10	0.90	17.00	23.46	18.04	0.16	0.01	0.01
MRI46	CHOP_F46	0.169	0.710	4.48		2.25		4.65	2.33	0.04	#DIV/0!	0.04
MRI47	CHOP_F47	0.320	1.089	1.85	22.35	1.30	15.74	24.52	17.27	0.17	0.01	0.01

Patient ID	GT ID	CO (L/min)	CI (L/min/m2)	Qs	Qp	Qp_Qs_ratio	Dao flow	IVC Flow	SVC Flow	LPA Flow	RPA Flow	RPV flow	LPV flow
MRI1	CHOP_F1	3.6	3.30	2.70	3.50	1.30	1.38	1.10	0.90	0.90	1.60	2.00	1.50
MRI3	CHOP_F3	3.42	4.51	2.30	2.45	0.80	1.43	1.15	1.15	0.65	1.09	1.19	1.26
MRI4	CHOP_F4	3.45	2.28	3.20	3.50	1.10	1.76	2.07	1.45	1.21	1.69	1.99	1.49
MRI5	CHOP_F5	5.4	5.40	2.60	5.40	1.90	1.90	1.20	1.70	0.63	2.40	3.10	2.30
MRI6	CHOP_F6	3.89	2.46	3.33	4.14	1.24	2.74	2.34	0.99	1.28	2.16	2.27	1.87
MRI7	CHOP_F7	2.66	2.68	1.82	2.05	1.12	1.02	1.10	0.72	0.32	0.70	1.14	0.82
MRI11	CHOP_F11	7.29	4.01	3.94	5.96	1.50	3.20	2.83	1.11	1.92	1.32	3.26	2.70
MRI12	CHOP_F12	5.18	2.76	4.46	5.18	1.16	2.73	2.63	1.13	1.72	2.83	2.82	2.36
MRI14	CHOP_F14	4	2.52	3.10	4.00	1.30	2.44	2.27	0.81	1.73	1.21	1.93	2.05
MRI15	CHOP_F15	6.6	3.47	5.20	5.00	0.96	2.80	2.81	2.30	2.10	2.20	2.50	2.50
MRI16	CHOP_F16	7.3	4.56	4.10	5.70	1.20	3.80	2.80	1.30	1.30	3.20	3.40	2.30
MRI17	CHOP_F17	4.5	3.46	3.00	3.30	1.10	2.20	1.50	0.79	1.00	1.10	1.70	1.60
MRI18	CHOP_F18	5.15	3.10	4.31	4.72	1.10	2.63	2.72	0.64	1.92	1.90	2.39	2.33
MRI19	CHOP_F19	3.48	2.72	2.77	2.78	1.00	2.45	1.87	0.90	0.99	1.44	1.64	1.14
MRI20	CHOP_F20	1.67	0.84	3.70	4.42	1.19	2.35	2.18	1.52	2.13	1.48	2.27	2.15
MRI22	CHOP_F22	5.5	3.09	4.41	4.91	1.10	3.48	2.90	1.51	1.41	3.23	3.14	1.77
MRI25	CHOP_F25	4.5	2.87	3.40	4.70	1.40	2.77	2.36	1.00	1.83	1.64	2.28	2.45
MRI27	CHOP_F27	3.53	2.97	3.40	3.50	1.03	1.87	0.74	0.43	2.00	1.20	1.22	2.30
MRI28	CHOP_F28	4.9	3.71	3.50	4.90	1.40	1.60	1.73	1.74	1.68	1.80	2.54	2.40
MRI29	CHOP_F29	3.7	2.42	2.00	3.50	1.80	1.65	1.30	0.71		2.00	2.30	2.40
MRI31	CHOP_F31	4.6	3.41	3.20	4.10	1.30	2.20	1.80	1.20	1.10	1.60	2.10	2.00
MRI32	CHOP_F32	7.5	3.75	8.00	7.00	0.88	6.20	5.18	1.50	2.80	4.20	4.00	3.00
MRI33	CHOP_F33	4.4	2.29	3.60	4.80	1.33	2.50	2.30	1.20	1.50	2.60	2.46	2.20
MRI34	CHOP_F34	2.5	2.36	1.50	3.10	2.10	1.00	0.80	0.71	0.90	1.20	1.50	1.60
MRI35	CHOP_F35	5.1	3.07	3.90	4.90	1.26	3.20	2.90	1.00	1.10	1.90	3.00	1.90
MRI36	CHOP_F36	5.2	2.80	4.50	5.70	1.33	2.54	3.10	0.40	1.60	2.70	3.40	2.30
MRI39	CHOP_F39	4.77	3.33	2.50	2.50	1.00	2.32	2.56	1.54	1.79	1.91	DNE	DNE
MRI41	CHOP_F41	4.91	3.53	3.90	2.90	0.74	2.30	2.00	1.28	1.00	1.26	DNE	DNE
MRI42	CHOP_F42	5.69	4.16	3.70	3.70	1.00	2.29	2.89	2.49	1.34	1.48	DNE	DNE
MRI44	CHOP_F44	5	2.66	5.10	5.10	1.00	3.23	0.74	0.90	1.70	2.67	3.30	1.80
MRI45	CHOP_F45	4.9	3.77	3.50	4.20	1.20	2.70	2.50	1.00	1.00	1.80	2.54	1.50
MRI46	CHOP_F46	6.4	3.22	4.20	6.60	1.57	2.90	2.70	1.50	1.70	2.30	3.50	3.10
MRI47	CHOP_F47	4.3	3.03	3.40	3.50	1.03	2.50	2.30	1.10	0.60	2.00	2.00	1.50

Patient ID	GT ID	IVC PI	IVC PI (%)	IVC flow max	EDV (mL)	Indexed _EDV	ESV (mL)	Indexed _ESV	Stroke_ Volume (mL)	Indexed _stroke_ volume	Ejection _Fraction (%)
MRI1	CHOP_F1	n/a	n/a	n/a	143.0	131.0	62.0	57.0	81.0	74.3	57.0
MRI3	CHOP_F3	0.83	82.70	2.22	94.9	125.3	43.8	57.8	51.1	67.4	53.8
MRI4	CHOP_F4	0.36	35.80	2.81	110.5	73.0	45.3	30.0	65.2	43.0	59.0
MRI5	CHOP_F5	0.57	56.58	1.69	102.0	102.0	40.0	40.0	62.0	62.0	61.0
MRI6	CHOP_F6	0.23	22.68	3.02	103.8	65.8	42.0	26.6	61.9	39.2	59.6
MRI7	CHOP_F7	0.32	32.41	1.34	123.4	124.3	76.2	76.8	47.2	47.5	38.0
MRI11	CHOP_F11	0.36	35.89	3.36	138.0	76.0	44.0	24.0	94.0	51.6	68.0
MRI12	CHOP_F12	0.35	34.50	4.26	116.4	61.9	51.1	27.2	65.3	34.7	56.1
MRI14	CHOP_F14	0.29	28.76	2.89	72.4	45.0	10.9	7.0	61.5	38.7	85.0
MRI15	CHOP_F15	0.38	38.04	3.69	180.0	94.7	90.0	47.4	90.0	47.4	50.0
MRI16	CHOP_F16	0.25	24.83	3.70	195.0	121.9	90.0	56.3	105.0	65.6	54.0
MRI17	CHOP_F17	0.63	62.57	3.14	121.0	93.1	59.0	45.4	62.0	47.7	51.0
MRI18	CHOP_F18	0.29	29.37	3.69	118.5	71.5	30.6	18.4	87.9	53.0	74.2
MRI19	CHOP_F19	0.29	29.43	2.82	218.5	171.2	159.3	124.8	59.2	46.3	27.1
MRI20	CHOP_F20	1.62	162.00	4.53	217.4	107.9	107.7	53.5	109.7	54.9	50.5
MRI22	CHOP_F22	0.31	31.42	3.91	323.0	181.0	218.0	122.0	105.0	59.0	33.0
MRI25	CHOP_F25	0.63	62.79	4.00	163.7	104.1	71.6	45.5	92.1	58.7	56.0
MRI27	CHOP_F27	1.29	129.29	1.70	122.0	102.6	43.3	36.4	78.7	66.1	64.5
MRI28	CHOP_F28	0.34	34.06	2.66	178.0	135.9	72.3	54.8	105.9	80.2	59.0
MRI29	CHOP_F29	0.45	44.62	1.97	119.0	77.6	44.1	28.7	75.0	49.0	63.0
MRI31	CHOP_F31	0.33	32.86	2.77	143.5	106.1	65.8	48.7	77.7	57.6	54.1
MRI32	CHOP_F32	0.25	25.17	6.22	253.0	126.7	80.1	40.1	173.0	86.5	68.4
MRI33	CHOP_F33	0.80	79.82	4.01	229.2	120.0	85.0	44.3	144.2	75.1	62.9
MRI34	CHOP_F34	1.18	117.68	1.94	138.5	130.6	62.0	58.4	76.5	72.2	5.3
MRI35	CHOP_F35	1.06	105.84	5.61	136.9	82.7	64.5	38.7	72.4	43.6	52.9
MRI36	CHOP_F36	0.24	24.27	4.52	301.0	162.0	190.0	102.0	111.0	59.8	36.0
MRI39	CHOP_F39	0.42	42.03	3.16							
MRI41	CHOP_F41	0.19	18.97	2.45							
MRI42	CHOP_F42	0.50	50.12	4.43							
MRI44	CHOP_F44	1.04	104.13	1.40	141.0	73.0	72.0	37.0	68.0	36.2	49.0
MRI45	CHOP_F45	0.36	36.43	2.94	159.1	123.7	65.9	51.3	93.1	71.6	58.5
MRI46	CHOP_F46	0.67	67.14	4.06	183.6	92.3	96.7	48.6	87.0	43.7	47.4
MRI47	CHOP_F47	0.33	33.01	2.92	129.2	91.1	58.8	41.5	70.4	49.6	55.0

Patient ID	GT ID	IVC_min_diameter	IVC_mean_diameter	IVC_max_diameter	SVC_min_diameter	SVC_mean_diameter	SVC_max_diameter	LPA_min_diameter	LPA_mean_diameter	LPA_max_diameter	RPA_min_diameter	RPA_mean_diameter	RPA_max_diameter
MRI1	CHOP_F1	10.234	11.294	12.454	8.0679	9.3338	10.387	8.2107	10.433	11.005	7.0476	8.5579	11.195
MRI3	CHOP_F3	10.526	16.197	20.767	10.569	11.557	12.616	3.5359	6.1029	12.983	7.1311	8.8451	13.051
MRI4	CHOP_F4	16.75	22.323	28.198	10.804	16.086	21.228	6.16	9.6431	20.15	6.4634	11.159	24.659
MRI5	CHOP_F5	13.957	15.388	20.336	13.515	14.226	14.801	2.7327	6.9594	14.757	9.8677	11.237	16.059
MRI6	CHOP_F6	12.093	17.639	28.101	12.67	14.382	15.921	9.7491	11.507	15.874	10.379	11.2	12.71
MRI7	CHOP_F7	14.626	15.811	17.329	14.012	16.938	18.378	7.4159	9.0659	14.359	7.6309	10.357	17.176
MRI11	CHOP_F11	13.636	16.293	25.111	11.434	12.072	13.222	9.3518	11.93	16.336	6.1145	8.6935	10.728
MRI12	CHOP_F12	18.085	23.056	29.664	9.7089	12.874	17.992	8.4707	12.45	19.819	10.978	12.142	17.353
MRI14	CHOP_F14	12.484	19.016	24.123	9.5095	12.872	16.311	10.262	12.347	19.531	6.9181	10.275	17.167
MRI15	CHOP_F15	17.816	21.241	24.958	17.045	18.06	20.837	13.63	15.656	21.3	10.412	12.778	21.816
MRI16	CHOP_F16	17.119	21.564	25.719	11.062	15.827	21.714	6.832	10.765	21.007	10.634	13.547	22.034
MRI17	CHOP_F17	16.092	20.19	26.029	10.336	11.578	14.546	7.3168	9.9328	16.02	8.9745	8.9754	8.9764
MRI18	CHOP_F18	9.7259	12.299	17.612	7.8906	10.199	13.131	7.9052	10.257	17.986	9.708	10.865	13.672
MRI19	CHOP_F19	11.078	15.29	18.293	13.997	16.06	19.045	5.3736	9.3465	19.197	6.796	9.0922	16.531
MRI20	CHOP_F20	11.863	16.2	23.49	14.137	17.22	20.243	10.103	13.916	19.679	9.4821	10.654	15.712
MRI22	CHOP_F22	15.991	19.915	24.981	14.683	17.71	20.751	5.2454	11.304	19.567	9.108	12.86	21.353
MRI25	CHOP_F25	12.99	15.966	19.779	12.654	13.377	13.952	7.6445	10.216	14.711	7.8838	9.3486	13.388
MRI27	CHOP_F27	8.3227	9.2007	10.247	6.886	7.9817	10.38	7.1152	10.081	14.016	6.1329	6.9318	9.0883
MRI28	CHOP_F28	11.108	12.266	14.822	13.215	13.432	13.589	6.6371	9.2507	13.578	7.9534	9.1815	11.204
MRI29	CHOP_F29	16.464	21.339	25.972	11.17	14.76	21.103	6.2404	11.596	23.682	9.7603	12.298	21.528
MRI31	CHOP_F31	12.749	15.502	22.106	13.989	14.627	14.984	7.6389	9.0512	14.208	7.1974	8.6964	14.477
MRI32	CHOP_F32	18.073	21.138	28.438	12.933	15.518	19.602	9.482	13.393	21.423	9.062	12.725	20.82
MRI33	CHOP_F33	13.828	20.352	26.401	13.233	17.364	23.423	11.01	16.167	26.261	11.738	14.364	22.412
MRI34	CHOP_F34	9.5052	13.376	18.628	9.1758	12.147	14.961	8.5203	9.7862	13.649	14.409	14.999	16.455
MRI35	CHOP_F35	20.954	23.399	29.409	9.646	13.47	18.87	4.7253	11.425	19.011	7.4309	10.204	20.216
MRI36	CHOP_F36	12.308	14.105	16.456	9.02	10.862	15.095	6.4009	8.8266	12.653	10.224	11.91	15.081
MRI39	CHOP_F39	14.724	16.299	21.933	10.704	11.922	14.219	8.3787	11.638	14.668	11.042	12.63	14.116
MRI41	CHOP_F41	12.303	14.533	21.728	9.1237	10.575	12.45	3.9056	7.5102	13.835	6.4391	8.2256	13.072
MRI42	CHOP_F42	12.851	13.534	14.639	13.108	14.876	17.1	5.2656	10.517	15.683	10.036	12.807	18.23
MRI44	CHOP_F44	10.521	12.089	12.866	9.9523	13.177	16.056	9.2595	10.453	12.188	6.5432	7.3948	11.284
MRI45	CHOP_F45	11.373	14.04	16.82	9.1784	13.763	16.929	5.2331	9.5578	16.758	9.4899	11.396	16.127
MRI46	CHOP_F46	19.018	23.377	28.313	12.984	14.501	17.108	9.699	12.087	19.253	13.223	15.28	20.28
MRI47	CHOP_F47	13.824	17.454	20.96	13.371	14.304	16.124	4.553	7.2064	15.877	6.9928	9.4523	17.558

Patient ID	GT ID	IVC Stenosis	SVC stenosis	LPA Stenosis	RPA Stenosis	Overall PA Stenosis	IVC_area (cm2)	Congestion index	smallest IVC area (cm2)	Collateral flow	Collateral flow (% of AO)
MRI1	CHOP_F1	17.8902	25.2856	38.0642	32.1815	35.6981	1.23		1.009951154	0.8	24.9
MRI3	CHOP_F3	57.7665	16.367	66.4318	35.0009	45.1381	2.54	0.00291	1.072732118	0.915	27
MRI4	CHOP_F4	43.6979	54.89	59.1936	66.4516	63.3487	6	0.01279	3.378125303	0.45	13.5
MRI5	CHOP_F5	17.7341	9.74599	84.5816	22.8864	39.9902	3.7	0.0081	3.043837938	2.45	47
MRI6	CHOP_F6	52.9976	22.3905	28.2198	14.1234	21.3621	6.98	0.01614	3.280768662	0.6305	16.5
MRI7	CHOP_F7	14.4278	31.5654	33.0877	45.7145	40.2368	3.04	0.0069	2.601393462	1.194	31.5
MRI11	CHOP_F11	29.9558	10.2906	38.5517	50.5311	42.7066	6.4	0.01218	4.482825607	2.995	41.5
MRI12	CHOP_F12	38.4725	43.1261	53.7086	18.2541	36.4253	10.36	0.02518	6.374246507	0.68	13
MRI14	CHOP_F14	56.9008	45.4213	30.9218	54.6675	40.6378	4.6	0.00733	1.98256308	1.03	26
MRI15	CHOP_F15	29.649	10.9244	24.2068	33.6039	27.9639	6.23	0.01051	4.382869471	1.05	17.5
MRI16	CHOP_F16	36.9771	51.1494	59.722	38.3821	46.6417	5.17	0.00722	3.258282086	2.2	30
MRI17	CHOP_F17	36.4746	20.3037	45.7376	0.02005	25.1878	5.04	0.00809	3.201680172	1.25	27.5
MRI18	CHOP_F18	37.4655	40.1444	40.6002	20.1638	29.7942	1.12	0.00034	0.700386908	0.841	16.3
MRI19	CHOP_F19	47.5062	24.0411	66.9453	44.1313	55.8529	2.61	0.00241	1.370087355	0.53	15.17
MRI20	CHOP_F20	46.376	32.6018	47.2926	20.7893	37.4987	5.56	0.00682	2.981493201	0.69	41.32
MRI22	CHOP_F22	35.5251	31.2627	78.4676	49.8392	62.3175	7.21	0.01329	4.648639732	0.46	8.27
MRI25	CHOP_F25	33.8049	10.5175	44.0067	28.8822	37.1137	3.92	0.00384	2.594849173	1.20	26.73
MRI27	CHOP_F27	18.1749	25.5708	50.1842	21.722	41.0471	1.27	0.00095	1.039179238	0.10	2.83
MRI28	CHOP_F28	17.9902	3.20499	48.5237	24.9625	36.8315	3.61	0.00489	2.960554248	1.45	29.49
MRI29	CHOP_F29	40.4718	42.7291	71.0393	37.0121	53.0269	5.46	0.01513	3.250238503	1.60	43.11
MRI31	CHOP_F31	32.3642	8.53334	28.7722	31.5029	30.083	5.61	0.01137	3.794369655	1.50	32.61
MRI32	CHOP_F32	26.8974	30.5412	49.8762	49.2855	49.5959	7.02	0.00792	5.131801179	0.00	0.00
MRI33	CHOP_F33	53.8359	41.9213	53.6216	33.2214	44.622	6.83	0.01162	3.153009342	0.80	12.50
MRI34	CHOP_F34	49.5025	42.9376	24.1978	7.71246	12.6348	3.17	0.00518	1.600771195	1.00	39.80
MRI35	CHOP_F35	19.8065	48.7187	82.8941	46.9675	66.9525	10.15	0.01835	8.139642422	1.20	23.53
MRI36	CHOP_F36	23.8572	31.0406	47.411	26.3084	33.7897	2.51	0.00139	1.911184065	1.05	20.19
MRI39	CHOP_F39	18.3926	19.3891	48.1682	23.5656	34.8629	5.87	0.01092	4.790356107	0.67	14.05
MRI41	CHOP_F41	28.3343	25.5643	72.9559	38.7205	54.285	4.79	0.00935	3.432788245	1.63	33.20
MRI42	CHOP_F42	9.83842	22.3573	74.9324	38.5918	53.2282	1.94	0.00085	1.749134608	0.31	5.45
MRI44	CHOP_F44	24.2586	42.9555	21.5319	21.7062	21.59	1.31	0.00122	0.992212243	0.00	0.00
MRI45	CHOP_F45	34.3831	55.5258	70.022	30.6545	46.9111	3.76	0.00481	2.467196315	1.32	26.94
MRI46	CHOP_F46	33.8161	19.8283	35.6102	25.1118	29.1526	7.96	0.0156	5.268235739	2.55	39.84
MRI47	CHOP_F47	37.2697	12.6199	60.0829	45.2698	50.7149	4.52	0.007	2.83541049	0.90	20.93

APPENDIX G – SPECIFIC AIM 2A SERIAL STUDY PATIENT DATA

This appendix contains data for all patients included in the longitudinal portion of Specific Aim 2A. This includes 21 unique patients. Of these 21, six have multiple CMR data sets. The scans are numbered chronologically such as "LB06_1" and "LB06_2." This indicates that patient "LB06" had two scans. The earliest CMR scan was used to investigate correlations between flow rates, ventricular function and other metrics with collagen deposition.

In addition, 11 patients overlapped between the two studies in Specific Aim 1A. This allowed an investigation of how fluid mechanics and anatomic metrics changed from a time point ~ 7 years prior to biopsy to the time of biopsy. The naming key for these overlapping patients is given below.

Overlapping Patients	
Concurrent study ID	**Serial study ID**
MRI6	LB03_1
MRI11	LB06_1
MRI14	LB07_2
MRI15	LB08_1
MRI17	LB09_2
MRI18	LB10_1
MRI27	LB13_2
MRI32	LB16_1
MRI39	LB18_2
MRI41	LB19_1
MRI5	LB20_2

Patient ID/ GT ID	SiriusRed	Gender (1=male)	morphology (1=HLHS, 2=other)	Age at MRI (yrs)	Liver Biopsy Date	MRI scan date	Time between MRI biopsy (yrs)	Age at biopsy (yrs)	Fontan urgery date
LB03_1	22.9	2	1	20	41177	38589	7.09	27.09	32735
LB04_1	19	2	1	11	41010	39338	4.58	15.58	35908
LB05_1	41.8	2	1	14	40722	38567	5.9	19.9	34087
LB06_1	36.6	1	2	10	41184	38433	7.54	17.54	35817
LB06_2	36.6	1	2	11	41184	38755	6.65	17.65	35818
LB06_3	36.6	1	2	12	41184	39415	4.85	16.85	35819
LB06_4	36.6	1	2	13	41184	40056	3.09	16.09	35820
LB06_5	36.6	1	2	14	41184	40435	2.05	16.05	35821
LB07_2	14	2	2	23	41225	40305	2.52	25.52	35916
LB07_3	14	2	2	24	41225	40655	1.56	25.56	36281
LB08_1	18.2	1	2	16	41229	40672	1.53	17.53	34984
LB09_2	20.1	2	1	15	41246	39464	4.88	19.88	35172
LB10_1	49	2	2	9	41262	37873	9.28	18.28	34950
LB12_1	34.6	2	1	17	41415	40779	1.74	18.74	34821
LB13_2	12.1	2	2	3	41477	38282	8.75	11.75	38279
LB15_1	8.7	2	1	11	41604	37845	10.3	21.3	34339
LB15_2	8.7	2	1	15	41604	39259	6.42	21.42	34340
LB16_1	22.6	1	2	9	41649	37802	10.54	19.54	35241
LB17_2	46	2	1	22	42093	39469	7.19	29.19	31856
LB17_4	46	2	1	26	42093	41106	2.7	28.7	31857
LB18_2	37.8	2	1	3	42144	38666	9.53	12.53	38470
LB19_1	32.9	2	1	6	42184	39660	6.92	12.92	38072
LB20_2	20	1	1	7	42181	40868	3.6	10.6	38966
LB21_1	14.4	1	2	15	42429	40602	5.01	20.01	35816
LB21_2	14.4	1	2	17	42429	41502	2.54	19.54	35817
LB22_1	30	1	1	12	42514	39476	8.32	20.32	35922
LB23_1	22	2	1	5	42545	38470	11.16	16.16	37686
LB24_1	7	1	1	9	42548	40764	4.89	13.89	38630
LB25_1	22	1	1	6	42681	39119	9.76	15.76	37711
LB25_2	22	1	1	10	42681	40898	4.88	14.88	37712

Patient ID/ GT ID	Fontan duration at MRI (yrs)	Fontan duration biopsy (yrs)	BSA (m2)	Power loss (mW)	iPL	TCPC Resistance (WU)	TCPC Pressure drop (mmHg)	CO	CI
LB03_1	16.04	23.13	1.53	1.62748	0.01985	0.06356	0.21575	3.90	2.55
LB04_1	9.4	13.98	0.98	3.18452	0.1068	0.44212	0.79597	1.90	1.94
LB05_1	12.27	18.18	1.29	5.2286	0.03858	0.18339	0.65688	4.50	3.49
LB06_1	7.17	14.7	1.21	3.57222	0.03142	0.15342	0.49662	-	-
LB06_2	8.05	14.7	1.1	13.2176	0.09531	0.56461	1.83255	6.00	5.45
LB06_3	9.85	14.7	0.88	8.53003	0.03582	0.34214	1.14599	5.80	6.59
LB06_4	11.61	14.7	1.41	21.7465	0.10603	0.51393	2.24261	7.10	5.04
LB06_5	12.64	14.69	1.6	5.2695	0.05476	0.17426	0.64283	7.60	4.75
LB07_2	12.02	14.55	1.48	1.32243	0.02409	0.07055	0.20489	4.10	2.77
LB07_3	11.98	13.55	1.57	6.91411	0.05709	0.20115	0.7911	4.74	3.02
LB08_1	15.58	17.11	1.96	7.03389	0.02384	0.08408	0.51588	6.75	3.44
LB09_2	11.76	16.64	1.02	2.08092	0.03167	0.16174	0.38917	3.90	3.82
LB10_1	8.01	17.29	1.1	2.30405	0.03206	0.15256	0.39771	3.05	2.77
LB12_1	16.32	18.07	1.48	2.58194	0.11048	0.24337	0.53176	4.94	3.34
LB13_2	0.01	8.76	0.62	3.40141	0.03104	0.36514	0.74759	2.10	3.39
LB15_1	9.61	19.9	1.23	5.39196	0.06904	0.291	0.84028	5.30	4.31
LB15_2	13.48	19.9	1.63	7.87366	0.06475	0.21732	0.8775	4.90	3.01
LB16_1	7.02	17.56	1.04	0.9874	0.02209	0.0967	0.20728	3.70	3.56
LB17_2	20.86	28.05	1.4	8.46206	0.06214	0.26526	1.00503	4.60	3.29
LB17_4	25.34	28.04	1.44	10.3019	0.07131	0.29902	1.17738	4.60	3.19
LB18_2	0.54	10.07	0.58	1.04476	0.01552	0.16959	0.28237	2.40	4.14
LB19_1	4.35	11.27	0.8	1.40089	0.04032	0.23022	0.38096	3.63	4.53
LB20_2	5.21	8.81	1	4.45902	0.03738	0.23913	0.69269	5.39	5.39
LB21_1	13.11	18.12	1.68	9.05774	0.03567	0.14698	0.77401	6.02	3.58
LB21_2	15.58	18.12	1.9	7.19642	0.0455	0.13588	0.66334	5.80	3.05
LB22_1	9.74	18.06	1.1	1.24286	0.02064	0.09257	0.22754	3.60	3.27
LB23_1	2.15	13.31	0.66	1.11194	0.0278	0.21498	0.32798	2.00	3.03
LB24_1	5.85	10.73	1	1.53286	0.0264	0.13286	0.30273	3.60	3.60
LB25_1	3.86	13.62	0.63	1.06267	0.00973	0.11194	0.23136	1.76	2.79
LB25_2	8.73	13.61	1.03	0.61721	0.01637	0.06856	0.138	2.70	2.62

Patient ID/ GT ID	IVC flow	IVC Flow (% of CO)	IVC Flow (% of VC)	SVC flow	LPA flow	RPA flow	PFD	Collateral flow	IVC PI (%)
LB03_1	2.52	65	74	0.878	1.43	1.785	0.44479	0.505	19
LB04_1	1.20	63	60	0.8	0.9	1.1	0.45	0	146
LB05_1	1.68	37	64	0.939	1.4	2.2	0.38889	1.88	89
LB06_1	1.83	-	57	1.403	1.217	2.019	0.37608		11
LB06_2	2.00	33	61	1.3	1.5	1	0.6	2.7	28
LB06_3	1.90	33	58	1.4	1.5	0.8	0.65217	2.5	15
LB06_4	2.70	38	68	1.3	1.7	1.4	0.54839	3.1	14
LB06_5	2.50	33	64	1.4	1.7	1.3	0.56667	3.7	27
LB07_2	2.00	49	71	0.83	1.5	1.1	0.57692	1.27	17
LB07_3	3.04	64	74	1.05	1.83	1.78	0.50693	0.65	21
LB08_1	4.30	64	67	2.1	3.09	3.29	0.48433	0.35	31
LB09_2	1.43	37	59	0.981	1.088	0.745	0.59356	1.493	64
LB10_1	1.48	48	72	0.57	1.39	0.6	0.69849	0.442	10
LB12_1	1.84	37	84	0.34	0.6976	1.4824	0.32	2.757	15
LB13_2	0.53	25	41	0.75	1.701	0.399	0.81	0	93
LB15_1	2.01	38	70	0.878	0.856	1.497	0.36379	2.412	8
LB15_2	2.77	57	62	1.7	1.4	3.4	0.29167	0.4	13
LB16_1	1.29	35	60	0.858	1.058	0.809	0.56668	1.557	43
LB17_2	3.10	67	82	0.7	1.2	1.5	0.44444	0.8	130
LB17_4	3.10	67	82	0.7	1.3	1.5	0.46429	0.8	134
LB18_2	0.94	39	57	0.724	0.755	0.644	0.53967	0.735	51
LB19_1	1.05	29	60	0.689	0.531	0.906	0.36952	1.456	110
LB20_2	1.16	21	40	1.7	0.63	2.4	0.20792	2.536	44
LB21_1	3.46	57	79	0.933	2.79	2.47	0.53042	1.017	8
LB21_2	4.00	69	80	1	2.9	2.1	0.58	0.65	15
LB22_1	1.76	49	71	0.71	0.897	1.019	0.46816	1.135	31
LB23_1	0.74	37	48	0.791	0.583	0.918	0.38841	0.474	62
LB24_1	1.10	31	50	1.1	1	1.1	0.47619	1.4	89
LB25_1	1.17	66	57	0.894	0.612	0.666	0.47887	0	19
LB25_2	1.70	63	63	1	0.8	1.1	0.42105	0	156

Patient ID/ GT ID	Ejection fraction (%)	EDV (mL)	ESV (mL)	Stroke volume (mL)	IVC_d_ avg	IVC_d_ min	SVC_d_ avg	SVC_d_ min	LPA_d_ avg	LPA_d_ min
LB03_1					22.4	15.4	15.3	14.1	13.8	9.9
LB04_1	62	97	37	60	16.4	15.3	21.4	21.2	9.2	7.9
LB05_1	60	139	56	84	16.6	15.1	16.4	16.4	11.7	10
LB06_1					16.9	16.2	13.1	13.1	13.9	10.9
LB06_2	53	104	50	55	16.3	15.6	13.6	13.4	12.8	7.3
LB06_3	66.2	86.8	29.3	57.4	17.5	15.5	12.9	12.8	12.3	8.4
LB06_4	59	114	47	67	16.6	15.6	12.4	12.3	11.8	6.6
LB06_5	64	123	44	79	16.2	16	13.8	13.1	15.1	13.6
LB07_2	72	89	25	64	18.1	14.2	12.8	12.8	15.6	15.4
LB07_3	71.7	110.4	31.2	79.2	18.3	14.5	12.7	12.7	13	11.2
LB08_1	62.5	127.3	47.7	79.5	20.2	19.6	17.9	17.7	18.6	17.7
LB09_2				46	22.3	17.5	15.3	13.1	12.2	9.7
LB10_1					14.6	12.8	10.7	9.5	8.8	8.8
LB12_1					15.2	13.5	11	10.5	9.1	6.8
LB13_2	56	42.7	18.7	24	12.8	12.2	7.5	6.9	8.3	8.3
LB15_1					17.5	15.1	13.6	13.3	12.5	4.5
LB15_2	61	128	50	78	19.6	15.8	17.7	16.5	13.1	7.6
LB16_1					19.8	16.7	12.5	12.5	11.7	9.4
LB17_2				59						
LB17_4	74	77.2	20	57.3						
LB18_2				24	18.7	18.1	10.7	9.7	10.2	9.8
LB19_1	56	46	20	26	17.2	15.4	9.9	9.2	8.7	5.1
LB20_2					17	15.5	23.5	21.9	6.5	5.1
LB21_1	70	71.6	21.4	50.2	15.7	14.4	16.7	16.7	13.8	13.8
LB21_2	58	144.9	60.8	84.1	18	16.1	22.7	22.3	13.1	12.4
LB22_1				64	26	22.2	19.6	13.3	9.9	7.4
LB23_1				24	18.5	17.2	10.7	10.7	12.9	5.5
LB24_1	57	80.3	35	45.3	20.6	18.3	13.3	13	10.7	8.7
LB25_1					17.9	16.5	14.7	14.5	9.4	8.6
LB25_2	65	99	35	64	17.2	16.4	14.8	14.6	10.6	10

Patient ID/ GT ID	RPA_d_ avg	RPA_d_ min	IVC stenosis (%)	SVC stenosis (%)	LPA stenosis (%)	RPA stenosis (%)	Overall PA stenosis (%)	Smallest IVC area (cm2)
LB03_1	14	13.9	53	14.3	49.1	0.9	24.78	1.86
LB04_1	13.7	5.5	13.5	1.3	25.6	83.7	65.7	1.83
LB05_1	11.6	11.6	17.1	0	27.2	0	13.71	1.79
LB06_1	7	7	7.5	0.9	38.2	0	30.43	2.07
LB06_2	5.8	5.2	7.5	2	67.5	17.3	59.02	1.92
LB06_3	5.1	4.7	21.6	1.9	52.7	17.6	47.45	1.89
LB06_4	7	6.5	11.3	2.3	69.2	14.3	55.07	1.91
LB06_5	9.3	8.5	2.5	9.4	19.9	16.2	18.87	2.01
LB07_2	10.7	10.7	38.9	0	2.4	0	1.64	1.58
LB07_3	9.9	9.4	37.2	0	25.2	9.9	19.58	1.64
LB08_1	13.8	12.5	5.8	2.1	9.5	17.5	12.31	3.01
LB09_2	11.5	7.8	38.7	27.4	37.3	54	45.15	2.4
LB10_1	12.9	10.1	22.3	20.6	0	38.7	26.45	1.29
LB12_1	11.6	10.1	20.7	7.5	43.4	24.4	31.62	1.44
LB13_2	5.3	5.1	8.8	17.4	0	8.1	2.36	1.18
LB15_1	10	10	25.2	3.4	87.3	0	53.18	1.79
LB15_2	10.8	8.9	34.9	13.6	66.7	31.9	52.56	1.96
LB16_1	23.3	13.5	28.7	0	35.5	66.4	60.2	2.19
LB17_2								
LB17_4								
LB18_2	7.5	7.5	5.5	16.9	9	0	5.86	2.58
LB19_1	7.2	7.2	20.3	14.1	64.9	0	38.46	1.86
LB20_2	16.6	10.7	17	12.9	37.6	58	37.02	1.87
LB21_1	12.9	11.6	16.2	0	0	19.5	9.11	1.63
LB21_2	13.9	12.7	19.8	3.5	10.1	16.5	16.47	2.04
LB22_1	11.3	11.3	27.2	54.1	43.8	0	18.97	3.86
LB23_1	11.3	9.4	13	0	81.9	31.1	34.64	2.34
LB24_1	17	9.6	21.1	4.3	33.3	67.7	39.03	2.63
LB25_1	13.1	10.2	15.5	3	16.4	39.5	22.69	2.13
LB25_2	10.8	10.8	9.3	3.5	10.5	0	5.14	2.11

Data used to make Figure 7-7:

Patient_ID	SiriusRed	Time_between_MRIs	Time_between_MRI_biopsy	IVC_flow	IVC_flow_ind
LB03_1	22.9	20	7.09	2.517	1.65
LB03_overlap	22.9	26		2.34	1.481012658
LB03_change	22.9	6		-0.177	-0.168987342
LB06_1	36.6	10	7.54	1.833	1.51
LB06_overlap	36.6	16		2.83	1.554945055
LB06_change	36.6	6		0.997	0.044945055
LB07_2	14	14	2.52	2	1.35
LB07_overlap	14	26		2.27	1.427672956
LB07_change		12		0.27	0.077672956
LB08_1	18.2	16	1.53	3.5	1.785714286
LB08_overlap	18.2	18		2.64	1.478947368
LB08_change		2		-0.86	-0.306766917
LB09_2	20.1	15	4.88	1.426	1.4
LB09_overlap	20.1	19		1.5	1.153846154
LB09_change		4		0.074	-0.246153846
LB10_1	49	9	9.28	1.478	1.34
LB10_overlap	49	19		2.72	1.638554217
LB10_change		10		1.242	0.298554217
LB13_2	12.1	3	8.75	0.53	0.85
LB13_overlap	12	12		0.74	0.621848739
LB13_change		9		0.21	-0.228151261
LB16_1		9	10.54	1.285	1.24
LB16_overlap	22.6	19			2.59
LB16_change		10		-1.285	1.35
LB18_2	37.8	3	9.53	0.941	1.62
LB18_overlap	37.8	12		2.56	1.785216179
LB18_change		9		1.619	0.165216179
LB19_1	32.9	6	6.92	1.05	1.31
LB19_overlap	32.9	12		2	1.438848921
LB19_change		6		0.95	0.128848921

APPENDIX H – VIDEOS

See separate PDF file.

REFERENCES

1. Rosano A, Botto LD, Botting B, Mastroiacovo P, Germany W. Infant mortality and congenital anomalies from 1950 to 1994 : an international perspective L D Botto O Y ce For National. *J Epidemiol Community Health*. 2000;54(9):660-666. doi:10.1136/jech.54.9.660.

2. Hoffman JIE. The global burden of congenital heart disease : review article. *Cardiovasc J Afr*. 2013;24(4):141-145. doi:10.5830/CVJA-2013-028.

3. Norwood WI, Lang P, Casteneda AR, Campbell DN. Experience with operations for hypoplastic left heart syndrome. *J Thorac Cardiovasc Surg*. 1981;82(4):511—519. http://europepmc.org/abstract/MED/6168869.

4. Sano S, Ishino K, Kado H, et al. Outcome of Right Ventricle-to-Pulmonary Artery Shunt in First-Stage Palliation of Hypoplastic Left Heart Syndrome: A Multi-Institutional Study. *Ann Thorac Surg*. 2018;78(6):1951-1958. doi:10.1016/j.athoracsur.2004.05.055.

5. Fontan F, Baudet E. Surgical repair of tricuspid atresia. *Thorax*. 1971;26(3):240-248. doi:10.1136/thx.26.3.240.

6. Holder TM. An operation for the correction of tricuspid atresia. *J Pediatr Surg*. 2018;9(2):261. doi:10.1016/S0022-3468(74)80150-8.

7. De Leval, M. R., Kilner, P., Gewillig, M., & Bull C. Total cavopulmonary connection: a logical alternative to atriopulmonary connection for complex Fontan operations. Experimental studies and early clinical experience. *J Thorac Cardiovasc Surg*. 1988;96(5):682.

8. Gentles TL, Gauvreau K, Mayer J, et al. Functional outcome after the Fontan operation: Factors influencing late morbidity. *J Thorac Cardiovasc Surg*. 1997;114(3):392-405. doi:10.1016/S0022-5223(97)70184-3.

9. Dobell ARC, Trusler G a., Smallhorn JF, Williams WG. Atrial Thrombi after the Fontan Operation. *Ann Thorac Surg*. 1986;42(6):664-667. doi:10.1016/S0003-4975(10)64602-4.

10. Kanter KR, Haggerty CM, Restrepo M, et al. Preliminary clinical experience with a bifurcated Y-graft Fontan procedure - A feasibility study. *J Thorac Cardiovasc Surg*. 2012;144(2):383-389. doi:10.1016/j.jtcvs.2012.05.015.

11. Trusty PM, Slesnick TC, Wei ZA, et al. Fontan Surgical Planning: Previous Accomplishments, Current Challenges, and Future Directions. *J Cardiovasc Transl Res*. 2018:1-12. doi:10.1007/s12265-018-9786-0.

12. Pundi KN, Johnson JN, Dearani J a., et al. 40-Year Follow-Up after the Fontan Operation Long-Term Outcomes of 1,052 Patients. *J Am Coll Cardiol*. 2015;66(15):1700-1710. doi:10.1016/j.jacc.2015.07.065.

13. Srivastava D, Preminger T, Lock JE, et al. Hepatic Venous Blood and the Development of Pulmonary Arteriovenous Malformations in Congenital Heart Disease. *Circulation*. 1995;92(5):1217 LP - 1222. http://circ.ahajournals.org/content/92/5/1217.abstract.

14. Shinohara T, Yokoyama T. Pulmonary Arteriovenous Malformation in Patients with Total Cavopulmonary Shunt: What Role Does Lack of Hepatic Venous Blood Flow to the Lungs Play? *Pediatr Cardiol*. 2001;22(4):343-346. doi:10.1007/s002460010243.

15. Rychik J, Veldtman G, Rand E, et al. The precarious state of the liver after a fontan operation: Summary of a multidisciplinary symposium. *Pediatr Cardiol*. 2012;33(7):1001-1012. doi:10.1007/s00246-012-0315-7.

16. Rychik J, Goldberg D, Rand E, et al. End-organ consequences of the Fontan operation: liver fibrosis, protein-losing enteropathy and plastic bronchitis. *CardiolYoung*. 2013;23(May):831-840. doi:10.1017/S1047951113001650.

17. Rychik J. The Relentless Effects of the Fontan Paradox. *Semin Thorac Cardiovasc Surg Pediatr Card Surg Annu*. 2016;19(1):37-43. doi:10.1053/j.pcsu.2015.11.006.

18. Bernstein HS, Brook MM, Silverman NH, Bristow J. Development of Pulmonary Arteriovenous Fistulae in Children After Cavopulmonary Shunt. *Circulation*. 1995;92(9):309 LP - 314. http://circ.ahajournals.org/content/92/9/309.abstract.

19. Khairy P, Fernandes SM, Mayer JE, et al. Long-term survival, modes of death, and predictors of mortality in patients with Fontan surgery. *Circulation*. 2008;117(1):85-92. doi:10.1161/CIRCULATIONAHA.107.738559.

20. Ohuchi H, Negishi J, Noritake K, et al. Prognostic value of exercise variables in 335 patients after the fontan operation: A 23-year single-center experience of cardiopulmonary exercise testing. *Congenit Heart Dis*. 2015;10(2):105-116. doi:10.1111/chd.12222.

21. Veldtman GR, Opotowsky AR, Wittekind SG, et al. Cardiovascular adaptation to the Fontan circulation. *Congenit Heart Dis*. 2017;12(6):699-710. doi:10.1111/chd.12526.

22. Gewillig M, Brown SC. The Fontan circulation after 45 years: update in physiology. *Heart*. 2016;102(14):heartjnl - 2015-307467. doi:10.1136/heartjnl-2015-307467.

23. Duncan BW, Desai S. Pulmonary arteriovenous malformations after cavopulmonary anastomosis. *Ann Thorac Surg*. 2003;76(5):1759-1766. doi:10.1016/S0003-4975(03)00450-8.

24. Brown JW, Ruzmetov M, Vijay P, Rodefeld MD, Turrentine MW. Pulmonary arteriovenous malformations in children after the Kawashima operation. *Ann Thorac Surg*. 2005;80(5):1592-1596. doi:10.1016/j.athoracsur.2005.04.043.

25. Khurshid I, Downie GH. Pulmonary arteriovenous malformation. *Postgrad Med J*. 2002;78(918):191-197. doi:10.1136/PMJ.78.918.191.

26. McElhinney DB, Marshall AC, Lang P, Lock JE, Mayer JE. Creation of a brachial arteriovenous fistula for treatment of pulmonary arteriovenous malformations after cavopulmonary anastomosis. *Ann Thorac Surg*. 2005;80(5):1604-1609. doi:10.1016/j.athoracsur.2005.05.100.

27. Vettukattil JJ. Pathogenesis of pulmonary arteriovenous malformations: role of hepatopulmonary interactions. *Heart*. 2002;88(6):561-563. doi:10.1136/heart.88.6.561.

28. Sundareswaran KS, de Zélicourt D, Sharma S, et al. Correction of Pulmonary Arteriovenous Malformation Using Image-Based Surgical Planning. *JACC Cardiovasc Imaging*. 2009;2(8):1024-1030. doi:10.1016/j.jcmg.2009.03.019.

29. Shah MJ, Rychik J, Fogel MA, Murphy JD, Jacobs ML. ORIGINAL ARTICLES : CARDIOVASCULAR Pulmonary AV Malformations After Superior Cavopulmonary Connection : Resolution After Inclusion of Hepatic Veins in the Pulmonary Circulation. 1997;4975(96):0-3.

30. Goldberg DJ, Surrey LF, Glatz AC, et al. Hepatic Fibrosis Is Universal Following Fontan Operation, and Severity is Associated With Time From Surgery: A Liver Biopsy and Hemodynamic Study. *J Am Heart Assoc*. 2017;6(5):e004809. doi:10.1161/JAHA.116.004809.

31. Bryant T, Ahmad Z, Millward-Sadler H, et al. Arterialised hepatic nodules in the Fontan circulation: Hepatico-cardiac interactions. *Int J Cardiol*. 2011;151(3):268-272. doi:10.1016/j.ijcard.2010.05.047.

32. Mori M, Aguirre AJ, Elder RW, et al. Beyond a broken heart: Circulatory dysfunction in the failing Fontan. *Pediatr Cardiol*. 2014;35(4):569-579. doi:10.1007/s00246-014-0881-y.

33. Romero R. Liver in congenital heart disease: Implications of the fontan procedure for pediatric and adult liver specialists. *Clin Liver Dis*. 2013;2(5):210-214. doi:10.1002/cld.241.

34. Ghaferi A a., Hutchins GM. Progression of liver pathology in patients undergoing the Fontan procedure: Chronic passive congestion, cardiac cirrhosis, hepatic adenoma, and hepatocellular carcinoma. *J Thorac Cardiovasc Surg*. 2005;129(6):1348-1352. doi:10.1016/j.jtcvs.2004.10.005.

35. Chokshi A, Cheema FH, Schaefle KJ, et al. Hepatic dysfunction and survival after orthotopic heart transplantation: Application of the MELD scoring system for outcome prediction. *J Hear Lung Transplant*. 2012;31(6):591-600. doi:10.1016/j.healun.2012.02.008.

36. Wei Z (Alan), Trusty PM, Tree M, et al. Can time-averaged flow boundary conditions be used to meet the clinical timeline for Fontan surgical planning? *J Biomech*. 2016;50:172-179. doi:10.1016/j.jbiomech.2016.11.025.

37. Slesnick TC, Yoganathan AP. Computational modeling of Fontan physiology: At the crossroads of pediatric cardiology and biomedical engineering. *Int J Cardiovasc Imaging*. 2014;30(6):1073-1084. doi:10.1007/s10554-014-0442-8.

38. Fogel M a., Khiabani RH, Yoganathan A. Imaging for preintervention planning pre- and post-fontan procedures. *Circ Cardiovasc Imaging*. 2013;6(6):1092-1101. doi:10.1161/CIRCIMAGING.113.000335.

39. Haggerty CM, de Zélicourt DA, Restrepo M, et al. Comparing Pre- and Post-operative Fontan Hemodynamic Simulations: Implications for the Reliability of Surgical Planning. *Ann Biomed Eng*. 2012;40(12):2639-2651. doi:10.1007/s10439-012-0614-4.

40. Marsden AL, Bernstein AJ, Reddy VM, et al. Evaluation of a novel Y-shaped extracardiac Fontan baffle using computational fluid dynamics. *J Thorac Cardiovasc Surg*. 2009;137(2):394-403.e2. doi:10.1016/j.jtcvs.2008.06.043.

41. Yang W, Chan FP, Reddy VM, Marsden AL, Feinstein J a. Flow simulations and validation for the first cohort of patients undergoing the Y-graft Fontan procedure. *J Thorac Cardiovasc Surg*. 2015;149(1):247-255. doi:10.1016/j.jtcvs.2014.08.069.

42. Haggerty CM, Kanter KR, Restrepo M, et al. Simulating hemodynamics of the Fontan Y-graft based on patient-specific in vivo connections. *J Thorac Cardiovasc Surg*. 2013;145(3):663-670. doi:10.1016/j.jtcvs.2012.03.076.

43. Yang W, Feinstein J a, Shadden SC, Vignon-Clementel IE, Marsden AL. Optimization of a Y-graft design for improved hepatic flow distribution in the fontan circulation. *J Biomech Eng*. 2013;135(1):011002. doi:10.1115/1.4023089.

44. Yang W, Feinstein J a., Marsden AL. Constrained optimization of an idealized Y-shaped baffle for the Fontan surgery at rest and exercise. *Comput Methods Appl Mech Eng*. 2010;199(33-36):2135-2149. doi:10.1016/j.cma.2010.03.012.

45. Haggerty CM, Restrepo M, Tang E, et al. Fontan hemodynamics from 100 patient-specific cardiac magnetic resonance studies: A computational fluid dynamics analysis. *J Thorac Cardiovasc Surg*. 2013;148(4):1-10. doi:10.1016/j.jtcvs.2013.11.060.

46. Tang E, Restrepo M, Haggerty C, et al. a Retrospective Cohort of 100 Fontan Connections: Relationship Between Geometric Features and Hemodynamics Outcomes. *J Am Coll Cardiol*. 2013;61(10):E490. doi:10.1016/S0735-1097(13)60490-8.

47. Marsden AL, Vignon-Clementel IE, Chan FP, Feinstein J a., Taylor C a. Effects of exercise and respiration on hemodynamic efficiency in CFD simulations of the total cavopulmonary connection. *Ann Biomed Eng*. 2007;35(2):250-263. doi:10.1007/s10439-006-9224-3.

48. Lewis GD, Shah R, Shahzad K, et al. Sildenafil improves exercise capacity and quality of life in patients with systolic heart failure and secondary pulmonary hypertension. *Circulation*. 2007;116(14):1555-1562. doi:10.1161/CIRCULATIONAHA.107.716373.

49. Whitehead KK, Pekkan K, Kitajima HD, Paridon SM, Yoganathan AP, Fogel M a. Nonlinear power loss during exercise in single-ventricle patients after the Fontan: Insights from computational fluid dynamics. *Circulation*. 2007;116(11 SUPPL. 1). doi:10.1161/CIRCULATIONAHA.106.680827.

50. Khiabani RH, Whitehead KK, Han D, et al. Exercise capacity in single-ventricle patients after Fontan correlates with haemodynamic energy loss in TCPC. *Heart*. 2015;101(2):139-143. doi:10.1136/heartjnl-2014-306337.

51. Gewillig MH, Lundström UR, Bull C, Wyse RKH, Deanfield JE. Exercise responses in patients with congenital heart disease after Fontan repair: patterns and determinants of performance. *J Am Coll Cardiol*. 1990;15(6):1424-1432. doi:10.1016/S0735-1097(10)80034-8.

52. Mertens L, Hagler DJ, Sauer U, Somerville J, Gewillig M. Protein-losing enteropathy after the Fontan operation: an international multicenter study. PLE study group. *J Thorac Cardiovasc Surg*. 1998;115(5):1063-1073. doi:10.1016/S0022-5223(98)70406-4.

53. Asrani SK, Asrani NS, Freese DK, et al. Congenital heart disease and the liver. *Hepatology*. 2012;56(3):1160-1169. doi:10.1002/hep.25692.

54. Wu FM, Ukomadu C, Odze RD. STATE OF THE ART ARTICLES Liver Disease in the Patient with Fontan Circulation. 2011:190-201.

55. Deshpande SR, Maher KO, Morales DL. Mechanical Circulatory Support in Children: Challenges and Opportunities. *Prog Pediatr Cardiol*. 2016;43:31-41. doi:10.1016/j.ppedcard.2016.08.016.

56. Weinstein S, Bello R, Pizarro C, et al. The use of the Berlin heart EXCOR in patients with functional single ventricle. *J Thorac Cardiovasc Surg*. 2014;147(2):697-705. doi:10.1016/j.jtcvs.2013.10.030.

57. Niebler R a., Ghanayem NS, Shah TK, et al. Use of a HeartWare ventricular assist device in a patient with failed fontan circulation. *Ann Thorac Surg*. 2014;97(4):e115-e116. doi:10.1016/j.athoracsur.2013.11.075.

58. Rodefeld MD, Boyd JH, Myers CD, et al. Cavopulmonary Assist: Circulatory Support for the Univentricular Fontan Circulation. *Ann Thorac Surg*. 2003;76(6):1911-1916. doi:10.1016/S0003-4975(03)01014-2.

59. Prêtre R, Häussler A, Bettex D, Genoni M. Right-Sided Univentricular Cardiac Assistance in a Failing Fontan Circulation. *Ann Thorac Surg*. 2008;86(3):1018-1020. doi:10.1016/j.athoracsur.2008.03.003.

60. Tree M, Trusty P, Munz B, et al. In Vitro Examination of the HeartWare Circulite VAD in the Fontan Circulation. *ASAIO*. 2016;35(4):S46. doi:10.1016/j.healun.2016.01.123.

61. Tang E, Restrepo M, Haggerty CM, et al. Geometric characterization of patient-specific total cavopulmonary connections and its relationship to hemodynamics. *JACC Cardiovasc Imaging*. 2014;7(3):215-224. doi:10.1016/j.jcmg.2013.12.010.

62. Restrepo M, Mirabella L, Tang E, et al. Fontan pathway growth: A quantitative evaluation of lateral tunnel and extracardiac cavopulmonary connections using serial cardiac magnetic resonance. *Ann Thorac Surg*. 2014;97(3):916-922. doi:10.1016/j.athoracsur.2013.11.015.

63. Restrepo M, Tang E, Haggerty CM, et al. Energetic implications of vessel growth and flow changes over time in fontan patients. *Ann Thorac Surg*. 2015;99(1):163-170. doi:10.1016/j.athoracsur.2014.08.046.

64. Cheng CP, Herfkens RJ, Lightner AL, Taylor C a, Feinstein J a. Blood flow conditions in the proximal pulmonary arteries and vena cavae: healthy children during upright cycling exercise. *Am J Physiol Heart Circ Physiol*. 2004;287(2):H921-H926. doi:10.1152/ajpheart.00022.2004.

65. Driscoll DJ, Danielson GK, Puga FJ, Schaff H V., Heise CT, Staats B a. Exercise tolerance and cardiorespiratory response to exercise after the Fontan operation for tricuspid atresia or functional single ventricle. *J Am Coll Cardiol*. 1986;7(5):1087-1094. doi:10.1016/S0735-1097(86)80227-3.

66. Fredriksen PM, Therrien J, Veldtman G, et al. Lung function and aerobic capacity in adult patients following modi ed Fontan procedure. *Society*. 2001:295-299.

67. Giardini A, Hager A, Pace Napoleone C, Picchio FM. Natural history of exercise capacity after the Fontan operation: a longitudinal study. *Ann Thorac Surg*. 2008;85(3):818-821. doi:10.1016/j.athoracsur.2007.11.009.

68. Grewal J, Mccully RB, Kane GC, Lam C, Pellikka P a, Factors a NY. Left Ventricular Function and Exercise Capacity. 2009;301(3).

69. Hjortdal VE, Christensen TD, Larsen SH, Emmertsen K, Pedersen EM. Caval Blood Flow During Supine Exercise in Normal and Fontan Patients. *Ann Thorac Surg*. 2008;85(2):599-603. doi:10.1016/j.athoracsur.2007.08.062.

70. Shachar GB, Fuhrman BP, Wang Y, Lucas R V, Lock JE. Rest and exercise hemodynamics after the Fontan procedure. *Circulation*. 1982;65(6):1043-1048. doi:10.1161/01.CIR.65.6.1043.

71. Friedrich-Rust M, Koch C, Rentzsch A, et al. Noninvasive assessment of liver fibrosis in patients with Fontan circulation using transient elastography and biochemical fibrosis markers. *J Thorac Cardiovasc Surg*. 2008;135(3):560-567. doi:10.1016/j.jtcvs.2007.09.039.

72. Ginde S, Hohenwalter MD, Foley WD, et al. Noninvasive Assessment of Liver Fibrosis in Adult Patients Following the Fontan Procedure. *Congenit Heart Dis*. 2012;7(3):235-242. doi:10.1111/j.1747-0803.2012.00632.x.

73. Greenway SC, Crossland DS, Hudson M, et al. Fontan-associated liver disease: Implications for heart transplantation. *J Hear Lung Transplant*. 2016;35(1):26-33. doi:10.1016/j.healun.2015.10.015.

74. Martins T, Barbara A, Silva G, Faria T, Dalava B, Silva J. InVesalius: three-dimensional medical reconstruction software. *Virtual rapid Manuf*. 2007:135-141.

75. De Moraes, Thiago F and Amorim PH. InVesalius-An open-source imaging application. *Comput Vis Med Image Process*. 2011:405.

76. Yushkevich P a., Piven J, Hazlett HC, et al. User-guided 3D active contour segmentation of anatomical structures: Significantly improved efficiency and reliability. *Neuroimage*. 2006;31(3):1116-1128. doi:10.1016/j.neuroimage.2006.01.015.

77. Bidhult SL, Carlsson M, Steding-Ehrenborg K, Arheden H, Heiberg E. A new method for vessel segmentation based on a priori input from medical expertise in cine phase-contrast Magnetic Resonance Imaging. *J Cardiovasc Magn Reson*. 2014;16(Suppl 1):P355. doi:10.1186/1532-429X-16-S1-P355.

78. Heiberg E, Sjögren J, Ugander M, Carlsson M, Engblom H, Arheden H. Design and validation of Segment - freely available software for cardiovascular image analysis. *BMC Med Imaging*. 2010;10(1):1. doi:10.1186/1471-2342-10-1.

79. Wei ZA, Tree M, Trusty PM, Wu W, Singh-Gryzbon S, Yoganathan A. The Advantages of Viscous Dissipation Rate over Simplified Power Loss as a Fontan Hemodynamic Metric. *Ann Biomed Eng*. 2018;46(3):404-416. doi:10.1007/s10439-017-1950-1.

80. Tree M, Wei Z, Munz B, et al. A Method for In Vitro TCPC Compliance Verification. *J Biomech Eng Asme*. 2017;139(June):1-5. doi:10.1115/1.4036474.

81. Sunagawa G, Karimov JH, Dessoffy R, et al. New Technology Mimics Physiologic Pulsatile Flow During Cardiopulmonary Bypass. *Artif Organs*. 2018;42(2):231-235. doi:10.1111/aor.12986.

82. Zhang J, Gellman B, Koert A, et al. Computational and experimental evaluation of the fluid dynamics and hemocompatibility of the centrimag blood pump. *Artif Organs*. 2006;30(3):168-177. doi:10.1111/j.1525-1594.2006.00203.x.

83. Robertis F De. End-stage Cardiac failure managed with Levitronix Centrimag short-term ventricular assist device (VAD). *Hear Lung*. 24(2):100-100.

84. Dasi LP, Pekkan K, Katajima HD, Yoganathan AP. Functional analysis of Fontan energy dissipation. *J Biomech*. 2008;41(10):2246-2252. doi:10.1016/j.jbiomech.2008.04.011.

85. Bradley S Marino, Mark Fogel, Laura Mercer-Rosa Mercer-Rosa, Zhenglun Alan Wei Wei, Phillip M Trusty, Micheal Tree, Elaine Tang, Maria Restrepo, Kevin K Whitehead, Stephen M Paridon AY. No Title. In: *Poor Fontan Geometry, Hemodynamics, and Computational Fluid Dynamics Are Associated With Worse Quality of Life*. Vol Circulation (Supp1); 2017:A18082.

86. Mark A Fogel, Phillip Trusty, Alan Wei, Matthew Harris, Kevin Whitehead AY. No Title. In: *Cardiac Magnetic Resonance and Computational Fluid Dynamic Parameters Are Important Predictors of Adverse Events in the Fontan Almost 10 Years After Imaging*. Vol Circulation (Supp1); 2017:A18160.

87. Pekkan K, Whited B, Kanter K, et al. Patient-specific surgical planning and hemodynamic computational fluid dynamics optimization through free-form haptic anatomy editing tool (SURGEM). *Med Biol Eng Comput*. 2008;46(11):1139-1152. doi:10.1007/s11517-008-0377-0.

88. Luffel M, Sati M, Rossignac J, et al. SURGEM: A solid modeling tool for planning and optimizing pediatric heart surgeries. *Comput Des*. 2015. doi:10.1016/j.cad.2015.06.018.

89. Restrepo M, Luffel M, Sebring J, et al. Surgical Planning of the Total Cavopulmonary Connection: Robustness Analysis. *Ann Biomed Eng*. 2014;43(6):1321-1334. doi:10.1007/s10439-014-1149-7.

90. Marsden AL, Esmaily-Moghadam M. Multiscale Modeling of Cardiovascular Flows for Clinical Decision Support. *Appl Mech Rev*. 2015;67(3):030804. doi:10.1115/1.4029909.

91. Sodian R, Weber S, Markert M, et al. Pediatric cardiac transplantation: Three-dimensional printing of anatomic models for surgical planning of heart transplantation in patients with univentricular heart. *J Thorac Cardiovasc Surg*. 2008;136(4):1098-1099. doi:10.1016/j.jtcvs.2008.03.055.

92. Ventola CL. Medical Applications for 3D Printing: Current and Projected Uses. *P T*. 2014;39(10):704-711. doi:10.1016/j.infsof.2008.09.005.

93. McCloy R, Stone R. Science, medicine, and the future. Virtual reality in surgery. *BMJ*. 2001;323(7318):912-915. doi:10.1136/bmj.323.7318.912.

94. Seymour NE, Gallagher a G, Roman S a, et al. Virtual reality training improves operating room performance: results of a randomized, double-blinded study. *Ann Surg*. 2002;236(4):454-458. doi:10.1097/01.sla.0000028969.51489.b4.

95. Schiavazzi DE, Kung EO, Marsden AL, et al. Hemodynamic effects of left pulmonary artery stenosis after superior cavopulmonary connection: A patient-specific multiscale modeling study. *J Thorac Cardiovasc Surg*. 2015;149(3):689-696.e3. doi:10.1016/j.jtcvs.2014.12.040.

96. Wootton DM, Ku DN. Fluid mechanics of vascular systems, diseases, and thrombosis. *Annu Rev Biomed Eng*. 1999;1:299-329. doi:10.1146/annurev.bioeng.1.1.299.

97. Rayz VL, Boussel L, Ge L, et al. Flow residence time and regions of intraluminal thrombus deposition in intracranial aneurysms. *Ann Biomed Eng*. 2010;38(10):3058-3069. doi:10.1007/s10439-010-0065-8.

98. Whitehead KK, Sundareswaran KS, Parks WJ, Harris M a, Yoganathan AP, Fogel M a. Cardiac Magnetic Resonance Velocity Mapping Study. *J Thorac Cardiovasc Surg*. 2010;138(1):96-102. doi:10.1016/j.jtcvs.2008.11.062.Blood.

99. Surrey LF, Russo P, Rychik J, et al. Prevalence and characterization of fibrosis in surveillance liver biopsies of patients with Fontan circulation. *Hum Pathol*. 2016;57:106-115. doi:10.1016/j.humpath.2016.07.006.

100. Kiesewetter CH, Sheron N, Vettukattill JJ, et al. Hepatic changes in the failing Fontan circulation. *Heart*. 2007;93(5):579-584. doi:10.1136/hrt.2006.094516.

101. Whitehead KKK, Harris M a., Glatz AC, et al. Status of Systemic to Pulmonary Arterial Collateral Flow After the Fontan Procedure. *Am J Cardiol*. 2015;115(12):1739-1745. doi:10.1016/j.amjcard.2015.03.022.

102. Bocca C, Novo E, Miglietta A, Parola M. Angiogenesis and Fibrogenesis in Chronic Liver Diseases. *C Cell Mol Gastroenterol Hepatol*. 2015;1(5):477-488. doi:10.1016/j.jcmgh.2015.06.011.

103. Eipel C, Abshagen K, Vollmar B. Regulation of hepatic blood flow: The hepatic arterial buffer response revisited. *World J Gastroenterol*. 2010;16(48):6046-6057. doi:10.3748/wjg.v16.i48.6046.

104. Egbe AC, Connolly HM, Miranda WR, et al. Hemodynamics of Fontan Failure: The Role of Pulmonary Vascular Disease. *Circ Hear Fail*. 2017;10(12). doi:10.1161/CIRCHEARTFAILURE.117.004515.

105. Trusty PM, Wei Z, Rychik J, et al. Impact of hemodynamics and fluid energetics on liver fibrosis after Fontan operation. 2018;9:1-10. doi:10.1016/j.jtcvs.2018.02.078.

106. Trusty PM, Restrepo M, Kanter KR, Yoganathan AP, Fogel M a, Slesnick TC. A pulsatile hemodynamic evaluation of the commercially available bifurcated Y-graft Fontan modification and comparison with the lateral tunnel and extracardiac conduits. *J Thorac Cardiovasc Surg*. 2016. doi:10.1016/j.jtcvs.2016.03.019.

107. Durham L a., Dearani J a., Burkhart HM, et al. Application of Computer Modeling in Systemic VAD Support of Failing Fontan Physiology. *World J Pediatr Congenit Hear Surg*. 2011;2(2):243-248. doi:10.1177/2150135110397386.

108. Kanakis M, Lioulias A, Samanidis G, Loukas C, Mitropoulos F. Evolution in experimental fontan circulation: A review. *Ann Thorac Cardiovasc Surg*. 2013;19(3):177-185. doi:10.5761/atcs.ra.13-00017.

109. Leverett LB, Lynch EC, Alfrey CP, Hellums JD. Red Blood-Cell Damage by Shear-Stress. *Biophys J*. 1972;12(3):257 - &. <Go to ISI>://A1972L848900005\nhttp://www.ncbi.nlm.nih.gov/pmc/articles/PMC1484094/pdf/biophysj00725-0044.pdf.

110. Arnaoutakis GJ, Blitzer D, Fuller S, et al. Mechanical Circulatory Support as Bridge to Transplantation for the Failing Single Ventricle. *Ann Thorac Surg*. 2017;103(1):193-197. doi:10.1016/j.athoracsur.2016.05.015.

111. Poh CL, Chiletti R, Zannino D, et al. Ventricular assist device support in patients with single ventricles: The Melbourne experience. *Interact Cardiovasc Thorac Surg*. 2017;25(2):310-316. doi:10.1093/icvts/ivx066.

112. Lacour-Gayet FG, Lanning CJ, Stoica S, et al. An Artificial Right Ventricle for Failing Fontan: In Vitro and Computational Study. *Ann Thorac Surg*. 2009;88(1):170-176. doi:10.1016/j.athoracsur.2009.03.091.

113. L.C. R, H. L, R. B, et al. Mechanical circulatory support for the fontan circulation. *J Hear Lung Transplant*. 2016;35(4):S131. doi:10.1016/j.healun.2016.01.358.